

**Controlled Sequential Delivery of Two Growth Factors for the Stimulation of Endogenous  
Brain Repair after Stroke**

By

Yuanfei Wang

A thesis submitted in conformity with the requirements  
for the degree of Doctor of Philosophy  
Department of Chemical Engineering and Applied Chemistry  
University of Toronto

© Copyright by Yuanfei Wang 2014

# Controlled Sequential Delivery of Two Growth Factors for the Stimulation of Endogenous Brain

Repair after Stroke

Yuanfei Wang

Doctor of Philosophy

Department of Chemical Engineering and Applied Chemistry

University of Toronto

2014

## Abstract

Stroke is a leading cause of disability in the world, for which there currently is no effective treatment. One potential method for treating stroke is to stimulate the endogenous neural stem/progenitor cells (NSPCs) in the subventricular zone (SVZ) of adult brain to replace the tissue lost during stroke. Two growth factors that have shown promise in eliciting functional repair in rodent models of stroke are epidermal growth factor (EGF) and erythropoietin (EPO). However, there is a significant challenge in delivering protein drugs in a minimally invasive yet effective manner. In this thesis, a minimally invasive polymer-based system is developed to control the sequential release of EGF followed by EPO. This system comprises of a hyaluronan-methylcellulose (HAMC) hydrogel and two types of polymeric particles, and is applied epicortically to deliver EGF and EPO to stroke-injured mouse brains in a minimally invasive manner. In this thesis, the following are demonstrated:

- 1) The ability of therapeutics delivered locally to reach the target site after delivery is crucial for the success of local delivery strategies. PEG-modification leads to enhanced penetration distance of EGF.

- 2) When delivered epicortically to the stroke-injured mouse brain using HAMC, PEG-EGF penetrates further into the brain compared to unmodified EGF. Both EGF and PEG-EGF stimulated NSPC proliferation in the SVZ, but the extent of stimulation is greater when PEG-EGF is delivered compared to unmodified EGF.
- 3) The transport of EPO is similar in the uninjured and the stroke-injured brain following epicortical delivery from HAMC. EPO delivered epicortically from HAMC is able to reach the SVZ and can enhance neurogenesis in the stroke-injured brain.
- 4) A composite delivery system is engineered where PEG-EGF and EPO are individually encapsulated in different polymeric particles, and the particles are embedded in the HAMC hydrogel matrix. Stroke-injured animals that receive composite-mediated growth factor treatments ultimately achieve repair comparable to that achieved using a conventional catheter/osmotic minipump infusion system, without causing tissue damage associated with insertion of the infusion system into the brain.

## **Acknowledgements**

First and foremost I would like to thank my supervisor, Professor Molly Shoichet, for her guidance and support during my degree. This work would not have been possible without her inspirations and insights, and her mentorship and support throughout the last five years has been immensely valuable. It is difficult to overstate the contributions of Dr. Michael Cooke, who was instrumental in my development as a scientist. His enthusiasm and dedication to science has been a constant source of motivation over the years. Special thanks also go to Dr. Ryan Wylie for his expertise in protein chemistry.

I want to acknowledge my committee members, Professor Cindi Morshead and Professor Yuling Cheng, for their help and support. Professor Morshead's expertise on stem cell biology and animal models of stroke exposed me to a new and exciting aspect of biology, and Professor Cheng's expertise in transport phenomena has been extremely helpful in my project.

I am grateful for the support and help from members, both past and present, of the Shoichet Research Group. My Ph.D. has been a rewarding journey, and I cannot adequately express my gratitude to my parents for encouraging me on this journey and through its ups and downs. Thanks also go to all my friends, without whom it would not have been the same.

## Table of Contents

Acknowledgements.....	iv
List of Figures .....	x
List of Tables.....	xvi
1. Introduction.....	1
1.1. Rationale.....	1
1.2. Hypothesis and Objectives .....	2
1.3. Stroke.....	4
1.3.1. Statistics.....	4
1.3.2. Pathology of stroke .....	4
1.3.3. Currently available clinical treatments and their limitations .....	6
1.4. Using regenerative medicine-based approaches for treating stroke.....	7
1.4.1. Animal models of stroke.....	8
1.4.2. Neuroprotection as a treatment strategy for stroke.....	11
1.4.3. Neuroregeneration as an alternative stroke treatment .....	13
1.4.4. Growth factor-mediated stimulation of endogenous NSPCs and brain tissue regeneration .....	16
1.5. Challenges in drug-delivery to the brain .....	18
1.5.1. Blood-brain barrier.....	18
1.5.2. Invasiveness of local delivery strategies.....	20
1.5.3. Epicortical controlled drug delivery systems .....	21
1.6. Polymeric drug delivery systems for achieving controlled drug delivery to the brain .....	28
1.6.1. Hydrogel-based drug delivery systems.....	28
1.6.2. Hydrogels based on synthetic polymers in drug delivery applications.....	30
1.6.3. Hydrogels based on naturally derived polymers in drug delivery applications .....	32
1.6.4. Hyaluronan-methylcellulose blend (HAMC) as a local drug delivery scaffold .....	34
1.6.5. Use of polymeric particles for controlling protein delivery to the brain.....	36
1.7. Summary of research .....	46
2. Transport of epidermal growth factor in the stroke-injured brain*.....	48
2.1. Abstract.....	48

2.2	Introduction.....	49
2.3	Materials and Methods .....	52
2.3.1	Materials .....	52
2.3.2	PEG modification of rhEGF and purification of PEG <sub>x</sub> -rhEGF .....	52
2.3.3	Fluorescent labeling of EGF and PEG-EGF .....	54
2.3.4	Mouse surgeries .....	55
2.3.5	Mouse brain cortical slice preparations.....	55
2.3.6	Cortical slice viability.....	56
2.3.7	Stroke Surgeries.....	56
2.3.8	Integrative optical imaging (IOI) to calculate protein diffusivity .....	57
2.3.9	Image analysis and mathematical modeling for estimating rate of elimination and protein penetration distance .....	58
2.3.10	Total cell count in pre- and post-stroke brains.....	63
2.3.11	Real time RT-PCR to detect EGFR upregulation post stroke .....	63
2.3.12	<i>In vivo</i> penetration distance of rhEGF and PEG <sub>1</sub> -rhEGF .....	64
2.3.13	Bioactivity assay for neural stem cell response towards EGF and PEG <sub>x</sub> -EGF .....	65
2.3.14	Statistical analysis .....	66
2.4	Results .....	66
2.4.1	The effect of PEG on the intrinsic diffusivity of rhEGF in agarose.....	66
2.4.2	Transport of rhEGF and PEG <sub>x</sub> -rhEGF in uninjured brain cortical slices .....	67
2.4.3	Transport of rhEGF and PEG <sub>x</sub> -rhEGF in brain with stroke injury.....	70
2.4.4	Calculated penetration distance for rhEGF and PEG <sub>x</sub> -rhEGF in brain cortical tissue ..	73
2.4.5	<i>In vivo</i> penetration distance of rhEGF and PEG <sub>1</sub> -rhEGF .....	75
2.5	Discussion .....	76
2.6	Conclusion.....	80
3	Controlled epi-cortical delivery of epidermal growth factor for the stimulation of endogenous neural stem cell proliferation in stroke-injured brain* .....	81
3.1	Abstract.....	81
3.2	Introduction.....	82
3.3	Materials and Methods .....	85
3.3.1	Materials .....	85
3.3.2	Preparation of sterile HAMC.....	86

3.3.3	In vitro release of EGF and PEG-EGF from HAMC.....	86
3.3.4	Mouse surgeries.....	87
3.3.5	Preparation of delivery device for HAMC implantation.....	87
3.3.6	Drug delivery device implantation surgeries.....	88
3.3.7	Analysis of in vivo protein penetration.....	88
3.3.8	Stability of EGF and PEG-EGF in proteases of the brain extracellular space.....	89
3.3.9	Effects of EGF and PEG-EGF released from HAMC on endogenous SVZ cell proliferation.....	91
3.3.10	Statistics.....	92
3.4	Results.....	92
3.4.1	In vitro release of EGF from HAMC.....	92
3.4.2	In vivo elimination of EGF and PEG-EGF in uninjured and stroke-injured animals.....	92
3.4.3	In vivo penetration profiles of EGF and PEG-EGF in uninjured and stroke-injured animals	95
3.4.4	In vitro proteolytic stability of EGF and PEG-EGF in brain extracellular space (ECS) and intracellular enzyme solutions.....	98
3.4.5	Effect of EGF and PEG-EGF delivered from HAMC on SVZ stem cell proliferation ..	100
3.5	Discussion.....	103
3.6	Conclusion.....	107
4	Local hydrogel delivery strategy to the brain of erythropoietin for endogenous stem cell stimulation after stroke injury*.....	108
4.1	Abstract.....	108
4.2	Introduction.....	109
4.3	Materials and Methods.....	111
4.3.1	Materials.....	111
4.3.2	Preparation of sterile HAMC hydrogel.....	112
4.3.3	In vitro release of EPO from HAMC.....	112
4.3.4	Stroke surgeries and injection of drug delivery device.....	113
4.3.5	Analysis of in vivo protein penetration.....	114
4.3.6	Brain tissue preparation for morphological analysis.....	115
4.3.7	Analysis of stroke cavity size.....	115
4.3.8	Immunohistochemistry.....	116
4.3.9	Analysis of apoptosis using TUNEL.....	116

4.3.10	Statistics.....	117
4.4	Results .....	117
4.4.1	Cortical EPO Receptor (EPOr) expression in uninjured and stroke-injured brains.....	117
4.4.2	Release and penetration of EPO in uninjured and stroke-injured brains .....	118
4.4.3	Effects of EPO delivered from HAMC on stroke cavity size .....	120
4.4.4	Effect of HAMC on the inflammatory response after stroke .....	122
4.4.5	Effect of EPO on Ki-67 <sup>+</sup> and double cortin <sup>+</sup> (DCX <sup>+</sup> ) Ki-67 <sup>+</sup> cells in the SVZ .....	124
4.4.6	Effect of EPO on NeuN <sup>+</sup> mature neurons in the injured cortex .....	126
4.4.7	Effect of EPO on TUNEL <sup>+</sup> apoptotic cells in the injured cortex and SVZ .....	128
4.5	Discussion .....	130
4.6	Conclusion.....	133
5.	Bioengineered sequential growth factor delivery stimulates brain tissue regeneration after stroke* .....	134
5.1	ABSTRACT .....	134
5.2	INTRODUCTION.....	135
5.3	MATERIALS AND METHODS .....	137
5.3.1	Materials .....	137
5.3.2	Encapsulation of EGF-PEG in PLGA nanoparticles .....	138
5.3.3	Encapsulation of EPO in biphasic microparticles.....	139
5.3.4	Preparation of HAMC/particle composite drug delivery system (DDS).....	140
5.3.5	In vitro degradation of the composite DDS.....	141
5.3.6	In vitro release profiles of EGF-PEG and EPO from composite DDS.....	141
5.3.7	Preparation of drug delivery device .....	141
5.3.8	Surgeries .....	142
5.3.9	Stroke surgeries and implantation of drug delivery device .....	142
5.3.10	Implantation of catheter/osmotic minipump system.....	143
5.3.11	Analysis of in vivo protein penetration.....	143
5.3.12	Immunohistochemistry.....	144
5.3.13	Analysis of stroke cavity size.....	144
5.3.14	Analysis of apoptosis using TUNEL .....	144
5.3.15	Statistics.....	145
5.4	RESULTS.....	145

5.4.1	Controlled Release of EGF-PEG and EPO.....	145
5.4.2	SVZ cellular response to growth factors delivered from epicortical composite vs. ICV pump at 18 days after stroke.....	148
5.4.3	Tissue Repair in the peri-infarct brain.....	148
	151	
5.4.4	Cellular response in the SVZ at 32 days after stroke.....	155
5.4.5	Preliminary functional assessments.....	156
5.5	DISCUSSION.....	156
5.6	CONCLUSION.....	160
6.	Thesis Discussion.....	161
6.1.	Growth factor-mediated tissue regeneration following stroke.....	161
6.2.	Engineering protein transport in the injured brain.....	164
6.3.	Optimizing protein delivery from polymeric drug delivery systems.....	168
6.4.	Comparison between composite delivery system and existing delivery strategies.....	171
6.5	Potential issues in translation.....	174
7.	Thesis Conclusions.....	178
7.1.	Achievement of objectives.....	178
7.2.	Major contributions.....	180
8.	Recommendations for future work.....	182
8.1	Encapsulating more clinically relevant proteins in composite DDS.....	182
8.2	Additional functional assessment of composite delivery system.....	183
8.3	Translating composite DDS into larger animal models.....	183
8.4	Develop more clinically translatable drug delivery casing.....	185
9.	References.....	186
	Appendix A: Abbreviations.....	223
	Appendix B: Supplementary Figures.....	225
	Appendix C: Supplementary Tables.....	243
	Appendix D: Supplementary Results.....	245
	Copyright Acknowledgements.....	249

## List of Figures

Figure 1.1   Common activated poly(ethylene glycol) derivatives .....	25
Figure 1.2   Structure of hyaluronan (HA, left) and methylcellulose (MC, right) .....	34
Figure 1.3   Schematic describing the composite drug delivery system (DDS). We envision using a composite system of HAMC and polymeric particles to localize and sustain the deliver of EGF and EPO. The HAMC hydrogel (HA – red, MC – blue) is fast gelling at 37°C and injectable, it also localizes the factors delivered to the site of injection. However, the high water content leads to rapid Fickian diffusion of factors out of the hydrogel. We can encapsulate EGF and EPO in different polymeric particles to achieve the desired temporal delivery. EGF can be encapsulated in bulk-eroding nanoparticles to facilitate immediate but sustained release, whereas EPO can be first encapsulated in bulk-eroding nanoparticles and then embedded in surface eroding microparticles to achieve delayed and sustained release. An additional advantage of adding hydrophobic polymeric particles to HAMC is that the particles may interact with the methyl groups on methyl cellulose to form transient crosslinks, thereby further stabilizing the hydrogel. The quantities of particles added to the system will be dictated by the amount of factors required to achieve therapeutic efficacy.....	37
Figure 1.4   General structures of the four generations of poly(orthoesters) (POES). .....	39
Figure 1.5   General structure of poly(anhydrides). .....	40
Figure 2.1   Progression of rhEGF and PEG-rhEGF fluorescence intensity in dilute agarose following injection. (a) Representative images showing diffusion of fluorescently labelled rhEGF in dilute agarose. (b) Fluorescence intensity profiles obtained from images are fitted to Eq. 2, where the vertical axis represents the fluorescent intensity in arbitrary units and the horizontal axis represents distance from the centre of the fluorescence. All images are shown at the same magnification (scale bar = 100µm). (c) Representative graph showing plot of $\gamma^2/4$ ( $10^{-7}\text{cm}^2$ ) vs. time (s) for (○) rhEGF, (■) PEG <sub>1</sub> -rhEGF, (▲) PEG <sub>2</sub> -rhEGF, and (□) PEG <sub>3</sub> -rhEGF in agarose where values of $\gamma^2/4$ were obtained from fitting data to Eq. 2, and the gradient of the plot returns a value of D ( $10^{-7}\text{cm}^2/\text{s}$ ).....	61
Figure 2.2   PEG modification decreases diffusivity of rhEGF in saturated brain tissue. (a) Diffusivities for rhEGF and PEG <sub>x</sub> -rhEGF are determined in agarose, saturated and non-saturated cortical tissue in uninjured animals. (b) Representative $\gamma^2/4D$ vs. time plots of (i) rhEGF, (ii) PEG <sub>1</sub> -rhEGF, (iii) PEG <sub>2</sub> -rhEGF, and (iv) PEG <sub>3</sub> -rhEGF diffusion in (■) saturated and (○) non-saturated tissue. Plot is linear in saturated tissue but deviates from linearity in non-saturated tissue. ....	69
Figure 2.3   PEG modification decreases diffusivity of rhEGF in saturated brain tissue. (a) Microscope image showing a mouse brain coronal section with the site of stroke injury indicated by black arrow, under 10X magnification. (b) PEG modification decreases diffusivity of rhEGF in brain with stroke. The effect of mono-PEG modification of rhEGF on tissue diffusivities is studied in ipsilateral and contralateral sides of stroke, as well as that in the absence and presence of elimination are also determined. (c) Calculated tortuosity of rhEGF and PEG <sub>1</sub> -rhEGF in tissue. Tortuosity values are reported as mean $\pm$ s.e.m. (n = 25). Differences between bars with the same letter are not statistically significant while bars with different letters differ significantly. (d) Total cell number as determined by DAPI stain (scale bar = 100 µm). Arrows represent DAPI	

stained cells. (e) Total cell number is not elevated either ipsilateral or contralateral to stroke compared to uninjured controls. Cell counts are shown as mean  $\pm$  s.e.m. (n = 9). (F) EGFR gene expression is upregulated post stroke in the ipsilateral cortex. Real time RT-PCR results show that following stroke, the EGFR expression is upregulated ipsilateral to injury (P = 0.014).

.....	73
Figure 2.4   PEG modification increases the predicted penetration distance of rhEGF, assuming constant source of protein. (a) Predicted penetration distances for PEG <sub>1</sub> -rhEGF (dashed line) and rhEGF (solid line) in uninjured tissue, ipsilateral to stroke, and contralateral to stroke calculated using Eq. 6 (Methods). (b) PEG modification increases in vivo penetration distance of rhEGF following bolus injection. 0 h post injection, both rhEGF and PEG <sub>1</sub> -rhEGF show maximum concentration at the site of injection (depth of 0.5 – 1 mm below the cortical surface). 4 h post injection, rhEGF shows peak concentration at 1.5 mm ventral to cortical surface while PEG <sub>1</sub> -rhEGF concentration peaks at 2.0 mm. At 24 h post injection, rhEGF peak concentration occurs at similar depths as that at 4 h (P = 0.594), while PEG <sub>1</sub> -EGF shows significantly further penetration compared to EGF. Values are reported as mean $\pm$ s.d. (n = 4).....	76
Figure 3.1   Schematic for localized and sustained delivery of drugs to the brain. (a) Sagittal view of stroke-injured mouse brain with (b) drug delivery system. (c) Coronal view of stroke-injured mouse brain with (d) drug delivery system. (e) Drug delivery system in expanded view.	84
Figure 3.2   PEG-modified EGF has slower rates of elimination compared to native EGF in vivo. The amount of (■) EGF and (□) PEG-EGF detected after 2 h, 6 h, 1 d and 2 d was quantified. (a) Quantification of the amount of protein remaining in HAMC normalized to starting mass in uninjured and (b) stroke-injured brains. (c) The amount of protein was first quantified in the brain tissue by ELISA, and this amount was then divided by the total amount of protein released from HAMC to determine mass percents in uninjured and (d) stroke-injured brains (p < 0.05, n=3, mean $\pm$ SD reported). .....	94
Figure 3.3   PEG-modification of EGF allows for deeper tissue penetration in uninjured brains after delivery from implanted HAMC. Following implantation in uninjured mouse brains, the diffusion profiles of (■) EGF and (□) PEG-EGF at different depths is assessed. (a) At 2 hr post implantation protein concentration is similar. (b) At 6 hr post implantation, while significantly more PEG-EGF is found between 1500 and 2000 $\mu$ m, the profiles remain similar in all other tissue sections. (c) 1 day post implantation, significantly higher concentrations of PEG-EGF are found 2500 – 3000 $\mu$ m below the cortical surface. (d) 2 days post implantation, more PEG-EGF is found at all depths examined (p < 0.05, n=3, mean $\pm$ SD reported). .....	96
Figure 3.4   PEG-modification of EGF allows for deeper tissue penetration in stroke-injured brains after delivery from implanted HAMC. Following implantation in stroke-injured mouse brains, the diffusion profiles of (■) EGF and (□) PEG-EGF at different depths is assessed. (A) At 2 h and (B) 6 h post-implantation diffusion profiles appear similar. (C) 1 day post implantation, significantly more PEG-EGF is found between 1000 and 3000 $\mu$ m. (D) 2 days post implantation, higher levels of PEG-EGF are found at all depths examined (p < 0.05, n=3, mean $\pm$ SD reported). .....	97
Figure 3.5   PEG-EGF is more stable compared to native EGF in ECS proteins extracted from healthy and injured brains. (a) In the uninjured brain, (O) PEG-EGF is degraded more slowly than (●) EGF in proteins extracted from the extracellular space. The stability of (▲) EGF and (Δ) PEG-EGF in PBS remained constant and similar to initial levels over time. The stability of (■)	

EGF and (□) PEG-EGF in protease inhibitor-treated ECS extract also remained constant. (b) The rates of degradation ( $k_e$ ) and the half-lives ( $t_{1/2}$ ) are quantified. (c) PEG-EGF degrades more slowly than EGF in proteins extracted from the extracellular space of stroke-injured brains (n= 3, mean + SD reported). ..... 99

Figure 3.6 | When delivered epi-cortically from HAMC, PEG-EGF stimulates higher levels of SVZ cell proliferation compared to EGF. Uninjured and stroke-injured mice are treated with EGF and PEG-EGF delivered epi-cortically from HAMC. (a – d) Representative images are shown for Ki67 staining of stroke-injured and (e – h) stroke-injured/PEG-EGF treated groups. Arrows indicate double-labeled cells in the SVZ. (i) Quantification of Ki67 positive cells in uninjured brains, both PEG-EGF and EGF increased SVZ cell proliferation, by 1.6 fold compared to control groups ( $p < 0.05$ ), while no significant difference was observed contralateral to the implant. (j) In stroke-injured brains EGF enhanced cell proliferation in the SVZ, compared to control groups ( $p < 0.05$ ). PEG-EGF showed greater effect in increasing proliferation relative to all control groups ( $p < 0.001$ ), and EGF ( $p < 0.05$ ). There were no significant differences among the groups contralateral to the implant. n=3, mean ± SD reported. A, E Scale: 100 μm, B-D, F-H Scale: 50 μm. .... 102

Figure 3.7 | Proliferating various precursor cell populations in the SVZ. Sections from stroke-injured and stroke-injured/PEG-EGF treated brains are stained with Ki67 and either nestin, double-cortin (DCX), or GFAP. (a) stroke-injured and (b) stroke-injured/PEG-EGF treated brains co-stained with GFAP and Ki67. (c) Quantification of cells double-stained with Ki67 and nestin. (d) stroke-injured and (e) stroke-injured/PEG-EGF treated brains co-stained with nestin and Ki67. (f) Quantification of cells double-stained with Ki67 and nestin. (g) stroke-injured and (h) stroke-injured/PEG-EGF treated brains co-stained with DCX and Ki67. (i) Quantification of cells double-stained with Ki67 and DCX. Significant differences were found between stroke-injured and stroke-injured/PEG-EGF treated groups ( $p < 0.005$ , n=3, mean ± SD reported). Images were taken at 20x magnification. Insets show arrow-indicated regions at 60x magnification. Scale: 100 μm. .... 104

Figure 4.1 | Surgical paradigm for epicortical delivery of EPO. Animals received endothelin-1 induced stroke injury on day 0. HAMC or EPO incorporated in HAMC was injected epicortically at either 4 or 11 days post stroke, as indicated by arrows. The drug delivery system was allowed to remain in-place for 7 days prior to sacrifice. Animals were sacrificed on either day 11 or day 18 post stroke. .... 114

Figure 4.2 | EPO<sub>r</sub> expression is similar between uninjured and stroke-injured brain tissues. (a) Diagrammatic representation of the stroke-injured brain and the regions of interest for EPO<sub>r</sub> quantification. Rectangles indicate regions examined for EPO<sub>r</sub> expression. (b) Total numbers of EPO<sub>r</sub><sup>+</sup> cells are similar in all three conditions and both ipsilateral and contralateral to injury (mean ± standard deviation, n = 3 animals, 16 tissue slices were analyzed per animal). ..... 118

Figure 4.3 | Penetration of EPO in stroke-injured brains. (a – b) Paradigm for surgical induction of stroke and injection of drug delivery device. (c) Mass of EPO released from HAMC at 4 h, 1 d, and 2 d after injection indicate similar rates of release when injected onto (■) uninjured tissue, (□) stroke-injured tissue 4 days post stroke, and (▨) stroke-injured tissue 11 days post stroke. (d) EPO detected in brain tissue as percentage released from HAMC at 4 h, 1 d, and 2 d after injection indicate similar rates of EPO elimination due to stroke alone, stroke with HAMC, and stroke with EPO in HAMC. Penetration profiles of EPO in uninjured and stroke-injured brain

tissues were examined by ELISA. EPO penetration in brain tissue examined at (e) 4 h, (f) 1 d, and (g) 2 d after injection. Penetration was similar between the three types of brain tissue: (●) uninjured, (○) 4 days after stroke injury, and (□) 11 days after stroke injury (mean ±standard deviation, n = 3 animals, 16 tissue slices were analyzed per animal). ..... 119

Figure 4.4 | EPO delivered epicortically from HAMC decreases the stroke cavity size at 4 and 11 days after stroke. (a) Image of a brain section with stroke cavity (indicated by arrow) shown at 1.25x (scale: 2 mm). (b) Quantification of the cavity sizes. Stroke-injured animals received treatments at either 4 or 11 d post-stroke. Treatment with EPO in HAMC significantly reduced cavity size at 4 d, while both HAMC and EPO in HAMC significantly reduced cavity size at 11d (mean ±standard deviation, n = 3 animals, 16 tissue slices were analyzed per animal). ..... 121

Figure 4.5 | Epi-cortical delivery of EPO from HAMC attenuates the reactive astrocyte response at 4 and 11 days after stroke injury. (a) Diagram of the stroke-injured brain with drug delivery device. Rectangle indicates the region of interest. Representative images of GFAP<sup>+</sup> reactive astrocytes in the ipsilateral cortex ventral-lateral to the lesion site are shown for animals that received (b) stroke alone and (c) stroke followed by HAMC injection at 4 d, as well as (d) stroke alone and (e) stroke with HAMC injection at 11 d. Scale: 100 μm. (f) Quantitative comparison of average number of GFAP<sup>+</sup> cells are shown for the ipsilateral cortex per field of view. Treatment with both HAMC and EPO in HAMC significantly reduced the total number of GFAP<sup>+</sup> cells at both 4 and 11 days while the total number of DAPI<sup>+</sup> cells remain the same (mean ±standard deviation, n = 3 animals, 16 tissue slices were analyzed per animal). ..... 122

Figure 4.6 | Epi-cortical delivery of EPO from HAMC attenuates the activated microglia response at 4 days after stroke injury. (a) Diagram of the stroke-injured brain with drug delivery device. Rectangle indicates the region of interest. Representative images of CD68<sup>+</sup> cells in the ipsilateral cortex are shown for animals that received (b) stroke alone and (c) stroke followed by HAMC injection at 4d, as well as (d) stroke alone and (e) stroke with HAMC at 11d. Scale: 100 μm. (f) Quantitative comparison of average number of CD68<sup>+</sup> cells are shown for the ipsilateral cortex per field of view. Treatment with both HAMC and HAMC with EPO significantly reduced the level of CD68<sup>+</sup> signal at both 4 and 11 days while the total number of DAPI<sup>+</sup> cells remain the same (mean ±standard deviation, n = 3 animals, 16 tissue slices were analyzed per animal). 123

Figure 4.7 | Epi-cortical delivery EPO in HAMC increases the number of Ki-67<sup>+</sup> proliferating cells and DCX<sup>+</sup> migratory neuroblasts in the SVZ at 4 and 11 days post injury. Representative images are shown for Ki-67<sup>+</sup> cells and DCX<sup>+</sup> Ki-67<sup>+</sup> double-labeled cells in the SVZ ipsilateral to the stroke injury following (a – e) stroke injury and (f – j) EPO injected with HAMC 11 days after stroke. The lateral ventricle (LV) and the striatum are labelled. Scale: (a, f) 500 μm at 10x, (b – e, g – j) 100 μm at 20x. The number of Ki-67<sup>+</sup> cells in the ipsilateral SVZ at (K) 4 d and (L) 11 d is significantly increased by HAMC-mediated EPO treatment while the number of Ki-67<sup>+</sup> cells in the contralateral SVZ remain similar between treatments. DCX<sup>+</sup> Ki-67<sup>+</sup> double positive cells in the ipsilateral SVZ at (M) 4 d and (N) 11 d post stroke also increased following HAMC-mediated EPO treatment (mean ±standard deviation, n = 3 animals, 16 tissue slices were analyzed per animal). ..... 124

Figure 4.8 | EPO delivered from HAMC enhances the number of NeuN<sup>+</sup> mature neurons in the injured cortex at 4 and 11 days post injury. Representative images are shown for NeuN<sup>+</sup> cells in the cortex of stroke-injured, sham treated animals (a) ipsilateral and (b) contralateral to the injury, as well as stroke-injured, EPO treated animals (c) ipsilateral and (d) contralateral to the

injury at 4 days post stroke. Scale: 100  $\mu$ m. (e) Diagram of the brain with rectangles showing the regions analysed. Quantification of NeuN<sup>+</sup> cells are shown for (f) 4 d and (g) 11 d after stroke (mean  $\pm$  standard deviation, n = 3 animals, 16 tissue slices were analyzed per animal). ..... 127

Figure 4.9 | Treatment with EPO delivery at both 4 d and 11 d post stroke led to decreased number of TUNEL<sup>+</sup> cells in the ipsilateral SVZ and cortex. When stroke-injured animals were treated with EPO, the number of TUNEL<sup>+</sup> apoptotic cells decreased both in the (a, b) ipsilateral SVZ and the (c, d) ipsilateral cortex at 4 d or 11 d post stroke. HAMC alone had no effect relative to stroke alone. .... 129

Figure 5.1| Sequential delivery of EGF-PEG followed by EPO can be achieved using composite drug delivery system (DDS). (a) Schematic of the drug delivery system and in vivo EGF-PEG and EPO release from the composite on a microscopic level. Time course of the desired release profile is a sequential release of EGF-PEG for one week, followed by EPO. (b) In vitro release profiles of (□)EGF-PEG and (■) EPO engineered to yield the desired release profiles, with the majority of EGF-PEG released within the first week, followed by EPO released linearly for two weeks. (c) In vivo the release profiles of EGF-PEG and EPO from composite shows that EGF-PEG is released first followed by EPO release. (d) EGF-PEG can be observed in the stroke-injured brain tissue within days of injection, with the peak concentration detected at 1 week. EPO is not detected in the tissue in the first week, but accumulation is observed after the initial delay. (e) Endogenous stem cells reside in the SVZ. Accumulation of protein in the tissue corresponding to this region of the brain was examined and found to occur over the desired time course. All data are based on ELISA analysis (Mean  $\pm$  standard deviation, n = 3). ..... 147

Figure 5.2 | EGF-PEG and EPO delivered from composite increase proliferation of NSPCs and decrease cell death in the SVZ 18 days after stroke. (a – d) Representative images and (e) quantification of Ki67<sup>+</sup> proliferating cells in the ipsilateral SVZ at 18 d. Compared to vehicle controls, growth factor treatment using either pump or composite significantly increase the number of Ki67<sup>+</sup> proliferating cells in the ipsilateral SVZ. Stroke + G/F composite delivery animals showed significantly more Ki67<sup>+</sup> cells than Stroke + G/F pump delivery animals (p = 0.001), and only G/F composite delivery showed significantly more Ki67<sup>+</sup> cells than stroke alone (p = 0.008). When aCSF is infused through osmotic minipumps to the ventricles, the level of proliferation decreases significantly compared to stroke alone controls (p = 0.004). (f – i) Representative image and (j) quantification of Mash-1<sup>+</sup> neuroprecursors in the ipsilateral SVZ on day 18. Stroke + G/F pump infusion increases the number of Mash-1<sup>+</sup> neural precursor cells in the SVZ compared to Stroke + aCSF pump infusion controls (p = 0.045); and Stroke + G/F composite increases the number of Mash-1<sup>+</sup> cells compared to Stroke + vehicle composite (p = 0.033). Stroke + aCSF pump intraventricular infusion resulted in a significant reduction in Mash-1<sup>+</sup> cells compared to Stroke + vehicle composite (p = 0.001) and stroke alone (p = 0.002). No significant differences in Mash-1<sup>+</sup> cells were found between stroke alone and Stroke + vehicle composite or between stroke alone and Stroke + G/F composite. (k – n) Representative image and (o) quantification of TUNEL<sup>+</sup> apoptotic cells in the ipsilateral SVZ on day 18. At 18 d after stroke, the number of apoptotic cells in the SVZ was characterized by TUNEL<sup>+</sup> cell staining following stroke vs. the other interventions. Stroke + G/F composite delivery significantly reduced the number of apoptotic TUNEL<sup>+</sup> cells relative to both Stroke + vehicle composite delivery (p = 0.043) and Stroke + GF pump infusion (p = 0.027). (Mean  $\pm$  standard deviation, n

= 3. Results are normalized to Stroke animals. Scale: a, f, k: 100  $\mu\text{m}$ ; b – d, g – i, l – n: 50  $\mu\text{m}$ .) ..... 149

Figure 5.3| Sequential composite-mediated delivery EGF-PEG and EPO attenuates the injury response and cell death, and increases NeuN<sup>+</sup> mature neurons in the penumbra 18 d after stroke. At 18 d post stroke, (a – d) the level of TUNEL<sup>+</sup> cells decreases significantly in the injured cortex following growth factor treatment compared to stroke + vehicle controls. Importantly, stroke + G/F composite leads to a significant decrease in TUNEL<sup>+</sup> cells compared to stroke alone ( $p = 0.015$ ) and stroke + G/F pump ( $p = 0.038$ ). (e - h) Both stroke + G/F composite and stroke + G/F pump animals have significantly more NeuN<sup>+</sup> cells in the peri-infarct region compared to vehicle controls ( $p = 0.001$ ). The level of NeuN<sup>+</sup> neurons is significantly higher after stroke + G/F composite vs. stroke + G/F pump ( $p = 0.044$ ), yet still significantly less than uninjured tissue controls. (i) All animals showed a significant reduction in cavity size relative to stroke alone except for the stroke + aCSF pump group. (All results normalized to Stroke animals, mean + standard deviation,  $n = 5$ ). Scale: 100  $\mu\text{m}$ . ..... 151

Figure 5.4 | Epicortical delivery of the composite vehicle attenuates inflammatory response in the peri-infarct region 18 d after stroke. Given that HAMC demonstrates anti-inflammatory effects in the CNS, we examined the peri-infarct cortical tissue for inflammation. Only those animals that were treated with HAMC – either HAMC alone or vehicle composite comprised of HAMC and polymeric particles – showed significantly reduced (a – d) GFAP<sup>+</sup> reactive astrocytes and (e – h) CD68<sup>+</sup> macrophages/microglia around the lesion. For stroke + aCSF bolus, stroke-injured animals had aCSF injected in an identical manner to HAMC, thereby providing a control for epicortical delivery of HAMC. (All results normalized to Stroke animals, mean + standard deviation,  $n = 3$ , \* $p < 0.05$ ; \*\* $p < 0.01$ ; \*\*\* $p < 0.001$ ). Scale: 100  $\mu\text{m}$ . ..... 153

Figure 5.5 | Epicortical delivery of composite vehicle attenuates peri-infarct inflammatory response at 32 d post stroke, and sequential composite-mediated delivery of EGF-PEG and EPO attenuates the injury response and cell death, and increases NeuN<sup>+</sup> mature neurons at the same time point. Injection of vehicle composite post stroke reduces the number of (a) GFAP<sup>+</sup> reactive astrocytes and (b) CD68<sup>+</sup> activated microglia at 32 d compared to stroke alone and stroke with osmotic minipump treatments. This is similar to the effects seen at 18 d post stroke. (c) Growth factor treatment significantly reduces the stroke cavity size compared to vehicle controls. Quantification of (d) TUNEL<sup>+</sup> and (e) NeuN<sup>+</sup> stains at 32 d indicates G/F composite attenuates apoptosis and increases the number of mature neurons in the peri-infarct region compared to vehicle control. No significant difference was observed for NeuN<sup>+</sup> cells at 32 d between stroke + G/F composite and uninjured tissue, suggesting tissue repair to pre-injury levels (All results normalized to Stroke animals, mean + standard deviation,  $n = 5$ , \* $p < 0.05$ ; \*\* $p < 0.01$ ; \*\*\* $p < 0.001$ ). ..... 154

## List of Tables

Table 2.1   Elimination rate constants in uninjured and stroke brains. Values of $k_e$ were obtained by numerically solving Eq. 5 using the parameters listed in Table 4. Values are reported as mean $\pm$ s.d. (n = 25).....	70
Table 2.2   Predicted penetration distance from a point source (a) and a constant source (b) by rhEGF and PEG <sub>1</sub> -rhEGF in uninjured and stroke brains. Distances travelled are presented in units of millimetres. Diffusion is assumed to stop when concentration is less than 3 nM, which is the minimum EGF concentration required to stimulate NPCs in vitro.....	74

## 1. Introduction

### 1.1. Rationale

Similar to most central nervous system (CNS) disorders and injuries, stroke is a debilitating disorder for which no effective treatment exists today <sup>1</sup>. It is currently the third cause of death in the world, and a leading cause of disability <sup>2</sup>. There are two types of strokes: ischemic stroke, which results from blockages in cerebroarteries; and hemorrhagic stroke, which results from ruptures of the arteries <sup>3</sup>. The only FDA approved drug for stroke treatment is tissue plasminogen activator (tPA) <sup>4,5</sup>, which reduces the extent of stroke injury but does not allow for recovery <sup>4</sup>. tPA is effective if administered within 6 hours of stroke onset <sup>6</sup>, but as it dissolves thromboembolytic clots, tPA can only be used to treat ischemic stroke <sup>7</sup>. A number of drug-based treatments that show preclinical efficacy in animal models have also failed to elicit any benefit when translated into human subjects <sup>8-11</sup>.

Over the last decade, research efforts have been focused on using tissue engineering approaches that demonstrate the potential of regenerating brain tissue lost during stroke <sup>12-14</sup>. Neuroregeneration is a technique that involves administration of exogenous growth factors to stimulate endogenous neural stem/progenitor cells (NSPCs) in the subventricular zone (SVZ) of the lateral ventricles in the adult brain <sup>15-21</sup>. Specifically, one treatment that sequentially delivers epidermal growth factor (EGF) followed by erythropoietin (EPO) into the lateral ventricles for seven days each elicited tissue regeneration and functional recovery in rodent stroke models <sup>22</sup>.

A number of issues, however, prevent the clinical translation of these strategies <sup>23</sup>. One issue is the current lack of effective yet minimally invasive drug delivery strategies (DDS) <sup>24</sup>. Currently available DDS suffer a number of limitations when used for targeting the brain. Therapeutic

agents delivered systemically have limited ability to traverse the blood brain barrier (BBB), consequently high dosages must be administered to allow therapeutically relevant levels to accumulate in the brain. This may result in systemic toxicity and other undesired side effects. Local strategies such as intracerebral (IC) or intracerebroventricular (ICV) delivery to the brain allow for a large array of drugs to be delivered to the brain parenchyma at a constant rate. The surgical procedures involved, however, are invasive and associated with risks of infection<sup>25,26</sup>. Secondary surgeries may also be required for implant removal upon termination of the treatments.

The optimal drug delivery system for the brain should build upon the controlled profile and therapeutic efficacy of the local delivery systems, but minimize the invasiveness intrinsic in such systems. The following criteria should be met when engineering a DDS for the brain: 1) achieve controlled delivery profiles that match the treatment paradigm with optimum efficacy; 2) minimally invasive; 3) biocompatible; 4) biodegradable such that no surgical removal is required. The goal of this thesis is to design a DDS that encompasses all the above-mentioned properties, such that it can be used to improve the efficacy of growth factors used to treat stroke as well as other disorders of the CNS.

## **1.2. Hypothesis and Objectives**

The hypothesis governing this body of work is:

*A drug delivery system consisting of a hyaluronan-methylcellulose (HAMC) hydrogel and polymeric particles will enable epicortical delivery of EGF followed by EPO to the brain to elicit tissue regeneration in a mouse model of stroke.*

To test this hypothesis, the following objectives were set:

1. Evaluate EGF diffusion in the brain.
  - a) Compare EGF penetration in the uninjured and the stroke-injured brain.
  - b) Investigate the effect of PEG-modification on EGF penetration distance.
2. Assess the feasibility of epicortical HAMC-mediated PEG-EGF delivery for stroke treatment.
  - a) Examine the ability of PEG-EGF to penetrate from the cortex to the SVZ in the stroke-injured mouse brain following delivery from HAMC.
  - b) Examine the biological response of the stroke-injured brain to PEG-EGF delivered from HAMC.
3. Assess the feasibility of epicortical HAMC-mediated EPO delivery for stroke treatment.
  - c) Examine the ability of EPO to penetrate from the cortex to the SVZ in the stroke-injured mouse brain following delivery from HAMC.
  - d) Examine the biological response of the stroke-injured brain to EPO delivered from HAMC.
4. Design and optimize a composite DDS for epicortical delivery of PEG-EGF followed by EPO.
  - a) Engineer a composite DDS to achieve sequential release of PEG-EGF followed by EPO.
  - b) Investigate cellular response in the SVZ and peri-infarct region to PEG-EGF and EPO delivered epicortically from the composite DDS.
  - c) Investigate the effect of the composite on the brain's injury response after stroke.
  - d) Investigate the tissue benefit achieved by PEG-EGF and EPO delivered epicortically using the composite DDS.

## **1.3. Stroke**

### **1.3.1. Statistics**

Stroke is a devastating condition for which no effective treatment is currently available. It is a leading cause of disability and the 3<sup>rd</sup> leading cause of death worldwide, resulting in approximately 15 million injuries and 5 million deaths each year <sup>27</sup>. Stroke primarily affects the population over 50 <sup>28</sup>, although there are trends indicating that younger populations are increasingly susceptible to it today <sup>29</sup>. Stroke patients who survive the initial injury often still lose some or all abilities of self care <sup>30,31</sup>, and this is a significant burden on the health care system and society <sup>32</sup>.

### **1.3.2. Pathology of stroke**

The two broadest categories of stroke are ischemic strokes and hemorrhagic strokes <sup>33</sup>. Hemorrhagic stroke, resulting from cerebral hemorrhage following ruptured blood vessels, constitutes 20% of all stroke injuries <sup>34</sup> while ischemic stroke, resulting from blood vessel occlusion, constitutes the remaining 80% <sup>35</sup>. As hemorrhagic stroke typically causes immediate death <sup>36</sup> and the majority of stroke cases are ischemic stroke, the focus of this thesis will be on ischemic stroke.

There are two stages in ischemic stroke <sup>37</sup>. The site of the initial ischemic insult is referred to as the core region. Here, thromboembolic blockage of arteries leads to near-immediate necrotic cell death, which is referred to as the primary injury. Following the primary injury, the tissue that surrounds the core (penumbra) experiences a shortage of blood, which leads to reduction in oxygen and glucose concentrations in the penumbra. The subsequent ATP depletion leads to a

buildup of toxic substances such as glutamate and  $\text{Ca}^{2+}$ , and eventually leads to significant apoptosis and necrosis in the penumbra. This series of events following the primary injury are collectively referred to as the secondary injury <sup>38</sup>.

There are two main injury mechanisms involved in secondary stroke: excitotoxicity <sup>39</sup> and oxidative stress <sup>40</sup>. Excitotoxicity results from the ATP reduction in the penumbra following primary injury <sup>41</sup>. Without adequate energy supply, cells in the penumbra cannot maintain their normal  $\text{Ca}^{2+}$ ,  $\text{K}^+$ ,  $\text{Na}^+$  and  $\text{Li}^+$  ionic gradient, and intracellular glutamate is released <sup>42</sup>. Under normal circumstances, the released glutamate would be recycled by the cells during their metabolic process. However, due to the energy shortage, this recycle of glutamate does not occur. The intracellular glutamate released by pre-synaptic neurons binds to post-synaptic receptors, promoting  $\text{Ca}^{2+}$  entry <sup>43</sup>. High intracellular  $\text{Ca}^{2+}$  levels trigger a series of intracellular signaling events, leading to disruption of cytoskeletal proteins and important cellular enzymes, and generation of radicals such as peroxynitrite.  $\text{Ca}^{2+}$  also triggers apoptotic pathways by activating the  $\text{BCL}_{\text{XL}}$  class of apoptotic transcription factors <sup>44</sup>.

The other major mechanism involved in secondary injury in stroke is oxidative stress <sup>40</sup>. The main source of oxidative stress is the reactive oxygen species (ROS) generated during reperfusion (re-establishment of blood flow) <sup>45</sup>. Reperfusion is a process whereby blood flow is re-established after ischemia, which typically occurs minutes after the initial onset of stroke. These ROS lead to mitochondrial failure and compromises cell survival <sup>45</sup>. Both necrosis and apoptosis occur as a consequence of both the ROS attack on neurons and the excitotoxic pathway, and lead to large scale cell death in the penumbra.

### 1.3.3. Currently available clinical treatments and their limitations

Little may be done to prevent the primary injury in stroke as it results from a combination of genetic factors and lifestyle issues <sup>46-50</sup>, so the majority of stroke treatments being developed today aim at reducing the severity of secondary injury <sup>1</sup>, protecting neurons in the penumbra against excitotoxic and oxidative stress (neuroprotection) <sup>51</sup>, and regeneration of new functional neural cell types (neuroregeneration) <sup>52</sup>.

Acute stroke treatments available today need to be administered within hours of the onset of stroke in order to be effective <sup>53</sup>. Upon hospitalization, patients are typically first subjected to brain scans such as computed tomography (CT) <sup>54</sup> or magnetic resonance imaging (MRI) <sup>55</sup>. This allows a quick diagnosis to be performed, such that the nature and severity of stroke may be assessed. Most patients are then placed under hypothermia, a treatment that reduces the extent of injury <sup>56,57</sup>. Subsequently, ischemic stroke patients are typically treated with intravenous injection of thrombolytic agents <sup>58</sup>.

Thrombolysis is one of the treatments most commonly administered to acute ischemic stroke patients (within hours of onset) <sup>53</sup>. It is also the most effective of all the clinically available treatments, with better efficacy than treatments such as stroke unit intensive care and extended hypothermia. Thrombolytic agents are used in reperfusion therapy to dissolve the blood clots (thromboemboli) that occlude cerebral blood vessels <sup>59</sup>. Reperfusion therapy re-establishes the blood flow to the penumbra, thus salvaging the tissue <sup>60</sup>. A large number of thrombolytic agents, typically fibrin-specific agents, have been developed, although the only agent approved by the FDA for human use is tissue plasminogen activator (tPA) <sup>61</sup>. Despite its effectiveness as a clot-buster, tPA has a very limited time window for administration: if used more than 6 hours after

the onset of stroke, tPA does not elicit any beneficial effects. Furthermore, tPA only leads to a reduction in the extent of injury, and not tissue regeneration <sup>61</sup>.

Today, recovery after stroke in humans is typically achieved through long-term rehabilitation and physiotherapy <sup>62</sup>. While there has been some successful cases, most patients do not regain full motor and cognitive function, and the time required to achieve significant recovery can range from a few months to several decades <sup>63</sup>, depending on the severity of stroke <sup>62,64</sup>.

#### **1.4. Using regenerative medicine-based approaches for treating stroke**

Given the current lack in clinically proven treatments that can stimulate effective repair after stroke, extensive research efforts have been devoted to the development of new therapies. To date, regenerative medicine-based strategies such as exogenous stem cell transplants (Section 1.4.2) <sup>65</sup> and endogenous stem cell stimulation (Section 1.4.3) <sup>66</sup> have shown significant promise in many pre-clinical models and some clinical trials. Neuroprotection aims at preserving the host tissue after stroke, while neuroregeneration attempts to regenerate brain tissue to restore function lost during stroke. Neither approach, however, has been approved for clinical use <sup>67</sup>. More than 700 drugs have been tested preclinically and clinically since early 2000, but none has been approved, either due to lack of efficacy or due to safety concerns <sup>68</sup>. A number of factors may contribute to this lack of success. First, the causes of stroke are numerous and different for each individual. This makes it difficult to interpret and compare the outcome of medical interventions <sup>46</sup>. Second, drugs that are suitable for one condition may have no benefit or even have adverse effects in another situation, and the results from various pre-clinical studies are often contradictory <sup>69</sup>. Third, even when a suitable model of stroke has been developed and a potential drug or therapeutic agent been identified in animal models, clinical translation is extremely challenging <sup>70</sup>. To gain a more complete understanding of human stroke, it is

important to first understand the biology of stroke in animal models, as a full understanding will likely reconcile the results obtained from different animal models. The next section will provide a discussion on animal models commonly used in developing treatments for stroke.

#### **1.4.1. Animal models of stroke**

Animal models have served as indispensable tools in studying human stroke <sup>71</sup>. The number of animal models has also expanded greatly over the recent decades, as our understanding on the causes of stroke increased.

Historically, larger animals such as dogs, pigs, and non-human primates have been predominantly used as models for studying the causes and risk factors in stroke <sup>72-74</sup>. Currently, however, most stroke-related animal studies are carried out in rats and mice <sup>75</sup>. Their relatively small sizes and lower cost, in addition to the similarity between the structure of their brains and that of human brains, make them suitable candidates for understanding the pathology of stroke and developing treatments. Additionally, the high degree of genetic homogeneity within each strain allow for highly controlled experimental conditions <sup>76</sup>.

The criteria used to assess the usefulness, practicality, and reliability of an animal model typically include the following <sup>77</sup>: 1) the pathophysiology of the animal selected should be relevant to humans; 2) the size of stroke cavity developed after injury should be reproducible between experiments; 3) the technique used to induce stroke should be relatively simple and minimally invasive; 4) variables in animal physiology should be easy to monitor and can be maintained within normal ranges; 5) brain samples should be easy to harvest and readily

available, such that histological analyses may be carried out; and 6) the cost should be reasonable.

Animal models of stroke can be divided into the following four major categories. Each one has its advantages and limitations, and each is used for addressing different aspects of stroke research.

#### **1.4.1.1. Middle cerebral artery occlusion (MCAO) <sup>78</sup>**

The MCAO model is most frequently used in stroke research today due to its relevance to human clinical cases. Experimentally, this condition is induced by inserting a transluminal suture into the internal carotid artery of the animal host. The suture is kept in place, either transiently for 30, 60, or 90 min, or permanently. The size of the stroke lesion is dependent on the length of blockage as well as the shape, size, insertion length, and coating material of the suture.

Advantages of the MCAO model include that the size of the penumbra with respect to the brain size is relevant to human strokes, and the extent of injury can be controlled through the time-to-reperfusion. Some limitations of this model include that the surgical technique involved is relatively complex and invasive, and although the model is theoretically reproducible, outcomes often vary in practice. Additionally, the animals' mastication functions are sometimes affected, which complicates data analysis and interpretation. These experiments are also difficult to perform on the mice, and as a result MCAO models are predominantly used in rat models of stroke.

#### **1.4.1.2. Thromboembolic stroke models <sup>79</sup>**

Thromboembolic strokes are typically induced by injecting either an autologous clot fragment or synthetic blocking agent (e.g. polymer microspheres) into an extracranial artery. The size of the blocking agent and the affected artery dictates the nature and severity of the resulting injury.

Thromboembolic models of strokes are popular due to its simple nature and resemblance to the pathophysiology of human ischemic stroke. Most human strokes are caused by thromboembolism, where an artery is blocked either by the buildup of clot(s) in the affected artery (thrombosis) or fragments broken off from a remote thrombus (embolus). This model allows for the evaluation of a large number of thrombolytic agents, and for the evaluation of the resulting ischemic lesion after thrombolysis. However, no standardized animal model exists, and there is a high degree of variability in this class of models. The polydispersity in the size of clot fragments, in combination with the uncontrolled location of blockage, renders the model highly variable, and the results obtained from different studies may be hard to compare.

#### **1.4.1.3. Photothrombosis models** <sup>80</sup>

Photothrombosis is performed by injecting a photosensitive dye systemically and irradiating a pre-determined cortical region using a light beam with a specific wavelength. This generates oxygen radicals and induces focal damage in the endothelial layers, and induces platelet activation and aggregation in both pial and intraparenchymal vessels. This model allows a highly defined cavity region to form with minimal surgical requirements. However, as vasogenic edema and breakdown of the BBB in the lesion site occur within minutes of initial induction, the formation of the penumbra is difficult to predict and also has low reproducibility.

#### **1.4.1.4. Pial vessel disruption (PVD) models**

PVD is a technique where blood vessels on the cortical surface of the brain are disrupted mechanically to create a stroke lesion <sup>22</sup>. This model has been used to study stroke in large rodents, but has seen limited use in mice, larger animals and non-human primate models <sup>81</sup>. The major advantages of the PVD model are its simplicity and reproducibility <sup>82</sup>. However, this model has a number of drawbacks in studying ischemic stroke, as hemorrhage and edema sometimes forms in animals following PVD, which increases the level of complexity in data analysis.

#### **1.4.1.5. Endothelin-1 models**

Endothelin-1 (ET-1) is a small peptide that acts as a vasoconstrictor. It can be applied, either directly into the MCA, close to the MCA <sup>83</sup>, or into the cortex <sup>84</sup>. This model typically produces lesion patterns that are similar to MCAO but smaller in size. The main advantages of the ET-1 models include simple surgeries, relatively low invasiveness compared to PVD and MCAO, and the ability to induce ischemia in any target region of the brain. Additionally, the vasoconstrictive action of ET-1 is dosage dependent and therefore variable stroke lesion sizes can be achieved. Furthermore, ET-1 induces transient focal ischemia, and reperfusion occur naturally. In this thesis, ET-1 is used to induce focal ischemic stroke in mice for its minimally invasive nature, ease of application, and the reproducibility of stroke lesion characteristics.

#### **1.4.2. Neuroprotection as a treatment strategy for stroke**

One class of treatment currently under development, referred to as neuroprotection, aims at improving neuronal survival <sup>85</sup>. A number of neuroprotective approaches have been developed over the last several decades. One of the most common neuroprotective approaches is the use of glutamate antagonists. Glutamate binds to the extracellular receptors on neurons, including N-methyl-D-aspartic acid (NMDA) receptors and  $\alpha$ -amino-3-hydroxyl-5-methyl-4-isoxazole-propionate (AMPA) receptors, and initiates  $\text{Ca}^{2+}$  influx and excitotoxic cell death. NMDA and AMPA receptor antagonists can bind competitively to these receptors to prevent glutamate binding <sup>86</sup>. This prevents the downstream activation of apoptotic enzymes that impede neuronal survival.

Both pre-clinical and clinical results, however, show that many NMDA receptor antagonists fail to elicit functional recovery in animal models of stroke <sup>86</sup>. Consequently some research groups are developing antioxidant-based neuroprotective treatments <sup>86</sup>. Reperfusion is necessary for the long-term survival of cells in the brain post stroke, but it also leads to accumulation of ROS in the penumbra. The purpose of antioxidants is to reduce the reperfusion-induced oxidative stress experienced by neurons. The therapeutic agent edaravone has shown limited pre-clinical success by inhibiting lipid peroxidation and vascular endothelial cell damage, and reducing fluid accumulation in the brain (edema) <sup>86</sup>.

Neurotrophic factors have also been used in the attempt to achieve neuroprotection after stroke. A number of factors, including basic fibroblast growth factor (bFGF) and erythropoietin (EPO), have been used in this class of treatment, and they act by activating survival genes and suppressing suicidal genes in neurons. Other less commonly used treatments include free radical scavengers,  $\text{Ca}^{2+}/\text{Na}^+/\text{K}^+$  channel blockers, anti-inflammatory agents that inhibit neutrophil intrusions,  $\gamma$ -aminobutyric acid (GABA) receptor antagonists, and caspase inhibitors

<sup>87</sup>.

To date, most neuroprotective therapies that have shown promise pre-clinically have been unsuccessful in achieving neuroprotection clinically <sup>22,86,88</sup>. Aside from limited clinical success, one other major drawback in neuroprotective treatments is that these approaches only help to increase the survival of existing neurons <sup>89</sup>. Since there is large scale neuronal death resulting from the trauma of stroke, cognitive functions are inevitably lost <sup>90</sup>. Thus to regain these functions, it is important to promote post-stroke regeneration of brain tissues.

### **1.4.3. Neuroregeneration as an alternative stroke treatment**

An emerging trend in treating neurological disorders is the use of neuroregenerative techniques <sup>86,90</sup>. Compared to anti-thrombolytic and neuroprotective strategies, tissue regeneration offers the possibility of regaining lost functions to greater extents. Given the promise that neuroregeneration holds for the future of stroke treatments, research efforts have been heavily invested into the development of potential therapies <sup>91</sup>.

There are two main approaches to regenerating brain tissue in the adult mammal. The first is mediated by transplanting exogenous stem cells into the injured brain. The most significant challenge in this approach is that transplantation success rate is low due to low post-implantation survival and lack of integration with the host tissue (typically less than 1% of the transplanted cells survive) <sup>92</sup>. The second method for achieving neuroregeneration takes advantage of the endogenous neural stem and progenitor cells (NSPCs) in the brain <sup>52</sup>. Both of these techniques are discussed in detail in the next two sections.

#### **1.4.3.1. Transplantation of exogenous cells**

In the penumbra, neurons<sup>93</sup> and oligodendrocytes<sup>94</sup> are the two types of cell most susceptible to ischemic injury. Even though there is some evidence of spontaneous neuroregeneration, the extent to which this occurs is inadequate for repairing stroke-induced tissue damage<sup>95</sup>. One method for eliciting brain repair involves transplanting exogenous cells into the injured penumbra<sup>96</sup>. Commonly used cell types in replacement therapies include neural stem/progenitor cells, embryonic stem cells drawn from allogeneic sources, and mesenchymal stem cells (MSCs). Most recently, induced pluripotent stem cells (iPSC) have also been proposed and tested as candidates for cell replacement therapies as they allow for autologous transplant<sup>97</sup>.

Exogenous cell transplantation mediates brain repair through two mechanisms. One route relies on the integration of transplanted cells with host tissue: it is hoped that the newly transplanted cells will integrate with host tissue as functional neurons and supporting cells<sup>98</sup>. Either immature stem/progenitor cells or mature cells may be transplanted. The main drawback of transplanting progenitors is that these cells are potentially tumorigenic. The main limitation in using mature cells for transplantation is their lower survival rates post transplantation. The second mechanism of action relies not on direct cell-cell interaction between the host and the transplant, but rather on chemokines released by the transplanted cells. These chemokines may act either as neuroprotection or neuroregeneration agents. Both MSCs and NSPCs release cytokines such as leukemia inhibitory factor (LIF) and ciliary neurotrophic factor (CNTF) that are beneficial in promoting host tissue regeneration and repair<sup>99,100</sup>.

#### **1.4.3.2. Stimulation of endogenous neural stem/progenitor cells (NSPCs)**

The second approach used to promote tissue repair after stroke relies on endogenous neural stem/progenitor cells (NSPCs) in the brain<sup>101</sup>. In the adult mammalian brain, there are two stem cell centers that constitutively generate NSPCs: the subgranular zone (SGZ) of the dentate gyrus (DG) and the subventricular zone (SVZ) of the lateral ventricles<sup>101,102</sup>. The progenitor cells in the SGZ give rise to granular neurons that migrate to the nearby granule cell layer, and integrate into the DG<sup>103</sup>.

The NSPCs in the SVZ are considered true stem cells that exhibit the cardinal properties of self-renewal and multipotentiality. In culture, these cells respond to exogenous cues such as epidermal growth factor (EGF) and fibroblast growth factor (FGF), and can be expanded as free-floating neurospheres that originate from a single neural stem cell<sup>104</sup>.

In the adult brain, they proliferate at low levels constitutively, and the newly generated NSPCs migrate towards the olfactory bulb and differentiate into mature cell types<sup>90,102</sup>. Following stroke, there is an increase in proliferation of neural stem cells in the SVZ<sup>105</sup> both ipsilateral and contralateral to the injury. The newly generated NSPCs follow endogenous chemotactic cues and migrate towards the sites of injury<sup>102</sup>. Studies have shown that there is a ten-fold increase in progenitor cells at the site of injury 3 – 4 days following global ischemia in mice and rats<sup>106</sup>, and similar effects are observed following focal cerebral ischemia<sup>90,106</sup>.

One challenge in stimulating endogenous NSPCs is that the extent of precursor cell proliferation and migration after injury is limited<sup>22</sup>. It has also been shown previously that the premature neurons that leave the SVZ and migrate toward the site of stroke have limited ability to survive and differentiate into mature neurons once they are in the injured cortex<sup>22</sup>. Therefore exogenous interventions are required to help promote this process in order to improve recovery in stroke patients. A variety of growth factors has been identified that enhance NSPC

proliferation in animal models of stroke. The following section discusses a number of these candidates in detail.

#### **1.4.4. Growth factor-mediated stimulation of endogenous NSPCs and brain tissue regeneration**

##### **1.4.4.1. Growth factors with potential benefits in brain regeneration**

A number of growth factors have shown promise in stimulating tissue repair in the brain <sup>107</sup>. These growth factors act to directly promote NSPC proliferation, preferentially guide NSPC differentiation into mature neurons, enhance cell survival, or increase re-establishment of axonal connections between new tissue and host tissue. Examples of growth factors commonly associated with neural regeneration are discussed below.

Fibroblast growth factor-2 (FGF-2) is a member of the FGF superfamily. It is an 18 kDa glycoprotein that is upregulated in the brain both during development and following injury. FGF-2 acts both as a neuroprotective and a neuroregenerative agent in the injured brain <sup>108</sup>. As a neuroprotective agent, FGF-2 supports the survival of neurons, astrocytes, and oligodendrocytes by protecting them against toxins involved in the excitotoxic pathways and by upregulating the expression of free radical scavenging enzymes <sup>109</sup>. FGF-2 affords neuroregeneration primarily by promoting axonal outgrowth from neurons, and the proliferation of glial and vascular cells in the brain. It has also been shown that both mouse and rat NSPCs increase proliferation in the presence of FGF-2. Benefits associated with FGF-2 treatment in animal models include reduction in infarct volume and increase in neurological outcome <sup>110</sup>.

Another growth factor that promotes neuroregeneration after stroke is granulocyte-colony stimulating factor (G-CSF) <sup>111</sup>. This is a 19.6 kDa glycoprotein is used to treat neutropenia, but also exerts neuroprotective and neuroregenerative effects. G-CSF receptors are found predominantly on neurons in the cortex and hippocampus, as well as progenitors in the SVZ and SG. G-CSF is thought to inhibit apoptosis through the PI3K/Akt pathway <sup>112</sup>, and drives progenitor cells to preferentially differentiate into neurons through the JAK2/STAT3 pathway <sup>113</sup>. The combined action of these two pathways lead to decreased infarct volume and improved neurological outcome in stroke.

Epidermal growth factor (EGF) is a potent mitogen that has repeatedly been shown to stimulate the proliferation and migration of NSPCs both in vitro and in vivo <sup>114</sup>. Infusion of EGF at various times after stroke into the stroke injured cortex led to improved proliferation of progenitors in the SVZ, and these cells migrated to the injured cortex <sup>115</sup>. However, EGF alone neither exerts neuroprotection for the newly generated progenitors, nor encourages progenitors to preferentially differentiate down the neuronal lineage.

Erythropoietin (EPO) is a hematopoietic factor that increases erythropoiesis, or the generation of new red blood cells. In the central nervous system it exerts both neuroprotective effects <sup>116</sup>, through inhibition of neuronal apoptosis, and neuroregenerative effects <sup>117</sup>, through stimulation of endogenous SVZ progenitors and neuronal differentiation. Intranasal and intravenous administration of EPO after stroke has been shown to significantly reduce stroke cavity volume and improve behavioural recovery <sup>118,119</sup>.

#### **1.4.4.2. Sequential treatment of epidermal growth factor and erythropoietin**

A study by Kolb *et. al.* demonstrated the efficacy of a combined neuroregenerative therapy where EGF and EPO are sequentially infused into the lateral ventricles for treating PVD stroke in rats <sup>22</sup>. When EGF and then EPO were sequentially infused for 7 days each into the lateral ventricles of stroke-injured rats using a catheter/osmotic minipump system, regeneration of brain tissue at the peri-infarct site and functional recovery were observed. EGF induces increased proliferation of NSPCs in the SVZ, while EPO helps to enhance survival and integration, and promote differentiation into mature neurons <sup>22</sup>. This new treatment paradigm offers a possibility for treating ischemic stroke based on endogenous tissue regeneration.

However, this growth factor therapy, like many other regenerative medicine-based treatments for stroke, is currently administered using a catheter/osmotic minipump system, which is highly invasive. In this system, a catheter is inserted through the cortex into the SVZ, and an osmotic minipump is attached to the animal host throughout the entire treatment period. This strategy is invasive and induces inflammatory response and infection at the site of insertion. The alternative is to use systemic delivery, but this method requires high doses because only a small amount of drugs can penetrate the blood brain barrier. The high dosage may lead to systemic toxicity. Since currently available delivery strategies are either systemic or localized but highly invasive, there is a strong incentive to develop better delivery systems.

## **1.5. Challenges in drug-delivery to the brain**

### **1.5.1. Blood-brain barrier**

Drug delivery to the brain is a challenge because the brain is isolated from the rest of the body by the blood brain barrier (BBB) <sup>120</sup>. The endothelial cells lining the cerebral vessels form tight junctions that permit small hydrophobic molecules (<400Da) and nutrients to enter the brain at low levels (approximately 2% of drugs systemically administered will enter the brain <sup>121</sup>), but prevent the traffic of most foreign substances and macromolecules such as proteins <sup>122</sup>. This presents a challenge to drug delivery, especially growth factor delivery, to the brain.

Systemic delivery strategies are relatively non-invasive and easy to administer <sup>123</sup>. However, these are not suitable for targeting the brain because many drugs are hydrophilic, have high molecular weights, and do not readily permeate the BBB. Drug diffusion across the BBB may be induced by administering large doses systemically, but high drug dosage will likely lead to toxic side effects <sup>122</sup>. Additionally, even though a small fraction of foreign molecules does cross the BBB into the brain parenchyma, they are often exported rapidly by surface transporters on the BBB, such as the non-selective G-protein coupled-receptors <sup>124-127</sup>. This is a significant challenge for moving drugs that are effective in preclinical studies into clinical studies. Hundreds of model drugs have been developed which had been predicted to cross the BBB based on complex pharmacokinetic models. Most of these drugs are effective in vitro or in animal models, but nevertheless fail their clinical trials because of their inability to cross the BBB <sup>128,129</sup>.

Intranasal delivery of insulin had been investigated clinically in Alzheimer's patients and was shown to be effective in reducing cognitive loss. However, patients complained of discomfort, which can lead to low compliance level in practice <sup>130</sup>. Additionally, the concentration of the drug delivered that reaches the olfactory bulbs significantly exceeds that reaching other areas of the brain, and does not allow for truly targeted delivery.

Significant efforts have been devoted to designing strategies that are capable of transporting drugs across the BBB. One strategy that allows systemically administered therapeutic agents to enter the intracranial space is to temporarily disrupt the BBB, either mechanically through the use of electrical stimuli, or chemically by the injection of hyperosmotic sugar solutions such as mannitol <sup>131</sup>. However, even though these strategies have been used in the clinic to treat brain tumors <sup>121</sup>, they elicit local inflammatory response and may have toxic side effects. Additionally, only a small number of neurosurgeons in the world have the ability to properly administer these treatments, and consequently this type of treatment is not widely available <sup>121</sup>. Another type of strategy developed by Pardridge et. al., referred to as the “Trojan horse” strategy, bypasses the BBB by conjugating the protein or drug of interest to antibodies that are capable of crossing the BBB <sup>132</sup>. The resulting fusion protein has shown high efficiency in crossing the BBB and efficacy in animal models of brain disorders <sup>133</sup>. For example, a fusion protein of EPO was shown to cross the BBB and effectively reduce the severity of stroke in a mouse model <sup>134</sup>. However, each system must be designed individually, and not all proteins can be easily expressed recombinantly. Therefore the currently available systemic delivery methods fall short of achieving safe yet efficacious drug delivery to the brain.

### **1.5.2. Invasiveness of local delivery strategies**

Local delivery of drugs is another approach that has been used to bypass the BBB <sup>131,135</sup>. Currently available drug administration strategies for achieving local delivery include intracerebroventricular (ICV) <sup>136</sup> and intracranial bolus injection and infusion <sup>137</sup>.

Each of these, however, is faced with severe limitations towards clinical translation. Bolus injection comprises of one-time injections of the drug solutions. For many therapeutically

effective drugs and proteins, however, prolonged delivery with constant delivery rates are required to achieve optimal clinical outcome<sup>138</sup>. Therefore, repeated injections must be carried out to maintain the level of drugs at the target site required to obtain therapeutic benefits. This drastically increases invasiveness and patient discomfort. The catheter/osmotic minipump system is an improved delivery strategy compared to bolus injection since there is a constant reservoir of therapeutic agent, and the drug solution is delivered locally through a catheter that is implanted into the recipient close to the site of interest. However, this system is highly invasive since it must be attached to the patient throughout the treatment interval, leads to local inflammation, and it still lacks the ability to localize the drugs at the site of delivery after injection<sup>139,140</sup>. Localized delivery is an important criterion in designing DDS for the CNS: if the drugs cannot be spatially confined to a target region after delivery, only a small portion of the delivered drug is actually acting on the target tissue. If this is the case then a large quantity of drugs must be administered to achieve the required therapeutic potential, which may lead to toxic side effects elsewhere in the brain.

### **1.5.3. Epicortical controlled drug delivery systems**

Given the limitations in currently available DDS, we aimed to design an improved DDS that would encompass the following characteristics: 1) causes minimal tissue damage; 2) allows the drugs delivered to reach the target tissue efficiently; 3) does not lead to adverse effects in the tissue, including inflammation and toxicity. We hypothesized that a DDS with this set of characteristics would allow us to sequentially deliver EGF and EPO to stimulate endogenous NSPCS in the SVZ and enable brain repair in a minimally invasive manner.

These criteria may be met by placing a drug reservoir on top of the brain cortex, such that there is no damage to the parenchyma, and the system can spatially and temporally control the release profiles of the drugs to be delivered. We term such systems “epicortical” delivery systems. Epicortical systems obviate the tissue damage caused by intracerebral catheter insertions, and the physicochemical properties of the system may be engineered to yield the desired delivery profiles.

To understand the pharmacokinetics of epicortically delivered protein drugs in stimulating NSPCs in the SVZ, we need to understand the transport process of proteins in the brain.

#### **1.5.3.1. Parameters governing protein transport in the brain**

The success of epicortical delivery strategies for targeting the brain relies on the ability of drugs to penetrate from the site of deposition to a remote target region. This is a challenge at present because the rapid elimination of most proteins from the brain limits diffusion distances to 1 – 2 mm<sup>141</sup>. The diffusion distance of molecules in tissue is primarily dependent on two factors. The first is the intrinsic diffusivity of the molecules, which is influenced by molecular size, hydrophilicity/hydrophobicity, and protein surface charge<sup>141</sup>. Protein diffusion is also dependent on the rate of elimination by receptor-mediated endocytosis, proteolytic degradation, immune cell phagocytic uptake, and clearance through interstitial fluid flow<sup>141</sup>. Previous studies have shown that growth factors such as nerve growth factor (NGF) and brain-derived growth factor (BDNF) cannot diffuse more than 2 mm in the brain<sup>142</sup>. As both EGF and EPO receptors are abundant in the CNS, and elimination through all the different routes are possible, it can be conceived that diffusion distance would be limited for both of these proteins.

### **1.5.3.2. Potential strategies for improving penetration distance**

The retention time and consequently penetration distance of proteins in brain tissue can be modified using a number of techniques. The underlying principle is to reduce the rate of protein elimination and clearance from the diffusion path in the brain <sup>143</sup>. Most of these strategies involve increasing protein stability, increasing protein size, reducing recognition of proteins by cell surface receptors and binding moieties on the ECM.

One method for reducing protein elimination through reducing receptor recognition is site-specific modification of the protein, either by mutagenesis <sup>144,145</sup> or by post-translational amino acid substitution <sup>146</sup>. Here, amino acid residues in the receptor binding site of the protein can be changed in a manner such that the binding constant between the protein and their receptors are significantly decreased, but the stability and biological function of the proteins are not affected <sup>147</sup>. Protein binding can be significantly altered through replacing amino acid residues in the receptor molecule <sup>148</sup>. The drawback of this approach, however, is the impracticality of genetically modifying the host animal or patient, such that their receptors will bind the protein drugs of interest differently. The alternative is to modify the protein drugs themselves. The rationale for this technique takes advantage of the fact that protein homologues from different species may have different receptor binding properties, but have similar levels of biological functions <sup>149</sup>. For example, although recombinant human EGF is only 70% homologous to murine EGF in structure and binds weakly to mouse cells compared to human cells, it remains an effective mitogen in murine cell cultures <sup>150</sup>. However, the success of this type of approach is low and highly protein-dependent <sup>151</sup>.

Another method for increasing protein stability and diffusion distance in tissues is by conjugating polymer chains to proteins <sup>152</sup>. This acts through two mechanisms: increasing local viscosity to

reduce chain movement and protein misfolding <sup>153</sup>, and increasing the hydrodynamic radius of the protein and coating the protein surface, thereby reducing elimination through enzymatic degradation and receptor recognition <sup>127</sup>. Polymers that have been studied for this application include chitosan, polystyrene, dextran, and most commonly poly(ethylene glycol) (PEG). Chitosan has only been used in a small number of studies in systemically administered therapeutics, and the amount of information available is limited <sup>127,154</sup>. Polystyrene is a hydrophobic polymer, and as such has been shown to elicit significant cell adhesion and increase immunogenicity. The two polymers most commonly used to improve protein stability and residence time *in vivo* are dextran and PEG.

Dextran is one of the earliest polymers to be used in protein-polymer conjugation reactions. It is an  $\alpha$ -D-1,6-glucose-linked glucan with side-chains linked to the polymer backbone. The branches are typically 1-2 glucose units long, and the degree of side-branching is approximately 5%. A large number of proteins, including insulin <sup>155</sup>, lysozyme <sup>156</sup>,  $\beta$ -glucosidase <sup>157</sup>, and superoxide dismutase (SOD) <sup>158</sup> have been modified through dextran conjugation, and changes in their pharmacokinetics and therapeutic properties have been characterized. Dextran-conjugated proteins have shown improved stability against proteolysis and longer circulation time in the body compared to unmodified native proteins. However, dextran has been shown to elicit immune responses in some cases. For instance, both native dextran and dextran-conjugated serum albumin was shown to stimulate higher IgG and IgM production in animal models <sup>159</sup>. Additionally, the bioactivity of some therapeutic proteins have been observed to decrease after dextran conjugation <sup>159</sup>. Therefore the use of dextran to prolong proteins' tissue residence time is not optimal.

PEG is another polymer often conjugated to proteins to increase their hydrodynamic radius, protect against proteolysis, and reduce immune recognition <sup>160</sup>. Each ethylene oxide unit on

PEG binds 2 – 3 water molecules on average, which, in addition to a high degree of backbone flexibility, allows PEG to attain a hydrodynamic radius equivalent to a soluble protein 5 – 10 times its molecular weight <sup>160</sup>. The high degree of hydrophilicity and polymer chain flexibility contribute to PEG's popularity as a protein stabilizer <sup>161</sup>.

PEG is available in multiple conformations, including linear, branched, mono-functionalized, and multi-functionalized. The most basic structure of PEG contains hydroxyl groups on its chain ends, and cannot form covalent linkages with proteins. However, these OH groups may be replaced (i.e. activated) by functional moieties to mediate conjugation reactions, and PEG with chain-end functionalities are referred to as activated PEG <sup>162,163</sup>. Common activated PEG species used in protein conjugation include PEG-aldehydes (Fig. 1.1a) <sup>164</sup>, PEG-maleimides (Fig. 1.1b) <sup>165</sup>, N-hydroxysuccinimide (NHS) esters of PEG (Fig. 1.1c) <sup>152</sup>. Activated PEG molecules can react with different amino acid residues on proteins, but the most common amino acids involved in PEGylation reactions include lysine, asparagines, and glutamine. These amino acids contain amine groups that can react with NHS-PEG and PEG-aldehydes (in the presence of reducing agents); thiol groups on cysteines and methionine, which react with PEG-maleimide derivatives; or carboxy groups on the C-terminus, which can participate in thiol reactions <sup>152</sup>. Most PEG-conjugation reactions involve the nucleophilic attack by the protein (NH<sub>2</sub>, SH, etc) on PEG functional groups. The kinetics of PEGylation reactions depend on the nucleophilicity of the protein side chains and the affinity of the leaving group on PEG to be displaced <sup>166</sup>.

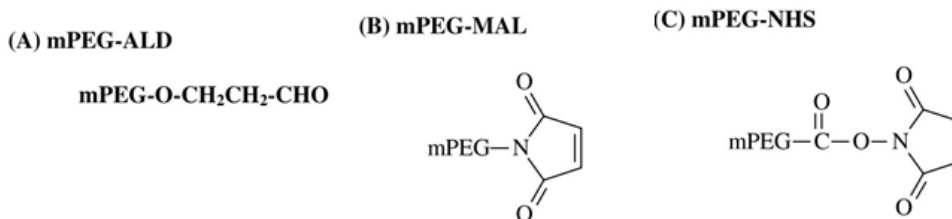


**Figure 1.1 | Common activated poly(ethylene glycol) derivatives**

The degree of branching and the molecular weight of PEG, the extent and degree of PEG-modification, and the conjugation chemistry have significant impacts on the stability, bioactivity, and pharmacokinetics of the PEG-conjugates <sup>167,168</sup>. For each protein, the appropriate PEG species must be selected to optimize the therapeutic efficacy of the conjugate. Generally, higher degrees of PEG modification or longer PEG chains will lead to longer circulation time, but receptor binding and bioactivity are often compromised. Additionally, since multiple modification sites are often available on most proteins, there may be multiple degrees of conjugation. The resulting heterogeneous product population may lead to unpredictable and irreproducible properties. Controlling the degree and position of PEG modification, as well as the separation of different forms of PEG-protein conjugates are both challenging aspects of PEG modification of proteins.

PEG can react with proteins following a variety of reaction chemistries. Amine groups ( $\text{NH}_2$ ) are the most commonly used functionality on amino acid residue for PEG modification. Common amino acid residues involved in amine-mediated PEG-modification include lysine, asparagine, glutamine, and the N-terminus. The other common PEG modification sites include cysteines and the C-terminus carboxylic acid group. However, cysteines are often involved in forming disulfide bridges to stabilize protein structure; the C-terminus and amino acids on the interior of the protein's tertiary structures are often crucial for bioactivity and thus reactions at these sites should be avoided. Therefore many protein modification reactions are engineered to be specific to the N-terminus <sup>169</sup>.

N-terminus specific monoPEG-modification of proteins may be achieved using a number of methods. The simplest strategy is to control the reaction pH. The pKa of the  $\alpha$ -amine on the N-terminus is 7.8 while that of the  $\epsilon$ -amine on lysines is 10.1. The pH may be controlled such that only the N-terminus is deprotonated and reactive in nucleophilic attacks by the PEG molecule.

Previous studies by Kinstler *et. al.* <sup>170</sup> and Lee *et. al.* <sup>171</sup> showed that at pH 5.0, granulocyte-colony stimulating factor (G-CSF) and epidermal growth factor (EGF), respectively, may be modified with PEG on the N-terminus without significant loss of bioactivity. However, the yields obtained are less than 30%.

N-terminus-specific monoPEG-modification may also be achieved through site-specific mutagenesis. Lysine residues on the protein interior may be removed and replaced with other amino acid residues, typically arginine, without significant loss of bioactivity <sup>172</sup>. This allows for protein conjugation with PEG-NHS at high conversion rates. However, this method is time consuming, and stringent characterization must be carried out to ensure that the product does not contain endotoxins and is safe for human use <sup>173</sup>.

Another potential strategy for monoPEG-modification of EGF is to replace the N-terminal amine group with a reactive carboxyl group in a transamination reaction <sup>174</sup>. The carboxyl group may react with amine-functionalized PEG to form an oxime bond <sup>175</sup>. This reaction may be mediated by enzymes (e.g. transaminases) <sup>176,177</sup>, metals (typically  $\text{Cu}^{2+}$ ), or organic compounds (e.g. pyridoxal L-phosphate) <sup>178</sup>. Transaminase catalysed reactions are lengthy, and proteins may lose bioactivity during the process. Metal and organic catalysed reactions proceed more quickly, but present the potential problem of cytotoxicity <sup>179</sup>.

Finally, a relatively new method has been developed where proteins are PEG-modified at a single amino acid residue using the enzyme sortase <sup>180</sup>. Sortase is a bacterial transpeptidase that catalyzes cell-wall sorting reactions by cleaving the peptide bond between a threonine (T) and a glycine (G) in a LPXTG peptide sequence, where X may be a number of amino acids, including aspartic acid (D), glutamine (Q), glutamic acid (E), alanine (A), and asparagines (N) <sup>181</sup>. The threonine carboxyl group reacts with a pentaglycine (GGGGG) sequence on bacterial cell-wall peptoglycan. This method may be used to conjugate PEG to the protein on either the N- or

the C-terminus by modifying the PEG and the protein to contain the required LPXTG and the GGGGG sequences.

One of the aims of this thesis is to study the effect of PEGylation on protein transport in the brain. To this end we used EGF as a model protein, and conjugated PEG molecules of similar molecular weight to EGF using amine-NHS reactions. The number of conjugated PEG molecular is varied to investigate the effect of the degree of PEGylation on protein transport. The amine-NHS reaction was selected for its simplicity and versatility.

## **1.6. Polymeric drug delivery systems for achieving controlled drug delivery to the brain**

Over the last few decades, much research effort has been devoted to developing polymer-based, controlled drug delivery systems (DDS) for targeting the brain <sup>182-184</sup>. Polymeric systems, especially polymeric hydrogels, are ideal scaffolds for tissue engineering and drug delivery. Hydrogels are crosslinked networks of hydrophilic polymers chains with high water content. They are typically biocompatible, biodegradable, and have tunable mechanical properties to match that of the extracellular matrix (ECM).

### **1.6.1. Hydrogel-based drug delivery systems**

Today there is still no precise definition for the term hydrogel, although it is commonly used to refer to crosslinked polymer networks <sup>185</sup> where the crosslinked structure allow for large quantities of water to be absorbed and the gel to swell without dissolving. Most hydrogels are viscoelastic and resemble the stiffness of soft tissues <sup>186-189</sup>. The crosslinks can be either physical or chemical. Chemically crosslinked hydrogels are typically more stable than physically

crosslinked hydrogels and maintain their structure over longer time period. However, the synthesis of these hydrogels often require initiators, many of which are toxic. Physical crosslinks often involve hydrogen bonds or hydrophobic interactions and thus do not require initiators. The trade-off is lower degrees of structural stability <sup>190</sup>.

One of the most biologically relevant properties of hydrogels is their swelling properties <sup>191</sup>. Hydrogel swelling is a complex three-step process. First, the hydrophilic groups on the polymer chains interact with water, which results in “primary bound water”. Second, as the network swells, the hydrophobic groups on the polymer chains are forced to interact with water and form “secondary bound water”. Together, primary and secondary bound water are referred to as “total bound water”. Lastly, the osmotic driving force of the network towards infinite dilution is resisted by the crosslinks, and an additional amount of water is absorbed up to the equilibrium water content. This last quantity of water is referred to as the bulk water or free water, and fills the space between the network chains and the centres of pore structures <sup>185</sup>. The total amount of water absorbed by a hydrogel network depends on the temperature and specific interaction between water and polymer chains <sup>192</sup>.

In drug delivery and tissue engineering applications, the design criteria for hydrogel-based systems include: 1) biocompatibility; 2) minimal invasiveness; and 3) biodegradability. To be considered a biocompatible drug delivery device, the hydrogel used must not elicit a significant inflammatory response and toxic side effects in the host. Minimal invasiveness is important in drug delivery applications so that the damage to host tissue can be minimized. This is important especially in the brain and central nervous system, where devices that cause excessive tissue damage will exaggerate the disorder in question rather than repair it <sup>193</sup>. Biodegradability is a desirable feature in drug delivery devices, as devices that are non-degradable must be removed from the body, and the additional surgical procedure may cause further tissue damage.

Hydrogels used in drug delivery applications have been derived from both synthetic and natural sources. The first hydrogels were derived from biological sources, but today an increasing number of hydrogel materials are chemically synthesized <sup>194</sup>. Polyethylene glycol (PEG) and polyvinyl alcohol (PVA) are two of the most commonly used synthetic hydrogels. Naturally derived polymers, such as collagen, chitosan, alginate, hyaluronic acid (HA), and cellulose derivatives such as methylcellulose and hydroxypropyl methylcellulose have also been used extensively <sup>123</sup>. The two classes of hydrogels, those derived from synthetic and naturally derived polymers, are discussed below with respect to their uses in drug delivery applications.

#### **1.6.2. Hydrogels based on synthetic polymers in drug delivery applications**

This section contains a discussion of five common synthetic polymers used to synthesize hydrogel scaffolds for drug delivery. These are: poly(ethylene glycol) (PEG); poly(vinyl alcohol) (PVA); poly(imide); poly(acrylate); and poly(urethanes) <sup>185</sup>.

PEG and derivatives of PEG are some of the most commonly used polymers in biomedicine <sup>195</sup>. Most of these hydrogels have high degrees of biocompatibility and lack tissue toxicity, both of which make them good candidates for use in drug delivery and tissue engineering systems <sup>196-198</sup>. PEG can also be easily modified to contain a number of functional groups that are responsive to environmental cues, such as temperature and pH variations <sup>199</sup>. The resulting hydrogels can be made to release drugs in a highly controlled manner, and are thus referred to as smart hydrogels <sup>200</sup>. The main limitations in PEG-based hydrogels are that they are often not biodegradable unless modified, and as such native PEG hydrogels must be surgically removed after drug release is completed.

Another commonly used synthetic polymer used in preparing hydrogel DDS is PVA<sup>201</sup>. The main advantages of using PVA in hydrogel DDS include their mechanical stability and their ability to retain water in the structure for prolonged periods of time<sup>201</sup>. This ensures an environment that is necessary in applications such as contact lenses, artificial organs, drug delivery systems, as well as wound dressings. However, as PVA hydrogels are typically synthesized using photochemical crosslinking reactions, toxic side effects could negatively impact the recipients if byproducts of the reactions are not completely removed from the hydrogel system<sup>202</sup>. Similar to PEG hydrogels, PVA hydrogels are also not biodegradable and as such require removal from the body.

Poly(imides)<sup>203</sup> and poly(acrylamides)<sup>204</sup> are two other classes of synthetic hydrogels that are used in biomedical applications. These hydrogels have often been used to synthesize endoprosthetics and plastic reconstruction devices, and have shown high degrees of biocompatibility<sup>205</sup>. Recently, the electroconductive properties of some poly(imides) and poly(acrylamides) have facilitated their use as microvalves in microfluidics devices or artificial heart applications<sup>206</sup>. Some sustained release applications have also been investigated, although their use tends to be limited to wound dressing-related applications<sup>206</sup>. Their application in the brain has so far been very limited to coatings on intracortical electrodes used for neural recordings<sup>207</sup>.

Poly(urethanes) are a lucrative class of materials that are commonly used as drug delivery devices, wound dressing membranes, artificial kidney applications, as well as catheter coating and contact lens materials<sup>208,209</sup>. One advantage of using poly(urethane) hydrogels is that they can be modified extensively and in many ways, which allows for a broad spectrum of applications. Many novel hydrogels are prepared by synthesizing interpenetrating networks of poly(urethanes) and polymers such as poly(acrylamide)<sup>208</sup>, PEG<sup>210</sup>, and poly(vinyl pyrrolidone)

<sup>211</sup>. Poly(urethane) based materials tend to have a high degree of mechanical stability and can last for years in vivo. However, for short-term (i.e. delivery over weeks or months) drug delivery purposes, this may not be appropriate.

### **1.6.3. Hydrogels based on naturally derived polymers in drug delivery applications**

In addition to synthetic polymer-based hydrogels, those derived from natural polymers also play an important role in biomedicine and drug delivery. These naturally derived hydrogels are sometimes argued as being better than synthetic hydrogels because they offer better chemical and morphological cues to cells without any modification <sup>193</sup>. A number of common examples, including collagen, alginate, chitosan, and hyaluronic acid are discussed in this section.

Collagen is a commonly used material in tissue engineering, and it is the most abundant protein in the ECM of mammals <sup>212,213</sup>. There are 19 types of collagen, but the basic structure of all collagen consist of three polypeptide chains in a three-stranded rope structure <sup>213</sup>. Collagen is an attractive material in tissue engineering because it has mechanical properties resembling that of the natural ECM, and its properties are also tunable through crosslinking or by blending it with other polymers, such as poly(lactic acid) (PLA), poly(glycolic acid) (PGA), and chitosan. Additionally, collagen is biodegradable by metalloproteases, thus allowing for remodeling. However, collagen contains amino acid moieties that bind to cell surface receptors with high affinity <sup>213</sup>. This cell adhesiveness is detrimental in drug delivery applications because the adhered cells will secrete various biological agents that may form fibrous capsules around the polymer, thereby compromising the release profile of drugs and their bioactivities.

Alginate is another type of polymer commonly used in regenerative medicine and tissue engineering. Its applications include both drug delivery and cell encapsulation. It is a naturally

derived linear copolymer of (1-4)-linked  $\beta$ -D-mannuronic acid (M-block) and  $\alpha$ -L-guluronic acid (G-block), and is commonly extracted from brown seaweed <sup>214</sup>. Alginate gels are formed when the G blocks interact with divalent cations and form ionic bridges between the polymer chains <sup>214</sup>. The mechanical properties of alginate hydrogels may be manipulated by varying the number and distribution of M and G blocks. One disadvantage of alginate in DDS is that gelation of alginate requires divalent ions such as  $\text{Ca}^{2+}$ , and the concentration of  $\text{Ca}^{2+}$  is important in controlling crosslinking density. Since the transport of  $\text{Ca}^{2+}$  in vivo is difficult to control, and the levels in different areas in the body fluctuate greatly, in situ gelation is difficult to control. Therefore alginates are usually used as implantable tissue engineering scaffolds rather than injectable DDS.

Another polymer commonly used in tissue-engineering is chitosan, a biocompatible and biodegradable polymer. Chitosan's popularity is due to its structural similarity to natural glycosaminoglycan (GAG) found in mammalian tissue and extracellular fluids. It is also biodegradable through enzymatic cleavage. Chitosan is a linear polysaccharide derived from chitin, consisting of (1-4)-linked D-glucosamine and N-acetyl-D-glucosamine <sup>215</sup>. It can be dissolved by dilute acids, and the dissolved polymer gels *via* either increasing pH or addition of a nonsolvent. Chemical crosslinking is another method used to induce chitosan gelation <sup>215</sup>. Chitosan degrades through lysozyme cleavage, and the ratio between the two constituent moieties determines the crystallinity of the chitosan fibres, and its degradation kinetics. Chitosan is sometimes used to synthesize "smart polymers", which are composite systems of chitosan with other polymers such as PVA and PLGA, and which respond to environmental stimuli <sup>216</sup>.

Hyaluronic acid is a glycosaminoglycan present in all mammals. In the body, high concentrations are found in connective tissues and the brain; it can also be manufactured by bacterial fermentation or derived from rooster combs <sup>217</sup>. Hyaluronic acid is degradable by

hyaluronidase in the body, and this property gives it an important advantage for drug delivery and other biomedical applications where biodegradability is important <sup>218</sup>. It also has the added advantage of being shear-thinning, thus allowing hydrogels with HA components to be injectable through thin gauge needles. Additionally, amine moieties on the HA also allow for extensive modification, such as photo-patterning of cell-recognition moieties like RGD <sup>219</sup>. HA by itself, however, does not form physical crosslinks, and therefore hydrogels of HA alone must be prepared using chemical and photocrosslinking techniques. There is therefore the possibility that toxic photoinitiators will remain in the system and may cause adverse side effects.

#### 1.6.4. Hyaluronan-methylcellulose blend (HAMC) as a local drug delivery scaffold

The Shoichet research group has previously developed a hydrogel that consists of a physical blend of hyaluronan, HA, and methylcellulose, MC, HAMC <sup>220</sup>. MC is an inverse thermal gelling polymer that forms physical crosslinks through hydrophobic interactions between the methyl groups (Fig 61.2) <sup>220</sup>. This allows therapeutic agents delivered to be localized at the site of injection.

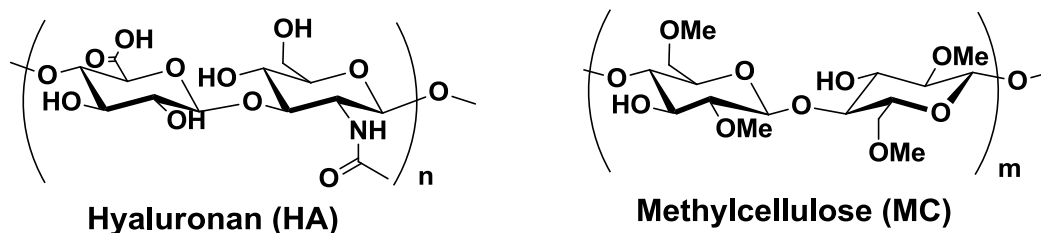


Figure 1.2 | Structure of hyaluronan (HA, left) and methylcellulose (MC, right)

The gelation of MC is a slow process at body temperature, and MC hydrogels may significantly erode before gelation is complete <sup>221</sup>. Blending HA with MC overcomes this limitation. HA is a high molecular weight glycosaminoglycan (GAG) composed of two repeating subunits: N-acetyl-D-glucosamine and D-glucuronic acid. The high molecular weight allows HA to form extensive entanglements among the MC network, keeping the MC groups in close contact and increasing the solution viscosity immediately after injection, thus enhancing the rate of gelation. As a charged polymer, HA also has salting-out effect on MC, thereby lowering its gelation temperature <sup>222</sup>. Furthermore, HA also has shear thinning properties that allow HAMC to be injectable at room temperature through high gauge needles when pressure is applied. Once injected into the intracranial space between the cortex of the brain and the skull, HA allows HAMC to rapidly gel at the site of injection, thereby allowing localization of the delivered therapeutic agents and minimizing loss. HA has also been shown to reduce inflammatory responses <sup>223</sup> and to minimize tissue adhesion and scar formation, all of which are advantageous in promoting wound healing <sup>223</sup>.

#### ***1.6.4.1 Advantages of using HAMC for brain drug delivery***

The physicochemical properties of HA and MC allow HAMC to have a number of characteristics ideal for DDS used in the CNS. Previous studies have shown HAMC to be injectable, fast-gelling, biocompatible, biodegradable, minimally swelling, and non-cell adhesive <sup>220</sup>. These properties are important in the DDS because injectable systems can be delivered in a minimally invasive manner; the fast-gelling hydrogel prevents the delivered therapeutic agents from being

washed away; biocompatibility, minimal degree of swelling, and non-cell adhesiveness ensure *in vivo* compatibility of the system; biodegradability avoids surgical removal of the device once drug release is complete; and minimal degree of swelling prevents unnecessary pressure from being imposed on the tissue. An additional characteristic of HAMC is that its properties are highly tunable by varying the percentage of HA and MC in the polymer and the molecular weight of the two constituents.

#### ***1.6.4.2 Limitations in using HAMC alone for application in drug delivery***

Despite its usefulness as a drug delivery scaffold, HAMC alone cannot sustain delivery for EGF and EPO over a 14-day period. While HAMC is appropriate for controlling and sustaining the delivery of hydrophobic drugs such as nimodipine<sup>224</sup>, it cannot sustain release of hydrophilic protein drugs because the majority of the hydrogel structure constitutes of water, and thus it does not impose significant diffusion barriers to the proteins. Since both EGF and EPO are hydrophilic and relatively small in size, these growth factors will diffuse rapidly out from the HAMC network. HAMC will be effective for localizing the growth factors, but another type of delivery vehicle is required to allow for 7-day sustained release of EGF followed by 7-day release of EPO.

#### **1.6.5. Use of polymeric particles for controlling protein delivery to the brain**

Due to the inability of HAMC to sustain protein delivery for more than several days, we must have another strategy to achieve sustained release profiles for EGF and EPO. Strategies that may allow 7-14 day delivery from HAMC include chemical modification of the hydrogel and the incorporation of an additional component such as polymeric particles into the DDS to control

delivery. Chemical modifications, such as crosslinking the hydrogel or conjugating the fusion proteins to the hydrogel through affinity-based binding pairs, may allow the required release profiles to be obtained <sup>225</sup>. Similarly the use of an additional component to control release may allow highly controlled delivery with tunable profiles. For the purpose of this thesis, focus will be placed on the addition of polymeric particles to control drug release from a hydrogel scaffold. We envision using a composite system of polymeric particles in the HAMC hydrogel to control the spatial and temporal delivery of EGF and EPO, where HAMC localizes the factors delivered at the site of injection, and the particles sustains the release to achieve the desired profiles (Fig. 1.3).

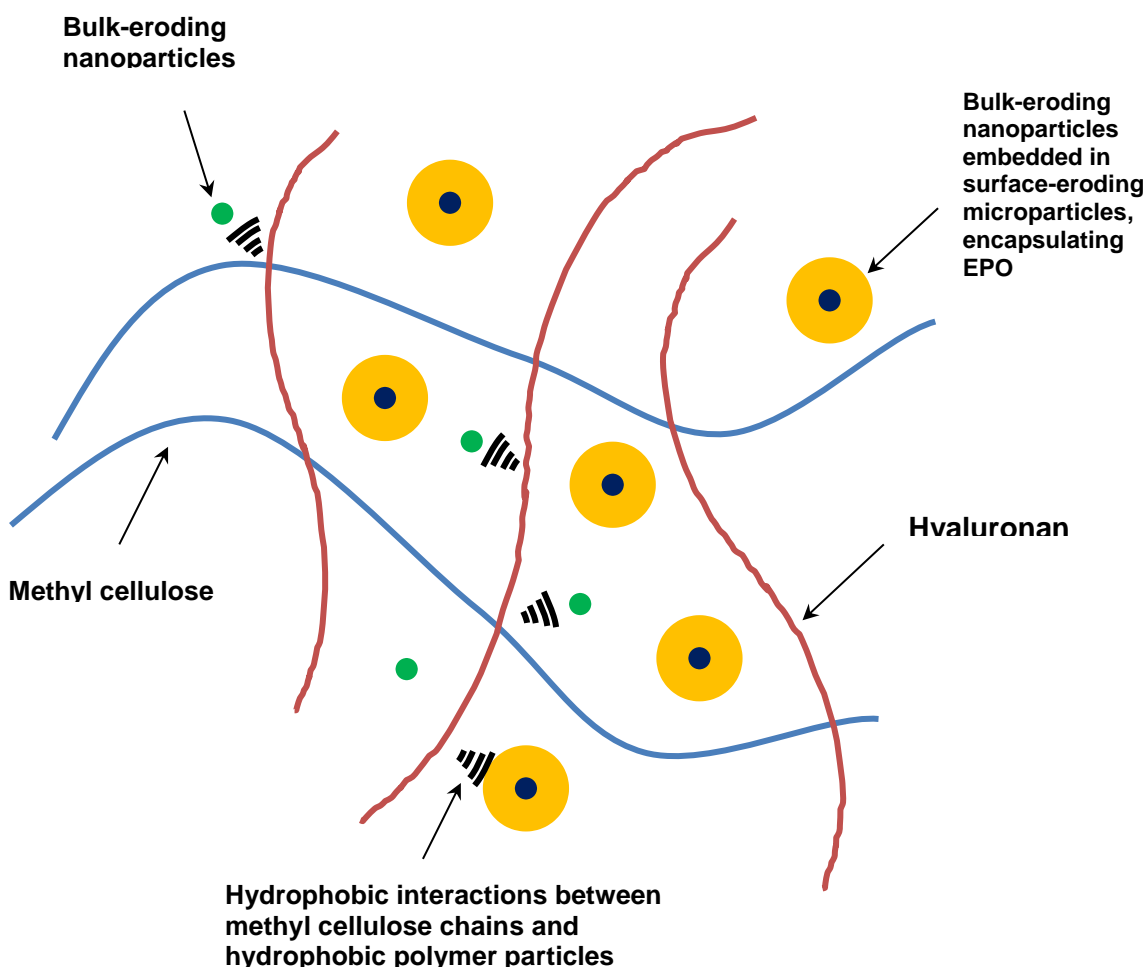


**Figure 1.3 | Schematic describing the composite drug delivery system (DDS).** We envision using a composite system of HAMC and polymeric particles to localize and sustain the deliver of

EGF and EPO. The HAMC hydrogel (HA – red, MC – blue) is fast gelling at 37°C and injectable, it also localizes the factors delivered to the site of injection. However, the high water content leads to rapid Fickian diffusion of factors out of the hydrogel. We can encapsulate EGF and EPO in different polymeric particles to achieve the desired temporal delivery. EGF can be encapsulated in bulk-eroding nanoparticles to facilitate immediate but sustained release, whereas EPO can be first encapsulated in bulk-eroding nanoparticles and then embedded in surface eroding microparticles to achieve delayed and sustained release. An additional advantage of adding hydrophobic polymeric particles to HAMC is that the particles may interact with the methyl groups on methyl cellulose to form transient crosslinks, thereby further stabilizing the hydrogel. The quantities of particles added to the system will be dictated by the amount of factors required to achieve therapeutic efficacy.

Polymeric particles with diameters ranging from several hundred nanometers to approximately 100 µm have been used in controlled drug delivery devices. Particles with diameters between 1 and 100 µm are generally referred to as microparticles, while those with submicron diameters are referred to as nanoparticles<sup>226,227</sup>. Micro/nanoparticles were first developed in the 1970s after it was discovered that particles made from poly(lactic acid) can extend the release of small molecule drugs for up to three months<sup>182</sup>. Since then a large number of polymers have been investigated as candidates for synthesizing these colloidal particles for different drug delivery applications. Three of the most intensely investigated classes of polymers used for the synthesis of colloidal particles for controlled release are poly(orthoesters)<sup>228</sup>, poly(anhydrides)<sup>229</sup>, and poly(esters)<sup>230</sup>.

#### **1.6.5.1 Poly(orthoester) (POE) nanoparticles**

There are four generations of poly(orthoesters) (POEs) available today with the general structure (Fig. 1.4)<sup>231</sup>:

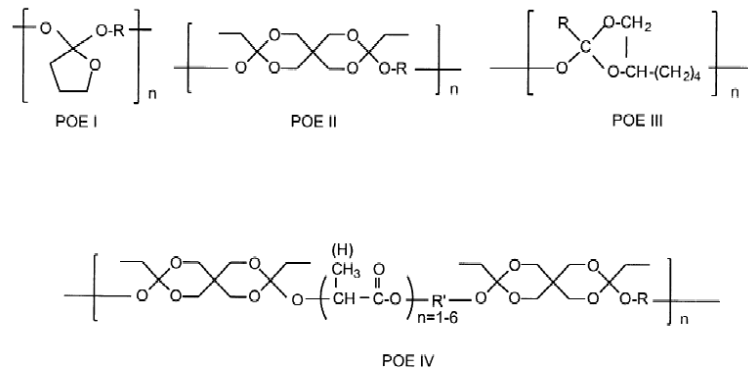


**Figure 1.4 | General structures of the four generations of poly(orthoesters) (POEs).**

The degradation of polymeric particles is dependent on the hydrophobicity of the polymer: hydrophilic polymer chains will imbibe water at a faster rate than chain scission through hydrolysis, and consequently the microparticles will degrade by bulk erosion. Alternatively, hydrophobic polymers chains hydrolyze faster than they take up water, and consequently the microparticles will be surface eroding. Since POE is highly hydrophobic, the microparticles synthesized from POEs are surface eroding<sup>231</sup>. The rate of POE degradation through hydrolysis is very slow, so the time period for drug release is typically several months to over a year<sup>231</sup>. In order to achieve short-term surface-erosion-mediated drug delivery, acidic recipients must either be added to the release medium or to the polymer matrix to increase the rate of polymer degradation. Additives such as short segments of lactic or glycolic acids are often used to catalyze the hydrolysis of POE degradation, but these acidic components severely compromise the stability of proteins encapsulated<sup>232</sup>. The hydrophobicity of the POEs also results in an initial delay period before any degradation can occur. This induction period typically lasts for 5 – 20 days even with the addition of acidic recipients<sup>231</sup>. Due to the long release period typically obtainable in POEs, this class of polymers is not suitable for our specific application.

### 1.6.5.2 Poly(anhydrides) (PA)

Poly(anhydrides) are a class of hydrophobic polymers that were first used in biomedical applications in the 1980s<sup>229</sup>. They have the general structure of (Fig. 1.5):

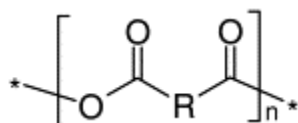


**Figure 1.5 | General structure of poly(anhydrides).**

One of the advantages of using poly(anhydrides) for drug delivery is that, similar to POEs, they are surface eroding polymers and their degradation period corresponds to the period of drug release. This property allows a linear release profile over the period of several days to be achieved<sup>229</sup>.

Poly(anhydrides) have been used primarily in the synthesis of polymeric millicylinders and microspheres. Millicylinders are rods with typical dimensions of either 5 mm diameter/0.5 mm height, 9 mm diameter/0.8 mm height, or 12.5 mm diameter/1.4 mm height<sup>229</sup>. The rate of water uptake is dependent on the size and geometry of the cylinders. Poly(anhydrides) have also been used in the synthesis of microspheres with diameters typically between 50 – 100  $\mu\text{m}$ <sup>229</sup>. Particles with smaller diameters are associated with low yields and poor release properties. The typical period of release for small molecule drugs or proteins range between 100 h and 400 h for these microspheres, with the larger microspheres having longer release times. While the sizes obtainable from DDS based on poly(anhydrides) are suitable for implants and orally administered therapeutic agents, they are not appropriate for the injectable DDS. This is because the needles used for *in vivo* injection have a typical inner diameter of 100 – 200  $\mu\text{m}$ ,

making microspheres difficult to inject. In the mid-1990s, a novel class of poly(anhydride)-poly(lactide)/poly(glycolic) double-walled microspheres <sup>233,234</sup> emerged, and they have shown versatile use in controlled delivery. However, the synthesis of double-walled microspheres relies on interfacial energy difference, and is only applicable for a few polymer systems. Therefore even though poly(anhydrides) alone are able to yield the desirable release period, it does not meet our design criteria of versatility and injectability.

### **1.6.5.3 Poly(esters)**

Poly(esters) are one of the largest classes of polymers used in controlled delivery systems. Many poly(esters) are biodegradable and can be used to encapsulate a variety of ingredients for biological applications. Examples include radioactive imaging and therapy <sup>235</sup>, protein and small molecule drug delivery <sup>236</sup>, gene and viral delivery <sup>237</sup>, and cell delivery <sup>238</sup>.

Block copolymers of poly(lactic-co-glycolic acid), PLGA, are one of the most widely used poly(esters) in the field of controlled drug delivery because it is one of the few biodegradable polymers approved for biological use by the FDA <sup>184,230,239</sup>. It is a block copolymer of lactic acid (LA) and glycolic acid (GA) with highly tunable properties such as intrinsic viscosity and rate of degradation <sup>240</sup>.

PLGA is a bulk-eroding polymer, in which the rate of water uptake exceeds the rate of hydrolytic chain cleavage, and the typical drug release profile of PLGA particles is triphasic. During the

synthesis of PLGA particles, a fraction of the drugs reside in interconnected pores close to the surface of the particles, and are able to diffuse out from the polymer matrix quickly. This results in the first burst release phase that typically occurs over 1 – 2 days. Following the burst release, a period of very slow release is maintained over several days, the exact length of which depends on the composition of the PLGA. This is because PLGA is a bulk-degrading polymer, the formation of interconnected pores in the polymer matrix through hydrolysis of their ester bonds require days to months. Since most drugs cannot diffuse easily through the hard hydrophobic PLGA shell, they are released only when particle erosion occurs. After this plateau region, another period of rapid drug release occurs in response to extensive PLGA degradation

<sup>240</sup>.

PLGA has highly tunable properties that may be used to achieve a variety of release profiles for drugs with large range of sizes and hydrophilicity. Studies have shown that by varying the relative ratios of LA and GA or the chain length of the copolymer, the overall molecular weight of the copolymer, and the terminal functional groups on PLGA, the period of release can range from one or two weeks to several months <sup>241</sup>. Process parameters during particle synthesis are also tunable, such that different geometries of the particles may be obtained. Particle geometry is another determinant in the type of release profile obtainable in PLGA particles.

#### **1.6.5.4 Rationale for using PLGA-based particles and limitations of PLGA**

PLGA particles are currently one the most extensively studied drug delivery vehicles in literature, and they can be used to encapsulate drugs with a wide range of properties <sup>125,242-244</sup>. PLGA also offers the possibility of synthesizing particles with a large range of sizes. By varying process parameters such as PLGA content in the organic phase and shear rate during emulsion, the

resulting particle sizes may range from several hundred nanometers to approximately 200  $\mu\text{m}$ <sup>229</sup>. This large range of possible particle sizes in PLGA particles allow them to be used in injectable systems. This is not possible by other polymers such as polyanhydride, which is predominantly used in the fabrication of microparticles whose diameters range between 50 – 100  $\mu\text{m}$ <sup>229</sup>. Thus PLGA offers a wide range of properties that may be tuned to satisfy the design criteria for our application. Since our goal is to develop a DDS that can be tuned to provide appropriate drug encapsulation and release for several different therapeutic agents, PLGA is the ideal candidate.

However, the use of PLGA for drug delivery applications also has a number of limitations. First, the sonication and aqueous/organic interface formed during the emulsion process leads to extensive protein denaturing<sup>245</sup>. Proteins are amphiphilic, and when they adsorb to the aqueous/organic interface, they assume the structural conformation with the lowest energy. This causes proteins to unfold and lose bioactivity. Denatured proteins are insoluble in aqueous solutions, and consequently there is incomplete protein release and reduced biological activity. Second, during the degradation process of PLGA through hydrolysis of ester bonds, acidic by-products are generated. While these products have not shown toxicity *in vitro* and *in vivo*, they contribute to the denaturing of encapsulated proteins<sup>246</sup>. Third, the drug release profile from PLGA particles follow a triphasic profile, as described before, and a linear, constant release profile is difficult to achieve. Additionally, the relative lengths of each of the three release phases are difficult to predict and control due to the large number of variables involved in PLGA particle synthesis. Thus, even when given a precise set of design criteria, there is no general formula that can be followed to optimally engineer a PLGA drug delivery system. Hence, for each application, the particles used to facilitate delivery must be individually designed.

#### 1.6.5.5 Methods of PLGA particle synthesis for protein delivery

The formulation process of PLGA particles may be varied to allow encapsulation and release of different proteins for specific applications. Two most common methods for preparing PLGA particles are salting-out<sup>227</sup> and emulsion/solvent evaporation<sup>243</sup>.

The salting-out method of preparing polymeric colloidal particles requires a water-soluble polymer to be dissolved in a high-salt concentration aqueous environment, such that a viscous gel is obtained. The therapeutic compounds to be encapsulated are dissolved in a water-miscible organic solvent. When the viscous gel is added to this solvent, phase separation occurs in a manner similar to the water-in-oil emulsions. The salt dissolved in the gel phase is capable of producing the salting-out of the organic solvent, leading to the formation of polymer particles. The drawback in this method is that the protein needs to be dissolved in organic solvents, which may lead to denaturation and toxicity<sup>227</sup>.

Emulsion/solvent evaporation is one of the most versatile techniques available for particle synthesis. Two variations of the emulsion technique commonly used to synthesize PLGA particles for encapsulating proteins and growth factors are the solid-in-oil (s/o) single emulsion, the oil-in-water emulsion (o/w) single emulsion, and the water-in-oil-in-water double emulsion ( $w_1/o/w_2$ )<sup>247</sup>.

The s/o emulsion is a relatively simple technique, where dry protein powders are first processed to obtain particulates of similar size, either by sonication or sieving (solid phase)<sup>248</sup>. Excipients, such as PEG, may be added at this stage to help stabilize the proteins of interest. The polymer is then dissolved in an organic solvent and the protein is also added to this organic solution (oil phase). The solution is then emulsified to produce nano- or micron-sized droplets, the solvent is

extracted and particles allowed to harden. The limitation in this strategy is that sizes of particles formed tend to be large ( $>100\ \mu\text{m}$ ), and the size distribution is large <sup>248</sup>.

The oil-in-water (o/w) emulsion was one of the first emulsion techniques developed <sup>247</sup>. It uses an inner organic phase that contains both the polymer and the therapeutic agent to be encapsulated. Typically, the therapeutic agents are soluble in organic solvents. The organic solvent used to synthesize PLGA particles is usually dichloromethane or ethyl acetate. This organic phase is introduced into a larger volume of aqueous solution containing excipients such as polyvinyl alcohol (PVA). During this stage the organic solvent is extracted from the polymer matrix, and the particles are allowed to harden. This technique is typically used to encapsulate drugs that are soluble in organic solutions. However, the o/w method has low encapsulation efficiency and loading capacity for water-soluble drugs. This is because during the hardening phase, the water-soluble drugs in the organic phase will preferentially partition into the outer aqueous phase, thereby reducing the amount of drugs encapsulated. It is therefore not suitable for the encapsulation of growth factors and cytokines, which are typically highly water soluble.

A more appropriate formulation of PLGA particles to encapsulate water-soluble drugs or proteins is the  $w_1$ -o- $w_2$  double emulsion/solvent evaporation technique <sup>230,247</sup>. Here the drug is dissolved in an inner aqueous phase of buffered solution ( $w_1$ ).  $w_1$  is introduced to an organic phase (o) containing PLGA dissolved in either dichloromethane or ethyl acetate. This mixture is sheared at high frequency to form the primary emulsion. The primary emulsion is then introduced into an outer aqueous phase ( $w_2$ ), and the mixture further emulsified to allow the microspheres to form. The secondary emulsion is then introduced into a hardening bath of aqueous buffer solution containing PVA, in which the organic solvent is extracted and the particles are allowed to harden. This technique has been shown to have better encapsulation

efficiency than other emulsion techniques for a number of proteins and growth factors, such as EGF<sup>244</sup>, EPO<sup>242</sup>, nerve growth factor (NGF), and lysozyme<sup>125,242,249</sup>.

## 1.7 Summary of research

The following chapters will discuss the development and characterization of a polymeric composite DDS that allows for sequential release of EGF followed by EPO, and facilitates epicortical drug delivery to the stroke-injured brain.

In chapter 2, the transport of proteins in the stroke-injured brain is investigated using EGF as a model protein<sup>250</sup>. Protein elimination in the brain is rapid, which results in short penetration distance. This distance is further decreased after stroke due to EGF receptor upregulation along the diffusion path. We conjugate to EGF a single PEG molecule with comparable molecular weight and show, using integrative optical imaging and mathematical modeling, that PEG-modification significantly enhances protein penetration in both uninjured and stroke-injured mouse brain by decreasing the rate of elimination.

In chapter 3, we examine the transport of PEG-EGF<sup>251</sup> in the stroke-injured brain following epicortical delivery from HAMC. We show that PEG-EGF can penetrate from the cortical surface to the SVZ in an endothelin-1 mouse model of stroke. We also demonstrate that PEG-EGF demonstrates greater stability against enzymatic degradation *in vitro*, which contributes to reduced rates of elimination *in vivo*. Consequently, higher amount of PEG-EGF penetrates to the SVZ following delivery compared to unmodified EGF, and greater stimulation of NSPCs in the SVZ is achieved using PEG-EGF.

In chapter 4, we examine the transport of EPO to the stroke-injured brain following HAMC-mediated epicortical delivery<sup>252</sup>. Unlike EGF, which diffused a significantly shorter distance in stroke-injured tissue compared to uninjured tissue, EPO transport is similar between the two types of tissues. We demonstrate that this is partially due to the lack of EPO receptor upregulation after injury. We also show that EPO penetrates to the SVZ following epicortical delivery and remain bioactive upon reaching the SVZ. In demonstrating the bioactivity of the EPO delivered, we show that EPO enhances neurogenesis.

In chapter 5, we demonstrate the development of the composite DDS to enable sequential delivery of PEG-EGF and then EPO. We show that the growth factors can be released following the desired profile and maintain bioactivity over time. We also demonstrate that when delivered epicortically from the composite, the combined treatment of PEG-EGF and EPO leads to tissue regeneration in the endothelin-1 mouse model of stroke. Additionally, performance of the composite DDS is comparable to that of the osmotic minipump delivery system, which is one of the most commonly used pre-clinical systems today. We also conducted preliminary functional assays, and showed that animals receiving composite-mediated treatment achieve significant functional improvement. These results are presented in Appendix D.

## 2 Transport of epidermal growth factor in the stroke-injured brain\*

\*This chapter was published in the Journal of Controlled Release.

Wang, Y<sup>1</sup>.; Cooke, M.J.; Lapitsky, Y.; Wylie, R.G.; Sachewsky, N.; Corbett, N.; Morshead, C.M.; Shoichet, M.S. 2010. “**Transport of Epidermal Growth Factor in the Stroke-injured Brain**” J Control Release, 149: 225-35

### 2.1 Abstract

Stroke is a neurological disorder that currently has no cure. Intrathecal delivery of growth factors, specifically recombinant human epidermal growth factor (rhEGF), stimulates endogenous neural precursor cells in the subventricular zone (SVZ) and promotes tissue regeneration in animal models of stroke. In this model, rhEGF is delivered with an invasive minipump/catheter system, which causes trauma to the brain. A less invasive strategy is to deliver rhEGF from the brain cortex; however, this requires the protein to diffuse through the brain, from the site of injection to the SVZ. Although this method of delivery has great potential, diffusion is limited by rapid removal from the extracellular space and hence for successful translation into the clinic strategies are needed to increase the diffusion distance. Using integrative optical imaging we investigate diffusion of rhEGF vs. poly(ethylene glycol)-modified rhEGF (PEG-rhEGF) in brain slices of both healthy and stroke-injured animals. For the first time, we quantitatively show that PEG modification reduces the rate of growth factor elimination by over an order of magnitude. For rhEGF this corresponds to a two to threefold increase in predicted brain penetration distance, which we confirm with *in vivo* data.

---

<sup>1</sup> Contribution by Y. Wang: designed and performed all in vitro and ex vivo experimental work; derived mathematical models used to extract transport parameters; designed and tested MATLAB algorithm used in deriving theoretical transport parameters from experimental data; collected experimental and modeling data; conducted data analysis and interpretation; prepared the manuscript.

## 2.2 Introduction

Each year more than 15 million stroke injuries occur worldwide, leading to 5 million deaths [1]. Stroke is a neurodegenerative condition caused by the occlusion or rupture of cerebral arteries [2, 3]. Currently there is no cure for stroke, and the only FDA approved treatment is tissue plasminogen activator (tPA), a thrombolytic agent with limited therapeutic benefit[1].

An emerging trend in treating neurodegenerative disorders is the use of regenerative techniques [3-5]. One method for achieving regeneration is to stimulate endogenous stem cell proliferation and differentiation to promote repair. A population of neural stem cells and their progeny (together termed neural precursor cells, NPCs) are located in the subventricular zone (SVZ) of the lateral ventricles [6] and the dentate gyrus of the hippocampus [7]. Following stroke, there is an increase in proliferation of NPCs in the SVZ. In response to injury, the NPCs will migrate towards the site of injury <sup>3</sup>. However, the extent of regeneration after stroke is limited. It is proposed that administering exogenous factors could enhance this process and improve tissue regeneration.

A number of growth factors have shown benefits in animal models of stroke [8-11]; however, the methods of delivery are not ideal, thereby limiting clinical translation. Systemic delivery is inadequate because most drugs either cannot cross the blood-brain barrier (BBB) or lead to adverse systemic side effects at the high doses required [12]. Direct delivery to the tissue is not ideal because minipump/catheter systems are highly invasive when implanted in the brain and have the risk of infection. Therefore a minimally-invasive delivery strategy, such as a drug delivery scaffold placed on the brain, is required (**Fig. S2.1**).

We first sought to define protein diffusion in the brain to understand whether protein released at a distant tissue site would reach the target cells. Protein transport in the brain is predominantly governed by: the intrinsic diffusivity ( $D$ ) of the protein; tissue tortuosity ( $\lambda = (D/D^*)^{1/2}$  where  $D^*$  is

the protein's apparent diffusivity in brain); and removal from the diffusing protein population as denoted by the first order elimination rate constant  $k_e$  [13]. One challenge we face in developing a minimally invasive drug delivery system is that proteins are rapidly eliminated from the diffusion path *via* binding to the extracellular matrix (ECM) and cell surface receptors<sup>14</sup>. Following binding, proteins are taken up by cells, enzymatically degraded or removed to the systemic circulation [14]. This leads to only 1 – 2 mm penetration distances, which are often insufficient to reach the target site.

One strategy to improve protein penetration is to conjugate poly(ethylene glycol) (PEG) to the protein of interest to decrease its rate of elimination [15, 16]. PEG is a hydrophilic polymer that acts as a stealth agent to mask proteins from cellular/macrophage uptake and enzymatic degradation [17-21]. While reports to date have provided some promising results, previous studies on the diffusion of proteins in tissues and the effect of PEG modification did not quantify the effect of PEG modification on elimination rate. Moreover, these previous studies used mixed populations of proteins with different degrees of modification [22, 23], which complicates the analysis, making the effect of PEG modification difficult to assess.

Here we investigate the transport and elimination of recombinant human epidermal growth factor (rhEGF) and PEG-rhEGF in brain cortical tissue using *ex vivo* integrative optical imaging (IOI) [13]. This technique uses epi-fluorescent microscopy to determine transport properties of a diffusing protein population [13]. To the best of our knowledge, IOI has never been used to quantify protein elimination rate. Thus, our use of IOI to study drug elimination presents an important extension of this tool. Furthermore, IOI studies have not been previously conducted in brains with stroke injuries. However, given that neural injury, including stroke, affects the structural organization, cells and molecules in the brain tissue [4, 24-27], it is important to study the transport of proteins in both injured and uninjured tissue. To gain further insight into tissue

penetration, we compared the transport calculated in tissue slices to that in animals using a rhEGF ELISA.

Human EGF is a 6.2 kDa protein with three lysine amino acid residues, thus providing three amine groups as potential sites for PEG modification [28]. It is known that EGF induces proliferation of NPCs and stimulates generation of radial glial cells in the brain that support neuronal migration [29, 30]. Kolb *et. al.* showed that in an animal stroke model, infusion of rhEGF followed by erythropoietin into the lateral ventricle increased proliferation of NPCs and enhanced functional recovery [10].

We demonstrate that 5 kDa methoxy-PEG-propionaldehyde (mPEG-PPA) can be conjugated to rhEGF in a site-specific manner resulting in one of mono- (PEG<sub>1</sub>), di (PEG<sub>2</sub>), or tri- (PEG<sub>3</sub>) PEG<sub>x</sub>-rhEGF. Controlling the pH and reactant ratios results in higher yield than previously reported [31, 32]. Using IOI, we demonstrate that mono-PEG modification reduces the rate of rhEGF elimination. Moreover, we show that stroke injuries lead to lower tissue tortuosity and higher rates of irreversible protein binding/elimination. The effect of PEG modification on rhEGF penetration distance is confirmed *in vivo* using a mouse stroke model. These data demonstrate the potential to increase penetration distance, thereby allowing for a minimally invasive delivery strategy where the protein does not need to be injected directly into the brain tissue but instead can be applied at the surface following stroke.

## 2.3 Materials and Methods

### 2.3.1 Materials

Recombinant human epidermal growth factor (rhEGF) and the rhEGF ELISA detection kit were purchased from PeproTech Inc. (Rocky Hill, NJ, USA). Methoxy-poly(ethylene glycol, 5 kDa) activated with propionaldehyde (mPEG-PPA) or N-hydroxysuccinimide (mPEG-NHS) were purchased from NOF Corp. (Tokyo, Japan). Alexa Fluor 488-NHS, Alexa Fluor 488-hydrazide fluorescent dyes and 10x PBS buffered solution were obtained from Invitrogen Inc. (Burlington, ON, Canada). 4-(4,6-Dimethoxy-1,3,5-triazin-2-yl)-4-methylmorpholinium chloride (DMTMM), sodium cyanoborohydride ( $\text{NaCNBH}_3$ ), NaCl,  $\text{MgCl}_2$ ,  $\text{CaCl}_2$ ,  $\text{BaCl}_2$ ,  $\text{Na}_2\text{HPO}_3$ ,  $\text{NaH}_2\text{PO}_3$  TES, MES, ethylenediamine tetraacetic acid (EDTA), ethylene glycol-bis(2-aminoethyl)-N,N,N', N'-tetraacetic acid (EGTA), phenylmethanesulfonyl fluoride (PMSF), dithioereitol, sodium acetate buffer salts, and low electroendosmosis (low EEO) agarose were supplied by Sigma Aldrich (Oakville, ON, Canada). Artificial cerebrospinal fluid (aCSF) and all buffers were prepared with distilled and deionized water prepared from a Millipore Milli-RO 10 Plus and Milli-Q UF Plus at 18 M $\Omega$  ·m resistivity (Millipore, Bedford, USA). MicroBCA protein assay kit was obtained from Thermo Fisher Scientific (Rockford IL, USA.) and used as per the manufactures instructions.

### 2.3.2 PEG modification of rhEGF and purification of PEG<sub>x</sub>-rhEGF

The three primary amines on rhEGF allow PEG to be conjugated at up to three sites. The degree of PEG modification was controlled by pH since the N-terminus  $\alpha$ -amine has a pKa of 7.8 while the  $\epsilon$ -amines on Lys 28 and 48 have pKa's of 10.1<sup>253</sup>. Methoxy-PEG-propionaldehyde (mPEG-PPA) was used to synthesize PEG<sub>1</sub>-rhEGF and PEG<sub>2</sub>-rhEGF (**Fig. S2.2**). rhEGF was dissolved in 50 mM sodium acetate buffer (pH 5.0) to a final concentration of 1 mg/ml. 140 molar excess  $\text{NaCNBH}_3$  and either 3 (for PEG<sub>1</sub>-rhEGF) or 6 (for PEG<sub>2</sub>-rhEGF) molar excess of

mPEG-PPA were added to the solution. The reaction was agitated for 1 h and incubated at room temperature for 23 h. The product solution was dialysed against 20 mM pH 5.0 sodium acetate buffer in 3.5 kDa MWCO slide-a-lyzer dialysis cassettes (Thermo Scientific, Rockford, IL, USA.). Greater than 80% yield of a pure population of PEG<sub>1</sub>-rhEGF was obtained using 3 molar excess of mPEG-PPA and a mixed population of PEG<sub>1</sub>- and PEG<sub>2</sub>-rhEGF (referred to as PEG<sub>2</sub>-rhEGF) was produced using 6 molar excess mPEG-PPA.

Methoxy-PEG-N-hydroxysuccinimide (mPEG-NHS) was used to synthesize PEG<sub>3</sub>-rhEGF (**Fig. S2.2**). rhEGF was dissolved in 50 mM TES buffer (pH 8.6) to a final concentration of 0.33 mg/ml. Twenty-five molar excess of mPEG-NHS was added to the reaction mixture and the solution was agitated at room temperature for 2 h. Twenty-five molar excess of mPEG-NHS and 100  $\mu$ l of TES buffer were added to the solution every 2 h until a total of 100 molar excess of mPEG-NHS was reached. The NHS ester of PEG was selected for its higher reactivity compared to mPEG-PPA, and a pure population of pure PEG<sub>3</sub>-rhEGF was produced using these reaction conditions (**Fig. S2.3**).

Upon completion, unreacted PEG was separated from the reaction mixture using fast protein liquid chromatography (UPC 900/P-920, Amersham Pharmacia Biotech, Piscataway, NJ, USA) with an anion exchange column (Pharmacia Biotech MonoQ, column volume  $\sim$  7.7 ml). The ionic exchange gradient was set with a low-salt buffer (buffer A: 10 mM TES, pH 8.2) and a high-salt buffer (buffer B: 50 mM TES with 1 M NaCl, pH 8.2). Buffer A was first introduced into the column and a linear salt gradient up to 100% buffer B was established over 20 column volumes. The column was run with a flowrate of 2 ml/min. The purified product was analysed using gel electrophoresis (Bio-Rad Mini Format 1D electrophoresis system, Bio-Rad Laboratories, Mississauga, ON, Canada). The gel was stained for EGF using SimplyBlue SafeStain (Invitrogen, Burlington, ON, Canada) and then stained for PEG using a solution of 10%

BaCl<sub>2</sub>, 2.5% KI and 1.3% I<sub>(s)</sub> in distilled water. The gel images were taken on Bio-Rad Gel Doc XR 170-8170 and processed using Quantity One-4.6.1 software.

### 2.3.3 Fluorescent labeling of EGF and PEG-EGF

To allow real time imaging of protein transport, rhEGF and PEG<sub>x</sub>-rhEGF were fluorescently labeled with Alexa 488. The Alexa dye was chosen for its relative pH stability and photostability<sup>254</sup>. For rhEGF, PEG<sub>1</sub>-rhEGF and PEG<sub>2</sub>-rhEGF, 1.6 x 10<sup>-4</sup> M solutions of rhEGF or PEG<sub>x</sub>-rhEGF were mixed with 10 molar excess Alexa 488-NHS and the reaction was carried out for 2 h at room temperature. Unreacted dye was separated from fluorescent protein using a G25 Sephadex size exclusion column with 20 mM pH 7.4 PBS as running buffer. PEG<sub>3</sub>-rhEGF was conjugated with Alexa 488-hydrazide using a 100 molar excess DMTMM as the coupling reagent. 25 molar excess of the fluorescent dye was added to a 1.6 x 10<sup>-4</sup> M PEG<sub>3</sub>-rhEGF solution. The reaction mixture was agitated at room temperature for 24 h. Upon completion, excess Alexa 488 dye and DMTMM were separated from the product by dialysing the product solution against 50 mM TES buffer (pH 8.6) for 24 h.

The final protein concentration after fluorescent conjugation was determined by measuring the absorbance at 280 nm using NanoDrop ND-1000 spectrophotometer (NanoDrop, Wilmington, DE, USA.) and correcting for the absorbance of the dye<sup>255</sup>. The protein and dye concentrations were determined by Beer's Law at an absorbance wavelength of 280 nm and an extinction coefficient of 17780 M<sup>-1</sup>cm<sup>-1</sup> for rhEGF, and an absorbance at 495 nm and an extinction coefficient of 71,000 M<sup>-1</sup>cm<sup>-1</sup> for Alexa 488. The relative concentration of protein and fluorescent probe were used to determine the degree of fluorescent tagging. On average there is approximately one fluorescent molecule conjugated on each protein molecule (**Table S2.1**).

### **2.3.4 Mouse surgeries**

All experiments were carried out in accordance with the Guide to the Care and Use of Experimental Animals developed by the Canadian Council on Animal Care and approved by the Animal Care Committee at the University of Toronto. All animals used in this study were 8 – 10 week old C57BL/6 mice (Charles River, QC, Canada).

### **2.3.5 Mouse brain cortical slice preparations**

Mice were sacrificed by cervical dislocation, the brain removed and immersed in 4°C artificial cerebrospinal fluid (aCSF). The composition of aCSF is as follows: 124 mM NaCl; 5 mM KCl; 26 mM NaHCO<sub>3</sub>; 1.25 mM NaH<sub>2</sub>PO<sub>4</sub>; 1.3 mM MgCl<sub>2</sub>; 1.5 mM CaCl<sub>2</sub>; and 10 mM D-(+)-glucose bubbled with 95% O<sub>2</sub>/5% CO<sub>2</sub> (pH 7.0). Brains were mounted onto a specimen plate with the anterior of the brain pointed up with the dorsal surface of the brain perpendicular to the cutting blade and immersed in aCSF (4°C). Coronal slices 400 µm thick were prepared from the interaural 4-5 mm plane using a microtome sectioning system (Series 1000, LR59590, Vibratome, Richmond, IL, USA) with a speed of 2.5 and amplitude of 9.0. Slices were transferred to aCSF (4°C) and the temperature of the aCSF and brain slices were allowed to equilibrate to room temperature while bubbled with 95% O<sub>2</sub>/5% CO<sub>2</sub>. Individual slices were transferred to a Lab-Tek® II chambered #1.5 coverglass system and aCSF (37°C) was added to the chamber immediately before imaging.

### **2.3.6 Cortical slice viability**

The viability of cortical slices over time was determined using the lactate dehydrogenase (LDH) cytotoxicity detection kit (Roche Canada). Briefly, 400 µm cortical tissue slices were obtained and kept in oxygenated aCSF at room temperature. The slices were removed and placed into 48-well tissue culture plates at various times between 1 and 8 h post sacrifice. Slices were incubated for 1 h at room temperature in 500 µl aCSF without oxygenation to imitate the microinjection environment. One hundred µl of the supernatant was then removed and the cytotoxicity assay was carried out according to the manufacturer's instructions. To determine the maximum concentration of LDH in cells, freshly prepared cortical slices were homogenized in 500 µl aCSF with 1.0 mm diameter Zirconia beads (BioSpec Products, 11079110zx, Bartlesville, OK, USA.) using a Mini BeadBeater tissue homogenizer (Biospec). The LDH assay was performed on the homogenate. All measurements were normalized to the homogenate LDH concentration. Measurements at all time points were performed on two slices from two individual animals.

### **2.3.7 Stroke Surgeries**

Stroke surgeries were carried out as described by Tennant *et. al.*<sup>256</sup>. Mice were anesthetised with isoflurane, shaved and placed into a Kopf stereotaxic instrument. A midline incision in the scalp was made. A small burr hole was made in the skull at the coordinates 2.25 lateral to the midline and 0.6 anterior to the Bregema. Using a 26G needle, endothelin-1 (400 pmol, Calbiochem, Gibbstown, NJ, USA.) was injected 1.0 ventral to the surface of the brain at a rate of 0.1 µl/min with a total volume of 1 µl. The needle was left in place for 10 min prior to removal to minimize back flow. The incision was sutured, antibiotic ointment applied and the animal left

to recover under a heat lamp. Animals were sacrificed 4 d post stroke and the cortical slices were prepared as described above for uninjured tissue.

### 2.3.8 Integrative optical imaging (IOI) to calculate protein diffusivity

Integrative optical imaging (IOI) was used to study the diffusion of proteins in *ex vivo* brain cortical slices as previously reported<sup>142,154,257</sup>. All protein samples were diluted with aCSF to a final protein concentration of  $1.8 \times 10^{-4}$  M prior to IOI. Intrinsic diffusivity ( $D$ ) of rhEGF and PEG<sub>x</sub>-rhEGF was determined through IOI in 0.3% agarose gel. The apparent diffusivities in brain were determined using 400  $\mu$ m thick uninjured or stroke-injured mouse brain slices saturated with 0.1 mg/ml non-fluorescent rhEGF solution. This concentration was selected to ensure saturation of the cell-surface rhEGF receptors such that there is no elimination of fluorescently labeled proteins from the diffusion path. Finally to study the elimination of rhEGF and PEG<sub>x</sub>-rhEGF in tissue, IOI was conducted in cortical tissue slices without pre-saturation.

A Nanoliter 2000 microinjection system (World Precision Instruments, Sarasota, FL, USA) was used to routinely inject 4.6 nl of fluorescently labeled protein solution into either agarose (**Fig. 2.1a**) or brain cortical slices at a depth of  $\sim 200\mu$ m in the barrel field and trunk region of the primary somatosensory cortex, layers III-VI<sup>258</sup>. A minimum of 25 injections were made for each protein species in every diffusing medium. For diffusion in tissue, a minimum of 6 tissue slices prepared from 3 animals were used for each group. A fine-tip glass capillary with 1.2 mm outside diameter and 4" length (World Precision Instruments, 1B120-4) was fire-polished to produce tips with 5  $\mu$ m inside diameter (PUL 100 vertical pipette puller, World Precision Instrument) and used for injection. The evolution in the fluorescence over time was observed using a Zeiss Axio Observer Z1 epi-fluorescence microscope and captured with a Hamamatsu 13940RCA-ERA camera at 2 s interval. The intensity profiles of the diffusing source along a

fixed axis were generated using the ImageJ (Image Processing and Analysis in JAVA, <http://rsbweb.nih.gov/ij>) analysis software, and quantitative analyses were conducted using Origin8 (OriginLab Corp.) and MATLAB (MathWorks).

### 2.3.9 Image analysis and mathematical modeling for estimating rate of elimination and protein penetration distance

Integrative optical imaging uses a point source-protein delivery, where the relationship between the diffusing protein concentration and the distance travelled at given time points is described by (Eq. 2-1) <sup>142</sup>:

$$C_{free}(r,t) = \frac{UC_p \lambda^3}{\alpha [4D\pi(t+t_o)]^{3/2}} \exp\left(\frac{-\lambda^2 r^2}{4D(t+t_o)}\right) \exp[-k_e(t)] \quad \text{Equation 2-1}$$

where  $C_{free}(r,t)$  is the free ECS protein concentration,  $U$  is the volume of protein solution injected,  $C_p$  is the concentration of injected protein solution,  $\alpha$  is the volume fraction of ECM in the brain, typically assumed to be 0.2 <sup>142</sup>;  $r$  is the radial distance away from the injection site,  $t$  is the time elapsed since injection, and  $t_o$  is the time required for a point source with a radius of zero to spread to the area that the protein occupies at the point of injection ( $t = 0$ ).

In the absence of protein elimination from the diffusion pathway (i.e.  $k_e = 0$ ), the intensity profile of the protein in the diffusing medium can be correlated to the effective diffusivity using the following set of equations (Eq. 2-2) <sup>142</sup>:

$$I_i(r, \gamma_i) = E_i \exp \left[ - \left( \frac{r}{\gamma_i} \right)^2 \right] \quad \text{Equation 2-2a}$$

$$\gamma_i = [4D \cdot (t + t_o)]^{1/2} \quad \text{Equation 2-2b}$$

where  $I_i(r, \gamma_i)$  is the intensity at a radial distance away from the source measured by IOI and  $E_i$  is a de-focused point-spread function of the objective <sup>142</sup>. Numerical values of  $I_i$  were generated using ImageJ along an axis through the fluorescent image as a function of time and radial distance from the centre (**Fig. 2.1a**), and the profile may be fitted in Origin 8 to generate the values of  $\gamma_i$  at specific time points (**Fig. 2.1b**). Graphing  $\gamma_i^2/4$  (normalized such that the plot passes through the origin) vs.  $t$  yields a linear plot with gradient equal to the effective diffusivity  $D$  in the appropriate medium in the absence of elimination (**Fig. 2.1c**). A time frame of 30 s, over which the  $\gamma_i^2/4$  vs.  $t$  plot remains linear, is typically used for determining the values of  $D$ . The tortuosity experienced by each protein species is determined from the diffusivities in the agarose and saturated cortical slices, as  $\lambda = (D/D^*)^{1/2}$  <sup>142</sup>.

When the protein is eliminated from the ECS during diffusion, the plot of  $\gamma_i^2/4$  can be normalized to the diffusivity ( $D$ ), and the  $\gamma_i^2/4D$  vs.  $t$  yields a curve that deviate from linearity (**Fig. 2.2b**), indicating the effect of protein elimination. In this case we need to account for the contributions to total fluorescent intensity by both proteins in the ECS and the irreversibly-bound, non-mobile proteins. This may be estimated as (Eq. 2-3):

$$I(r, t) = I_o C_{free}(r, t) + \epsilon I_o C_{bound}(r, t) \quad \text{Equation 2-3}$$

where  $I_o$  is the proportionality constant between the local fluorescence intensity and protein concentration. Once the values of  $D$  and  $\lambda$  have been obtained using IOI in agarose and

saturated tissue, we can estimate  $I_o$  by calculating the area under the fluorescent intensity peak at  $t_o$ . The approximate value of  $I_o$  determined here is approximately 0.1 – 0.5 nl/nmol·AU, where AU is the arbitrary fluorescent intensity units. The parameter  $\varepsilon$  accounts for the decrease in detected intensity upon internalization. Since the time required for rhEGF/EGF receptor complex internalization varied between 5 – 30 min depending on the tissue type<sup>259</sup>, which exceeds the time scale of IOI (3 min), we assumed the value of  $\varepsilon$  to be 1. From simple mass balance, the irreversibly-bound protein concentration  $C_{bound}(r,t)$  may be described by (Eq. 2-4):

$$C_{bound}(r,t) = k_e \int_0^t C_{free}(r,t) dt \quad \text{Equation 2-4}$$

Combining Eqs. 1, 3 and 4, an expression for the evolution in spatial fluorescence profiles is obtained (Eq. 2-5):

$$I(r,t) = \frac{I_o C_p U \lambda^3}{\alpha [4\pi D(t+t_o)]^{3/2}} \exp\left[-\frac{\lambda^2 r^2}{4D(t+t_o)}\right] \exp[-k_e(t)] + \varepsilon I_o k_{bound} \int_0^t \frac{C_p U \lambda^3}{\alpha [4D(t+t_o)]^{3/2}} \exp\left[-\frac{\lambda^2 r^2}{4D(t+t_o)}\right] \exp[-k_e(t)] dt \quad \text{Equation 2-5}$$

We numerically solve this equation using MATLAB to obtain the values of  $k_e$  since all other parameters may be either obtained from literature or determined experimentally. For each set of intensity profiles, the value of  $k_e$  is iterated between 0 and  $10^{-1} \text{ s}^{-1}$  with an increment of  $10^{-7} \text{ s}^{-1}$ . The fitted value of  $k_e$  yielding the least squares residual (LSR) from the experimental data is taken to be the elimination constant.

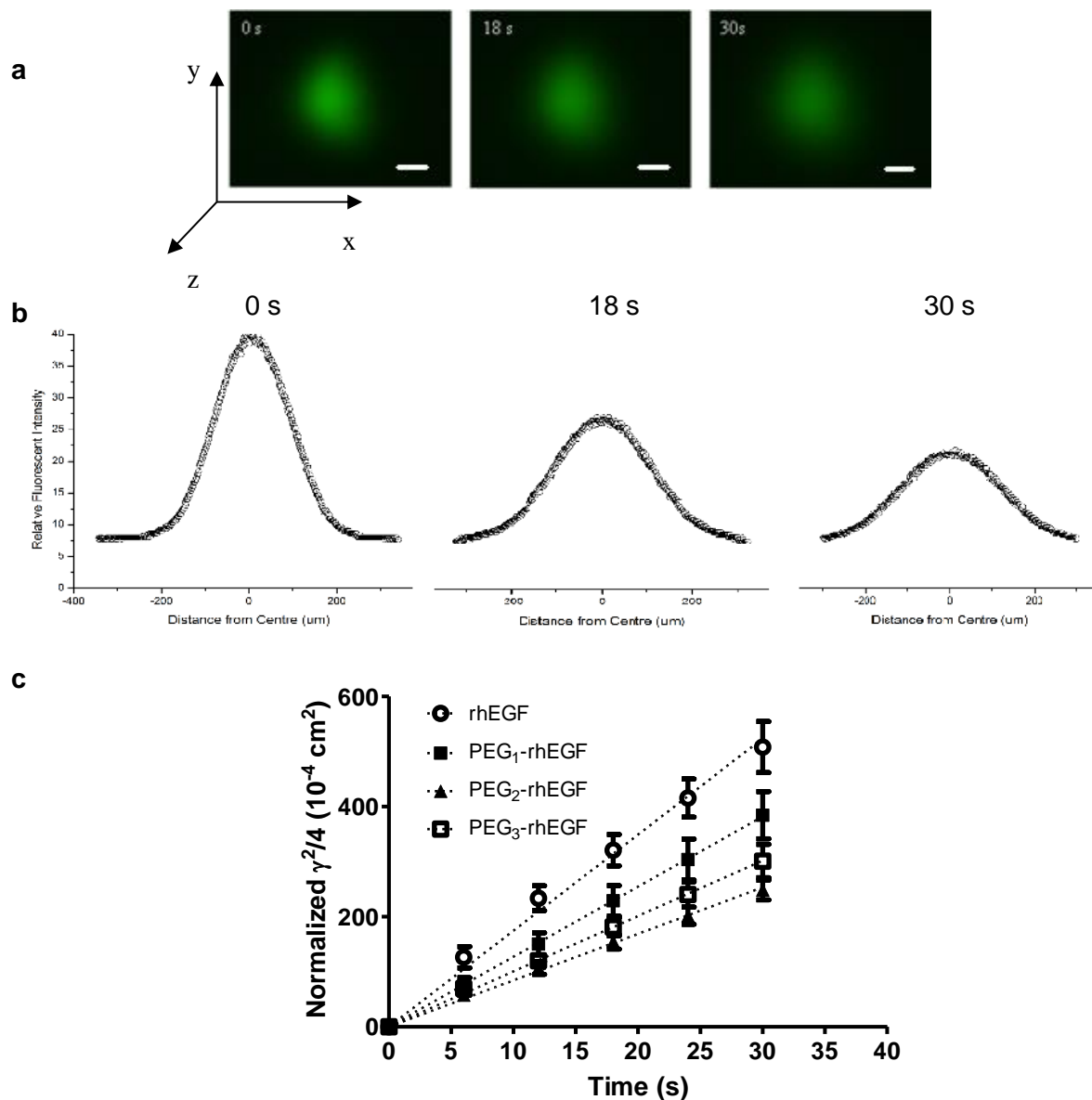


**Figure 2.1 / Progression of rhEGF and PEG-rhEGF fluorescence intensity in dilute agarose following injection.** (a) Representative images showing diffusion of fluorescently labelled rhEGF in dilute agarose. (b) Fluorescence intensity profiles obtained from images are fitted to Eq. 2, where the vertical axis represents the fluorescent intensity in arbitrary units and the horizontal axis represents distance from the centre of the fluorescence. All images are shown at the same magnification (scale bar =  $100\mu\text{m}$ ). (c) Representative graph showing plot of  $\gamma^2/4$  ( $10^{-7}\text{cm}^2$ ) vs. time (s) for (○) rhEGF, (■) PEG<sub>1</sub>-rhEGF, (▲) PEG<sub>2</sub>-rhEGF, and (□) PEG<sub>3</sub>-rhEGF in agarose where values of  $\gamma^2/4$  were obtained from fitting data to Eq. 2, and the gradient of the plot returns a value of  $D$  ( $10^{-7}\text{cm}^2/\text{s}$ ).

We confirmed the method validity using agarose and saturated tissue. Since both agarose and saturated brain tissue should yield values of  $k_e$  equal to zero for any diffusing species, they serve as appropriate controls for the system. For rhEGF and PEG<sub>x</sub>-rhEGF, the values of  $k_e$  calculated by the model were indeed 0 s<sup>-1</sup>, confirming the validity of the model.

To ensure accuracy in fitting, the model-generated values of  $k_e$  were used, along with experimental values of  $D$  and  $\lambda$ , to reproduce the series of theoretical intensity profiles with respect to time. These theoretical profiles were again fitted to Eq. 2.2 in Origin® to produce theoretical plots for  $\gamma^2/4D$  vs. time, which were compared with experimentally-derived plots of  $\gamma^2/4D$  vs. time (**Fig. S2.4**). Good agreement was found between all model fits and experimental data.

A polymer scaffold represents a constant source of protein drugs on top of the brain cortex, and the steady state concentration profile of the protein in the tissue can be represented as (Eq. 2-6)

141,260.

$$\frac{C}{C_o} = \exp\left(-\sqrt{\frac{k_e}{D}} \lambda x\right) \quad \text{Equation 2-6}$$

where  $C/C_o$  is the normalized concentration of protein at a certain distance,  $x$ , away from the source. Eq. 6 allows us to predict how far a protein can penetrate in the brain in the presence of a constant source before its concentration drops below the therapeutic threshold. Calculations are accurate to  $\pm 15\%$ , as estimated by error propagation theory<sup>261</sup>.

### **2.3.10 Total cell count in pre- and post-stroke brains**

Four days following stroke, mice were transcardially perfused, the brains were removed and cryoprotected overnight in 20% sucrose. Brains were sectioned coronally at 15µm sections using a cryostat and placed on X slides. Sections were viewed under a light microscope (Olympus CKX41). The lesion cavities were measured using ImageJ 1.38X to determine the epicenter of the lesion and pictures were taken of sections at the epicentre, 300µm rostral and 300µm caudal to the epicentre, using SonyI IDC version 1.2.0.2. Equivalent anatomical sections in control animals were stained with DAPI mounting media and coverslipped. The medial, ventral, and lateral areas surrounding the lesion cavity, contralateral cortex, or uninjured cortex were photographed using a fluorescent microscope (Zeiss Stemi 2000, KL1500 LCD) under 10X magnification. The total numbers of nuclei were counted per 276.25mm<sup>2</sup> per region. Comparisons between the counts obtained from the lesioned, contralateral, and uninjured cortices were made by ANOVA using GraphPad Prism.

### **2.3.11 Real time RT-PCR to detect EGFR upregulation post stroke**

The upregulation of EGFR following stroke injuries was investigated using real-time RT-PCR. Uninjured control animals and animals with 4 day stroke injuries were sacrificed, and the brains were harvested and divided along the midline to obtain the ipsilateral and contralateral hemispheres. Tissues were homogenized using Zirconia beads in a Mini BeadBeater tissue homogenizer. Extraction of mRNA was carried out as per the manufacturer's instructions (RNeasy Lipid Tissue Mini Kit, Qiagen) and OligodT primers were used to synthesize cDNA as per the manufacturers' instructions (AffinityScript Multi Temperature cDNA synthesis kit, Agilent Technologies). The following primers were used for cDNA amplification: 5'-GAA CTG GGC TTA GGG AAC TGC-3' (EGFR forward); 5'-CAT TGG GAC AGC TTG GAT CAC-3' (EGFR

reverse)<sup>262</sup>. The house keeping gene used was hypoxanthine phosphoribosyltransferase (HRPT): 5' – CTC ATG GAC TGA TTA TGG ACA GGA C – 3' (forward) and 5' – GCA GGT CAG CAA AGA ACT TAT AGC C – 3' (reverse), Real-time RT-PCR was carried out using Lightcycler 480 II (Roche) with the following cycle: 95°C; 60°C; 72°C. A melt curve and gel electrophoresis were carried out to verify primer specificity.

### **2.3.12 *In vivo* penetration distance of rhEGF and PEG<sub>1</sub>-rhEGF**

The *in vivo* penetration distance of rhEGF and PEG<sub>1</sub>-rhEGF in brain tissue was measured using uninjured animals. Mice were anesthetised with isoflurane and a small burr hole was made in the skull at the coordinates 2.25 lateral to the midline and 0.5 anterior to Bregema. A 30 gauge sterile Hamilton syringe was inserted 1.0 mm into the cortex and 0.5 µl of either protein or control solutions was injected. The injections were made at a rate of 0.1 µl/min, the needle was left in place for 10 min to reduce back flow, and the needle was retracted over 5 min. Treatment groups include sterile-filtered rhEGF or PEG<sub>1</sub>-rhEGF solutions (8 x 10<sup>-5</sup> M), saline controls, and mPEG-propionaldehyde dissolved in saline controls (8 x 10<sup>-5</sup> M). Mice injected with protein solutions or control solutions were sacrificed at immediately (15 min), 4, and 24 h post injection.

Brains were extracted and snap frozen using CO<sub>2(s)</sub> cooled isopropane and stored at -80°C. Three 1 mm coronal slices were prepared, at the injection site and rostral and caudal to the injection site. Coronal slices were prepared using McIlwain tissue chopper (790744-11, Mickle laboratory engineering company, Surrey, UK). Dorsal-ventral sections (0.5 mm) were then obtained from each coronal slice using Leica CM3050S cryostat system operating at -18°C. Each 0.5 mm section was transferred into 2 ml polystyrene microtubes (Sarstedt 72.694.006, Montreal, Quebec, Canada) and 200 µl homogenizing buffer (20 mM HEPES, 10 mM KCl, 1.5 mM MgCl<sub>2</sub>, 1 mM EDTA, 1 mM EGTA, 1 mM dithiothreitol, 1 mM PMSF) was added to each

tube. Tissue sections were homogenized with 1.0 mm diameter zirconia beads. To remove tissue fragments, homogenized tissue was centrifuged at 15,000 RPM for 15 min at 4°C and the homogenate was transferred into 1.75 ml Eppendorf tubes. 200 µl ELISA diluent solution was used to dilute homogenate to a total volume of 400 µl.

ELISAs were performed as per manufacturer's instructions on the homogenate solutions to determine the concentration of rhEGF at different depths from the cortical surface. Recombinant human EGF ELISA detection kit was used to avoid cross-contamination with endogenous mouse EGF. Protein concentrations detected in each animal were normalized to the amount of protein detected at the initial time to construct the diffusion profiles. A mass balance on the tissue rhEGF content showed that immediately post injection, approximately 90% of the injected protein was accounted for. The detectable concentration of proteins decreased over time, likely due to enzymatic degradation. Control groups injected with either saline solution or PEG dissolved in saline did not show detectable rhEGF concentrations at any of the time points studied (data not shown).

### **2.3.13 Bioactivity assay for neural stem cell response towards EGF and PEG<sub>x</sub>-EGF**

The bioactivity of rhEGF released from the DDS was determined *in vitro* using mice neural stem cell cultures. Neural stem cells were isolated from the subventricular zone (SVZ) of 9 week old male C57/BL6 mice and grown in 25 cm<sup>2</sup> tissue culture flasks (Corning CLS430639, Sigma Aldrich, Oakville, ON, Canada). Cells were passaged every 7 days for two weeks. Neurospheres were dissociated and plated in tissue culture treated 96-well plates (Corning CLS3696, Sigma Aldrich) at an initial cell density of 10 cells/µl in SFM and a total volume of 100 µl. rhEGF or PEG<sub>x</sub>-rhEGF solutions were diluted in serum free culture media (SFM, 30% glucose, 7.5% NaHCO<sub>3</sub>, 0.5% HEPES, 1% L-glutamine, 10% hormone mix, 1% Pen/Strep, 10%

DMEM/F12, 74% dH<sub>2</sub>O) and added to each well to a final concentration of 3.2 nM. The cells were incubated for 7 days at 37°C without media change, following which MTT assays were performed to evaluate metabolic activities of cells in culture.

#### 2.3.14 Statistical analysis

The distribution of data was determined by the Kolmogorov-Smirnov normality test. For normally distributed data, comparisons between multiple groups were conducted using ANOVA. For pair-wise comparison of normally distributed data, t-test was carried out. For comparison of data that were not normally distributed, the Mann-Whitney-U test with Bonferonni correction was used<sup>263</sup>. Significance levels were indicated by  $p < 0.05$  (\*), 0.01 (\*\*), and 0.001 (\*\*\*).

## 2.4 Results

### 2.4.1 The effect of PEG on the intrinsic diffusivity of rhEGF in agarose

Fluorescently-labeled rhEGF and PEG<sub>x</sub>-rhEGF (**Fig. S2.1, S2.2** and **Table S2.1**) were separately injected into 0.3% agarose gels to study their intrinsic diffusivities. Dilute agarose gel was used to mimic a non-tortuous diffusing medium while avoiding convection. To calculate diffusivity, we injected fluorescently labeled proteins and monitored their intensity profiles over 30 s (**Fig. 2.1a, b**). By plotting the  $y^2/4$  parameter vs. time (Eq. 2) protein diffusivity was calculated from the slope, as shown in **Fig. 2.1c**. The intrinsic diffusivity ( $D$ ) of rhEGF in agarose was  $16.8 \times 10^{-7} \text{ cm}^2/\text{s}$  whereas that of PEG<sub>x</sub>-rhEGF, where  $x = 1, 2, \text{ or } 3$ , was significantly less at  $13.2 \times 10^{-7} \text{ cm}^2/\text{s}$  ( $P < 0.001$ ),  $8.88 \times 10^{-7} \text{ cm}^2/\text{s}$  ( $P < 0.001$ ), and  $7.68 \times 10^{-7} \text{ cm}^2/\text{s}$  ( $P = 0.0328$ ), respectively (**Fig. 2.1c, Table S2.2**). The decrease in intrinsic diffusivity of rhEGF with increasing PEG modification was likely due to its increase in hydrodynamic radius ( $R_H$ ).

## 2.4.2 Transport of rhEGF and PEG<sub>x</sub>-rhEGF in uninjured brain cortical slices

To understand the effect of tissue tortuosity on rhEGF vs. PEG<sub>x</sub>-rhEGF diffusion independent of receptor binding, the EGF receptors (EGFR) of uninjured mouse brain cortical tissue slices were saturated with non-fluorescently-tagged rhEGF prior to the study. We also ensured that all brain tissue slices were > 90% viable for over 8 h, which is longer than the duration of the diffusion study (**Fig. S2.5**). The apparent tissue diffusivity  $D^*$  of rhEGF ( $5.01 \times 10^{-7} \text{ cm}^2/\text{s}$ ) decreased with PEG modification for PEG<sub>1</sub>-rhEGF ( $3.34 \times 10^{-7} \text{ cm}^2/\text{s}$ ), PEG<sub>2</sub>-rhEGF ( $2.09 \times 10^{-7} \text{ cm}^2/\text{s}$ ) and PEG<sub>3</sub>-rhEGF ( $1.66 \times 10^{-7} \text{ cm}^2/\text{s}$ ) (**Fig. 2.2a, Table S2.2**). There was a significant difference in  $D^*$  between all groups except for PEG<sub>2</sub>-rhEGF and PEG<sub>3</sub>-rhEGF ( $P = 0.103$ ), likely due to an insignificant difference in  $R_H$  between PEG<sub>2</sub>-rhEGF and PEG<sub>3</sub>-rhEGF <sup>264,265</sup>.

The tortuosity ( $\lambda$ ) experienced by proteins in brain tissue was also calculated. In uninjured tissue, rhEGF experiences a  $\lambda$  of 1.83 whereas PEG<sub>x</sub>-rhEGF had a  $\lambda$  of 1.99, 2.06, and 2.15 for  $x = 1, 2, 3$ , respectively. Thus, the diffusion of smaller rhEGF is obstructed significantly less by the brain tissue than the larger, PEG-modified rhEGF ( $p < 0.001$ ).

The apparent diffusivity was calculated in tissue with elimination, where the tissue slices were not pre-saturated with non-fluorescent rhEGF. As in the case of pre-saturated tissue, the plot of  $\gamma^2/4$  over 30 s revealed a significant decrease in  $D^*$  from rhEGF to PEG<sub>3</sub>-rhEGF ( $P = 0.0054$ , **Fig. 2.2a, Table S2.2**). The diffusivity of each protein species, however, was lower than in the former case. This decrease in apparent diffusivity likely reflects the binding of rhEGF to the ECM. Importantly, this decrease was dramatic for rhEGF (from  $5.01 \pm 0.88$  for saturated to  $2.22 \pm 0.32 \text{ cm}^2/\text{s}$  in non-saturated uninjured brain tissue) and insignificant for PEG-modified rhEGF (e.g., from  $3.34 \pm 0.52$  to  $2.64 \pm 0.35 \text{ cm}^2/\text{s}$ ), which suggests that PEG modification reduces the reversible binding of rhEGF to the ECM.

While the gradient of  $\gamma^2/4D$  vs. time in saturated tissue remained linear, that in tissue with elimination deviated from linearity between 30 and 60 s, demonstrating the effect of protein elimination (**Fig. 2.2a**). In *ex vivo* tissue slices with elimination, although enzymatic degradation occurs over longer time scales<sup>266</sup>, it is likely that rhEGF is primarily removed through either irreversible binding to the tissue, or cellular uptake. In an IOI experiment, this leads to the immobilization of the fluorescently-tagged growth factors, and thus a reduction in the slope of the  $\gamma^2/4D$  vs. time curve.

Using the diffusivity and tortuosity determined above, we calculated the protein elimination rate constant  $k_e$  for rhEGF and PEG<sub>x</sub>-rhEGF in uninjured tissue. This was achieved by fitting fluorescent intensity profiles in tissue with elimination over 3 min to Eq. 5 using MATLAB. Parameters used in the model are listed in **Table S2.3**. The  $k_e$  of rhEGF in uninjured tissue was determined to be  $52.0 \times 10^{-4} \text{ s}^{-1}$  (**Table 2.1**) and those of PEG<sub>x</sub>-rhEGF were  $2.14 \times 10^{-4} \text{ s}^{-1}$ ,  $1.95 \times 10^{-4} \text{ s}^{-1}$ , and  $1.45 \times 10^{-4} \text{ s}^{-1}$  for  $x = 1, 2, 3$  ( $P < 0.001$  for all 3 groups compared against rhEGF). The greatest difference in terms of reducing the rate of protein binding was between rhEGF and PEG<sub>1</sub>-rhEGF, with a diminishing effect with di- and tri-PEG modification. This illustrates that PEG modification led to significantly slower protein elimination.

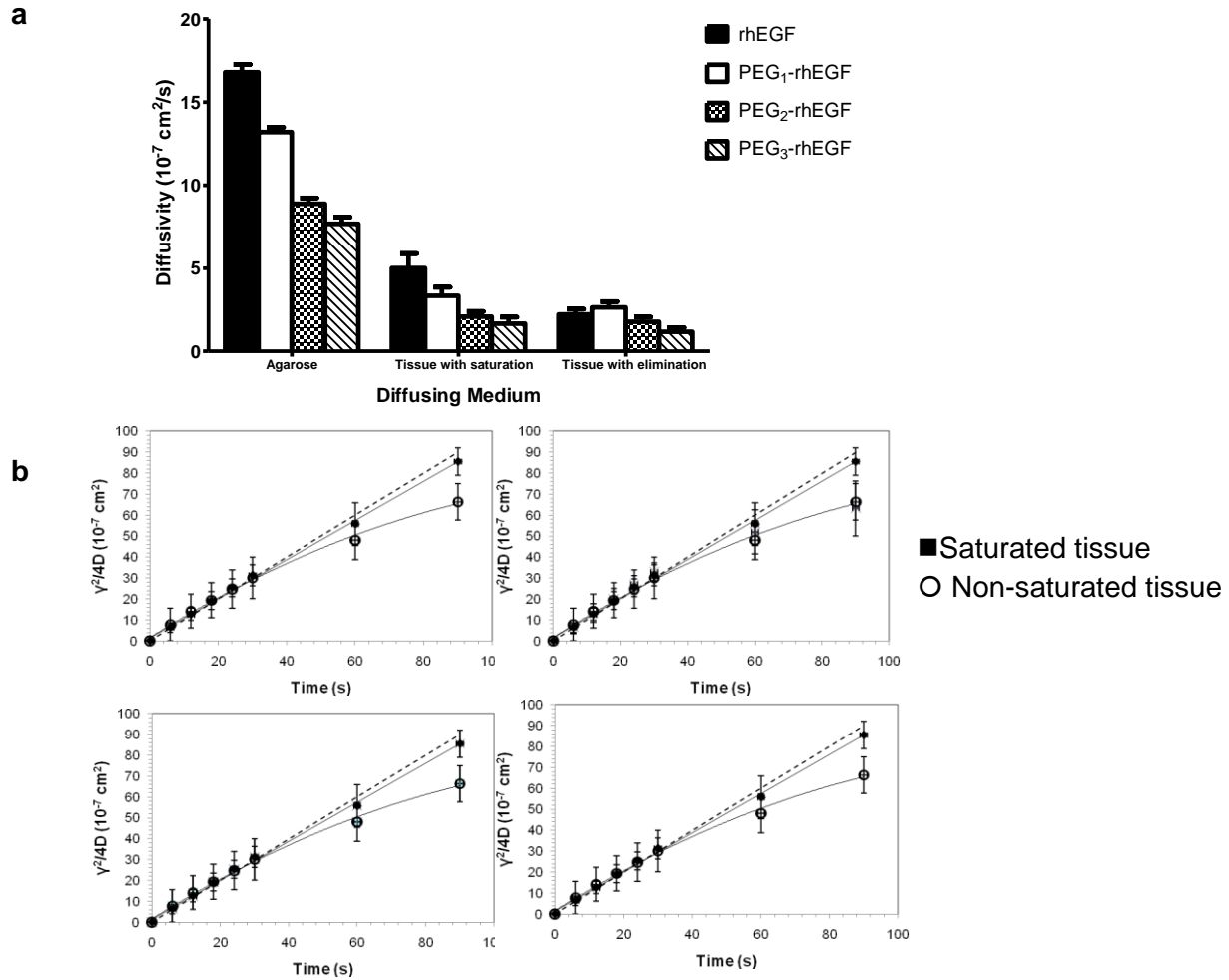


**Figure 2.2 | PEG modification decreases diffusivity of rhEGF in saturated brain tissue.** (a) Diffusivities for rhEGF and PEG<sub>x</sub>-rhEGF are determined in agarose, saturated and non-saturated cortical tissue in uninjured animals. (b) Representative  $y^2/4D$  vs. time plots of (i) rhEGF, (ii) PEG<sub>1</sub>-rhEGF, (iii) PEG<sub>2</sub>-rhEGF, and (iv) PEG<sub>3</sub>-rhEGF diffusion in (■) saturated and (○) non-saturated tissue. Plot is linear in saturated tissue but deviates from linearity in non-saturated tissue.

**Table 2.1 | Elimination rate constants in uninjured and stroke brains.** Values of  $k_e$  were obtained by numerically solving Eq. 5 using the parameters listed in Table 4. Values are reported as mean  $\pm$  s.d. ( $n = 25$ ).

Sample	Elimination Rate ( $k_e$ ( $10^{-4}$ s $^{-1}$ ))		
	Ipsilateral to stroke injury	Contralateral to stroke injury	Uninjured Brain Cortical Slices
rhEGF	659 $\pm$ 26.1† **	193 $\pm$ 21.2† **	52.0 $\pm$ 1.01† **
PEG <sub>1</sub> -rhEGF	29.0 $\pm$ 2.99 **	19.7 $\pm$ 1.76 **	2.14 $\pm$ 0.24 **

†Values are significantly different from other values in the same column at  $p < 0.05$ .

\*\*Values are significantly different from other values in the same row at  $p < 0.05$ .

### 2.4.3 Transport of rhEGF and PEG<sub>x</sub>-rhEGF in brain with stroke injury

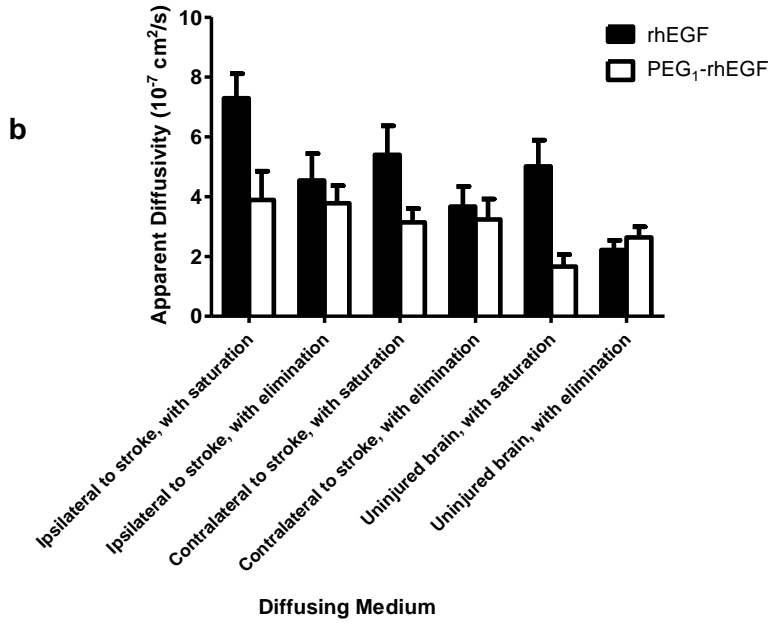
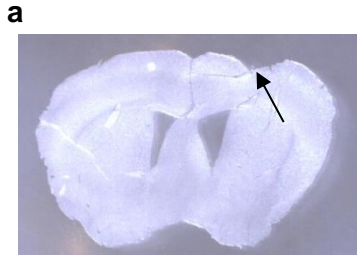
To better understand the diffusion in brain tissue following stroke injury, the endothelin-1 (Et-1) stroke-injury model was used<sup>267,268</sup> and tissue slices were taken after 4 days following the induction of stroke (**Figure 2.3a**), thereby mimicking the time period previously studied for the delivery of rhEGF<sup>22</sup>. Given that proteins maintain bioactivity better after conjugation with one PEG compared to multiple PEG chains<sup>269</sup>, and a significant reduction in the rate of protein elimination ( $k_e$ ) for PEG<sub>1</sub>-rhEGF was observed relative to rhEGF, the transport of rhEGF and PEG<sub>1</sub>-rhEGF were compared in stroke-injured brain tissues (**Fig. 2.3a, Table S2.4**). As predicted from diffusivity data in agarose and uninjured tissue,  $D_{rhEGF}^*$  exceeded  $D_{PEG1-rhEGF}^*$  in saturated tissue both ipsilateral ( $P < 0.001$ ) and contralateral ( $P = 0.007$ ) to the stroke injury. In saturated tissue,  $D_{rhEGF}^*$  ipsilateral to stroke was higher than both  $D_{rhEGF}^*$  contralateral to stroke ( $P = 0.0043$ ) and  $D_{rhEGF}^*$  in uninjured brain ( $P = 0.002$ ); yet no significant difference was observed for  $D_{rhEGF}^*$  between the contralateral hemisphere and the uninjured brain ( $P = 0.554$ ). These data indicate that stroke injury leads to change in tissue tortuosity.

To further investigate the effect of PEG modification on rates of rhEGF elimination in injured tissue, we calculated  $k_e$  both ipsilateral and contralateral to the stroke injury (**Table 2.1**).

Consistent with observations in uninjured tissue, the  $k_e$  of PEG<sub>1</sub>-rhEGF is 23-fold lower than rhEGF in tissue ipsilateral to stroke ( $29.0 \times 10^{-4} \text{ s}^{-1}$  vs.  $659 \times 10^{-4} \text{ s}^{-1}$ , respectively) and 10-fold lower in tissue contralateral to stroke ( $19.7 \times 10^{-4} \text{ s}^{-1}$  vs.  $193 \times 10^{-4} \text{ s}^{-1}$ , respectively). This demonstrates that PEG modification reduces the rate of protein removal from diffusion.

The difference observed for  $D_{PEG_1-rhEGF}^*$  in stroke vs. uninjured brains is likely due to a change in tissue composition following injury, discussed below. The tortuosity experienced by both rhEGF and PEG<sub>1</sub>-rhEGF was lower in ipsilateral stroke injury tissue than both contralateral stroke injury tissue and uninjured brain tissue (**Fig. 2.3c**). Changes in tissue tortuosity could result from either changes in cell density or changes in the ECM. We determined that the total number of cells in stroke injured brains and non-stroke brains were not significantly different between stroke ipsilateral, stroke contralateral and uninjured brain tissues (**Fig. 2.3d, e**).

We used real time RT-PCR to examine EGFR mRNA expression in the tissue. The results demonstrate that EGFR mRNA is significantly upregulated ipsilateral to the stroke injury compared to uninjured brain tissue ( $P = 0.014$ ; **Fig. 2.3f**), which could be accounted for by the increased expression in the ECM or cellular diversity within the injured tissue. EGFR expression contralateral to stroke does not differ significantly from uninjured controls ( $P = 0.166$ ). These data are consistent with the differences in tortuosity observed for rhEGF and PEG<sub>1</sub>-rhEGF; however, they do not account for the differences observed for  $k_e$  ipsilateral and contralateral to stroke that are both significantly higher than that in uninjured brains (**Table 2.1**) for EGF and PEG<sub>1</sub>-EGF. These data suggest that EGF/EGFR binding likely accounts for some, but not all, of the mechanisms influencing  $k_e$ .



**c**

Sample	Calculated Tortuosity ( $\lambda = (D/D^*)^{1/2}$ )		
	Ipsilateral to Stroke	Contralateral to Stroke	Uninjured Tissue
rhEGF	1.52 ± 0.12 †**	1.76 ± 0.19 †**	1.83 ± 0.18 †**
PEG <sub>1</sub> -rhEGF	1.84 ± 0.25 **	2.05 ± 0.16	1.99 ± 0.16 **

† Values are significant different from other values in the same column at  $p < 0.05$ .

\*\* Within each row, values indicated are significantly different at  $p < 0.05$ .

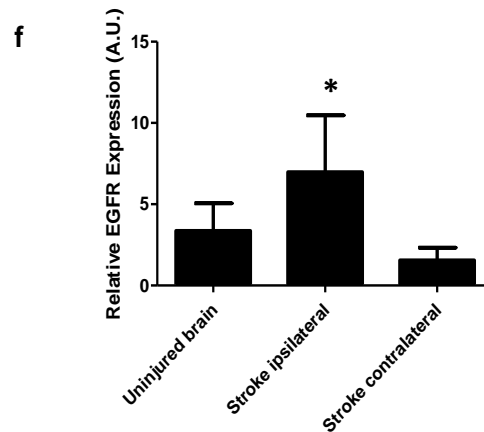
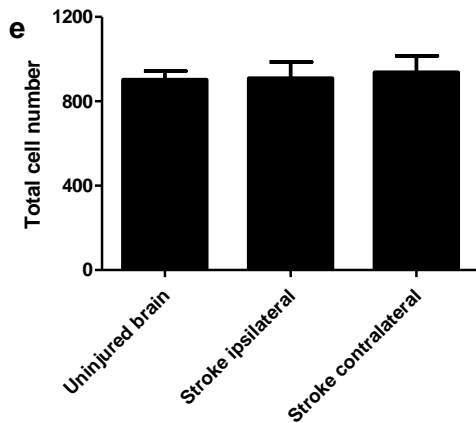
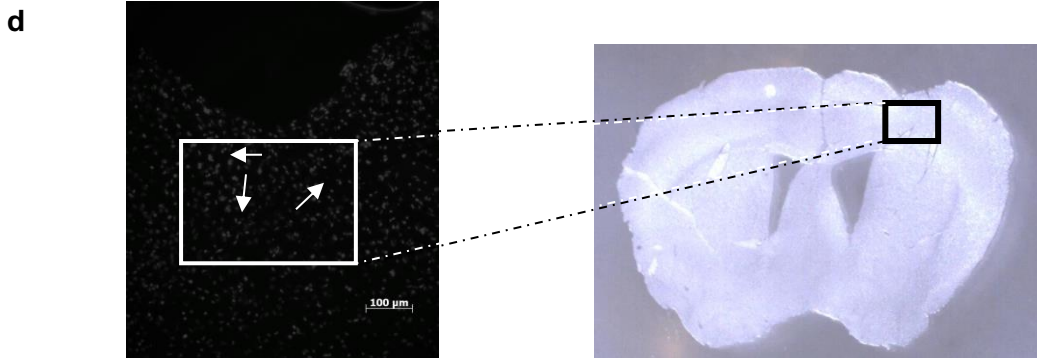


**Figure 2.3 / PEG modification decreases diffusivity of rhEGF in saturated brain tissue.** (a) Microscope image showing a mouse brain coronal section with the site of stroke injury indicated by black arrow, under 10X magnification. (b) PEG modification decreases diffusivity of rhEGF in brain with stroke. The effect of mono-PEG modification of rhEGF on tissue diffusivities is studied in ipsilateral and contralateral sides of stroke, as well as that in the absence and presence of elimination are also determined. (c) Calculated tortuosity of rhEGF and PEG<sub>1</sub>-rhEGF in tissue. Tortuosity values are reported as mean  $\pm$  s.e.m. (n = 25). Differences between bars with the same letter are not statistically significant while bars with different letters differ significantly. (d) Total cell number as determined by DAPI stain (scale bar = 100  $\mu$ m). Arrows represent DAPI stained cells. (e) Total cell number is not elevated either ipsilateral or contralateral to stroke compared to uninjured controls. Cell counts are shown as mean  $\pm$  s.e.m. (n = 9). (F) EGFR gene expression is upregulated post stroke in the ipsilateral cortex. Real time RT-PCR results show that following stroke, the EGFR expression is upregulated ipsilateral to injury (P = 0.014).

#### 2.4.4 Calculated penetration distance for rhEGF and PEG<sub>x</sub>-rhEGF in brain cortical tissue

Based on the experimental  $D$ ,  $\lambda$  and  $k_e$  values, we calculated the theoretical distance that rhEGF and PEG<sub>1</sub>-rhEGF would diffuse in the cortex. Because this distance will depend on the duration of delivery, we analyze two limiting cases: (1) a pulse injection, as done in the case IOI; and (2) a constant source, as in the case of an ideal drug delivery scaffold. Because all drug delivery vehicles perform between these two limits, these calculations provide the “best- and worst-case” estimates on the theoretical diffusion distance. In each case, the penetration distance was estimated based on concentration of the free protein in the extracellular space,  $C_{free}(r, t)$ , using Eq. 2.1 for the pulse injection and Eq. 2.6 for the constant source (**Fig. 2.4a**). A meaningful estimation of penetration distance requires that the amount of protein reaching the target site maintains therapeutic benefit. Since NSCs proliferate *in vitro* at an rhEGF concentration of 3.2 nM (20 ng/ml)<sup>270</sup> and we found no difference in bioactivity between rhEGF and PEG<sub>1</sub>-rhEGF at this concentration (**Fig. S2.6**), this value was used as  $C_{free}(r, t)$  in Eqs. 1 and 6 to estimate rhEGF penetration distance.

In each case the penetration distance achieved from a constant source was greater than that achieved from a pulse injection (**Tables 2.2a** and **2.2b**). The penetration distance of PEG<sub>1</sub>-rhEGF was also greater than that of rhEGF, regardless of the tissue type. In uninjured brain, we calculate that rhEGF penetrates 1.5 – 1.8 mm while PEG<sub>1</sub>-rhEGF penetrates to a distance to 4.4 – 7.0 mm. In injured tissue, rhEGF penetrated the tissue to 0.00 – 0.59 mm ipsilateral to stroke, likely due to rapid elimination, whereas PEG<sub>1</sub>-rhEGF diffused 1.7 – 2.5 mm. Similarly, rhEGF penetrated 0.87 – 0.95 mm and PEG<sub>1</sub>-rhEGF penetrated 1.8 – 2.3 mm in contralateral stroke-injured tissue. These results show that PEG modification increases the penetration distance of rhEGF, which falls within the range predicted by previous modeling studies <sup>154</sup>.

**Table 2.2 | Predicted penetration distance from a point source (a) and a constant source (b) by rhEGF and PEG<sub>1</sub>-rhEGF in uninjured and stroke brains.** Distances travelled are presented in units of millimetres. Diffusion is assumed to stop when concentration is less than 3 nM, which is the minimum EGF concentration required to stimulate NPCs in vitro.

**a**

Sample	Penetration Distance from Point Source (mm)		
	Ipsilateral to stroke injury	Contralateral to stroke injury	Uninjured Brain Cortical Slices
rhEGF	†	0.87	1.5
PEG <sub>1</sub> -rhEGF	1.7	1.8	4.4

† Value is negligible

**b**

Sample	Penetration Distance from Constant Source (mm)		
	Ipsilateral to stroke injury	Contralateral to stroke injury	Uninjured Brain Cortical Slices
rhEGF	0.59	0.95	1.8
PEG <sub>1</sub> -rhEGF	2.5	2.3	7.0

#### 2.4.5 *In vivo* penetration distance of rhEGF and PEG<sub>1</sub>-rhEGF

To confirm our model predictions, we investigated the *in vivo* penetration distance of rhEGF and PEG<sub>1</sub>-rhEGF in uninjured mouse brains. Bolus injections of protein solutions were made into the somatosensory cortex at the same coordinates used for Et-1 injections. The brains were then harvested and sectioned to analyse the rhEGF concentration at various depths by ELISA. We examined the diffusion profile of both native and PEG-modified rhEGF upon immediate sacrifice, and at 4 and 24 hours after injection of the protein solutions (**Fig. 2.4b**). Immediately after injection we find the highest concentrations of both rhEGF and PEG<sub>1</sub>-rhEGF at the site of injection (0.5 - 1 mm below the cortical surface). At 4 h after injection, rhEGF reaches a peak concentration at a depth of 1.0 – 1.5 mm from the cortical surface whereas PEG<sub>1</sub>-rhEGF is found at a depth of 1.5 – 2.0 mm, demonstrating greater tissue penetration than native rhEGF. At 24 h after injection, the diffusion profile of rhEGF is similar to that at 4 h ( $P = 0.594$ ) suggesting that a large fraction of the rhEGF is not freely diffusing between 4 and 24 h. In contrast, PEG<sub>1</sub>-rhEGF penetrates significantly deeper by 24 h ( $P = 0.003$  compared to 4 hours) with the peak concentration found at 2.0 – 2.5 mm and significant concentration of PEG<sub>1</sub>-rhEGF detected at 2.5 – 3.0 mm. The greater tissue penetration observed for PEG<sub>1</sub>-rhEGF vs. rhEGF is consistent with our model predictions.

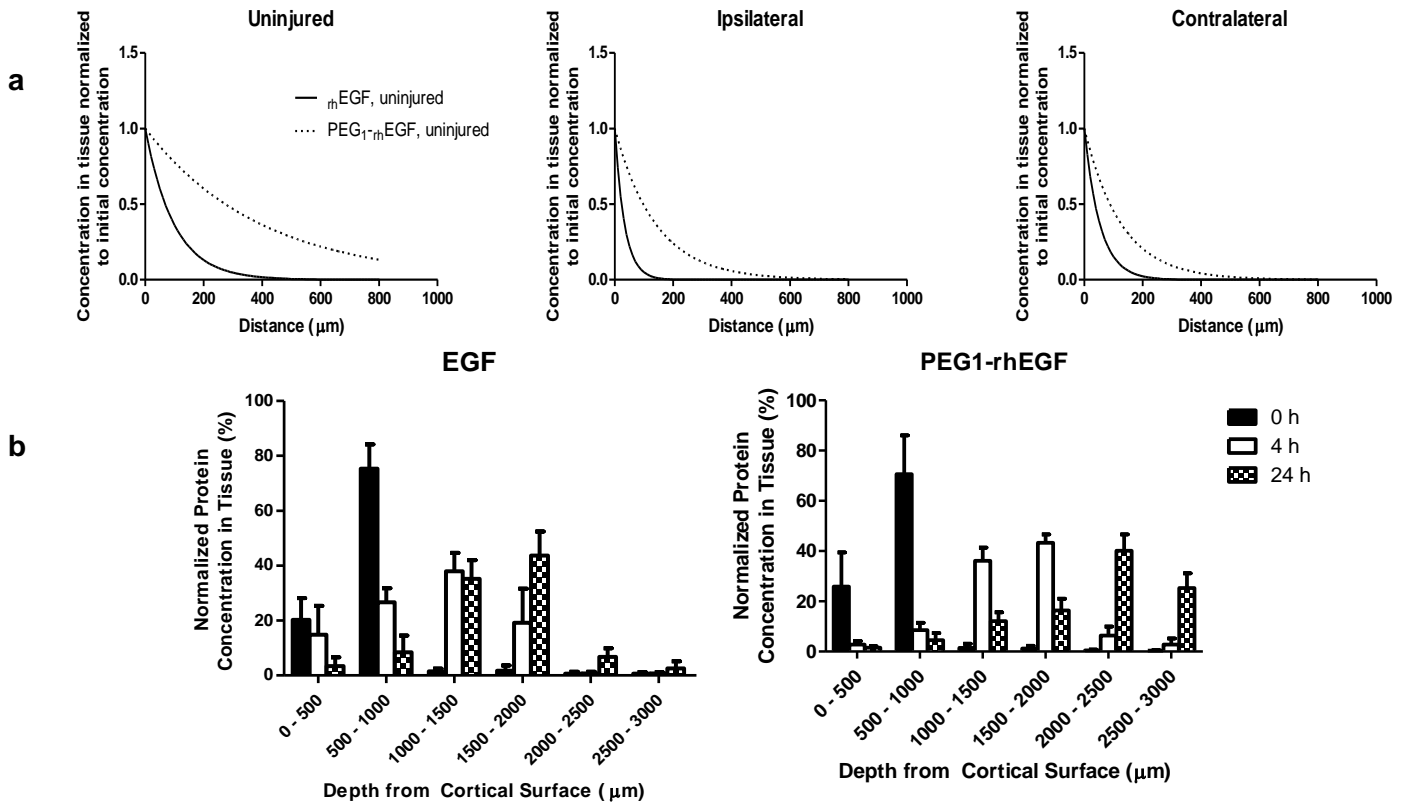


**Figure 2.4 | PEG modification increases the predicted penetration distance of rhEGF, assuming constant source of protein.** (a) Predicted penetration distances for PEG<sub>1</sub>-rhEGF (dashed line) and rhEGF (solid line) in uninjured tissue, ipsilateral to stroke, and contralateral to stroke calculated using Eq. 6 (Methods). (b) PEG modification increases in vivo penetration distance of rhEGF following bolus injection. 0 h post injection, both rhEGF and PEG<sub>1</sub>-rhEGF show maximum concentration at the site of injection (depth of 0.5 – 1 mm below the cortical surface). 4 h post injection, rhEGF shows peak concentration at 1.5 mm ventral to cortical surface while PEG<sub>1</sub>-rhEGF concentration peaks at 2.0 mm. At 24 h post injection, rhEGF peak concentration occurs at similar depths as that at 4 h ( $P = 0.594$ ), while PEG<sub>1</sub>-EGF shows significantly further penetration compared to EGF. Values are reported as mean  $\pm$  s.d. ( $n = 4$ ).

## 2.5 Discussion

Stroke-injured brains differ from uninjured brains in cell and molecular composition as well as tissue organization<sup>95,271-273</sup>. For both rhEGF and PEG<sub>1</sub>-rhEGF, we found  $D^*$  ipsilateral to stroke to be higher than that in uninjured brain. This suggests that the tissue surrounding the stroke

site loses integrity following injury and the diffusing proteins encounter less tortuous resistance. Since the total cell counts in brain tissue pre- and post-stroke injury are similar, the difference in tortuosity may be due to changes in the brain ECM.

Both the intrinsic and apparent diffusivities of rhEGF in uninjured brain measured herein are consistent with values previously reported in the literature<sup>142</sup>. PEG modification of rhEGF leads to an increase in protein hydrodynamic radius, which results in decreased diffusivity<sup>166</sup>: the  $R_H$  of rhEGF increases approximately by a factor of 1.5 with the addition of one 5 kDa PEG chain, by an additional factor of 1.2 with the second 5 kDa PEG chain, and by smaller increments with subsequent PEG additions<sup>265,274</sup>.

While some reports have suggested that PEG modification is detrimental towards protein/receptor interactions, the specific influence of PEG modification is protein specific and concentration dependent<sup>269</sup>. Lee *et. al.* showed that at concentrations above 1 nM, there was no significant difference in the binding affinity of EGFR to rhEGF and PEG<sub>1</sub>-rhEGF<sup>171</sup>. We also found with an *in vitro* bioactivity assay that there is no difference in the metabolic response of NPCs to rhEGF or PEG<sub>1</sub>-rhEGF at concentration of approximately 3 nM. Since rhEGF signaling relies on the binding between rhEGF and the extracellular domain of EGFR, this suggests that although PEG modification may retard the binding rate, the rhEGF/EGFR binding affinity is not significantly decreased. Moreover, the reduced rate of protein binding may be compensated through longer tissue residence time afforded by modification with PEG<sup>269</sup>.

It is known that PEG masks protein surfaces against phagocytosis and enzymatic degradation, and may reduce protein interactions with cells and other ECM components in the diffusion path<sup>265,275</sup>. To the best of our knowledge,  $k_e$  for rhEGF in the brain has not been reported. Using a pure population of PEG-modified proteins and IOI, we quantitatively show for the first time that

PEG modification leads to reduced rates of protein removal and increased protein penetration distances. In the context of IOI, protein elimination refers to the removal of protein from the diffusion pathway. Therefore  $k_e$  represents the rate of rhEGF/EGFR complex formation, non-specific rhEGF binding to the ECM, as well as endocytosis. Enzymatic degradation is not considered here because the time scale required exceeds that of IOI. The rhEGF/EGFR binding involves complex enzyme kinetics and the reported complex formation rates vary from  $5 \times 10^{-2} \text{ s}^{-1}$  to  $3 \times 10^{-4} \text{ s}^{-1}$  <sup>276</sup>. The rate of internalization following complex formation has also been investigated in a number of tissue types <sup>277-281</sup> and shown to vary between  $5 \times 10^{-4} \text{ s}^{-1}$  and  $6 \times 10^{-3} \text{ s}^{-1}$ . Therefore our value of  $k_{e, rhEGF}$  ( $5.2 \times 10^{-3} \text{ s}^{-1}$ ) in uninjured brain fall within these ranges and is a reasonable estimate.

Using IOI we found that binding of both rhEGF and PEG<sub>1</sub>-rhEGF occurs most rapidly ipsilateral to stroke, with significantly slower elimination in uninjured tissue. This is likely because EGFR is upregulated after injury <sup>259,282</sup>. Interestingly, while the rate of elimination contralateral to stroke is lower than that ipsilateral to stroke, it is higher than elimination in uninjured brain tissue. This was unexpected since the contralateral side is often used as a control in studying disorders of the brain. Buga *et. al.*, however, found changes in gene expression profiles contralateral to stroke relative to uninjured tissues in aged animals <sup>271</sup>. This suggests that the contralateral hemisphere in stroke animals is also affected by stroke and not identical to uninjured brain tissue. Real time RT-PCR demonstrated that EGFR over-expression was observed ipsilateral, but not contralateral, to the injury. Thus while rhEGF/EGFR complex formation contributes to the change in  $k_e$ , it is not the sole determinant. Global changes in growth factor expression following stroke, for example, may facilitate other mechanisms that contribute to the increase in contralateral  $k_e$ , including changes in the ECM that lead to higher levels of non-specific protein adhesion to ECM components, as well as protein uptake by inflammatory cells.

The values of  $k_e$  reported here show that PEG modification can overcome the rapid elimination of protein drugs in diseased brains. Our results demonstrate the need to study protein transport in injured or diseased brain tissue (relative to control uninjured brains) because the rate of elimination impacts penetration distance and changes with tissue type. Rapid removal leads to shallow penetration distances and impacts the efficacy of drug delivery strategies.

The penetration distances calculated from IOI were confirmed *in vivo*. Between 4 and 24 h after a bolus injection of protein solutions, the PEG<sub>1</sub>-rhEGF showed a 1.0 mm increase in penetration distance while the rhEGF itself demonstrated only a small change in tissue penetration distance. This suggests that more rhEGF was removed from the diffusing population compared to PEG<sub>1</sub>-rhEGF. Our results are consistent with previous data showing increased penetration distance due to PEG modification. For example, Soderquist *et al.* illustrated that PEG-modification of brain derived neurotrophic factor (BDNF) enhanced its *in vivo* half-life and tissue penetration<sup>283</sup>. Stroh *et al.* showed qualitatively that native BDNF undergoes negligible diffusion in the brain while a mixed population of PEG-BDNF, with various degrees of PEG modification, demonstrated significantly increased penetration<sup>257</sup>. Belcheva *et al.* demonstrated similar results where PEG-conjugated nerve growth factor improved its pharmacokinetic performance in the brain<sup>284</sup>. Similarly, Kang *et al.* found that conjugation of 5 kDa PEG to basic fibroblast growth factor (bFGF) increases its penetration distance in the spinal cord tissue<sup>285</sup>. In a related study, using dextran instead of PEG, Krewson *et al.* demonstrated that conjugation of a polymer to nerve growth factor increased tissue penetration<sup>286</sup>. Our finding demonstrates that PEG modification may enable the development of a less invasive strategy for delivering proteins to sites deep in the brain. PEG modification of growth factors provides a promising strategy for achieving minimally invasive and targeted protein therapy.

## 2.6 Conclusion

Current drug delivery strategies suffer from either an inability to obtain delivery profiles for optimum therapeutic efficacy or do not afford the level of minimal-invasiveness required in clinical applications. Quantification of the elimination constant demonstrated that PEG modification of rhEGF results in greater penetration in brain cortex. The calculated penetration distance was confirmed *in vivo* as PEG-modified rhEGF diffused deeper than the native form. While the actual penetration distance following release from a scaffold will be lower than that predicted by the constant source model due to protein depletion at the source, our findings suggest that the use of a controlled release, minimally-invasive drug delivery system of PEG-rhEGF holds promise for strategies to repair the injured brain, including the stimulation of endogenous neural precursor cells.

### **3 Controlled epi-cortical delivery of epidermal growth factor for the stimulation of endogenous neural stem cell proliferation in stroke-injured brain\***

\*This chapter was published in Biomaterials.

**Wang, Y.<sup>2</sup>; Cooke, M.J.<sup>3</sup>; Morshead, C.M.; Shoichet, M.S.** 2011. "***Controlled epi-cortical delivery of epidermal growth factor for the stimulation of endogenous neural stem cell proliferation in stroke-injured brain***" *Biomaterials*, 32: 5688-97.

#### **3.1 Abstract**

One of the challenges in treating central nervous system (CNS) disorders is minimizing the invasiveness associated with drug delivery. Stroke is the third leading cause of death in the industrialized world and currently has no effective treatment. Stimulation of endogenous neural stem/progenitor cells (NSPCs) by growth-factor treatment is a promising strategy for tissue regeneration. Epidermal growth factor (EGF) enhances proliferation of endogenous NSPCs in the subventricular zone (SVZ) when delivered directly to the ventricles of the brain; however, this strategy is highly invasive. To take advantage of endogenous stem cell stimulation for tissue repair, we designed a novel method to deliver molecules directly to the brain without tissue damage, thereby obviating the need to cross the blood-brain barrier. EGF or poly(ethylene glycol)-modified EGF (PEG-EGF) was dispersed in a hydrogel blend of hyaluronan and methylcellulose (HAMC) and placed epi-cortically on both uninjured and stroke-injured mouse brains. Moreover, PEG-modification decreased the rate of EGF degradation by proteases, leading to a significant increase in protein accumulation at greater tissue depths than previously shown, corresponding to that of the SVZ. EGF and PEG-EGF increased NSPC proliferation in uninjured and stroke-injured brains; and in stroke injured brains, PEG

---

<sup>2</sup> Contribution by Y. Wang: designed and conducted all in vitro and in vivo experimental work; collected, analyzed, and interpreted data from experiments; prepared the manuscript.

<sup>3</sup> Cooke and Wang are joint first authors on this manuscript

modification significantly increased NSPC stimulation. Our epi-cortical delivery system is a minimally-invasive method for local delivery to the brain, overcoming brain tissue damage that results from cannula insertion into the ventricle and providing a new paradigm for local delivery to the brain.

### **3.2 Introduction**

Effective treatment of disorders in the central nervous system (CNS), including the brain and the spinal cord, remain highly challenging today. This is partly due to the difficulties associated with delivering drugs to the CNS in a controlled and minimally invasive manner. Localized delivery is currently achieved in clinical studies using an osmotic minipump system<sup>287</sup>, but prolonged use of this system significantly increases the invasiveness of surgeries as well as the risks of infection<sup>288-290</sup>. Alternative strategies, such as systemic delivery, are limited by the blood-brain barrier (BBB), which prevents most systemically administered drugs from penetrating into the brain<sup>131,291</sup>. Those molecules that can cross the BBB are required in such high doses to achieve therapeutic levels in the brain that undesired systemic side effects result. There is demand for a delivery strategy that enables localized, sustained release to the brain without tissue damage.

Stroke is currently the third leading cause of death in the industrialized world, leading to 15 million injuries and 5 million deaths each year<sup>105</sup>. It is caused by the occlusion or rupture of cerebral arteries. While there is currently no effective treatment for stroke, tissue regeneration by endogenous stem cell stimulation holds promise<sup>22,292</sup>. This neuroregenerative approach may be facilitated by delivering growth factors to stimulate proliferation of endogenous stem cells in the brain. The neural stem cell niche in the subventricular zone (SVZ) is located along the walls of the lateral ventricles of the brain<sup>101,293,294</sup>. Following stroke, neural stem/progenitor cells (NSPCs) in the SVZ are stimulated to proliferate, but at insufficient levels to regenerate

damaged tissue <sup>295,296</sup>. Therapeutic factors infused into the ventricles of the brain promote endogenous stem cell activation, as has been shown with numerous factors, including: epidermal growth factor (EGF) <sup>22,297</sup>, erythropoietin (EPO) <sup>22</sup>, nerve growth factor (NGF) <sup>298</sup>, cyclosporine A <sup>292</sup>, colony stimulating factor (CSF) <sup>299</sup>, and basic fibroblast growth factor (bFGF) <sup>298</sup>.

Recombinant EGF administered intracerebroventricularly via an osmotic minipump system enhances the proliferation of endogenous NSPCs in the SVZ <sup>22</sup>. The resulting functional recovery in a rodent stroke model is highly promising <sup>22</sup>, but prolonged use of the osmotic minipump system is damaging towards brain tissue.

With the aim of designing a minimally-invasive system for sustained drug release to the brain, we developed a polymeric drug delivery vehicle comprised of a physical blend of hyaluronan (HA) and methylcellulose (MC), termed HAMC <sup>220</sup>. It is an injectable shear thinning hydrogel that is inversely thermal gelling, with MC forming hydrophobic physical crosslinks at reduced temperature due to the presence of HA, while retaining its ability to flow due to the shear thinning property of HA. HAMC gels upon injection into physiological environments, thus minimizing the need for invasive surgeries. HAMC has previously been shown to deliver proteins directly to the injured spinal cord <sup>300</sup>. In this report we examined the use of HAMC as a minimally invasive drug delivery vehicle to the brain and evaluated whether remote delivery of EGF would stimulate the endogenous stem cells in the SVZ.

To achieve local delivery to the brain, without injection directly into brain tissue, EGF in HAMC was deposited directly on the cortical surface within a drug delivery casing, which spatially confined HAMC and EGF to the target site (**Fig. 3.1**). While this is less invasive than direct injection into the ventricles of the brain, it was not known whether this remote mode of delivery

would allow proteins to diffuse through the cortical tissue to reach the SVZ. Diffusion of proteins in the brain tissue is primarily dependent on intrinsic diffusivity of the protein, tissue tortuosity, and protein elimination from the diffusion path. A combination of these factors limits protein diffusion distance in the brain to 1 – 2 mm<sup>260</sup>, while the SVZ resides approximately 2.5 – 3 mm below the cortical surface<sup>301</sup>. This penetration distance is inadequate for reaching the SVZ, thus severely impeding the development of an epi-cortical delivery system. N-terminus modification of EGF with a 5 kDa poly(ethylene glycol) (PEG) molecule increases the *in vivo* diffusion distance following bolus injection<sup>302</sup>.

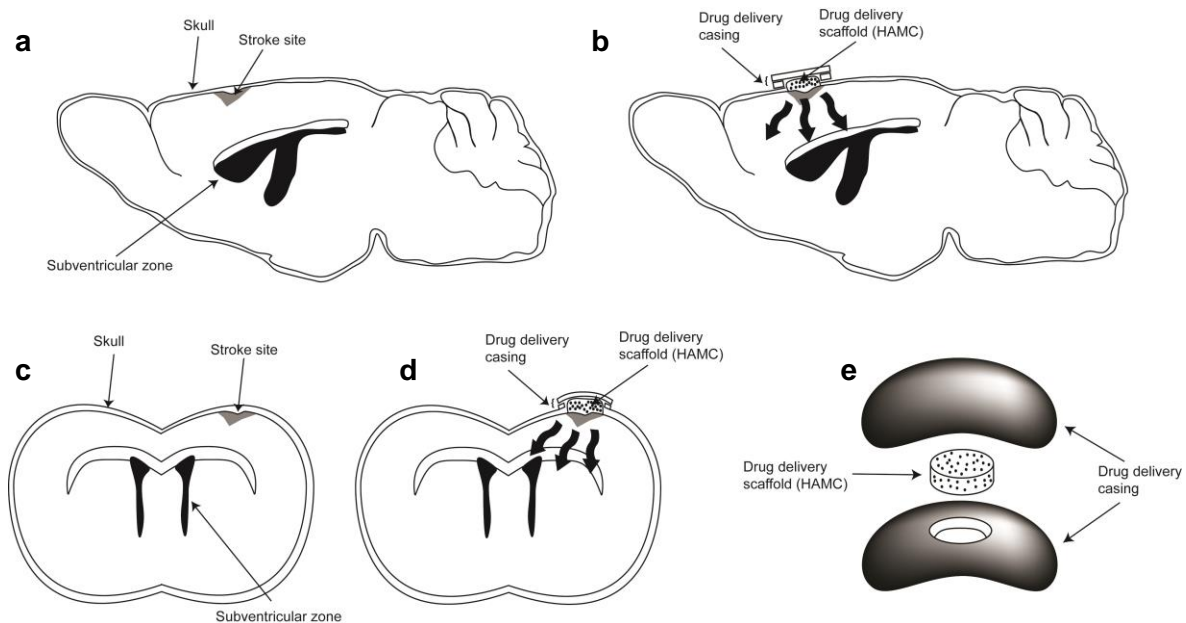


**Figure 3.1 | Schematic for localized and sustained delivery of drugs to the brain.** (a) Sagittal view of stroke-injured mouse brain with (b) drug delivery system. (c) Coronal view of stroke-injured mouse brain with (d) drug delivery system. (e) Drug delivery system in expanded view.

Here we investigated the penetration distance of EGF and mono-PEG-modified EGF (PEG-EGF) in uninjured and stroke-injured mouse brains following epi-cortical delivery from HAMC. Compared to EGF, we observed significantly greater amounts of PEG-EGF after 2 days at a depth of 3000  $\mu\text{m}$  (or 3 mm) from the cortex surface. To gain insight into the mechanism accounting for differences in tissue penetration, brain extracts were examined for proteolytic

degradation; we found that PEG modification significantly reduced EGF degradation. In both uninjured and stroke-injured brains, epi-cortical delivery of EGF and PEG-EGF resulted in enhanced cell proliferation, while in stroke-injured brains PEG-EGF significantly increased proliferation. These results demonstrate that HAMC can serve as a drug delivery vehicle for epi-cortical delivery to the brain, and that PEG-modification enhances the delivery of remotely delivered proteins, allowing deep penetration into the tissue.

### **3.3 Materials and Methods**

#### **3.3.1 Materials**

1.4-1.8 x 10<sup>6</sup> g/mol sodium hyaluronan (HA) was purchased from NovaMatrix (Sandvika, Norway). 3.4 x 10<sup>5</sup> g/mol methylcellulose (MC) was obtained from Shin Etsu (Chiyoda-ku, Tokyo, Japan). Recombinant human epidermal growth factor (EGF) and the EGF ELISA detection kit were purchased from PeproTech Inc. (Rocky Hill, NJ, USA). Methoxy-poly(ethylene glycol, 5 kDa) activated with propionaldehyde (mPEG-PPA) was purchased from NOF Corp. (Tokyo, Japan). Mouse anti-human Ki-67 and mouse anti-rat nestin were purchased from BD biosciences (Mississauga, ON, Canada), mouse anti-rat GFAP was obtained from Millipore Inc. (Billerica, MA, USA), rabbit anti-mouse Ki-67 and rabbit anti-mouse double-cortin were obtained from Abcam (Cambridge, MA, USA), and Vectashield with DAPI stain was purchased from Vectorlabs (Burlington, ON, Canada). Alexa 488 and Alexa 564 goat-anti-rabbit IgG, and Alexa 488 and Alexa 568 goat-anti-mouse IgG were obtained from Invitrogen Inc. (Burlington, ON, Canada). Sodium cyanoborohydride (NaCNBH<sub>3</sub>), NaCl, MgCl<sub>2</sub>, CaCl<sub>2</sub>, BaCl<sub>2</sub>, Na<sub>2</sub>HPO<sub>3</sub>, NaH<sub>2</sub>PO<sub>3</sub>, TES, MES, ethylenediamine tetraacetic acid (EDTA), ethylene glycol-bis(2-aminoethyl)-N,N,N', N'-tetraacetic acid (EGTA), phenylmethanesulfonyl fluoride (PMSF), dithioereitol, sodium acetate buffer salts, and protease inhibitor panel were supplied by Sigma Aldrich (Oakville, ON, Canada). Artificial cerebrospinal fluid (aCSF<sup>303</sup>) and all buffers were

prepared with distilled and deionized water prepared from a Millipore Milli-RO 10 Plus and Milli-Q UF Plus at 18 MΩ ·m resistivity (Millipore, Bedford, USA). MicroBCA protein assay kit was obtained from Thermo Fisher Scientific (Rockford IL, USA) and used as per the manufactures instructions.

### **3.3.2 Preparation of sterile HAMC**

HA and MC were dissolved in dH<sub>2</sub>O, sterile-filtered and lyophilized under sterile conditions. The resulting sterile polymers were kept at 4 °C until use. HAMC was produced with 1 w/v% HA and 2 w/v% MC dissolved in sterile aCSF, mixed using a (SpeedMixer DAC 150 FVZ, Siemens) and centrifuged to remove air bubbles. Subsequently, 10 µl of 1.6 mM solutions of EGF or PEG-EGF was added to 900 µL HAMC, mixed and centrifuged to eliminate air bubbles.

### **3.3.3 In vitro release of EGF and PEG-EGF from HAMC**

To estimate the time required for EGF and PEG-EGF to diffuse from the HAMC implant *in vivo*, we studied their release from HAMC *in vitro*. 100 µl of HAMC containing 0.16 mM of either EGF or PEG-EGF was injected into the bottom of a 2 ml Eppendorf tube and allowed to gel for 20 min at 37 °C. 900 µl of aCSF was incubated to 37 °C and slowly added to the gel. The supernatant was removed at each time point and replaced with fresh aCSF. The amount of protein released was analysed at t = 0, 15, 30 min, 1, 2, 3, 4, 5, 6, 8, 12, 24 h. The cumulative amount released at each time point was plotted against time.

### 3.3.4 Mouse surgeries

All experiments were carried out in accordance with the Guide to the Care and Use of Experimental Animals developed by the Canadian Council on Animal Care and approved by the Animal Care Committee at the University of Toronto. All animals used in this study were 9 – 11 week old C57BL/6 mice (Charles River, QC, Canada). A total of 75 animals were used in these studies.

Stroke surgeries were carried out as described by Tennant *et. al.* <sup>256</sup>. Mice were anesthetised with isoflurane, shaved and placed into a Kopf stereotaxic instrument. A midline incision in the scalp was made. A small burr hole was made in the skull at the coordinates 2.25 lateral to the midline and 0.6 anterior to the Bregma. Using a 26G needle, the vasoconstrictor endothelin-1 (400 pM, Calbiochem, Gibbstown, NJ, USA.) was injected 1.0 ventral to the surface of the brain at a rate of 0.1  $\mu$ l/min with a total volume of 1.0  $\mu$ l. The needle was left in place for 10 min prior to removal. The incision was sutured, antibiotic ointment applied and the animal left to recover under a heat lamp.

### 3.3.5 Preparation of delivery device for HAMC implantation

HAMC was contained on the cortex of the brain in a custom-made device. The device consists of two polycarbonate disks (0.5 mm height x 5.9 mm outside diameter). The central opening of one spacer was enlarged to 2 mm in diameter. The second spacer was unmodified. Both spacers were slightly heated and moulded into a concave shape to match the curvature of the skull (**Fig. 3.1**). The spacers were sterilized with ethylene oxide prior to use.

### **3.3.6 Drug delivery device implantation surgeries**

Uninjured mice were anaesthetised with isoflurane, shaved and placed into a Kopf stereotaxic instrument. A midline incision in the scalp was made. A small burr hole was made in the skull at the coordinates 2.25 lateral to the midline and 0.6 anterior to Bregma. The exposed dura was pierced using a 26G needle. A spacer with 2 mm opening was fixed over the burr hole with bone glue. 3 µl of either HAMC alone or HAMC with growth factor was placed into the central opening in direct contact with the brain cortical surface. A second spacer without an opening was placed above the first spacer and fixed with bone glue. The skin was sutured over the spacer system.

For mice with stroke surgeries, the drug delivery implant was inserted at day 4 post stroke. The sutures were removed to expose the burr hole and any tissue debris was removed using a 26G needle. HAMC or HAMC with growth factor was implanted as above. The animal was re-sutured after implantation.

### **3.3.7 Analysis of in vivo protein penetration**

Animals were sacrificed at 2 h, 6 h, 1 day, and 2 days post implantation. The spacers containing HAMC were removed from the skull and placed into a 2 ml Eppendorf tube and 0.5 ml of ELISA diluents solution (0.1% Tween 20 in dH<sub>2</sub>O) was added. The tube was kept on a rotary shaker at 4°C overnight to extract any growth factors remaining in the gel.

Brains were extracted and snap frozen using CO<sub>2(s)</sub> cooled isopropane and stored at -80 °C. Three 1 mm coronal slices were prepared, at the injection site and rostral and caudal to the injection site. Coronal slices were prepared using McIlwain tissue chopper (790744-11, Mickle laboratory engineering company, Surrey, UK). Dorsal-ventral sections (0.5 mm) were then

obtained from each coronal slice using Leica CM3050S cryostat system operating at -18 °C. Each 0.5 mm section was transferred into 2 ml polystyrene microtubes (Sarstedt 72.694.006, Montreal, Quebec, Canada) and 200 µl homogenizing buffer (20 mM HEPES, 10 mM KCl, 1.5 mM MgCl<sub>2</sub>, 1 mM EDTA, 1 mM EGTA, 1 mM dithioereitol, 1 mM PMSF) was added to each tube. Tissue sections were homogenized with 1.0 mm diameter zirconia beads. To remove tissue fragments, homogenized tissue was centrifuged at 15,000 RPM for 15 min at 4 °C and the homogenate was transferred into 1.75 ml Eppendorf tubes. 200 µl ELISA diluent solution was used to dilute homogenate to a total volume of 400 µl.

The amount of protein remaining in the gel and in the brain homogenate at each time point were analysed by EGF ELISA (PeproTech) as per the manufacturer's instructions. The amount of protein remaining in the gel at each time point was used to calculate the amount of protein released by difference. We assume that no protein is lost from HAMC during the period of release. To confirm the effect of denaturation on protein detectability by ELISA, known concentrations of EGF and PEG-EGF were boiled for 60 min in the presence of 2 mM β-mercaptoethanol. Detectability of thus treated proteins were compared to non-denatured proteins by ELISA. ELISA is a reliable method for detecting stable protein in tissue since proteins degraded or denatured are not detectable (**Fig. S3.1**). The concentrations in the homogenate were used to generate tissue penetration profiles for EGF and PEG-EGF as well as the protein mass balance at each time point.

### **3.3.8 Stability of EGF and PEG-EGF in proteases of the brain extracellular space**

The stability of EGF and PEG-EGF were investigated in solutions of proteases extracted from the brain extracellular space (ECS). Extracellular enzymes were extracted as described previously by Shashoua *et al.*<sup>304</sup>. An extraction buffer of 0.32 M sucrose and 1 mM calcium

acetate in dH<sub>2</sub>O was first prepared. Uninjured and stroke-injured C57/BL6 mice were perfused with the extraction buffer. The brains were harvested and incubated on a rotary shaker (Orbitron Rotator 1, Model # 260200, Boekel Scientific, Feasterville, PA, USA) in 25 ml of the extraction buffer for 2 h at 0 °C. The extract was concentrated using tubular protein concentrators (Ultracel 3 kDa MWCO UFC 900324, Millipore, Billerica, MA, USA) until the final volume was approximately 3 ml. The concentrate was then centrifuged at 16249 g for 90 min and the supernatant was dialysed in 3500 kDa MWCO dialysis cassettes (Slide-A-Lyzer 66330, Thermo Scientific, Rockford, IL, USA) against 150 mM PBS for 24 h. The total protein concentrations in both samples were estimated using a UV spectrophotometer (UV-vis ND-100, Nanodrop, Wilmington, DE, USA), and the solutions were diluted in PBS such that the total protein concentrations in all samples were equal.

The stability of EGF and PEG-EGF were determined in brain ECS samples over 48 h at 37 °C. 100 µl of the incubating media was added to 1.5 ml Eppendorf tubes and stored at 4 °C. At each time point, 5 µl of 10 µg/ml EGF or PEG-EGF solution was added to each extract and incubated at 37 °C. The time points examined were 0, 0.5, 1, 2, 3, 6, 8, 24 and 48 h. Immediately after the 0 h samples were taken, the stability of proteins in all samples were determined using EGF ELISA as per the manufacturer's instructions (PeproTech). The protein stability was compared to a sample in PBS incubated at 37 °C for the same period of time.

To verify that the mechanism of protein degradation is enzymatic proteolysis, a panel of protease inhibitor solutions was added to the ECS and homogenate solutions to inactivate the proteolytic enzymes present. The protease inhibitor panel was prepared with the following solution in dH<sub>2</sub>O: 1 mM 4-(2-aminoethyl) benzenesulfonyl fluoride hydrochloride (AEBSF), 1 mg/ml 6-aminohexanoic acid, 100 µM antipain, 800 mM aprotinin, 4 mM benzamidin HCl, 40 µM bestatin, 100 µM chymostatin, 10 µM E-64, 1 mM N-ethylmaleimide, 100 µM leupeptin, 1

µg/ml pepstatin, 10 µM phosphoramidon, and 10 mM trypsin inhibitor (INHIB1, Sigma-Aldrich). The protein stability assay was carried out as above and the ELISA detectable protein concentration was determined.

### **3.3.9 Effects of EGF and PEG-EGF released from HAMC on endogenous SVZ cell proliferation**

Both uninjured and stroke-injured mice subjected to implantation surgeries of EGF or PEG-EGF were sacrificed 2 d following implantation and perfused with 10 ml saline followed by 10 ml 4% PFA. The brains were harvested and post-fixed in 4% PFA for 24 h at 4 °C, and subsequently cryoprotected with 20% sucrose solution for 24 h.

Brains were cryosectioned at 10 µm and all tissue sections from Bregema 1.94 to Bregema - 2.92 were collected. Sections were stained with the following antibodies: rabbit anti-mouse Ki67 (1:200); mouse anti-human Ki56 (1:200); mouse anti-rat GFAP (1:200); mouse anti-rat nestin (1:200); rabbit anti-mouse DCX (1:200). With the following secondary antibodies: Alexa 568 goat IgG (1:200); Alexa 488 goat-anti-rabbit IgG (1:200); Alexa 564 goat-anti-rabbit IgG (1:200); Alexa 488 goat-anti-mouse IgG (1:200); Alexa 568 goat-anti-mouse IgG (1:200).

To determine the effect of EGF and PEG-EGF released from HAMC on endogenous SVZ cell proliferation, every 5<sup>th</sup> tissue section was stained and all Ki-67<sup>+</sup>/DAPI<sup>+</sup> cells along the lateral walls of the ipsilateral and contralateral ventricles were counted. Additionally, ten random sections were selected from each uninjured and stroke-injured, PEG-EGF treated animals, and co-stained with Ki67 nestin or DCX. Double-positive cells along the SVZ were quantified as a percent of total Ki67<sup>+</sup> cells.

### 3.3.10 Statistics

Data are presented as mean  $\pm$  standard deviation. Comparisons between multiple groups were conducted using one-way ANOVA with Bonferonni correction. Significance levels were indicated by  $p < 0.05$  (\*), 0.01 (\*\*), and 0.001 (\*\*\*).

## 3.4 Results

### 3.4.1 In vitro release of EGF from HAMC

The release of EGF and PEG-EGF from HAMC was first studied *in vitro*. We followed the release profile over 24 h (**Fig. S3.2a**). Approximately 80% of protein in HAMC was released within the first 8 h, and approximately 100% was released by 24 h. The release was diffusion controlled between 30 min and 8 h, as the fractional protein release was proportional to  $t^{0.5}$  (**Fig. S3.2b**)<sup>305</sup>. Between 0 and 30 min, the release did not follow diffusion-controlled profile due to swelling of HAMC, which reached equilibrium after 30 min of incubation in buffer. Diffusional release of PEG-EGF from HAMC is not slower than EGF, despite the hydrodynamic radius of PEG-EGF being larger than that of EGF<sup>264,306</sup>.

### 3.4.2 In vivo elimination of EGF and PEG-EGF in uninjured and stroke-injured animals

HAMC containing either EGF or PEG-EGF was implanted on top of both uninjured brains and stroke-injured mouse brains 4 days post stroke. *In vitro* EGF release data suggest that the majority of epi-cortically delivered EGF and PEG-EGF from HAMC are released within 2 days. We therefore extracted the EGF or PEG-EGF remaining in HAMC at 2 h, 6 h, 1 d, and 2 d post implantation and assessed the amount present using ELISA. As predicted, the amount of protein remaining in HAMC decreased at each subsequent time point in all cases examined (**Fig.**

**3.2a, b).** No significant differences are found between EGF and PEG-EGF groups, as well as injured and uninjured groups.

Similarly, to determine the elimination rate of delivered proteins, we measured detectable protein levels in brain tissues at 2 h, 6 h, 1 d, and 2 d. Proteins detected were normalized to the expected amount released at each time, as determined from the mass of protein detected in HAMC. PEG-EGF is eliminated at significantly slower rates than EGF from both uninjured (**Fig. 3.2c**) and stroke-injured brains (**Fig. 3.2d**). In uninjured brains, at 2 h post implant, 90% of the EGF and PEG-EGF released from HAMC is detected *via* ELISA. At 6 h, 1 d, and 2 d post implant, significantly more PEG-EGF is detectable in tissue compared to EGF ( $p < 0.05$ ). Indeed, at 2 d post implant, only 10% of EGF is detected whereas 60% of PEG-EGF is found. Similarly, in stroke-injured brains, significantly more PEG-EGF is detected in tissue compared to EGF at all times examined. Even at 2 d post implant, the quantity of PEG-EGF significantly exceeded that of EGF though only low levels of both EGF and PEG-EGF are detected ( $p < 0.05$ ).

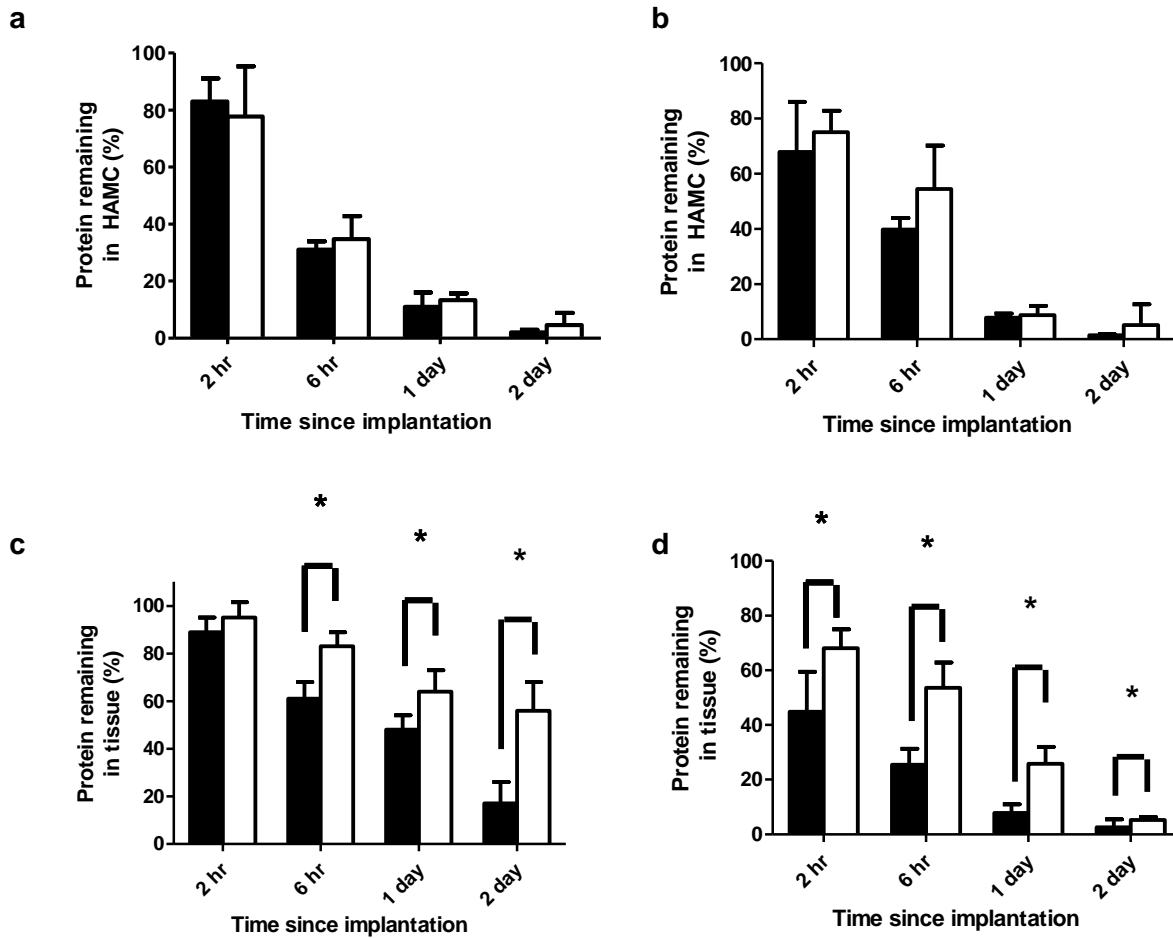


**Figure 3.2 | PEG-modified EGF has slower rates of elimination compared to native EGF in vivo.** The amount of (■) EGF and (□) PEG-EGF detected after 2 h, 6 h, 1 d and 2 d was quantified. (a) Quantification of the amount of protein remaining in HAMC normalized to starting mass in uninjured and (b) stroke-injured brains. (c) The amount of protein was first quantified in the brain tissue by ELISA, and this amount was then divided by the total amount of protein released from HAMC to determine mass percents in uninjured and (d) stroke-injured brains ( $p < 0.05$ ,  $n=3$ , mean  $\pm$  SD reported).

### 3.4.3 In vivo penetration profiles of EGF and PEG-EGF in uninjured and stroke-injured animals

Protein penetration in brain tissue is severely limited by rapid elimination<sup>141</sup>. Based on previous studies<sup>302</sup>, it was hypothesized that PEG-modification of EGF would reduce rates of elimination, thereby allowing the protein to diffuse further. To this end we investigated the tissue penetration profiles of EGF and PEG-EGF at 2 h, 6 h, 1 d, and 2 d following release from HAMC in both uninjured and stroke-injured mice. Six 500  $\mu\text{m}$  sequential tissue sections were prepared ventral to the cortical surface and the delivered proteins were extracted for analysis by ELISA.

In the uninjured brain, at 2 h post implantation, the majority of protein was found between 0 – 500  $\mu\text{m}$  below the cortical surface for both EGF and PEG-EGF (**Fig. 3.3a**). At 6 h post implantation (**Fig. 3.3b**), the majority of EGF is found at depths between 0 – 1500  $\mu\text{m}$  with trace amounts observed at 1500 – 2500  $\mu\text{m}$ . Significantly higher concentrations of PEG-EGF are found at 1500 – 2500  $\mu\text{m}$  compared to EGF at 6 h post implant ( $p < 0.05$ ), while at 1 d post implantation (**Fig. 3.3c**), the concentrations of PEG-EGF observed between 2500 – 3000  $\mu\text{m}$  significantly exceed that of EGF ( $p < 0.05$ ). At 2 d post implantation (**Fig. 3.3d**), the amounts of PEG-EGF found in all tissue sections exceed that of EGF ( $p < 0.05$ ), and there is at least a two-fold increase of protein accumulation due to PEG-modification. This suggests that EGF is cleared faster than PEG-EGF, and demonstrates that PEG-EGF is able to penetrate deeper into uninjured brain tissue than unmodified EGF.

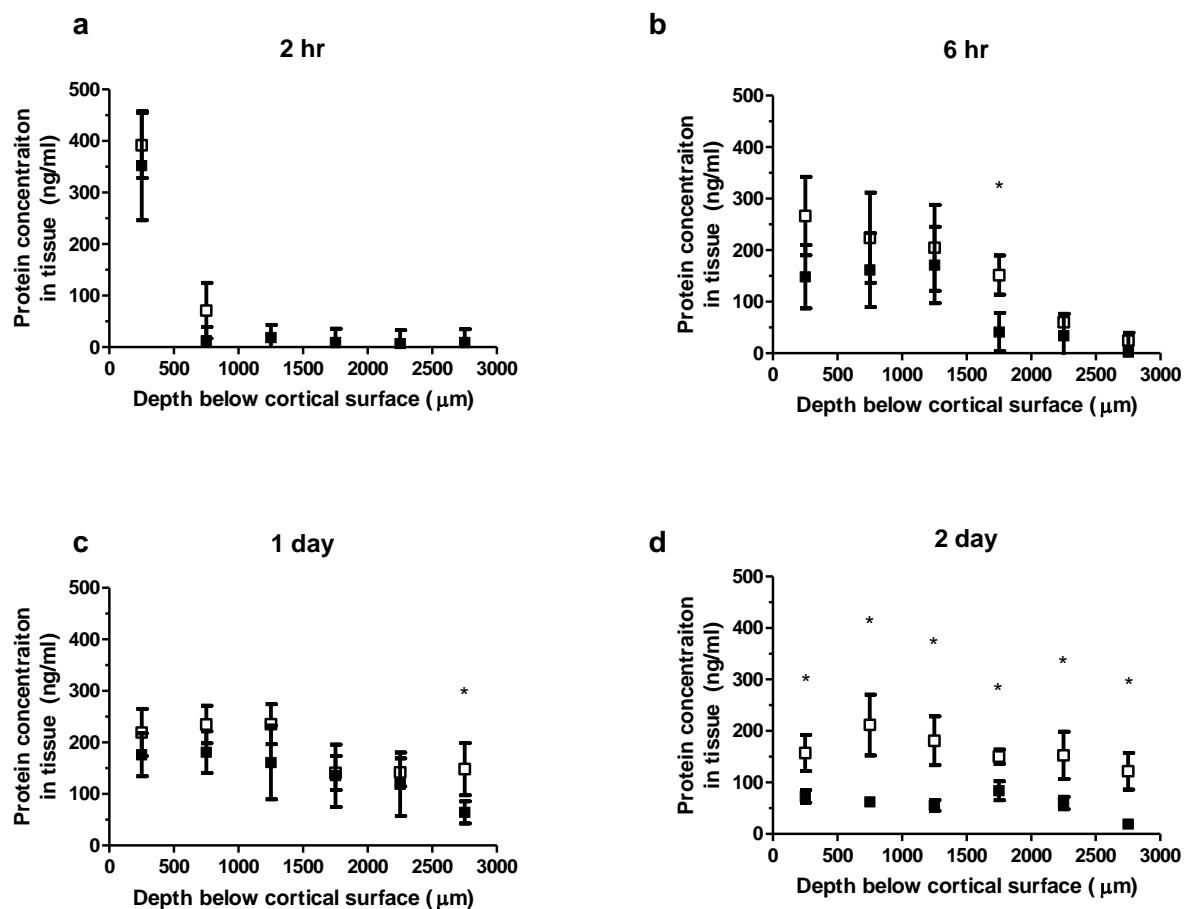


**Figure 3.3 | PEG-modification of EGF allows for deeper tissue penetration in uninjured brains after delivery from implanted HAMC.** Following implantation in uninjured mouse brains, the diffusion profiles of (■) EGF and (□) PEG-EGF at different depths is assessed. (a) At 2 hr post implantation protein concentration is similar. (b) At 6 hr post implantation, while significantly more PEG-EGF is found between 1500 and 2000 μm, the profiles remain similar in all other tissue sections. (c) 1 day post implantation, significantly higher concentrations of PEG-EGF are found 2500 – 3000 μm below the cortical surface. (d) 2 days post implantation, more PEG-EGF is found at all depths examined ( $p < 0.05$ ,  $n=3$ , mean  $\pm$  SD reported).

In stroke-injured brains, a similar trend is observed. At early times (**Fig. 3.4a, b**), the penetration profile of PEG-EGF resembles that of EGF. At 1 d post implant (**Fig. 3.4c**), PEG-EGF is observed throughout the 3000 μm of tissue analyzed while the amounts of EGF found deeper than 1000 - 1500 μm are negligible. PEG-modification leads to greater than seven-fold increase in protein accumulation. At 2 d post implantation (**Fig. 3.4d**), while there is minimal EGF and

PEG-EGF found in the deeper tissue slices, the protein accumulation achieved by PEG-modification is ten-fold greater between 500 – 2000  $\mu\text{m}$ , and more than twenty-fold greater between 2000 – 3000  $\mu\text{m}$ . This finding is promising for delivery to the stem cell niche in the SVZ, which is approximately 2000 – 3000  $\mu\text{m}$  ventral to the cortical surface. While unmodified EGF may not be able to reach the SVZ in efficacious doses, PEG-EGF will likely reach the SVZ at sufficiently high doses, thereby stimulating NSPC proliferation *in vivo*.

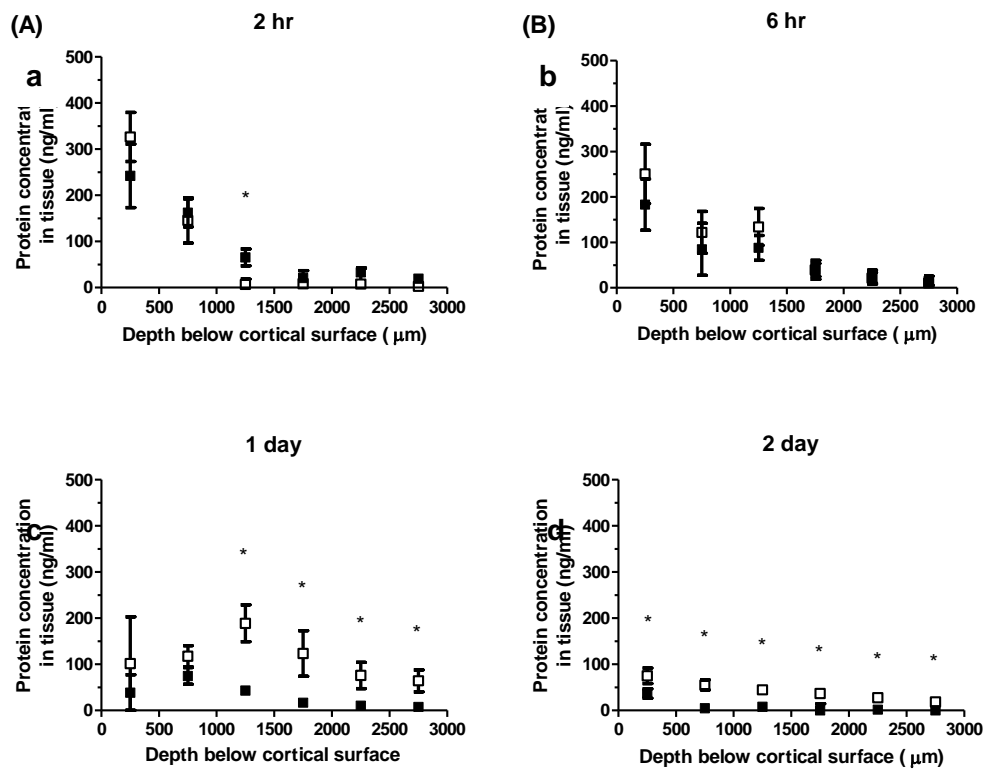


**Figure 3.4 | PEG-modification of EGF allows for deeper tissue penetration in stroke-injured brains after delivery from implanted HAMC.** Following implantation in stroke-injured mouse brains, the diffusion profiles of (■) EGF and (□) PEG-EGF at different depths is assessed. (A) At 2 h and (B) 6 h post-implantation diffusion profiles appear similar. (C) 1 day post implantation, significantly more PEG-EGF is found between 1000 and 3000  $\mu\text{m}$ . (D) 2 days post implantation, higher levels of PEG-EGF are found at all depths examined ( $p < 0.05$ ,  $n=3$ , mean  $\pm$  SD reported).

### 3.4.4 In vitro proteolytic stability of EGF and PEG-EGF in brain extracellular space (ECS) and intracellular enzyme solutions

According to the tissue mass balance of delivered EGF and PEG-EGF, it is clear that PEG-EGF is eliminated more slowly than EGF. One of the major mechanisms of protein elimination in the brain is enzymatic degradation<sup>307</sup>. To gain insight into this possible mechanism of degradation, we studied the stability of EGF and PEG-EGF in proteases extracted from the extracellular space of the brain *in vitro*. In protein extracts from uninjured brains, PEG-EGF exhibits significantly higher stability than EGF (**Fig. 3.5a**). The half-life ( $t_{1/2}$ ) of PEG-EGF is 3.52 h while that of EGF is 0.74 h (**Fig. 3.5b**). In extracts from stroke-injured brains, a similar trend is observed in the extracellular protein extracts (**Fig. 3.5c**), and the  $t_{1/2}$  of PEG-EGF and EGF are 3.85 and 1.69 h, respectively. The difference in half-life for EGF vs. PEG-EGF in stroke-injured brain is not as great as that in uninjured brain, likely due to high levels of protein over-expression after the stroke injury<sup>308,309</sup>. To confirm that the observed effect on protein stability is due to proteolytic degradation, we examined EGF and PEG-EGF stability in both PBS and protein extracts from stroke-injured brains treated with a panel of protease inhibitors (**Fig. 3.5a, c**). The stability of both EGF and PEG-EGF remained at initial levels over 8 h when incubated with protease inhibitors, suggesting that the degradation of EGF observed is predominately enzyme-mediated.

\

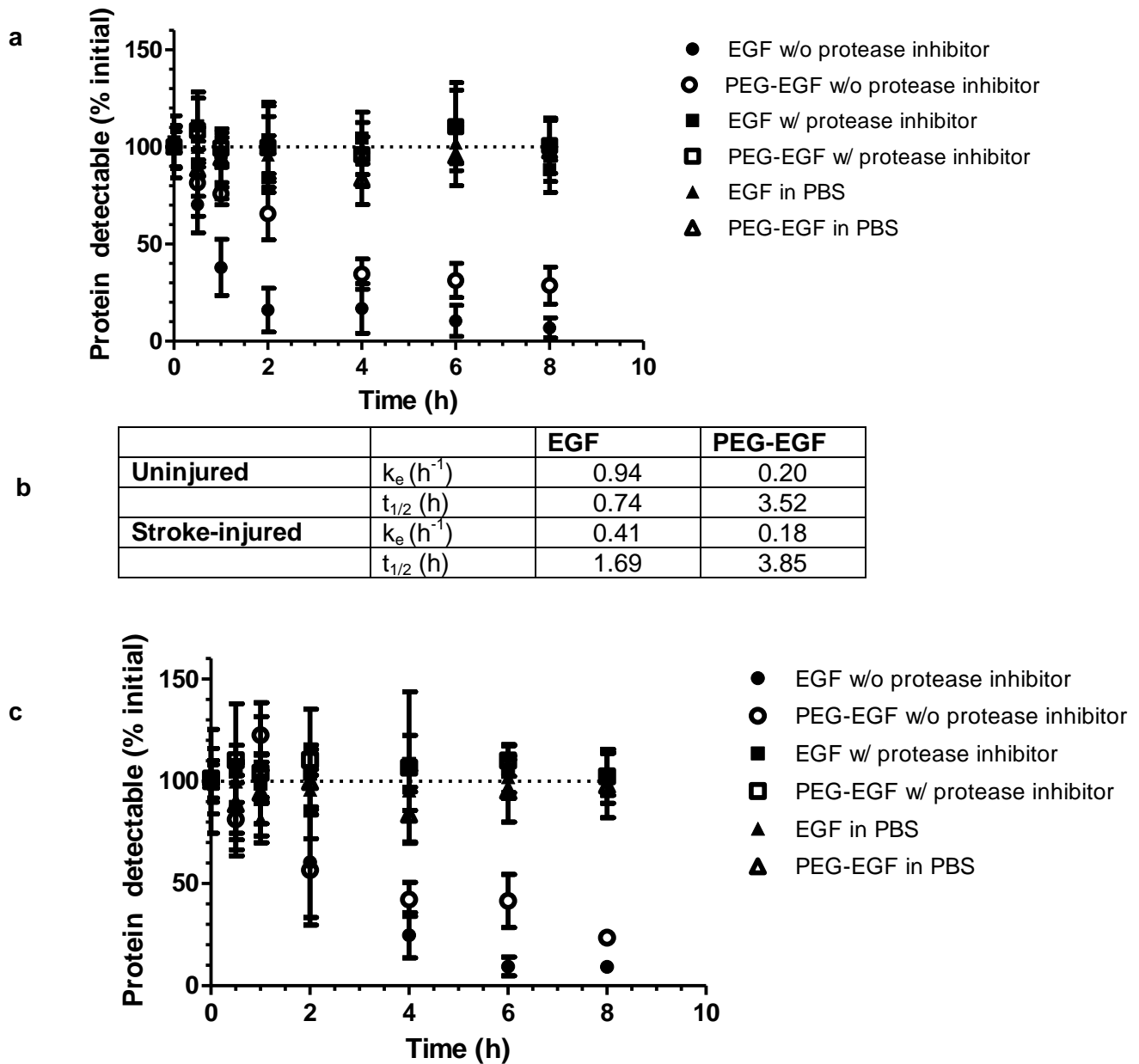


**Figure 3.5 | PEG-EGF is more stable compared to native EGF in ECS proteins extracted from healthy and injured brains.** (a) In the uninjured brain, (○) PEG-EGF is degraded more slowly than (●) EGF in proteins extracted from the extracellular space. The stability of (▲) EGF and (△) PEG-EGF in PBS remained constant and similar to initial levels over time. The stability of (■) EGF and (□) PEG-EGF in protease inhibitor-treated ECS extract also remained constant. (b) The rates of degradation ( $k_e$ ) and the half-lives ( $t_{1/2}$ ) are quantified. (c) PEG-EGF degrades more slowly than EGF in proteins extracted from the extracellular space of stroke-injured brains ( $n=3$ , mean  $\pm$  SD reported).

### 3.4.5 Effect of EGF and PEG-EGF delivered from HAMC on SVZ stem cell proliferation

Immunohistochemical staining with Ki67 is used as measure of proliferation in the SVZ <sup>310</sup>. To ensure that the Ki67<sup>+</sup> cells is an accurate measure of NSPC proliferation, sections from both stroke-injured mice and stroke-injured mice treated with PEG-EGF were co-stained with Ki67 and the NSPC markers nestin and DCX <sup>311</sup>. There is no significant difference between stroke-injured and the treatment group in the percentage of cells double staining for Ki67 and nestin (**Fig. S3.3a**) and DCX (**Fig. S3.3b**). Thus increased Ki67 immunostaining reflects increased proliferation of NSPCs.

Following epi-cortical implantation of EGF and PEG-EGF, we examined the proliferation of SVZ NSPCs to determine whether the protein reaching the SVZ is bioactive. Both uninjured and stroke-injured mice were sacrificed 2 d post implantation. Coronal brain sections from all treatment groups were stained with Ki67 and DAPI and co-stained cells along the lateral ventricles were quantified (representative images of SVZ from the stroke-injured group, **Fig. 3.6a – d**, and the stroke-injured/PEG-EGF treated group, **Fig. 3.6e – h**, are shown). The total number of Ki67<sup>+</sup> proliferating cells in the SVZ was quantified ipsilateral and contralateral to the implant.

In uninjured brains with and without blank HAMC implants, the total cell number is not significantly different between the ipsilateral and contralateral SVZ (**Fig. 3.6i**). We did not observe an increase in NSPC proliferation resulting from HAMC alone. When treated with EGF and PEG-EGF delivered from HAMC, the number of proliferating NSPCs ipsilateral to the implant significantly exceeded that from the HAMC implant alone ( $p < 0.05$ ). There was no difference observed contralateral to the implant between any of the test groups. The ipsilateral cell count exceeded the contralateral cell count following EGF/PEG-EGF treatment ( $p < 0.05$ ).

This suggests that within 2 d post implant, EGF delivered from the hydrogel delivery system preferentially reached the ipsilateral SVZ and thus enhanced stem cell proliferation. We observed no significant difference in cell proliferation between EGF and PEG-EGF treatments ipsilateral to the implant. This indicates that in uninjured brains, the dose of EGF reaching the SVZ is able to enhance NSPC proliferation, and the effect of EGF and PEG-EGF arriving at the SVZ within 2 d post implant is equivalent in terms of their ability to promote NSPC proliferation.

Stroke injuries increased the level of SVZ cell proliferation compared to uninjured controls, both ipsilateral and contralateral to the injury (**Fig. 3.6j**). Contralateral to the stroke injuries, sham implants of aCSF and HAMC did not lead to differences in the proliferating cell population of the SVZ. There were no statistical differences between the EGF and PEG-EGF treated animals compared to control animals in the contralateral tissue. Ipsilateral to the stroke injuries, sham implants of aCSF and HAMC did not affect the number of proliferating SVZ cells compared to stroke surgeries alone. The total number of proliferating cells in the ipsilateral SVZ was significantly enhanced by both EGF ( $p < 0.05$ ) and PEG-EGF ( $p < 0.001$ ). PEG-EGF led to higher numbers of proliferating cells ipsilateral to the implant compared to EGF ( $p < 0.05$ ). This demonstrates that PEG-EGF is bioactive *in vivo*. It also demonstrates that PEG-EGF is more effective than EGF in stimulating NSPC proliferation in stroke-injured brains, when delivered using the minimally-invasive HAMC epi-cortical delivery vehicle. The effect of PEG-EGF was only observed in the SVZ ipsilateral to the implant, suggesting that epi-cortical delivery is able to target the ipsilateral tissue, thereby confining the effect to the desired region.

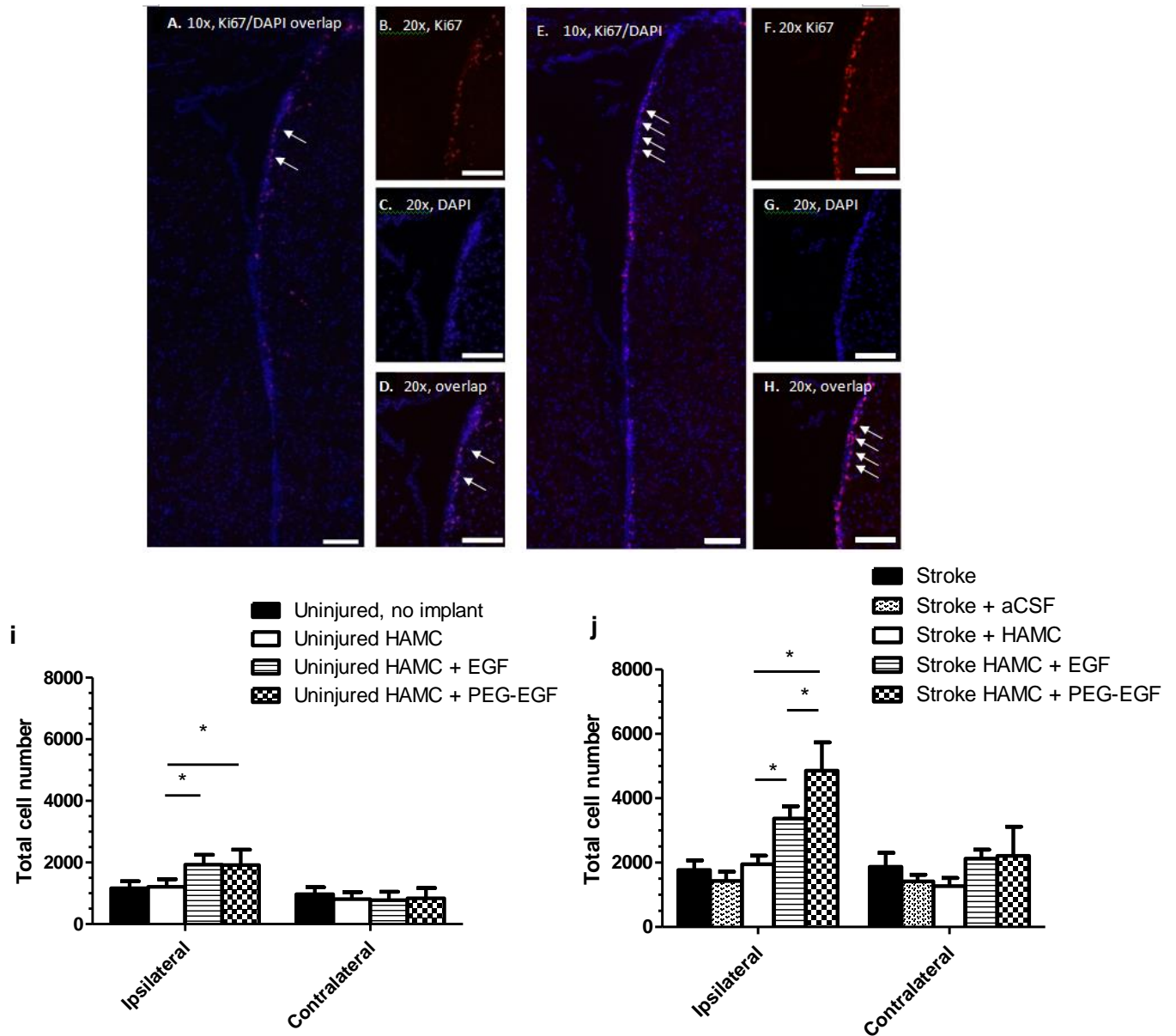
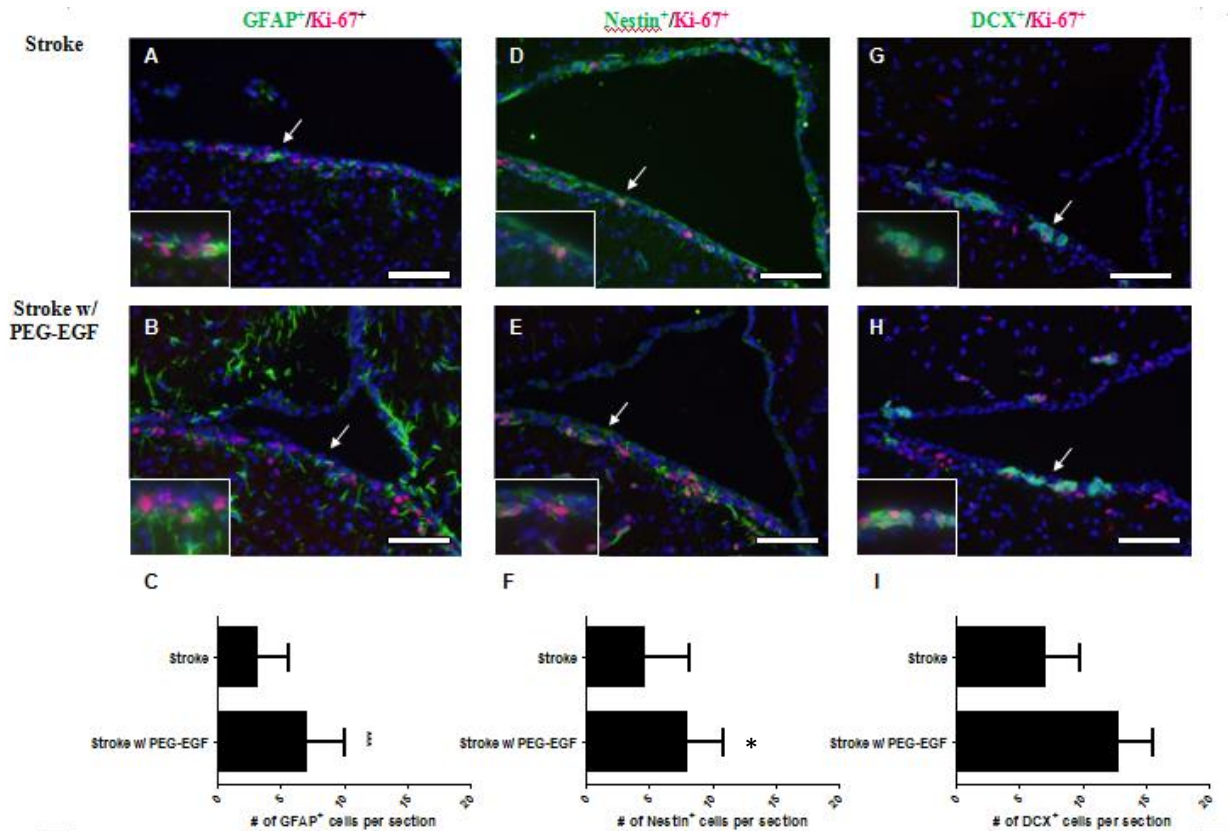


Figure 3.6 | When delivered epi-cortically from HAMC, PEG-EGF stimulates higher levels of SVZ cell proliferation compared to EGF. Uninjured and stroke-injured mice are treated with EGF and PEG-EGF delivered epi-cortically from HAMC. (a – d) Representative images are shown for Ki67 staining of stroke-injured and (e – h) stroke-injured/PEG-EGF treated groups. Arrows indicate double-labeled cells in the SVZ. (i) Quantification of Ki67 positive cells in uninjured brains, both PEG-EGF and EGF increased SVZ cell proliferation, by 1.6 fold compared to control groups ( $p < 0.05$ ), while no significant difference was observed contralateral to the implant. (j) In stroke-injured brains EGF enhanced cell proliferation in the SVZ, compared to control groups ( $p < 0.05$ ). PEG-EGF showed greater effect in increasing proliferation relative to all control groups ( $p < 0.001$ ), and EGF ( $p < 0.05$ ). There were no significant differences among the groups contralateral to the implant.  $n=3$ , mean  $\pm$  SD reported. A, E Scale: 100  $\mu$ m, B-D, F-H Scale: 50  $\mu$ m.

We also confirmed that the factors delivered epi-cortically from HAMC are efficacious towards the various precursor cell populations in the SVZ. EGF is a known mitogen for precursor cells in the SVZ<sup>102,311</sup>. We have determined that treatment with PEG-EGF leads to more pronounced SVZ cell proliferation compared to baseline conditions. Therefore sections from stroke-injured mice treated with and without PEG-EGF were double-stained with Ki67 and the NSPC marker nestin, the neuroblast marker DCX, or the astrocyte marker GFAP. We found the number of Ki67<sup>+</sup> cells that were also positive for either nestin (**Fig. 3.7a – c**), DCX (**Fig. 3.7d – f**), or GFAP (**Fig. 3.7g – i**) to be significantly increased in stroke injured and PEG-EGF treated animals compared to the stroke-only animals. This confirms that the PEG-EGF reaching the SVZ elicits responses from the SVZ precursor cell populations.

### 3.5 Discussion

Treatment for stroke, along with other disorders of the brain, presents a challenge for the field of controlled drug delivery. Efficacious treatments not only require a sustained dose of therapeutically relevant drugs to reach the target site, but also mandate maintaining bioactivity and minimizing invasiveness. To achieve effective neuroregeneration after stroke injuries, a number of growth factors including EGF have been tested. Compared to systemic delivery, local drug delivery is preferred because the former may have side effects on other tissues. While the osmotic minipump/catheter system achieves local delivery to the brain, it is highly invasive. Therefore hydrogel reservoirs, such as HAMC, present a desirable alternative.



**Figure 3.7 | Proliferating various precursor cell populations in the SVZ. Sections from stroke-injured and stroke-injured/PEG-EGF treated brains are stained with Ki67 and either nestin, double-cortin (DCX), or GFAP. (a) stroke-injured and (b) stroke-injured/PEG-EGF treated brains co-stained with GFAP and Ki67. (c) Quantification of cells double-stained with Ki67 and nestin. (d) stroke-injured and (e) stroke-injured/PEG-EGF treated brains co-stained with nestin and Ki67. (f) Quantification of cells double-stained with Ki67 and nestin. (g) stroke-injured and (h) stroke-injured/PEG-EGF treated brains co-stained with DCX and Ki67. (i) Quantification of cells double-stained with Ki67 and DCX. Significant differences were found between stroke-injured and stroke-injured/PEG-EGF treated groups ( $p < 0.005$ ,  $n=3$ , mean  $\pm$  SD reported). Images were taken at 20x magnification. Insets show arrow-indicated regions at 60x magnification. Scale: 100  $\mu$ m.**

Here we investigated the potential of using HAMC as a local drug delivery vehicle for treating stroke. By placing HAMC remotely from the target site, we avoid risks of trauma and infection involved with inserting cannula and needles into the brain tissue<sup>312</sup>. In our system, HAMC is delivered epi-cortically, thus improving safety compared to systems where the reservoir is either

directly inserted into the tissue <sup>141,313</sup> or a burr hole is drilled into the brain tissue to create a void for the reservoir <sup>131</sup>.

One important factor impeding the use of polymeric drug delivery systems in the brain is short protein penetration distance. Previous studies have shown protein diffusion to be restricted to 1 – 2 mm in brain tissue <sup>314</sup>, an inadequate distance for NSPC stimulation as the niche is deep within the brain. Our present study shows that by modifying EGF with PEG, we significantly increase the amount of protein accumulated 2 – 3 mm ventral to the cortical surface, 1 – 2 days after HAMC delivery. These distances exceed previously reported distances of protein diffusion in the uninjured brain and correspond to the expected depth of the SVZ <sup>286,315</sup>. These features demonstrate that HAMC is a suitable candidate for localized sustained drug delivery to the brain.

PEG-modification resulted in a 3-fold increase in EGF penetration distance in the uninjured brain and up to 27-fold increase in stroke-injured brain. The benefit of PEG-modification is amplified in the stroke-injured brain potentially due to EGFR upregulation post stroke <sup>302</sup>. One drawback currently is that while 3 mm of penetration allows therapeutics to reach the SVZ in animal models, it may not be adequate in human clinical studies. We propose that an increase in penetration distance can be further enhanced through the use of a constant protein source. We <sup>316</sup> and others <sup>141,314</sup> previously showed that proteins released from a constant source will increase diffusion in the brain by 2-fold compared to a single injection. We have also previously demonstrated that a number of proteins may be encapsulated in poly(lactide-co-glycolide) micro/nanospheres and may be incorporated into HAMC to achieve a range of delivery periods, between 7 and 30 days <sup>316</sup>. This type of long-term sustained delivery device will provide the constant source required to further increase protein diffusion distance in the brain. Additionally, depositing the growth factors close to their sites of action reduces the volume of tissue exposed

to the treatment, which decreases the chance of tumor development associated with long-term growth factor delivery.

Another benefit of our delivery system is the growth factor gradient that is established in the tissue. The penetration profiles of PEG-EGF in the brain tissue demonstrate that over the two days of diffusion-mediated release from HAMC, a concentration gradient forms between the brain/HAMC interface and the SVZ. This gradient may help NSPCs to migrate from the SVZ to the injury site<sup>297,317</sup>, thus further aiding tissue regeneration.

We studied the stability of EGF and PEG-EGF during diffusion by examining their rates of degradation in brain-extracted solutions. PEG modification of EGF improved EGF stability and corroborates previously reported results, where PEG improved the stability of various proteins *in vitro*<sup>318</sup>. We found both EGF and PEG-EGF to be eliminated faster in stroke-injured brains compared to uninjured brains. This is likely due to inflammatory cell activation<sup>307</sup> and proteolytic enzyme over-expression<sup>307</sup>.

The observation that stroke injuries increase cell proliferation in the SVZ is consistent with previous findings<sup>319</sup>. The effect of injury alone, however, does not adequately enhance proliferation and tissue regeneration<sup>320</sup>. While the total number of proliferating cells in uninjured brains is similar after EGF or PEG-EGF treatment, they are both significantly higher than untreated controls. The lack of differences observed between the treated groups may be due to a saturation effect<sup>321</sup>, where the amounts of protein reaching the SVZ both exceed the saturation level of EGFR<sup>142</sup>.

### 3.6 Conclusion

Our results demonstrate the potential of HAMC as a drug delivery vehicle for local release to the brain and the use of PEG as a modifier to enhance protein stability, diffusion distance, and *in vivo* bioactivity. We demonstrate that injection of HAMC on the brain cortex achieves direct delivery to the brain tissue, obviating the need to cross the BBB or use minipump/catheter systems. PEG-EGF enhances NSPC proliferation in both uninjured and stroke-injured brains with the greatest number of NSPCs stimulated ipsilateral to the stroke injury with PEG-EGF delivery. Significantly, the results reported herein have broad applicability to other areas of controlled molecule delivery to the brain. For example, our system could be used to deliver a myriad of clinically relevant agents, including small molecule drugs <sup>322</sup>, protein therapeutics <sup>22</sup>, and imaging agents <sup>323</sup>. This delivery system is beneficial because it achieves local delivery to the brain in a minimally-invasive way, and may enable the clinical translation of minimally-invasive epi-cortical drug delivery strategies.

## **4 Local hydrogel delivery strategy to the brain of erythropoietin for endogenous stem cell stimulation after stroke injury\***

\*This chapter was published in Biomaterials.

**Wang, Y.**<sup>4</sup>; Cooke, M.J.; Morshead, C.M.; Shoichet, M.S. 2012. "*Hydrogel delivery of erythropoietin to the brain for endogenous stem cell stimulation after stroke injury*" Biomaterials, 33 (2012): 2681-92

### **4.1 Abstract**

Drug delivery to the brain is challenging because systemic delivery requires high doses to achieve diffusion across the blood-brain barrier and often results in systemic toxicity. Intracerebroventricular implantation of a minipump/catheter system provides local delivery, yet results in brain tissue damage and can be prone to infection. An alternate local delivery strategy, epi-cortical delivery, releases the biomolecule directly to the brain while causing minimal tissue disruption. We pursued this strategy with a hyaluronan/methyl cellulose (HAMC) hydrogel for the local release of erythropoietin to induce endogenous neural stem and progenitor cells of the subventricular zone to promote repair after stroke injury in the mouse brain. Erythropoietin promotes neurogenesis when delivered intraventricularly, thereby making it an ideal biomolecule with which to test this new epi-cortical delivery strategy. We investigated HAMC in terms of the host tissue response and the diffusion of erythropoietin in the stroke-injured brain for neural repair. Erythropoietin delivered from HAMC at 4 and 11 days post-stroke resulted in attenuated inflammatory response, reduced stroke cavity size, increased number of both neurons in the peri-infarct region and migratory neuroblasts in the subventricular zone, and decreased apoptosis in both the subventricular zone and the injured cortex. We demonstrate

---

<sup>4</sup> Contribution by Y. Wang: designed and conducted all in vitro and in vivo experimental work; collected, analyzed, and interpreted data from experiments; prepared the manuscript.

that HAMC-mediated epi-cortical administration is promising for minimally invasive delivery of erythropoietin to the brain.

## 4.2 Introduction

Stroke is the fourth leading cause of death in the world and causes 15 million debilitating injuries each year [1]. Stroke is caused by a disruption in blood supply to the brain, and is classified as either ischemic or hemorrhagic. In ischemic stroke, decreased blood flow results in an insufficient supply of nutrients to cells in the core, which leads to necrotic cell death. A secondary phase of injury subsequently occurs in the tissue surrounding the core (the penumbra), resulting in apoptosis [1].

There is currently no cure for stroke and the only clinically proven drug is tissue plasminogen activator, an anti-thrombolytic agent used to reduce the extent of injury [2]. However, this treatment does not afford tissue regeneration. A number of neuroregenerative strategies have shown improved functional recovery in animal models of stroke, including stem cell transplantation and endogenous stem cell stimulation. For the latter, exogenous factors are delivered to the brain to stimulate endogenous neural stem/progenitor cells (NSPCs) in the subventricular zone (SVZ) to promote tissue repair after injury [3]. Endogenous NSPC stimulation with erythropoietin (EPO) has resulted in NSPC proliferation, migration, and maturation, as well as promoting regeneration and replacement of cells and tissues lost following stroke injury [4, 5].

EPO is a 30.4 kDa glycoprotein that has been shown to be both neuroprotective and neuroregenerative after injury to the CNS [6, 7], and it has been shown to reduce stroke cavity

size clinically [8]. In the brain, EPO binds with the erythropoietin receptor (EPOr), which is expressed on multiple cell types including neurons, astrocytes, and NSPCs in the SVZ [7]. When bound to EPOr on NSPCs, EPO promotes their survival and differentiation into mature neurons [9].

One limitation in using EPO, as well as a number of other growth factors, for stimulating endogenous brain repair after stroke is the lack of appropriate delivery systems. Systemic delivery of proteins, by intravenous or intranasal delivery, results in less than 1% crossing the blood-brain barrier BBB [10]. Moreover, intravenous delivery can lead to systemic toxicity at high concentrations [11, 12] while chronic intranasal delivery is associated with systemic toxicity, patient discomfort, low patient compliance and thus sub-optimal therapeutic benefit [13, 14]. Local drug delivery strategies typically involve the insertion of a cannula or drug delivery scaffold into the brain tissue, both of which are highly invasive [15, 16]. The optimum paradigm involves delivering drugs from the cortical surface using a minimally invasive strategy, controlling the release and transport of the drugs such that they reach the SVZ, and maintaining the bioactivity of the drugs in order that they stimulate the NSPCs upon reaching the SVZ.

With a view toward circumventing the blood-brain barrier and achieving delivery to the brain, we asked whether EPO could be delivered locally to the stroke-injured brain using an injectable hydrogel and what the brain host tissue response would be to this hydrogel. The physically crosslinked blend of hyaluronan (HA) and methyl cellulose (MC) (HAMC) is bioresorbable, injectable through a fine needle, and gels rapidly at physiological temperature [17]. HAMC spatially localizes the drug of interest at the site of delivery and facilitates short-term controlled release to the CNS [18, 19].

One of the major limitations of delivering protein drugs to the brain is the fast rate of protein elimination and the consequent short penetration distance. Unmodified proteins often do not

penetrate more than 1 mm in the uninjured brain, and penetration distance decreases significantly after brain injury because stroke injury results in the upregulation of many protein receptors in the brain [18, 20]. Modification of proteins with poly(ethylene glycol), PEG, has been used to increase protein penetration distance [18, 21-23].

Here we studied the diffusion of EPO from the HAMC hydrogel, delivered directly to the cortex, in the uninjured as well as stroke-injured mouse brain. In order to understand the kinetics of EPO penetration in the brain, EPO<sub>r</sub> expression was examined at the time points of EPO delivery: 4 and 11 days post-stroke. These two time points were selected because previous reports have delivered EPO at these time points, albeit using a highly invasive cannula/minipump system, and shown that in mice models of ischemia, cortical EPO<sub>r</sub> upregulation increases between 1 and 7 days post ischemia [24], and persists up to 28 days [25]. The host tissue response of EPO delivered from HAMC was examined in terms of: NSPC stimulation/migration and neurogenesis; and the inflammatory response by immunohistochemical staining for macrophages/microglia and astrocytes.

### **4.3 Materials and Methods**

#### **4.3.1 Materials**

Recombinant human erythropoietin (EPREX) was supplied by Ortho Biotech Canada (Toronto, ON, Canada). Sodium hyaluronan (HA,  $1.4-1.8 \times 10^6$  g/mol) was purchased from NovaMatrix (Sandvika, Norway). Methylcellulose (MC,  $3.4 \times 10^5$  g/mol) was obtained from Shin Etsu (Chiyoda-ku, Tokyo, Japan). Mouse anti-human Ki-67 was purchased from BD biosciences (Mississauga, ON, Canada), mouse anti-rat NeuN and GFAP were obtained from Millipore Inc. (Billerica, MA, USA), rat anti-mouse CD68<sup>+</sup> and rabbit anti-mouse double-cortin were obtained

from Abcam (Cambridge, MA, USA), and Vectashield with DAPI stain was purchased from Vectorlabs (Burlington, ON, Canada). Alexa 488 goat-anti-rat, Alexa 488 and 586 goat-anti-rabbit IgG, and Alexa 568 goat-anti-mouse IgG were obtained from Invitrogen Inc. (Burlington, ON, Canada). Sodium cyanoborohydride ( $\text{NaCNBH}_3$ ), NaCl,  $\text{MgCl}_2$ ,  $\text{CaCl}_2$ ,  $\text{BaCl}_2$ ,  $\text{Na}_2\text{HPO}_3$ ,  $\text{NaH}_2\text{PO}_3$ , trehalose, and cresyl violet acetate were supplied by Sigma Aldrich (Oakville, ON, Canada). Triton X-100 was supplied by ACROS (NJ, U.S.A.). Artificial cerebrospinal fluid (aCSF [23]) and all buffers were prepared with distilled and deionized water prepared from a Millipore Milli-RO 10 Plus and Milli-Q UF Plus at 18 M $\Omega$  ·m resistivity (Millipore, Bedford, USA). Recombinant EPO ELISA kit was purchased from BD biosciences (Mississauga, ON, Canada).

#### **4.3.2 Preparation of sterile HAMC hydrogel**

HA and MC were dissolved separately in  $\text{dH}_2\text{O}$  at 4°C overnight, sterile-filtered and lyophilized. The resulting sterile powders were kept at 4 °C until use. HAMC was prepared with 1.1% HA and 2.2% MC in sterile aCSF and mixed using a SpeedMixer (DAC 150 FVZ, Siemens). Immediately prior to injection, 100  $\mu\text{L}$  of sterile EPO solution (10,000 U/ml) was added to 900  $\mu\text{L}$  HAMC (yielding a final concentration of 1% HA and 2% MC), mixed and centrifuged to eliminate air bubbles.

#### **4.3.3 In vitro release of EPO from HAMC**

The time required for EPO to diffuse out of HAMC was determined in vitro. EPO was mixed into HAMC to yield a final concentration of 1000 U/ml, and 100  $\mu\text{L}$  was injected into the bottom of a 2 ml Eppendorf tube and gelled at 37 °C for 20 min. 900  $\mu\text{L}$  of aCSF at 37 °C was added. The

supernatant was completely replaced at each of the following time points and EPO concentrations determined using ELISA: 0, 30 min, 1, 2, 4, 6, 8, 12, 24 h.

#### **4.3.4 Stroke surgeries and injection of drug delivery device**

All animal work was carried out in accordance with the Guide to the Care and Use of Experimental Animals (Canadian Council on Animal Care) and approved by the Animal Care Committee at the University of Toronto. A total of 54 C57BL/6 mice (aged 9 – 11 weeks) were used in this study (Charles River, QC, Canada).

Stroke surgeries were carried out as described previously [26]. Mice were anesthetised with isoflurane, shaved and placed into a Kopf stereotaxic instrument. Scalps were cleaned and a midline incision made next, a small burr hole was made in the skull at the coordinates 2.25 lateral to the midline and 0.6 anterior to the Bregema. Using a 26G needle, 1.0  $\mu$ l of the vasoconstrictor endothelin-1 (400 pM, Calbiochem, Gibbstown, NJ, USA.) was injected 1.0 ventral to the brain surface at 0.1  $\mu$ l/min. The needle was left in place for 10 min prior to removal. The incision was sutured, antibiotic ointment applied and animal recovered under a heat lamp.

The drug delivery system was injected at either day 4 or day 11 post-stroke (7 d post stroke, **Fig. 4.1**). The sutures were removed to expose the stroke site and any tissue debris was removed. The drug delivery device was prepared as described previously [18] to spatially localize HAMC at the cortical surface. A disk with 2 mm opening was fixed over the burr hole with bone glue. 3  $\mu$ l of either HAMC containing EPO or HAMC alone was injected into the hole such that the gel is in direct contact with the brain cortical surface. A second disk with no opening was fixed over

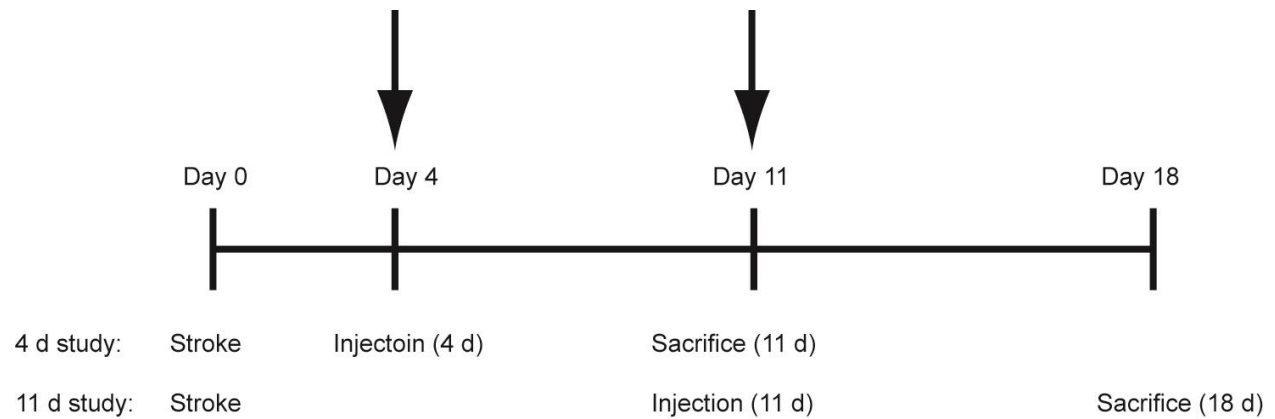


**Figure 4.1** / Surgical paradigm for epicortical delivery of EPO. Animals received endothelin-1 induced stroke injury on day 0. HAMC or EPO incorporated in HAMC was injected epicortically at either 4 or 11 days post stroke, as indicated by arrows. The drug delivery system was allowed to remain in-place for 7 days prior to sacrifice. Animals were sacrificed on either day 11 or day 18 post stroke.

the first spacer. The skin was sutured over the spacer system. For uninjured animals, the surgery was identical (without the stroke injury itself) to that of stroke-injured mice.

#### 4.3.5 Analysis of in vivo protein penetration

Animals were sacrificed at 4 h, 1 day, and 2 days post injection and the drug delivery device containing HAMC was retrieved. The extracted device was placed into 0.5 ml 0.1% Tween 20 in PBS and agitated overnight at 4°C overnight to extract any remaining EPO.

Brains were snap frozen with CO<sub>2(s)</sub> cooled isopentane and stored at -80 °C. A 3 mm coronal section around the injection site was prepared using the McIlwain tissue chopper (790744-11, Mickle laboratory engineering company, Surrey, UK). Dorsal-ventral sections (0.5 mm) were then cryosectioned from each coronal slice using a Leica CM3050S cryostat system. Each section was homogenized in 400 µl lysis buffer (40 mM trehalose, 1% Triton X-100 in dH<sub>2</sub>O),

and the homogenate supernatant was removed after centrifugation at 15,000 RPM for 15 min at 4 °C.

The amount of protein remaining in HAMC and in the brain homogenate at each time point was determined using a recombinant EPO ELISA kit (BD Biosciences) as per the manufacturer's instructions. The difference between the amounts of protein that remain in HAMC at each time was used to calculate the amount of protein released. We assume that no protein is lost from the entire system during the period of release and that all protein released has diffused into the brain tissue. The amount of EPO in the homogenate was used to generate tissue penetration profiles as well as the protein mass balance at each time point.

#### **4.3.6 Brain tissue preparation for morphological analysis**

At the appropriate time points animals were transcardially perfused with saline followed by 4% paraformaldehyde (PFA). Brains were extracted and fixed in 4% PFA at 4°C overnight, followed by cryoprotection in 30% sucrose. Cryoprotected brains were snap frozen and cryosectioned to 10 µm.

#### **4.3.7 Analysis of stroke cavity size**

Sections were defatted in 50:50 chloroform:ethanol solution overnight, and rehydrated in 100%, 95%, and dH<sub>2</sub>O for 2 min each. Cresyl violet acetate was dissolved at 0.1 w/v % in dH<sub>2</sub>O and 0.3 ml of glacial acetic acid was added to 100 ml of solution. Brain sections were incubated in cresyl violet solution for 1 h at 37°C, washed in H<sub>2</sub>O and serially dehydrated in 95%, 100% ethanol, and xylene. Sections were mounted and sealed.

Sections were examined for the start and end points of stroke cavity. Every 10<sup>th</sup> section was imaged from the start to the end of the cavity. The cavity size on each section was measured using ImageJ, summed and multiplied by 10 to obtain the cavity size.

#### **4.3.8 Immunohistochemistry**

From each brain 16 sections were analyzed using immunohistochemistry. Sections were permeabilized for 30 min with 1% Triton X-100 in PBS and blocked for 30 min with a solution of 0.1% Triton X-100 and 5% BSA in PBS. Sections were incubated with primary antibodies at 4°C overnight. Mouse anti-human Ki-67, mouse anti-rat GFAP, rat anti-mouse CD68<sup>+</sup> and rabbit anti-mouse double-cortin (DCX), and mouse anti-rat NeuN were used at 1:200 dilution. Sections were then washed 3 times in PBS and incubated in secondary antibodies for 1 h at room temperature. Alexa 488 goat-anti-rat IgG, Alexa 488 and 568 goat-anti-rabbit IgG, and Alexa 568 goat-anti-mouse IgG were used at 1:200 dilutions. Sections were washed 3 times in PBS, mounted with Vectashield and sealed.

#### **4.3.9 Analysis of apoptosis using TUNEL**

Terminal deoxynucleotidyl transferase dUTP nick end labelling (TUNEL) was used to determine apoptosis after stroke. The ApopTag Fluoresceine In Situ Apoptosis kit was purchased from Millipore (Danvers, MA, U.S.A.) and the TUNEL assay performed as per the manufacturer's instructions. A total of 8 sections were analysed from each brain.

#### 4.3.10 Statistics

All experiments were conducted with three replicates ( $n = 3$ ), and data are shown as mean  $\pm$  standard deviation. One-way ANOVA with Bonferonni correction was used to compare between multiple groups. Significance levels were indicated as  $p < 0.05$  (\*),  $0.01$  (\*\*), and  $0.001$  (\*\*\*)).

### 4.4 Results

#### 4.4.1 Cortical EPO Receptor (EPOr) expression in uninjured and stroke-injured brains

The rate of protein elimination in the brain is an important determinant of penetration distance, which can be significantly increased by reducing elimination kinetics. Receptor mediated endocytosis is a key route of EPO elimination from the brain [27] and since many cell types in the brain express EPO receptors (EPOr) [27, 28], it was important to quantify the number of EPOr<sup>+</sup> cells in both uninjured and stroke-injured brain tissues. By quantifying the number of EPOr<sup>+</sup> cells in two regions along the diffusion pathway and both ipsilateral and contralateral to the injury (**Fig. 4.2a**), we found that the total number of EPOr<sup>+</sup> cells in our two selected volumes of cortical tissue was similar between uninjured and stroke-injured animals (**Fig. 4.2b**). The similarity in brain EPOr expression before and after stroke injury suggests that EPO penetration in brain tissue will be unaffected by the stroke injury, and EPO may penetrate significantly in the tissue without requiring further modification with, for example, PEG, as has been required for other proteins [21, 22].

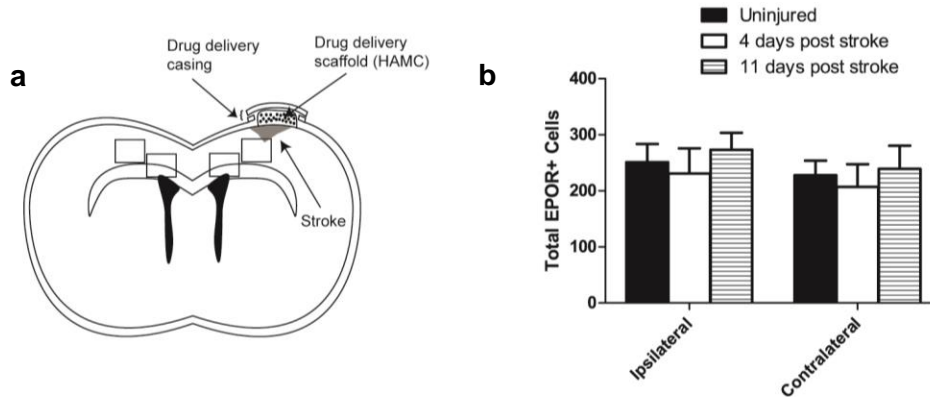


**Figure 4.2 | EPOr expression is similar between uninjured and stroke-injured brain tissues.** (a) Diagrammatic representation of the stroke-injured brain and the regions of interest for EPOr quantification. Rectangles indicate regions examined for EPOr expression. (b) Total numbers of EPOr<sup>+</sup> cells are similar in all three conditions and both ipsilateral and contralateral to injury (mean  $\pm$  standard deviation, n = 3 animals, 16 tissue slices were analyzed per animal).

#### 4.4.2 Release and penetration of EPO in uninjured and stroke-injured brains

Prior to studying EPO release from HAMC *in vivo*, we tested the *in vitro* release profile of EPO from HAMC and found that approximately 80% of EPO was released in the first 24 h, and all of the encapsulated protein was released within 48 h (Fig. S4.1a). Plotting the cumulative fractional release against the square root of time ( $t^{1/2}$ ) yields a linear relationship, indicating Fickian diffusion kinetics (Fig. S4.1b).

The *in vivo* release and penetration of EPO from HAMC in both uninjured and stroke-injured brains was quantified at 4 h, 1 d, and 2 d after injection at two different injection times after stroke injury: 4 and 11 days (Fig. 4.3a, b). For each set of time points and in all uninjured, 4 d injured and 11 d injured brain tissues, the amount of EPO remaining in HAMC was similar as quantified by ELISA. This demonstrates that the tissue type did not affect the rate of release of EPO from HAMC (Fig. 4.3c). In order to calculate the percent of EPO released from HAMC and



in the brain tissue, we compared the amount of EPO detected to a theoretical amount. The theoretical amount of EPO was estimated by assuming that the entire quantity of EPO released from HAMC diffused into the brain. The difference between theoretical and measured EPO was used to estimate the rate at which protein is eliminated from the tissue (**Fig 4.3d**).

The penetration depth of EPO in the uninjured brain and 4 and 11 day-stroke-injured brains were determined at 4 h, 1 d, and 2 d post injection (**Fig. 4.3e – g**). Similar penetration profiles were found between all groups at the three time points examined. Importantly, a significant amount of EPO was found between 2 and 3 mm ventral to the cortical surface, which corresponds to the location of the SVZ in the mouse brain. The lack of EPO $\alpha$  upregulation after stroke supports these data and enables significant EPO penetration in the brain. These promising results led us to investigate the effects of HAMC and EPO on cortical tissue and endogenous brain NSPCs.

#### **4.4.3 Effects of EPO delivered from HAMC on stroke cavity size**

To investigate the biological effect of EPO delivered epi-cortically from HAMC, stroke was induced on day 0 by injection of endothelin-1 into the mouse brain, and either HAMC alone or HAMC with EPO was injected on either day 4 or day 11 post injury (**Fig. 4.1**). The drug delivery system was injected ipsilateral to the stroke. The contralateral hemisphere served as an internal control in all groups examined.

Injection of endothelin-1 into the mouse brain led to the formation of a cavity at the injection site (**Fig. 4.4a**). We measured the cavity volume in stroke-injured animals, and compared this to that of stroke-injured animals treated with HAMC alone or HAMC with EPO (**Fig. 4.4b**). To establish

a time course on the effects of EPO, we examined two time points: 4 d and 11 d after stroke. When injected 4 d post stroke, the vehicle alone (HAMC) appeared to reduce cavity volume relative to stroke alone; however, when EPO was delivered in HAMC this reduction in cavity size was significant ( $p = 0.031$ ).

When injected 11 d post stroke, HAMC alone significantly decreased the cavity volume compared to injury alone ( $p = 0.033$ ). HAMC with EPO further reduced cavity size compared to both HAMC treated ( $p = 0.045$ ) and untreated ( $p = 0.006$ ) animals. The reduction in cavity size observed with HAMC alone was unexpected and led us to investigate the possible mechanism further.

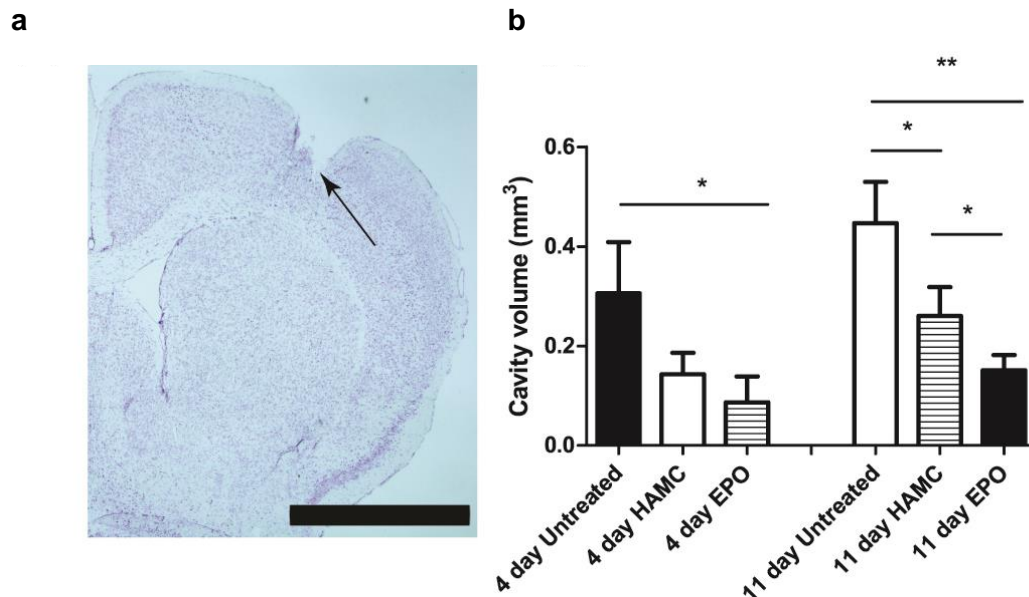


**Figure 4.4 | EPO delivered epicortically from HAMC decreases the stroke cavity size at 4 and 11 days after stroke.** (a) Image of a brain section with stroke cavity (indicated by arrow) shown at 1.25x (scale: 2 mm). (b) Quantification of the cavity sizes. Stroke-injured animals received treatments at either 4 or 11 d post-stroke. Treatment with EPO in HAMC significantly reduced cavity size at 4 d, while both HAMC and EPO in HAMC significantly reduced cavity size at 11d (mean  $\pm$  standard deviation,  $n = 3$  animals, 16 tissue slices were analyzed per animal).

#### 4.4.4 Effect of HAMC on the inflammatory response after stroke

When stroke-injured animals received injections of HAMC at both 4 d and 11 d post injury, the number of reactive astrocytes, as indicated by GFAP<sup>+</sup> immunostained cells with ramified morphology (Fig. 4.5a – e), decreased in the ipsilateral cortex ventral to the lesion site ( $p = 0.003$  at 4 d and  $p = 0.001$  at 11 d; Fig. 4.5f). Interestingly, there was no difference observed between injections of HAMC vs. HAMC with EPO, suggesting that the reduced glial response was due to the biomaterial and not EPO.

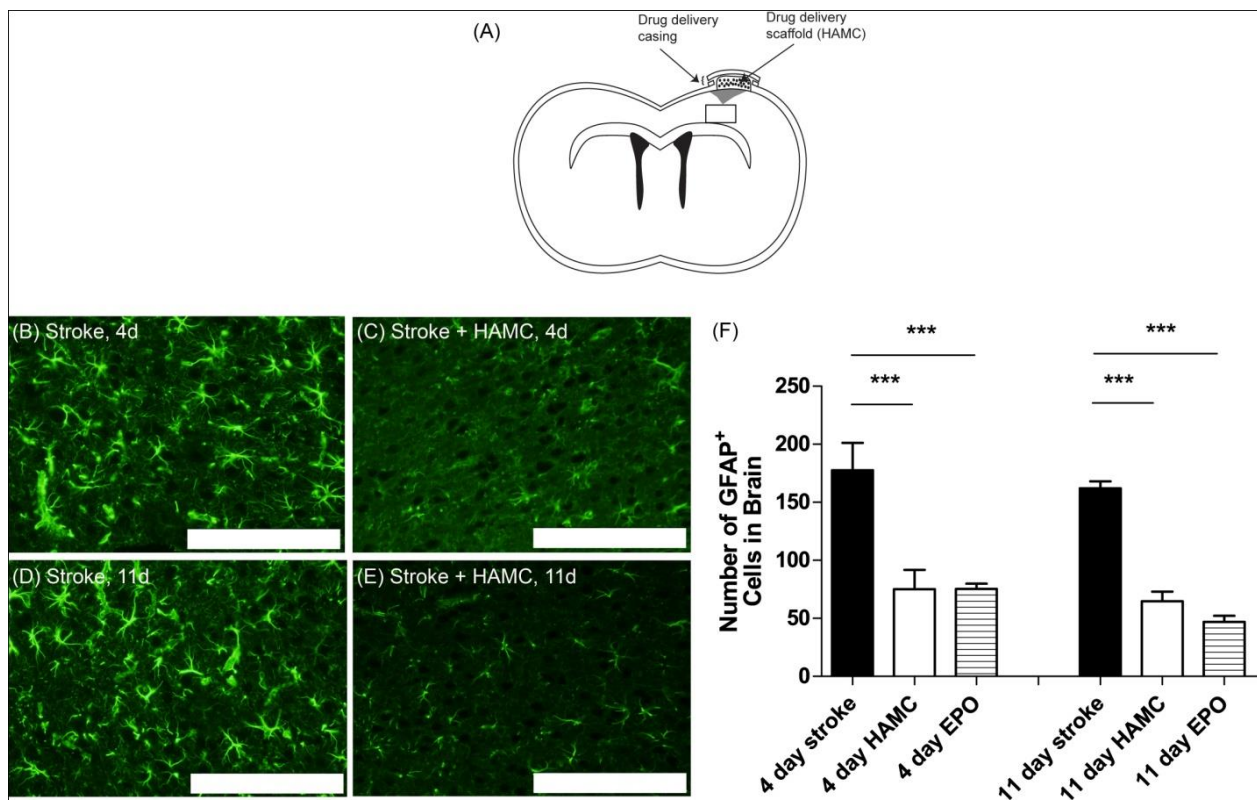


**Figure 4.5 | Epi-cortical delivery of EPO from HAMC attenuates the reactive astrocyte response at 4 and 11 days after stroke injury.** (a) Diagram of the stroke-injured brain with drug delivery device. Rectangle indicates the region of interest. Representative images of GFAP<sup>+</sup> reactive astrocytes in the ipsilateral cortex ventral-lateral to the lesion site are shown for animals that received (b) stroke alone and (c) stroke followed by HAMC injection at 4 d, as well as (d) stroke alone and (e) stroke with HAMC injection at 11 d. Scale: 100  $\mu$ m. (f) Quantitative comparison of average number of GFAP<sup>+</sup> cells are shown for the ipsilateral cortex per field of view. Treatment with both HAMC and EPO in HAMC significantly reduced the total number of GFAP<sup>+</sup> cells at both 4 and 11 days while the total number of DAPI<sup>+</sup> cells remain the same (mean  $\pm$  standard deviation,  $n = 3$  animals, 16 tissue slices were analyzed per animal).

The number of CD68<sup>+</sup> activated microglia and macrophages (**Fig. 4.6a - e**) also decreased around the lesion site in response to injection of HAMC at 4 d and 11 d post stroke ( $p = 0.01$  at 4 d and  $p = 0.004$  at 11 d, **Fig. 4.6f**). Similar to the astroglial response, there was no difference observed between injections of HAMC vs. HAMC with EPO in terms of the number of CD68<sup>+</sup> cells, suggesting that the attenuated inflammatory response was due to the biomaterial and not EPO. Taken together, the reduced stroke cavity can be predominantly attributed to the biomaterial, HAMC.

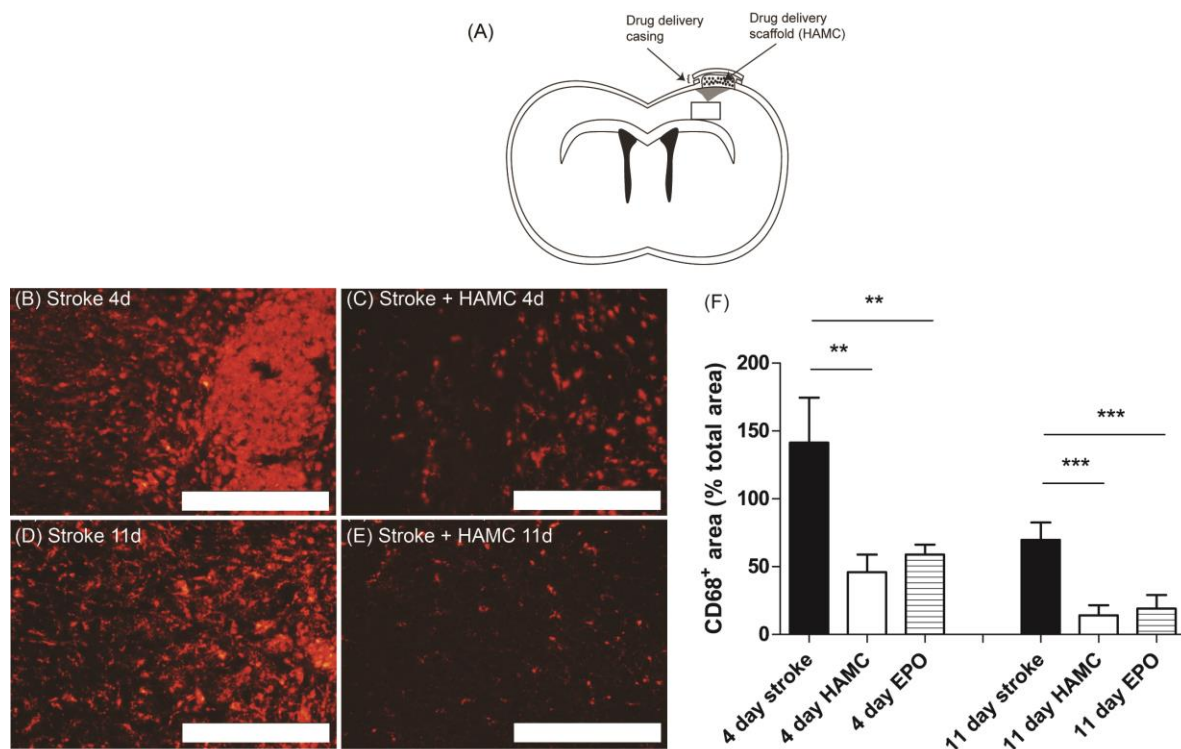


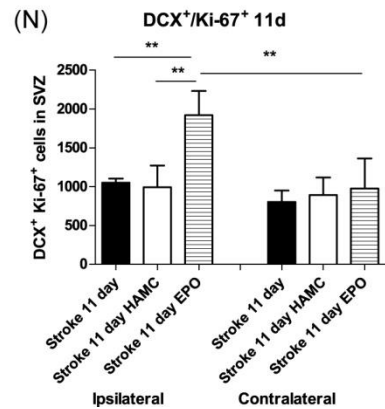
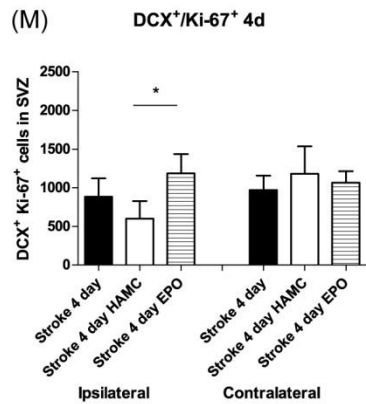
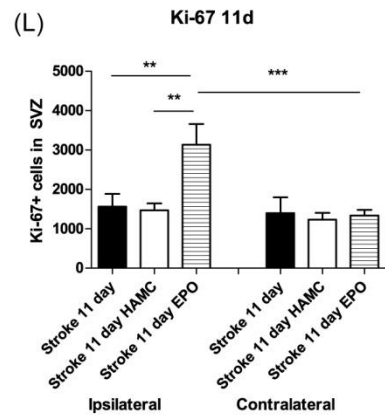
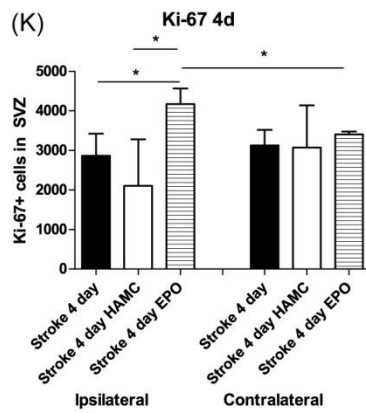
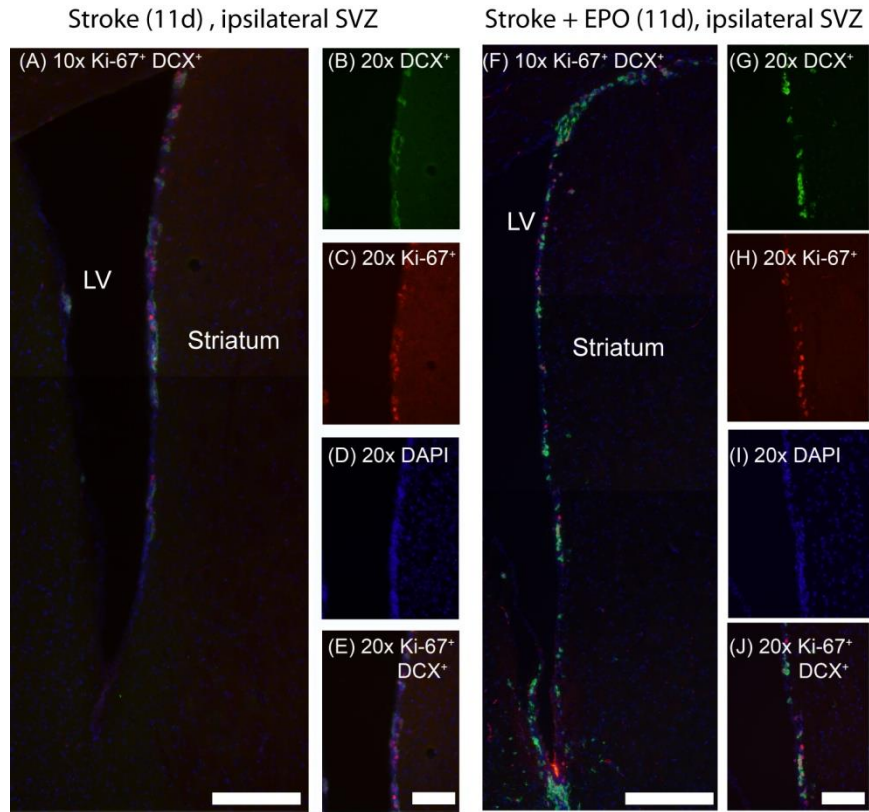
**Figure 4.6 | Epi-cortical delivery of EPO from HAMC attenuates the activated microglia response at 4 days after stroke injury.** (a) Diagram of the stroke-injured brain with drug delivery device. Rectangle indicates the region of interest. Representative images of CD68<sup>+</sup> cells in the ipsilateral cortex are shown for animals that received (b) stroke alone and (c) stroke followed by HAMC injection at 4d, as well as (d) stroke alone and (e) stroke with HAMC at 11d. Scale: 100  $\mu$ m. (f) Quantitative comparison of average number of CD68<sup>+</sup> cells are shown for the ipsilateral cortex per field of view. Treatment with both HAMC and HAMC with EPO significantly reduced the level of CD68<sup>+</sup> signal at both 4 and 11 days while the total number of DAPI<sup>+</sup> cells remain the same (mean  $\pm$  standard deviation,  $n = 3$  animals, 16 tissue slices were analyzed per animal).

#### 4.4.5 Effect of EPO on Ki-67<sup>+</sup> and double cortin<sup>+</sup> (DCX<sup>+</sup>) Ki-67<sup>+</sup> cells in the SVZ

Compared to controls of either stroke alone (**Fig. 4. 7a – e**) or stroke with HAMC, injection of HAMC with EPO onto stroke-injured mouse brains significantly increased the number of Ki-67<sup>+</sup> and DCX<sup>+</sup> Ki-67<sup>+</sup> double positive cells in the ipsilateral SVZ (**Fig. 4.67f – j**). Ki-67 is a marker for proliferating cells while DCX is a marker associated with migratory neuroblasts [29]. Similarly, when injected 4 d (**Fig. 4.7k**) and 11 d (**Fig. 4.7l**) post-stroke, HAMC with EPO treatment led to an approximate 2-fold increase in Ki-67<sup>+</sup> cells compared to HAMC treatment alone and stroke alone. Only the EPO-treated groups had significantly more Ki-67<sup>+</sup> cells in the ipsilateral SVZ than the contralateral SVZ at both time points ( $p = 0.031$  at 4 d and  $p = 0.005$  at 11 d). This shows that the hydrogel alone does not induce cell proliferation, and that exogenous EPO is required to stimulate cell proliferation in the SVZ. Furthermore, there was no difference between any groups in the contralateral SVZ, suggesting that EPO diffusion was specific to the ipsilateral cortex, where it was injected.

**Figure 4.7 | Epi-cortical delivery EPO in HAMC increases the number of Ki-67<sup>+</sup> proliferating cells and DCX<sup>+</sup> migratory neuroblasts in the SVZ at 4 and 11 days post injury.** Representative images are shown for Ki-67<sup>+</sup> cells and DCX<sup>+</sup> Ki-67<sup>+</sup> double-labeled cells in the SVZ ipsilateral to the stroke injury following (a – e) stroke injury and (f – j) EPO injected with HAMC 11 days after stroke. The lateral ventricle (LV) and the striatum are labelled. Scale: (a, f) 500  $\mu\text{m}$  at 10x, (b – e, g – j) 100  $\mu\text{m}$  at 20x. The number of Ki-67<sup>+</sup> cells in the ipsilateral SVZ at (K) 4 d and (L) 11 d is significantly increased by HAMC-mediated EPO treatment while the number of Ki-67<sup>+</sup> cells in the contralateral SVZ remain similar between treatments. DCX<sup>+</sup> Ki-67<sup>+</sup> double positive cells in the ipsilateral SVZ at (M) 4 d and (N) 11 d post stroke also increased following HAMC-mediated EPO treatment (mean  $\pm$  standard deviation,  $n = 3$  animals, 16 tissue slices were analyzed per animal).

Figure 4-7



Interestingly, the absolute numbers of Ki-67<sup>+</sup> cells in both the ipsilateral and contralateral SVZ were lower when EPO was delivered 11 d post stroke compared to 4 d post stroke ( $p = 0.031$ ). This suggests that proliferation of cells in the SVZ decreased with time after stroke injury, but may be partially restored with EPO treatment. The number of double positive DCX<sup>+</sup> Ki-67<sup>+</sup> cells in the SVZ was close to 2-fold greater with EPO delivery in the ipsilateral SVZ at both 4 d (**Fig. 4.7m**) and 11 d (**Fig. 4.7n**) post-stroke. This increase was not observed following treatment with HAMC alone. No difference was found between any groups in the contralateral SVZ.

When delivered 11 d post stroke, the number of double positive DCX<sup>+</sup> Ki-67<sup>+</sup> cells was also enhanced compared to 4 d post stroke ( $p = 0.033$ ). Moreover, only EPO delivery at 11 d post stroke resulted in significantly higher DCX<sup>+</sup> Ki-67<sup>+</sup> cells in the ipsilateral SVZ compared to the contralateral SVZ ( $p = 0.03$ ). These results indicate that when given 11 d (vs. 4 d) after stroke, EPO enhanced the migratory potential of proliferating cells in the ipsilateral SVZ. Since DCX is an immature marker for precursor cells but not found in mature neurons [30], these findings suggest that EPO promotes neuroregeneration.

#### **4.4.6 Effect of EPO on NeuN<sup>+</sup> mature neurons in the injured cortex**

We examined neuronal responses in stroke animals that received EPO. Stroke injuries cause neuronal death in the ipsilateral cortex (**Fig. 4.8a – d**). EPO delivery both 4 d and 11 d post stroke significantly increased the number of NeuN<sup>+</sup> mature neurons in the injured cortex relative to stroke alone ( $p = 0.001$  at 4 d,  $p = 0.032$  at 11 d, **Fig. 4.8e – g**), although the total number of mature neurons in the injured cortex was still more than ten-fold lower than that in the uninjured contralateral cortex.

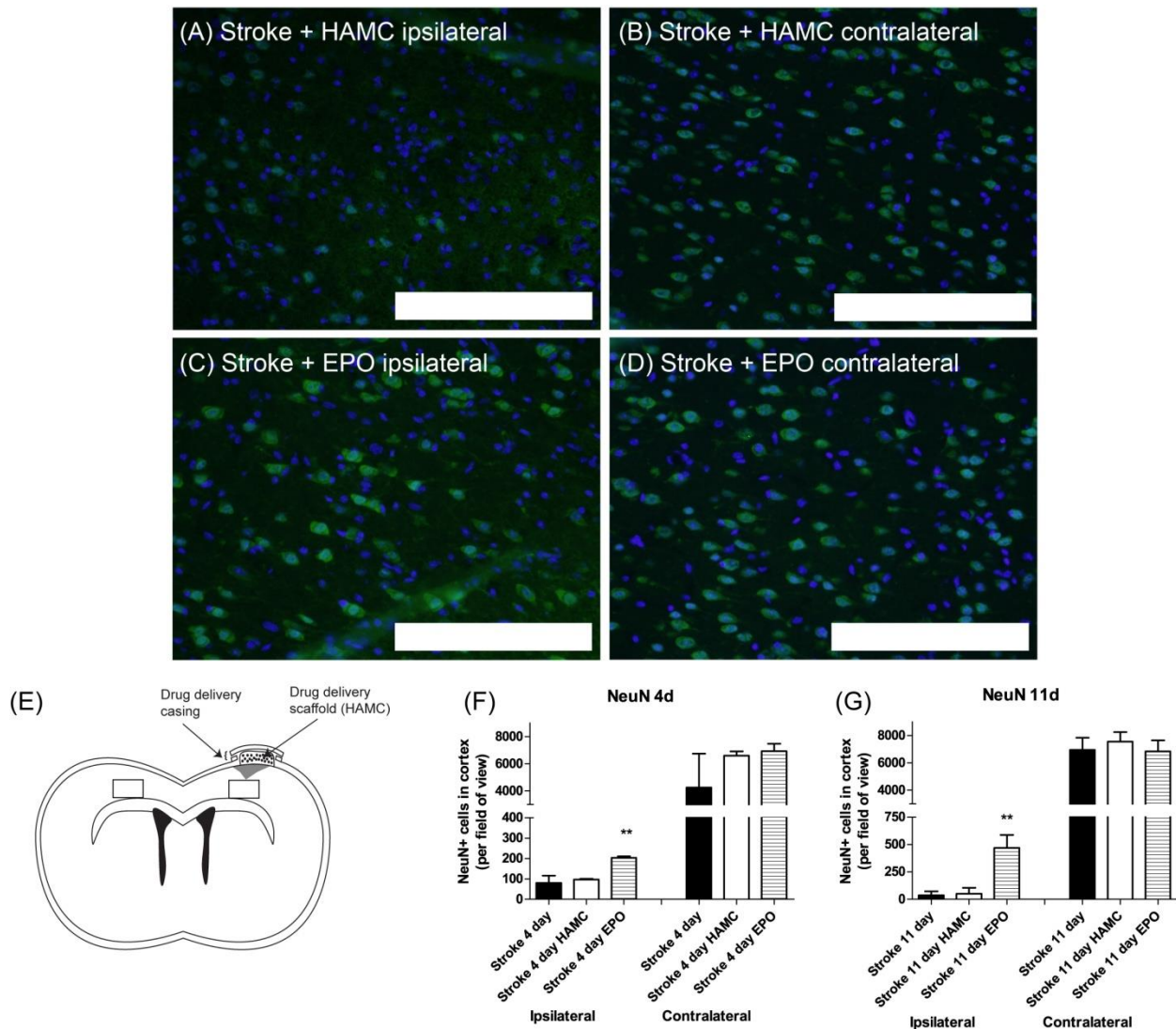


**Figure 4.8 | EPO delivered from HAMC enhances the number of NeuN<sup>+</sup> mature neurons in the injured cortex at 4 and 11 days post injury.** Representative images are shown for NeuN<sup>+</sup> cells in the cortex of stroke-injured, sham treated animals (a) ipsilateral and (b) contralateral to the injury, as well as stroke-injured, EPO treated animals (c) ipsilateral and (d) contralateral to the injury at 4 days post stroke. Scale: 100  $\mu$ m. (e) Diagram of the brain with rectangles showing the regions analysed. Quantification of NeuN<sup>+</sup> cells are shown for (f) 4 d and (g) 11 d after stroke (mean  $\pm$  standard deviation, n = 3 animals, 16 tissue slices were analyzed per animal).

When stroke injured animals received no treatment or HAMC alone, the number of NeuN<sup>+</sup> cells found in the ipsilateral cortex was higher at 4 days post-stroke compared to 11 days post-stroke, although the difference was not statistically significant. Cell death likely continues to occur

around the lesion site between 4 and 11 days after stroke injury. Unexpectedly, the number of NeuN<sup>+</sup> cells in the ipsilateral cortex was higher when EPO was delivered 11 d post-stroke than 4 d post-stroke ( $p = 0.017$ ). This result mirrors the increase of DCX<sup>+</sup> Ki-67<sup>+</sup> double positive cells in the SVZ at 11 d compared to 4 d, and indicates that epi-cortically delivered EPO has a direct benefit on increasing the number of neurons around the infarct site.

#### **4.4.7 Effect of EPO on TUNEL<sup>+</sup> apoptotic cells in the injured cortex and SVZ**

We studied the extent of apoptotic cell death by TUNEL-immunostaining in both the cortex and the SVZ after stroke and injection of either HAMC alone or HAMC with EPO. In the SVZ (**Fig. 4.9a, b**), injection of HAMC alone, at either 4 d or 11 d, did not change the TUNEL<sup>+</sup> response compared to stroke-injured groups. However, when EPO was delivered from HAMC, a significant decrease in the TUNEL<sup>+</sup> signal was found at both 4 d ( $p = 0.007$ ) and 11 d ( $p = 0.049$ ) compared to HAMC alone. This reduction in the number of apoptotic cells in the SVZ may be correlated to the increase in Ki67<sup>+</sup> proliferating cells in the SVZ and suggests a neuroprotective role for EPO. This effect is further supported by the data that show the number of TUNEL<sup>+</sup> cells in the ipsilateral SVZ being similar to that found in the contralateral SVZ only after EPO delivery at 4 d. Thus EPO delivery appeared to decrease cell death to the basal level in the SVZ. The data at 11 d follows similar trends to those at 4 d; however, the differences in ipsilateral and contralateral SVZ are not significant at 11 d, suggesting that neuroprotective effects associated with EPO delivery are more significant when it is present at earlier time points after stroke.

In the ipsilateral cortex, we also observed a decrease in the number of TUNEL<sup>+</sup> cells after EPO delivery relative to injection of HAMC alone or stroke alone (**Fig. 4.9c, d**). HAMC treatment did not lead to changes in cortical TUNEL stain relative to stroke alone. The decrease at 4 d was significantly different whereas that at 11 d post stroke was not statistically significant. The lack

of statistically significant improvement when EPO was delivered 11 d post-stroke further suggests the necessity of early EPO administration for neuroprotection.

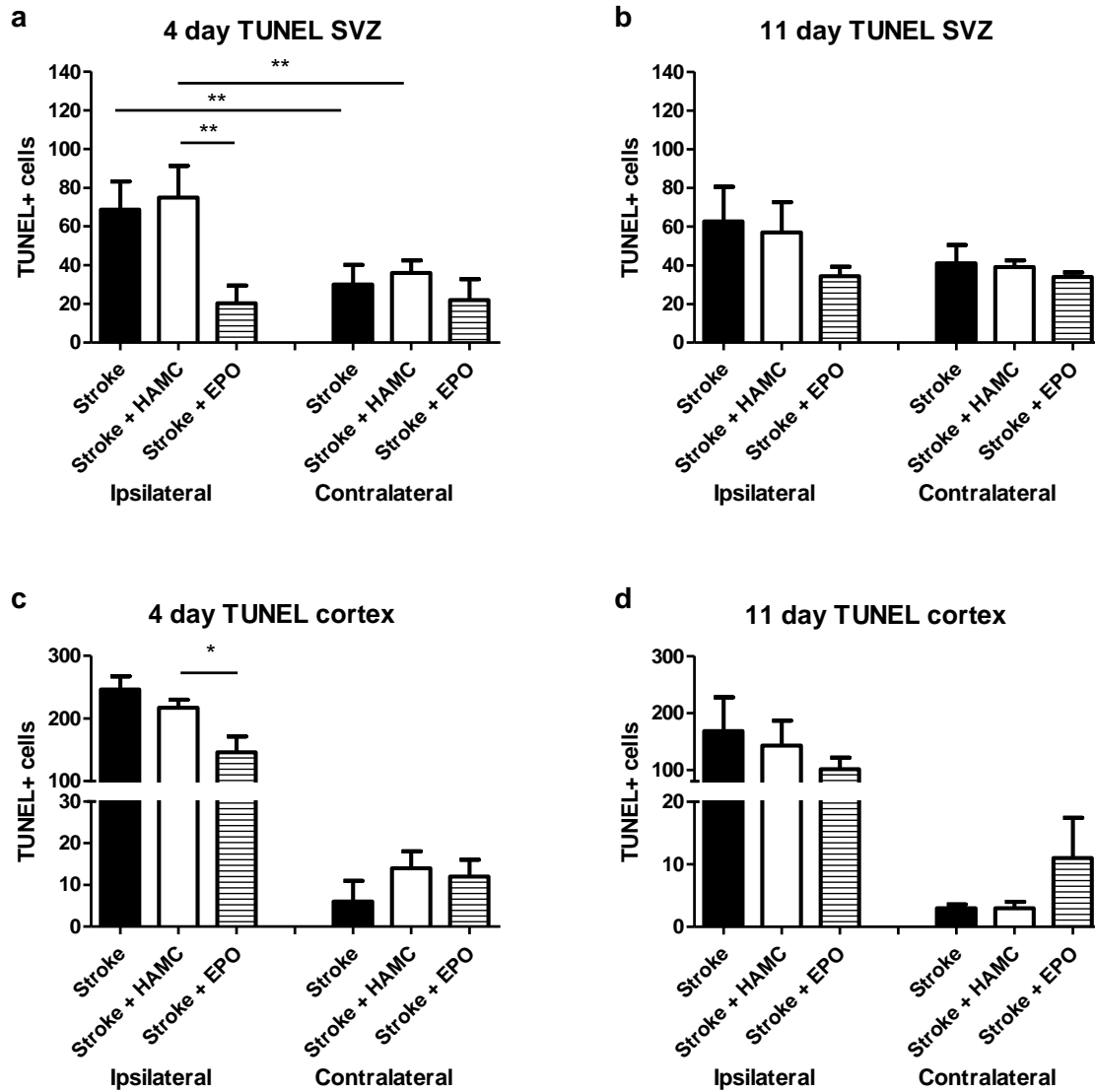


**Figure 4.9 | Treatment with EPO delivery at both 4 d and 11 d post stroke led to decreased number of TUNEL<sup>+</sup> cells in the ipsilateral SVZ and cortex.** When stroke-injured animals were treated with EPO, the number of TUNEL<sup>+</sup> apoptotic cells decreased both in the (a, b) ipsilateral SVZ and the (c, d) ipsilateral cortex at 4 d or 11 d post stroke. HAMC alone had no effect relative to stroke alone.

## 4.5 Discussion

The HAMC-mediated epi-cortical delivery of EPO allowed us to observe tissue benefit resulting from both EPO and HAMC. Injection of HAMC itself led to an attenuated inflammatory response after stroke, as indicated by fewer reactive astrocytes and activated microglia around the lesion site. HAMC has been shown to attenuate the inflammatory response after spinal cord injury [17]. HA itself has been reported to be anti-inflammatory [31] through reducing white cell migration to the site of injury [32], and through inhibiting pro-inflammatory molecules of the prostaglandin pathway [33]. It also enhances wound healing and angiogenesis after traumatic brain injury [34]. The attenuated inflammatory response may account for the reduced cavity size observed [35] with injection of HAMC following stroke injury and likely reflects the wound healing properties of HA [36].

We found that the penetration profiles and in vivo elimination rate of EPO are similar between the uninjured and stroke injured brains at two times after stroke. This was interesting given that epidermal growth factor (EGF) has been previously reported to be eliminated significantly faster in the infarct brain compared to the uninjured brain due to EGF receptor overexpression [18, 23]. The transport of epidermal growth factor (EGF) in the brain decreased more than three-fold after stroke injury [18, 23], and PEG-modification of EGF was required to enhance the amount of EGF reaching the SVZ. Conversely, EPO penetration was independent of injury and EPO was able to penetrate the brain tissue sufficiently to reach the SVZ after stroke.

Receptor-mediated endocytosis is one of the major routes for EPO clearance from the brain [28]. We found that the extent of EPOr expression was similar between uninjured and stroke injured brains in regions of the cortex and striatum through which it would have to diffuse to reach the SVZ, and which helps to explain the similar diffusion profiles of EPO in the brain before and

after stroke injury. While EPOr has been previously reported to be upregulated in the penumbra of stroke-injured brains, the specific regions where EPOr overexpression was observed were not reported [7, 37, 38], which may explain our different results. Interestingly, since neurons and astrocytes in the brain both express EPOr [39], and the number of reactive astrocytes, are reduced in the presence of HAMC, EPOr expression may have been further attenuated. It is clear that the in vivo environment has a profound impact on protein transport in the brain, as the rate of protein elimination is directly influenced by the number of cell surface receptors and binding moieties on the extracellular matrix (ECM) [40]. Since protein penetration is dictated by both the rates of diffusion and elimination, a good understanding of the in vivo environment allows protein penetration distance to be predicted and whether minimally invasive drug delivery from the cortical surface is feasible.

EPO delivered from HAMC shows significant benefits in the post-stroke brain. The effect of EPO on reducing the stroke cavity size agrees with results reported previously [8]. The numbers of SVZ neuroblasts as well as mature neurons following EPO delivery at 11 d are enhanced compared to those following EPO delivery at 4 d. This may be due to the fact that the environment in the brain 4 d post-stroke is more inflammatory than at 11 d post-stroke. We showed that at 11 d, the CD68<sup>+</sup> activated microglia/macrophages in the brain decreased compared to 4 d, which is consistent with others' findings that in the acute period after stroke, there is a higher degree of proteases, inflammatory cytokines, and scavenging inflammatory and immune cells in the brain [41, 42]. Thus the beneficial effect of EPO may be masked by these deleterious factors at 4 d [43].

EPO has been shown to have both neuroprotective and neuroregenerative properties in the CNS [44]. EPO delivered 4 d post-stroke decreased apoptosis in the SVZ and the injured cortex, and maintained higher numbers of mature neurons in the injured cortex. Since 4 d after stroke is

unlikely sufficient time for newly generated neuronal precursors to migrate to the stroke site and mature [45], the observed benefit is likely attributable to the neuroprotective role of EPO. EPO delivery 11 d post-stroke also led to qualitatively fewer apoptotic cells in the injured cortex, although the lack of statistically significant difference at 11 d suggests that acute EPO treatment post-injury is required to achieve neuroprotection. We also observed a neuroregenerative effect associated with epi-cortical EPO delivery. EPO delivered at 4 d and 11 d post stroke increased the number of both proliferating cells and migratory neuroblasts in the SVZ. The decrease in TUNEL<sup>+</sup> cells in combination with the increase in proliferative cells in the SVZ following EPO delivery at both 4 d and 11 d also suggests that EPO mediates neuroregeneration by promoting the survival of NSPCs in the brain as has been also reported by others [46, 47]. EPO delivery also increased the number of mature neurons 11 d post-stroke at the lesion site. This further suggests enhanced neuroregeneration following EPO treatment, and that delayed treatment provides a tissue benefit.

The benefits of epi-cortical EPO delivery observed here demonstrate that HAMC is a promising vehicle for enabling local delivery of therapeutics to the brain. The potential advantages of the system may be enhanced by increasing the length of delivery or by delivering a panel of factors. Many groups have shown that prolonged delivery of drugs to the brain, including EPO [48], significantly increases the benefits observed [15, 49]. HAMC is a hydrogel that itself will not facilitate prolonged delivery; however, tunable and controlled delivery of factors from HAMC may be achieved by incorporating polymeric particles that encapsulate drugs into the hydrogel [49]. Importantly, local epi-cortical delivery of drugs, such as EPO with HAMC, should result in a lower overall dose delivered and thus fewer side effects. For example, with intracerebroventricular delivery, cerebrospinal fluid is continually replenished resulting in the drug being distributed throughout the central nervous system. In fact, only 1 – 2% of drugs delivered to the ventricles can be found in the tissue 1 mm away from the ependyma [16]

whereas in our epicortical HAMC delivery strategy, EPO was found 3 mm from the injection site. This illustrates that HAMC-mediated epi-cortical delivery is a true local delivery strategy, and promising for eliciting tissue benefit with reduced side effects relative to both systemic and intraventricular delivery. Co-delivering a panel of factors often facilitates synergistic benefits. EPO has been delivered with EGF [50], brain derived neurotrophic factor [10], ciliary neurotrophic factor [10], and insulin-like growth factor [51], among others, to elicit neuroregeneration or neuroprotection after CNS injuries. HAMC has previously been used to deliver a multitude of proteins and small molecule drugs to the CNS to achieve tissue and functional benefits [17, 19, 49, 52-54]. The findings here illustrate that HAMC is a versatile drug delivery platform to improve the treatment of CNS disorders of the brain.

#### **4.6 Conclusion**

HAMC is an injectable hydrogel that attenuates the inflammatory response in the brain and can be used to achieve controlled short-term delivery of EPO, which is a versatile glycoprotein that induces both neuroprotection and neuroregeneration in the CNS. EPO penetrated deep into the brain, reaching the cells in the subventricular zone and had neuroprotective and neuroregenerative effects after stroke. The benefits observed from epi-cortical EPO delivery from HAMC suggest that this hydrogel can be used as a platform technology to enable minimally invasive CNS drug delivery.

## 5. Bioengineered sequential growth factor delivery stimulates brain tissue regeneration after stroke\*

\*This chapter was accepted for publication in the Journal of Controlled Release.

Wang Y.<sup>5</sup>, Cooke, M.J., Sachewsky, N., Morshead, C.M., Shoichet, M.S. 2013. “**Bioengineered sequential growth factor delivery stimulates brain tissue regeneration after stroke**”. Journal of Controlled Release, Accepted.

### 5.1 ABSTRACT

Stroke is a leading cause of disability with no effective regenerative treatment. One promising strategy for achieving tissue repair involves the stimulation of endogenous neural stem/progenitor cells through sequential delivery of epidermal growth factor (EGF) followed by erythropoietin (EPO). Yet currently available delivery strategies such as intracerebroventricular (ICV) infusion cause significant tissue damage. We designed a novel delivery system that circumvents the blood brain barrier and directly releases growth factors to the brain. Sequential release of the two growth factors is key in eliciting tissue repair. To control release, we encapsulate pegylated EGF (EGF-PEG) in poly(lactic-co-glycolic acid) (PLGA) nanoparticles and EPO in biphasic microparticles comprised of a PLGA core and a poly(sebacic acid) coating. EGF-PEG and EPO polymeric particles are dispersed in a hyaluronan methylcellulose (HAMC) hydrogel which spatially confines the particles and attenuates the inflammatory response of brain tissue. Our composite-mediated, sequential delivery of EGF-PEG and EPO leads to tissue repair in a mouse stroke model and minimizes damage compared to ICV infusion.

---

<sup>5</sup> Contribution by Y. Wang: designed and conducted all in vitro and in vivo experimental work; collected, analyzed, and interpreted data from experiments; prepared the manuscript.

## 5.2 INTRODUCTION

Stroke is a devastating neurological disorder and a leading cause of disability in the world<sup>2</sup>. Pathologically there are two stages in stroke, the primary and secondary injuries<sup>324</sup>. The primary injury refers to the initial insult and the affected area, the core region, is characterized by necrosis. The secondary injury follows the primary injury, and is caused by the depletion of oxygen and ATP in the tissue surrounding the core. This leads to apoptosis and forms an area of partial cell death, which is termed the penumbra<sup>324</sup>. The inflammatory response associated with stroke further devastates the injury<sup>325</sup> and impedes tissue repair<sup>326</sup>.

Given limited treatment options<sup>327</sup>, regenerative strategies such as stimulation of the endogenous neural stem/progenitor cells (NSPCs) in the subventricular zone (SVZ)<sup>328</sup> of the adult brain have been pursued. NSPCs proliferate at constitutive levels in the healthy adult brain and migrate to the olfactory bulbs. After injury, the level of NSPC proliferation in the SVZ increases, and some precursor cells migrate towards the injured cortex<sup>329,330</sup>. However, the level of proliferation and migration induced by stroke is insufficient to promote repair, as a large number of these newborn cells die before they can mature and integrate into the neuronal network<sup>331</sup>. The goal of regenerative strategies is to stimulate NSPC proliferation and migration to the injury site, thereby replenishing the tissue lost during stroke<sup>319</sup>. A number of growth factors, including erythropoietin (EPO)<sup>332</sup>, vascular endothelial growth factor (VEGF)<sup>333</sup> and fibroblast growth factor-2 (FGF-2)<sup>334</sup> have been shown to stimulate neurogenesis. Moreover, treatments where two or more factors are delivered in a controlled manner have demonstrated enhanced efficacy compared to single-factor treatments<sup>335</sup>.

Delivering growth factors to the brain is not trivial, as the blood brain barrier (BBB) isolates the brain from systemic circulation both physically and chemically<sup>336</sup>. Conventional systemic delivery strategies, such as intravenous infusion, are relatively simple and non-invasive, but

many growth factors cannot efficiently penetrate the BBB<sup>337</sup>, and thus high doses are required, which can result in systemic toxicity. Systemic delivery combined with localized disruption of the BBB, such as with ultrasound, provides an alternative strategy, but opens the BBB non-selectively and may permit harmful substances to enter the brain<sup>338</sup>. Local delivery strategies such as intracerebroventricular (ICV) infusion through the catheter/osmotic minipump system bypass the BBB, but require invasive surgeries<sup>339</sup>. Notwithstanding the invasiveness of this procedure, sequential infusion using a catheter/minipump system of EGF and EPO (but neither individually) led to tissue repair in a pial vessel disruption (PVD) rat model of stroke<sup>22</sup>. EGF stimulates the proliferation of NSPCs to expand the pool, while EPO is neuroprotective and reduces apoptosis of the newly generated cells. The temporally controlled infusion of EGF for the first 7 days followed by EPO for the subsequent 7 days is key to tissue repair, which was achieved with neither simultaneous EGF and EPO delivery nor each factor alone. Here we are interested in: (1) engineering a new, less invasive strategy for local delivery of each of EGF and EPO while maintaining temporal controlled release; and (2) testing this strategy relative to the conventional catheter/minipump system in a different animal model of stroke – the endothelin-1 mouse model of focal ischemic stroke.

Using an epicortical delivery strategy, our challenge was to achieve both controlled temporal growth factor release and sufficient penetration in brain tissue of the released factors for endogenous stem cell stimulation. EGF modified with poly(ethylene glycol) (EGF-PEG)<sup>250,340</sup> and EPO<sup>341</sup> were previously shown to penetrate through the ischemic cortex and reach the SVZ when delivered epicortically from a physical blend of hyaluronan and methylcellulose, HAMC<sup>220</sup>. However, protein delivery from a hydrogel scaffold is governed by Fickian diffusion and tends to occur rapidly. The sustained release over a minimum of 2 weeks, which is required for tissue repair, cannot be easily achieved from a hydrogel alone<sup>342</sup>. Here we developed a novel composite system that allows for sustained release of EGF-PEG followed by EPO. This was

achieved by encapsulating each of EGF-PEG and EPO in polymeric particles and incorporating the particles into the HAMC hydrogel.

We confirm the validity of the endothelin-1 model of stroke in the mouse by showing that sequential infusion of EGF-PEG and EPO using the catheter/minipump system promotes tissue repair in this model, similar to that observed previously with the PVD model. Importantly, we demonstrate a new method for local and sustained drug release to the brain with temporal control, comprised of a composite of HAMC hydrogel and polymeric particles encapsulating EGF-PEG and EPO. We show that this delivery vehicle achieves sequential release of each of EGF-PEG and EPO in vivo and stimulates endogenous NSPCs in the adult mouse brain, resulting in tissue repair in the endothelin-1 model of stroke. This new delivery strategy promotes greater tissue repair than the traditional catheter/minipump system and avoids the consequent tissue damage observed with the latter.

### **5.3 MATERIALS AND METHODS**

#### **5.3.1 Materials**

Recombinant human epidermal growth factor (EGF) and the EGF ELISA detection kit were purchased from PeproTech Inc. (Rocky Hill, NJ, USA). Recombinant human erythropoietin (EPREX) was supplied by Ortho Biotech Canada (Toronto, ON, Canada). Recombinant EPO ELISA kit was purchased from BD biosciences (Mississauga, ON, Canada). Methoxy-poly(ethylene glycol, 5 kDa) activated with propionaldehyde (mPEG-PPA) was purchased from NOF Corp. (Tokyo, Japan). Sodium hyaluronan (HA,  $1.4-1.8 \times 10^6$  g/mol) was purchased from NovaMatrix (Sandvika, Norway). Methyl cellulose (MC,  $3.4 \times 10^5$  g/mol) was obtained from Shin Etsu (Chiyoda-ku, Tokyo, Japan). Mouse anti-human Ki-67 was purchased from BD biosciences (Mississauga, ON, Canada), mouse anti-rat NeuN and GFAP were obtained from Millipore Inc. (Billerica, MA, USA), rat anti-mouse CD68<sup>+</sup> and rabbit anti-mouse double-cortin were obtained

from Abcam (Cambridge, MA, USA), and Vectashield with DAPI stain was purchased from Vectorlabs (Burlington, ON, Canada). Alexa 488 goat-anti-rat, Alexa 488 and 568 goat-anti-rabbit IgG, and Alexa 568 goat-anti-mouse IgG were obtained from Invitrogen Inc. (Burlington, ON, Canada). Sodium cyanoborohydride ( $\text{NaCNBH}_3$ ), NaCl,  $\text{MgCl}_2$ ,  $\text{CaCl}_2$ ,  $\text{BaCl}_2$ ,  $\text{Na}_2\text{HPO}_3$ ,  $\text{NaH}_2\text{PO}_3$ , trehalose, and cresyl violet acetate were supplied by Sigma Aldrich (Oakville, ON, Canada). Triton X-100 was supplied by ACROS (NJ, U.S.A.). Artificial cerebrospinal fluid (aCSF<sup>250</sup>) and all buffers were prepared with distilled and deionized water prepared from a Millipore Milli-RO 10 Plus and Milli-Q UF Plus at  $18 \text{ M}\Omega \cdot \text{m}$  resistivity (Millipore, Bedford, USA).

### **5.3.2 Encapsulation of EGF-PEG in PLGA nanoparticles**

EGF is modified with 5 kDa poly(ethylene glycol) (PEG) using a N-terminus specific mono-PEGylation chemistry as previously described<sup>250</sup>. A 16 mM EGF solution was prepared in sodium acetate (pH 5.5), and 3 molar excess of methoxy-PEG-aldehyde and 140 molar excess of  $\text{NaCNBH}_3$  was added to the reaction mixture. The reaction was allowed to proceed at room temperature overnight. The product is dialyzed against TES buffer (pH 8.2) and purified using size-exclusion FPLC and lyophilized for storage.

EGF-PEG was encapsulated in poly(lactic-co-glycolic acid) (PLGA) nanoparticles using a double-emulsion process. 6.3 mg EGF-PEG was reconstituted in 100  $\mu\text{l}$  PBS (pH 7.4) to form the inner aqueous phase. Either 60 mg or 120 mg of PLGA was dissolved in 900  $\mu\text{l}$  dichloromethane (DCM) to form the organic phase. The two phases were sonicated for 10 min over ice. The primary emulsion was transferred to an outer aqueous phase of 2.5% PVA and 10% NaCl in  $\text{ddH}_2\text{O}$ , and sonicated for 10 min over ice. The final emulsion was stirred overnight in a 2.5% PVA, and either 0% or 10% NaCl hardening bath. The particles were centrifuge-washed

five times and lyophilized for storage. Blank nanoparticles were similarly prepared by using 100  $\mu$ l of 10x PBS (pH 7.4) without protein as the inner aqueous phase.

Particle size was measured on a Malvern zeta-sizer (Mastersizer 2000, Worcestershire, UK). To determine protein encapsulation, EGF-PEG loaded particles were dissolved in 1 ml DCM. The protein was extracted into 9 ml of aCSF and an EGF ELISA was used to determine protein encapsulation as per manufacturer's instructions. The encapsulation efficiency was calculated as (Eq. 5.1):

$$\text{Encapsulation efficiency (EE\%)} = \frac{\text{Measured protein concentration}}{\text{Initial protein concentration in encapsulation}} \times 100\%$$

PLGA nanoparticles loaded with EGF-PEG have an average diameter of 800 nm (polydispersity index = 0.622) and are formed by the double emulsion solvent evaporation method<sup>343</sup>. The particles have an EGF-PEG encapsulation efficiency of  $54 \pm 3.3\%$  (**Supplementary Fig. S5.1a**).

### 5.3.3 Encapsulation of EPO in biphasic microparticles

EPO was encapsulated first in PLGA nanoparticles similar to EGF-PEG. To optimize encapsulation, various formulations were tested (**Supplementary Fig. S5.1b**). 500 U of EPO was encapsulated in test formulations. The optimal formulation with 3.5 wt % BSA (compared to weight of PLGA used) and 400 mM trehalose coencapsulated with 500 U EPO (A) was defined as that which yielded the highest encapsulation with least amount of additives required. This formulation was used to encapsulate 40,000 U of EPO for all subsequent batches.

PLGA nanoparticles containing EPO were subsequently embedded in poly(sebacic acid) (PSA) microparticles in a single emulsion process. 120 mg of EPO-loaded nanoparticles were

dispersed in an organic phase containing 120 mg PSA in 900  $\mu$ l THF. The primary emulsion was sonicated for 15 s and transferred to an outer aqueous phase of 1% PVA and 10% NaCl. The secondary emulsion was homogenized for 1 min and stirred for 4 h at room temperature in a 0.1% PVA, 10% NaCl hardening bath. The particles were centrifuge washed and lyophilized for storage. Blank biphasic particles were similarly prepared by using 100  $\mu$ l of PBS (pH 7.4) with no proteins as the inner aqueous phase of the PLGA nanoparticles.

Particle size was determined using a Malvern mastersizer 2000, and the particles diameter average  $137 \pm 48 \mu\text{m}$ . Surface morphology was examined using SEM and surface chemical composition was determined using XPS (**Supplementary Fig. S5.2**). Particles were dissolved as described above and encapsulation efficiency was measured using an EPO ELISA kit as per manufacturer's instructions. EPO encapsulation efficiency was determined to be  $23 \pm 4.8\%$ , and the particles have an average diameter of  $18 \pm 4.7 \mu\text{m}$  (**Supplementary Fig. S5.2**).

#### **5.3.4 Preparation of HAMC/particle composite drug delivery system (DDS)**

EGF-PEG was encapsulated in PLGA nanoparticles, and EPO was encapsulated in PLGA nanoparticles which were embedded into poly(sebacic acid) (PSA) microparticles. HAMC was prepared as described previously<sup>220</sup>. HA and MC as received were dissolved in ddH<sub>2</sub>O and sterile filtered and lyophilized under sterile conditions. A solution of 1% sterile HA and 2% sterile MC was prepared in sterile aCSF<sup>250</sup>. 120 mg EGF-PEG-loaded PLGA nanoparticles and 50 mg EPO-loaded PSA/PLGA biphasic microparticles were added to 1 ml of HAMC, mixed using SpeedMixer (DAC150FVZ, Landrum, SC, USA.), and kept at 4°C overnight to remove air bubbles.

### 5.3.5 In vitro degradation of the composite DDS

100 µl of the blank composite DDS was injected into the bottom of a 2 ml microcentrifuge tube and allowed to gel at 37 °C. Terminal samples were prepared for the same time points as the *in vitro* release study. Tubes were weighed before and after composite injection. Each tube was then filled with 900 µl of warm aCSF and incubated at 37 °C. The aCSF was removed at each time point and the tube was weighed to obtain the wet composite mass. The composite degradation was calculated as (Eq. 5.2):

$$\% \text{ remaining composite mass} = \frac{\text{Wet mass at time } t}{\text{Initial wet mass}} \times 100\%$$

### 5.3.6 In vitro release profiles of EGF-PEG and EPO from composite DDS

100 µl of composite was injected through a 26G needle into the bottom of 2 ml microcentrifuge tubes and allowed to gel at 37 °C for 10 min. 900 µl of aCSF equilibrated to 37 °C was added to each tube as the release medium. The buffer was completely removed at t = 0, 1, 2, 3, 4, 7, 10, 14, 21, 28, 35 d and replaced with fresh buffer. Samples were analyzed for protein concentration using EGF and EPO ELISA kits as per manufacturer's instructions. All samples were digested after the final time point to determine the amount of protein remaining in the composite.

### 5.3.7 Preparation of drug delivery device

The drug delivery casing was prepared as described previously<sup>340</sup>. The device consisted of two disks (0.5 mm height x 5.9 mm diameter) and was used to confine the composite at the site of injection. The bottom disk contained a 2 mm central opening, and both disks were molded to the shape of the mouse skull. Sterilization with ethylene oxide gas was carried out prior to use.

### 5.3.8 Surgeries

All animal work was carried out in accordance with the Guide to the Care and Use of Experimental Animals (Canadian Council on Animal Care) and approved by the Animal Care Committee at the University of Toronto. 9 – 11 week old male C57BL/6 mice were used in this study (Charles River, QC, Canada). A total of 60 animals were used in these studies.

### 5.3.9 Stroke surgeries and implantation of drug delivery device

Stroke surgeries were carried out as described previously<sup>256</sup>. Mice were anaesthetized with isoflurane, shaved and placed into a Kopf stereotaxic instrument. A midline incision in the scalp was made and a small burr hole was made in the skull at the coordinates 2.25 lateral to the midline and 0.6 anterior to the Bregma. 1  $\mu$ l of endothelin-1 (400 pmol, Calbiochem, Gibbstown, NJ, USA.) was injected 1.0 mm ventral to the brain surface at 0.1  $\mu$ l/min. The needle was left in place for 10 min prior to removal and the incision was sutured. Uninjured mice were similarly treated, but no injection was carried out (**Fig. S5.3**).

The drug delivery system was injected 4 days post stroke to ensure that the majority of neuronal death has occurred, and any neurons found in the peri-infarct site at the completion of treatment are due to neurogenesis. The burr hole was exposed and any tissue debris was removed. The disk with 2 mm central opening was fixed over the burr hole with bone glue. 3  $\mu$ l of the composite was injected into the hole such that it is in direct contact with the brain's cortical surface. A second disk with no opening was fixed over the first disk and the skin was sutured over the system.

### **5.3.10 Implantation of catheter/osmotic minipump system**

Stroke surgeries were carried out as described above. A cannula (Alzet Brain Infusion Kit 3, Durect Inc., Cupertino, CA, USA.) was stereotactically implanted at the coordinates -0.8 mm lateral to the midline and 0.2 mm anterior to the Bregma on the day of stroke, as adapted from Kolb et al<sup>22</sup>. On day 4 after stroke, an osmotic minipump (Alzet model 1007D, 0.5 µl/hr flow rate) containing 45 µg/ml EGF-PEG in sterile aCSF was inserted subcutaneously and attached to the cannula. On day 11 after stroke (i.e. 7 days later), the first pump was replaced with a pump containing 100 µl of 3,000 U/ml EPO. The pump was removed on day 18.

### **5.3.11 Analysis of in vivo protein penetration**

Protein penetration analysis was carried out as described previously<sup>340</sup>. Animals that received EGF-PEG and EPO treatment from the composite were sacrificed at 1, 4, 8, 11, 14, and 21 d post implantation and the drug delivery device containing the composite was removed and protein extracted into aCSF overnight at 4°C. Animals that received EGF-PEG and EPO through catheter/osmotic minipumps were sacrificed at 7 and 14 d post implant and treated similarly.

Brains were snap frozen in CO<sub>2(s)</sub>-cooled isopentane and three 1 mm coronal sections around the implant site was prepared using the McIlwain tissue chopper. Dorsal-ventral sections (0.5 mm each, 6 section totally 3 mm depth, with the deepest 3 sections corresponding to the depth of the SVZ in mice) were then prepared from each coronal slice using Leica CM3050S cryomicrotome. Each subsection was homogenized in 400 µl lysis buffer (40 mM trehalose, 1% Triton X-100), and the supernatant was removed after centrifuging at 15,000 RPM for 15 min at 4 °C.

The amount of protein remaining in the composite, as well as that in each brain section at each time point was determined using both an EGF-PEG and an EPO ELISA kit as per the

manufacturers' instructions. The level of EGF-PEG and EPO in the brain of sham-treated animals were subtracted as background.

### **5.3.12 Immunohistochemistry**

Brain tissue from sacrificed animals was prepared for immunohistochemical analysis as previously described<sup>341</sup>. Animals were sacrificed and transcardially perfused with saline followed by 4% paraformaldehyde (PFA). The brains were fixed in 4% PFA at 4°C overnight, followed by cryoprotection in 30% sucrose. Brains were snap frozen and cryosectioned at 10 µm. Primary antibodies for Ki-67, GFAP, CD68, Mash-1, and NeuN were used at 1:400 dilutions. Secondary antibodies (Alexa 488 or Alexa 568) were used at 1:200 dilutions. Sections were mounted using Vectashield with DAPI and sealed. Immunohistochemical analysis for each marker was performed on 10 tissue sections, 100 µm apart. The peri-infarct tissue surrounding the cavity was examined for NeuN, GFAP, and CD68, while the subependymal layer of the ipsilateral SVZ was examined for Ki-67 and Mash-1 (**Supplementary Fig. S5.4**).

### **5.3.13 Analysis of stroke cavity size**

Stroke cavity size analysis was carried out as previously described<sup>340</sup>. Sections were stained with cresyl violet, covered and sealed. The area of the cavity on each section was obtained using ImageJ analysis software and the cavity volume obtained by summing the cavity size of each section, multiplying by the total thickness of the 10 sections examined.

### **5.3.14 Analysis of apoptosis using TUNEL**

Terminal deoxynucleotidyl transferase dUTP nick end labelling (TUNEL) was used to determine apoptosis after stroke. The ApopTag Fluoresceine In Situ Apoptosis kit was purchased from Millipore (Danvers, MA, U.S.A.) and TUNEL assay performed as per manufacturer's instructions. A total of 8 sections were analysed from each brain.

### 5.3.15 Statistics

All data are shown as mean  $\pm$  standard deviation. One-way ANOVA with Bonferonni correction was used to compare between multiple groups. Significance levels are indicated as  $p < 0.05$  (\*),  $p < 0.01$  (\*\*), and  $p < 0.001$  (\*\*\*)).

## 5.4 RESULTS

### 5.4.1 Controlled Release of EGF-PEG and EPO

We first examined the *in vitro* degradation and release profiles of the composite system. Degradation of the drug delivery system was examined *in vitro*. The composite retains at least 50% of its initial wet mass over 35 days (**Supplementary Fig. S5.5a**). EGF-PEG is completely released within the first week and EPO is released linearly between days 4 and 21 *in vitro* thereby demonstrating temporally-controlled, sequential release of bioactive factors (**Fig. 5.1**, **Supplementary Fig. S5.5b**), similar to that used with catheter/osmotic minipump system.

To achieve sequential release of EGF-PEG followed by EPO, EGF-PEG is encapsulated in poly(lactic-co-glycolic acid) (PLGA) nanoparticles and EPO is encapsulated in PLGA nanoparticles that are coated with poly(sebacic acid) (**Fig. 5.1a**). The EGF-PEG and EPO particles are incorporated into a HAMC hydrogel comprised of 1% HA and 2% MC and the release profile is characterized both *in vitro* and *in vivo*. EGF-PEG is completely released within the first week and EPO is released linearly between 4 d and 21 d *in vitro* (**Fig. 5.1b**). This linear profile demonstrates temporally-controlled sequential release of bioactive factors. Notably, the *in vivo* release profiles of EGF-PEG and EPO from the composite system (**Fig. 5.1c**, **Supplementary Fig. S5.6**) mirror those observed *in vitro*. EGF-PEG is observed in brain tissue only in the first two weeks, reaching a maximum at 7 d whereas EPO is not detected until after the first week and peaks at 21 d (**Fig. 5.1d**). This demonstrates that sequential release and

accumulation of EGF-PEG followed by EPO is achieved. Importantly, by examining the accumulation of EGF-PEG and EPO at various depths in the brain tissue, we confirm that both proteins are able to penetrate through the injured cortex to the SVZ (**Fig. 5.1e**).

One key difference between epicortical delivery and ICV infusion is the amount of protein that accumulates in the tissue following delivery (**Supplementary Fig. S5.6, S5.7**). The maximum tissue accumulation of EGF-PEG (detected at day 7-8) and EPO (detected at day 14) are  $134 \pm 12$ -fold and  $552 \pm 48.6$ -fold higher, respectively, following epicortical delivery compared to catheter/minipump ICV infusion. Proteins delivered ICV are likely dispersed by the cerebrospinal fluid throughout the central nervous system (CNS), thereby accounting for the small amount of EGF-PEG and EPO detected in the brain.

Notwithstanding the differences in amount and region of protein accumulation achieved with epicortical composite vs. catheter/mini pump delivery systems, the latter is the best comparative group due to its widespread use and previous success in a rat PVD stroke model. The epicortical composite delivery represents a less invasive strategy than catheter/minipump for controlled temporal release of EGF-PEG and EPO enabling us to compare the tissue benefits in the endothelin-1 mouse model of stroke. We hypothesize that transiently higher concentrations of EGF-PEG and EPO in the brain will lead to enhanced NSPC stimulation and increased tissue benefit.

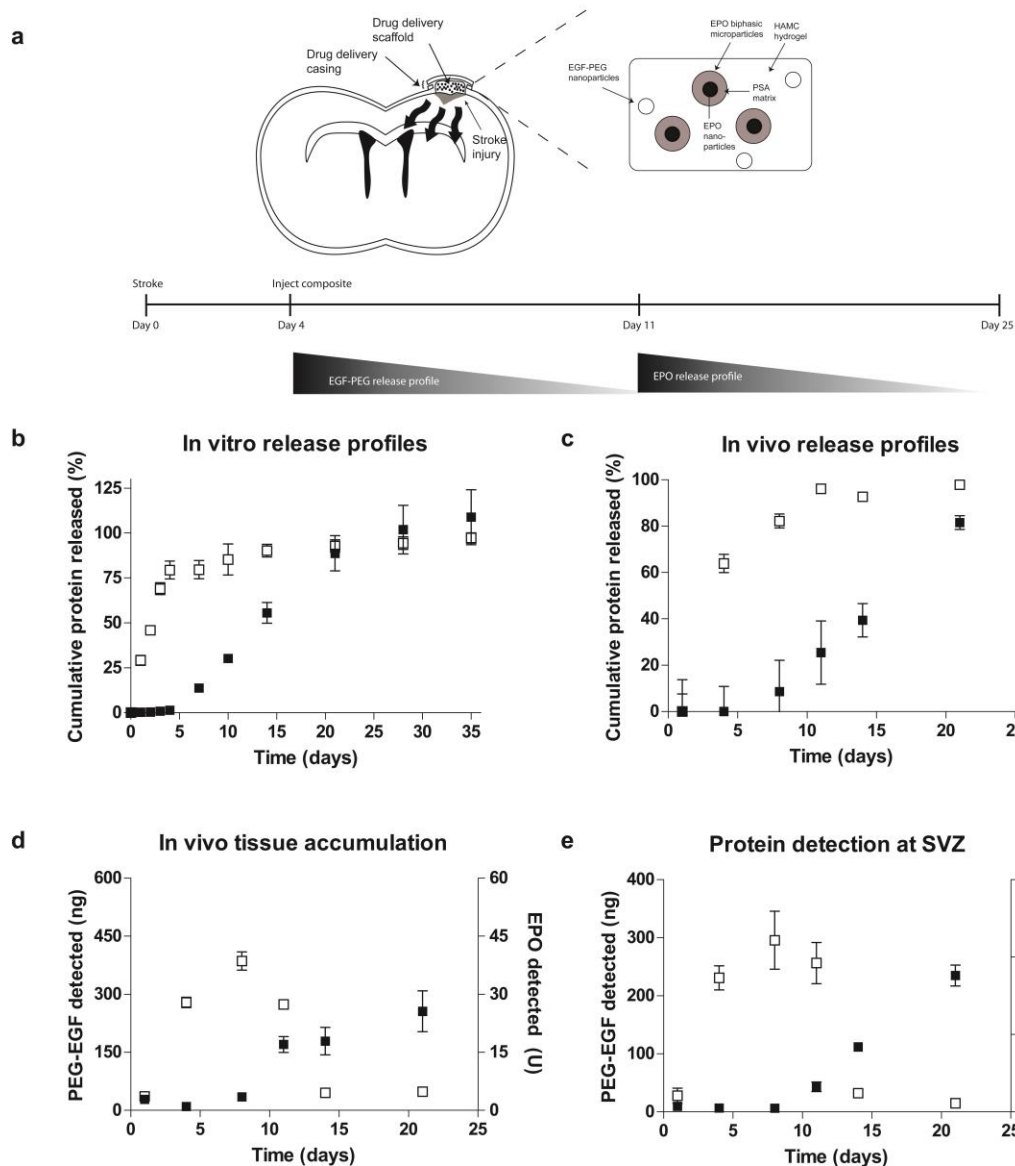


**Figure 5.1| Sequential delivery of EGF-PEG followed by EPO can be achieved using composite drug delivery system (DDS).** (a) Schematic of the drug delivery system and in vivo EGF-PEG and EPO release from the composite on a microscopic level. Time course of the desired release profile is a sequential release of EGF-PEG for one week, followed by EPO. (b) In vitro release profiles of (□)EGF-PEG and (■) EPO engineered to yield the desired release profiles, with the majority of EGF-PEG released within the first week, followed by EPO released linearly for two weeks. (c) In vivo the release profiles of EGF-PEG and EPO from composite shows that EGF-PEG is released first followed by EPO release. (d) EGF-PEG can be observed in the stroke-injured brain tissue within days of injection, with the peak concentration detected at 1 week. EPO is not detected in the tissue in the first week, but accumulation is observed after the initial delay. (e) Endogenous stem cells reside in the SVZ. Accumulation of protein in the tissue corresponding to this region of the brain was examined and found to occur over the desired time course. All data are based on ELISA analysis (Mean  $\pm$  standard deviation,  $n = 3$ ).

#### **5.4.2 SVZ cellular response to growth factors delivered from epicortical composite vs. ICV pump at 18 days after stroke**

The rationale for sequential delivery of EGF-PEG followed by EPO is based on previous studies demonstrating that EGF promotes NSPC proliferation<sup>344</sup> and expands the cell population, while EPO promotes neurogenesis from SVZ NSPCs<sup>332</sup>. We therefore analyze NSPC proliferation and neural progenitors in the SVZ ipsilateral to injury at 18 d after stroke to capture the cellular response following growth factor delivery.

Compared to vehicle controls, growth factor treatment using either pump or composite significantly increases the number of Ki67<sup>+</sup> proliferating cells (**Fig. 5.2a – e**) and Mash-1<sup>+</sup> neural precursors (**Fig. 5.2f – j**) in the SVZ. When aCSF is infused using catheter/minipumps following stroke, a reduction is observed for both Ki67<sup>+</sup> and Mash-1<sup>+</sup> compared to stroke alone, suggesting a negative tissue benefit with CSF flow alone in the ventricles (the rate = 0.5 µl/hr). Stroke + growth factor (G/F) composite delivery also significantly reduces the number of TUNEL<sup>+</sup> apoptotic cells in the SVZ (**Fig. 5.2k – o**) relative to both Stroke + vehicle composite delivery ( $p = 0.043$ ) and Stroke + G/F pump infusion ( $p = 0.027$ ). These data suggest that the composite delivery system promotes tissue repair beyond that resulting from temporally controlled release of EGF-PEG and EPO. Thus the epicortical HAMC composite delivery of EGF-PEG and EPO shows greater tissue repair than that of ICV infusion, suggesting an additional tissue benefit of the composite delivery vehicle itself.

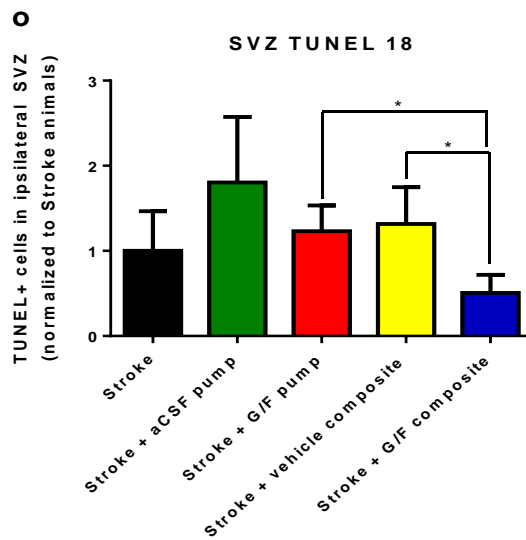
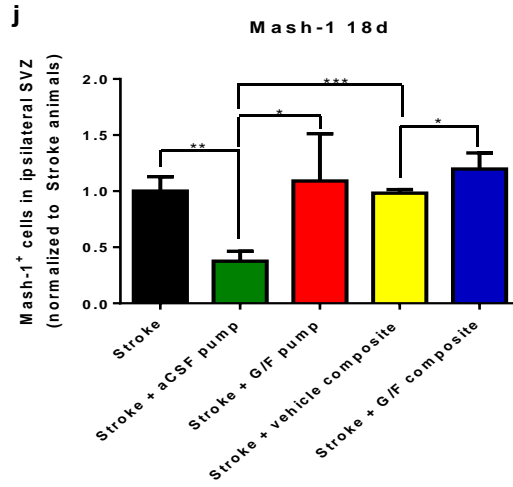
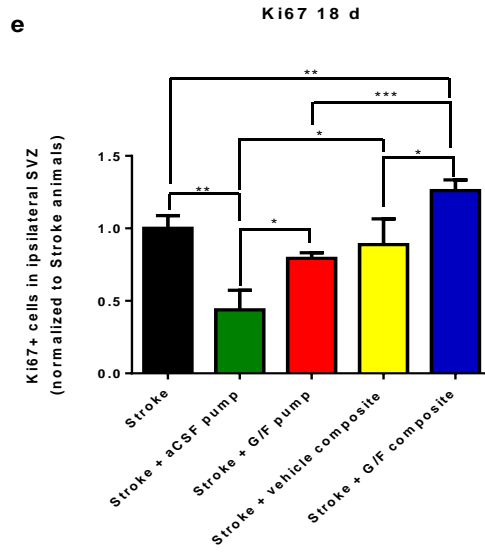
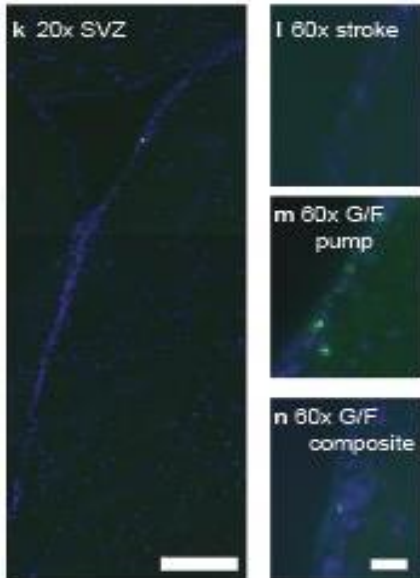
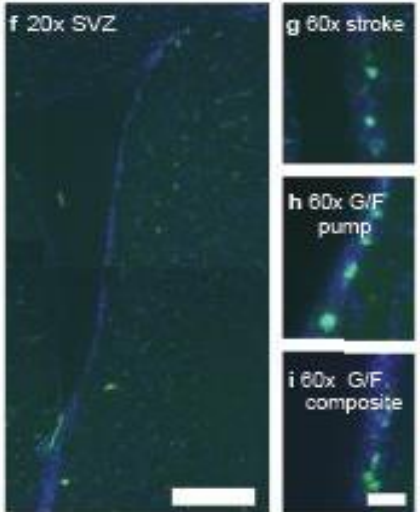
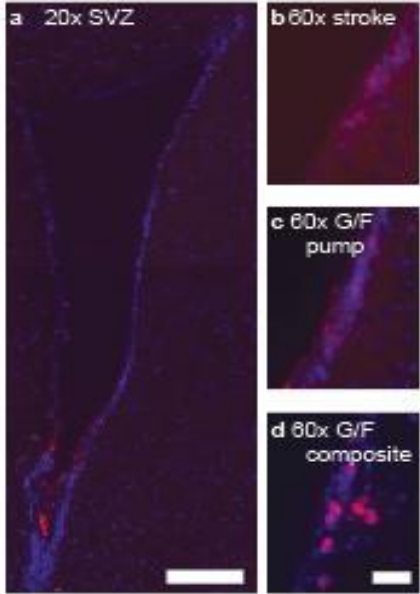
#### **5.4.3 Tissue Repair in the peri-infarct brain**

To gain greater insight into the tissue response following growth factor treatment, we assess the number of TUNEL<sup>+</sup> apoptotic cells and NeuN<sup>+</sup> mature neurons in the peri-infarct region, as well

as the size of cavity that forms after endothelin-1 stroke. These outcomes are assessed at 18 d and 32 d post stroke, two time points that were selected to both correspond to the completion of ICV growth factor delivery (18 d), and allow examination of tissue at longer time points (32 d).

At 18 d, treatment with growth factors decreases the extent of apoptosis (**Fig. 5.3a – d**) and increases the number of NeuN<sup>+</sup> mature neurons (**Fig. 5.3e – h**) in the peri-infarct region compared to stroke alone or Stroke + vehicle controls. Importantly, even though composite-mediated delivery of growth factors does not return the number of NeuN<sup>+</sup> cells to the pre-injury level, the number of cells is significantly higher compared to that achieved using catheter/minipump infusion. Additionally, all animals except the Stroke + aCSF pump group show a significant reduction in the cavity size relative to stroke alone (**Fig. 5.3i**).

**Figure 5.2 | EGF-PEG and EPO delivered from composite increase proliferation of NSPCs and decrease cell death in the SVZ 18 days after stroke.** (a – d) Representative images and (e) quantification of Ki67<sup>+</sup> proliferating cells in the ipsilateral SVZ at 18 d. Compared to vehicle controls, growth factor treatment using either pump or composite significantly increase the number of Ki67<sup>+</sup> proliferating cells in the ipsilateral SVZ. Stroke + G/F composite delivery animals showed significantly more Ki67<sup>+</sup> cells than Stroke + G/F pump delivery animals ( $p = 0.001$ ), and only G/F composite delivery showed significantly more Ki67<sup>+</sup> cells than stroke alone ( $p = 0.008$ ). When aCSF is infused through osmotic minipumps to the ventricles, the level of proliferation decreases significantly compared to stroke alone controls ( $p = 0.004$ ). (f – i) Representative image and (j) quantification of Mash-1<sup>+</sup> neuroprecursors in the ipsilateral SVZ on day 18. Stroke + G/F pump infusion increases the number of Mash-1<sup>+</sup> neural precursor cells in the SVZ compared to Stroke + aCSF pump infusion controls ( $p = 0.045$ ); and Stroke + G/F composite increases the number of Mash-1<sup>+</sup> cells compared to Stroke + vehicle composite ( $p = 0.033$ ). Stroke + aCSF pump intraventricular infusion resulted in a significant reduction in Mash-1<sup>+</sup> cells compared to Stroke + vehicle composite ( $p = 0.001$ ) and stroke alone ( $p = 0.002$ ). No significant differences in Mash-1<sup>+</sup> cells were found between stroke alone and Stroke + vehicle composite or between stroke alone and Stroke + G/F composite. (k – n) Representative image and (o) quantification of TUNEL<sup>+</sup> apoptotic cells in the ipsilateral SVZ on day 18. At 18 d after stroke, the number of apoptotic cells in the SVZ was characterized by TUNEL<sup>+</sup> cell staining following stroke vs. the other interventions. Stroke + G/F composite delivery significantly reduced the number of apoptotic TUNEL<sup>+</sup> cells relative to both Stroke + vehicle composite delivery ( $p = 0.043$ ) and Stroke + GF pump infusion ( $p = 0.027$ ). (Mean  $\pm$  standard deviation,  $n = 3$ . Results are normalized to Stroke animals. Scale: a, f, k: 100  $\mu\text{m}$ ; b – d, g – i, l – n: 50  $\mu\text{m}$ .)



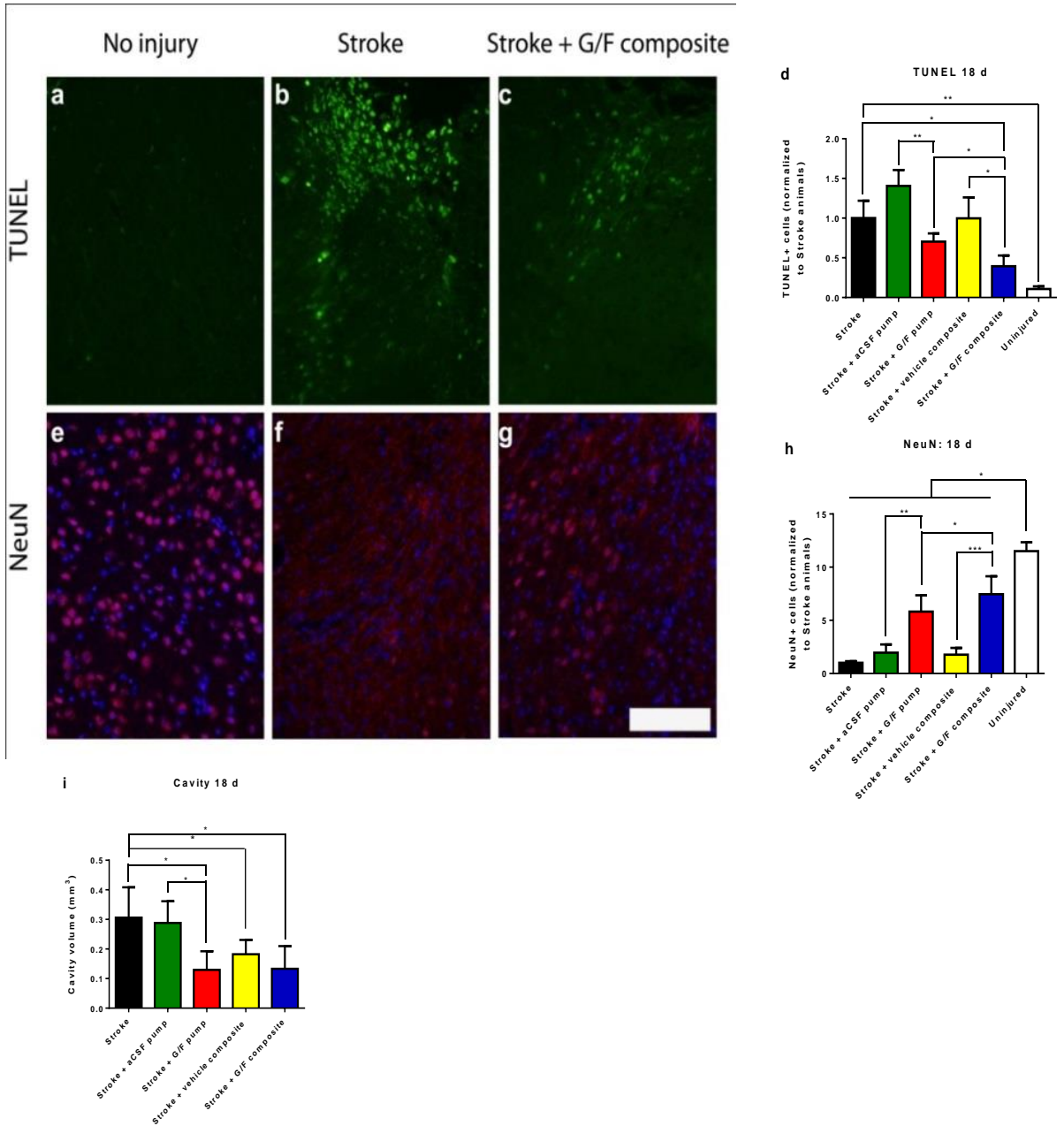


**Figure 5.51 Sequential composite-mediated delivery EGF-PEG and EPO attenuates the injury response and cell death, and increases NeuN<sup>+</sup> mature neurons in the penumbra 18 d after stroke.** At 18 d post stroke, (a – d) the level of TUNEL<sup>+</sup> cells decreases significantly in the injured cortex following growth factor treatment compared to stroke + vehicle controls. Importantly, stroke + G/F composite leads to a significant decrease in TUNEL<sup>+</sup> cells compared to stroke alone ( $p = 0.015$ ) and stroke + G/F pump ( $p = 0.038$ ). (e - h) Both stroke + G/F composite and stroke + G/F pump animals have significantly more NeuN<sup>+</sup> cells in the peri-infarct region compared to vehicle controls ( $p = 0.001$ ). The level of NeuN+ neurons is significantly higher after stroke + G/F composite vs. stroke + G/F pump ( $p = 0.044$ ), yet still significantly less than uninjured tissue controls. (i) All animals showed a significant reduction in cavity size relative to stroke alone except for the stroke + aCSF pump group. (All results normalized to Stroke animals, mean + standard deviation,  $n = 5$ ). Scale: 100  $\mu\text{m}$ .

The HAMC delivery vehicle is anti-inflammatory in the CNS<sup>220</sup>. As stroke causes inflammation in the peri-infarct area<sup>345</sup>, which is detrimental to recovery<sup>325</sup>, we examine the peri-infarct tissue at 18 d to assess whether the composite attenuates inflammation in the stroke injured brain. We observe that only those animals treated with HAMC – either HAMC alone or vehicle composite – have significantly lower inflammatory response in terms of the number of GFAP<sup>+</sup> reactive astrocytes (**Fig. 5.4a – d**) and CD68<sup>+</sup> activated microglia and macrophages (**Fig. 5.4e – h**). This confirms the anti-inflammatory effect of HAMC previously observed in other CNS injuries<sup>220</sup>.

At the 32 d terminal time point, stroke injured animals that received composite-mediated treatments (both vehicle alone and G/F) show a reduced number of GFAP<sup>+</sup> reactive astrocytes (**Fig. 5.5a**) and CD68<sup>+</sup> macrophages and microglia (**Fig. 5.5b**) compared to osmotic catheter/minipump-treated animals, again demonstrating the anti-inflammatory effect of HAMC in the CNS. Relative to controls, G/Fs delivered by either epicortical composite or ICV infusion also show reduced cavity volumes that are not significantly different from each other at 32 d (**Fig. 5.5c**). Apoptosis in the peri-infarct area continues to be evident at 32 d, with the greatest reduction in TUNEL<sup>+</sup> cells observed in the G/F composite delivery group (**Fig. 5.5d**). Additionally, the level of apoptosis in animals that received G/F from the epicortical composite is not significantly different from that of uninjured controls. This enhanced brain tissue repair observed after epicortical composite delivery may be attributed to either the greater concentration and longevity of EPO in the brain tissue of animals receiving G/Fs by epicortical composite and/or a combination of HAMC's anti-inflammatory effect and the reduced invasiveness of epicortical delivery compared to intraventricular infusion.

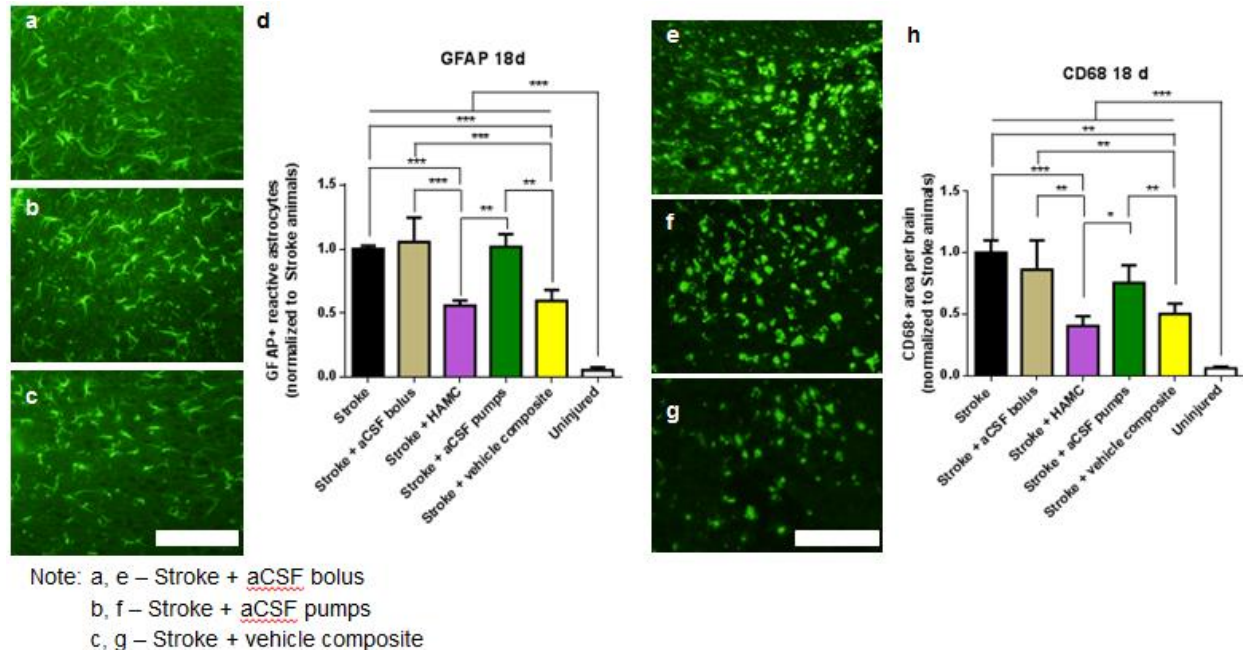


**Figure 5.4 | Epicortical delivery of the composite vehicle attenuates inflammatory response in the peri-infarct region 18 d after stroke.** Given that HAMC demonstrates anti-inflammatory effects in the CNS, we examined the peri-infarct cortical tissue for inflammation. Only those animals that were treated with HAMC – either HAMC alone or vehicle composite comprised of HAMC and polymeric particles – showed significantly reduced (a – d) GFAP<sup>+</sup> reactive astrocytes and (e – h) CD68<sup>+</sup> macrophages/microglia around the lesion. For stroke + aCSF bolus, stroke-injured animals had aCSF injected in an identical manner to HAMC, thereby providing a control for epicortical delivery of HAMC. (All results normalized to Stroke animals, mean + standard deviation, n = 3, \*p<0.05; \*\*p<0.01; \*\*\*p<0.001). Scale: 100 μm.

There are also significantly more NeuN<sup>+</sup> mature neurons in the peri-infarct area of G/F composite treated animals compared to the stroke alone and vehicle composite controls at 32 d (Fig. 5.e). While no significant difference in NeuN<sup>+</sup> cells is observed between G/F delivery by either composite or catheter/minipumps, no significant difference is observed in G/F treated and uninjured groups, suggesting tissue repair to pre-injury levels and a neuroregenerative effect of G/F treatment. Since we wait 4 d after stroke injury prior to G/F delivery, and most effective neuro-protective treatments need to be delivered within 1 – 4 days post injury<sup>346</sup>, the tissue repair observed is likely a neuroregenerative (vs. neuro-protective) effect. The increased

number of NeuN<sup>+</sup> cells and reduced cavity size is correlated with increased NSPC proliferation in the SVZ at 18 d.

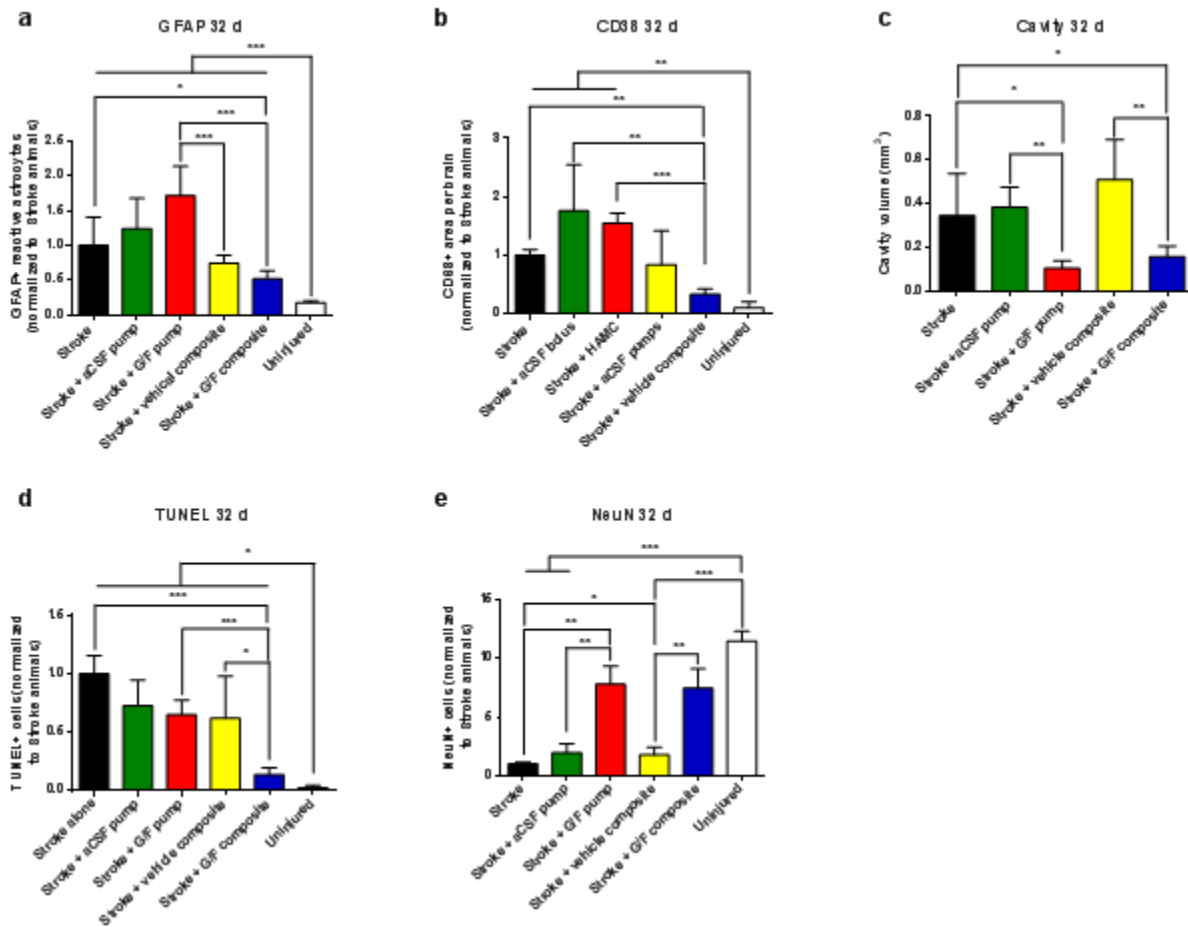


**Figure 5.5 | Epicortical delivery of composite vehicle attenuates peri-infarct inflammatory response at 32 d post stroke, and sequential composite-mediated delivery of EGF-PEG and EPO attenuates the injury response and cell death, and increases NeuN<sup>+</sup> mature neurons at the same time point.** Injection of vehicle composite post stroke reduces the number of (a) GFAP<sup>+</sup> reactive astrocytes and (b) CD68<sup>+</sup> activated microglia at 32 d compared to stroke alone and stroke with osmotic minipump treatments. This is similar to the effects seen at 18 d post stroke. (c) Growth factor treatment significantly reduces the stroke cavity size compared to vehicle controls. Quantification of (d) TUNEL<sup>+</sup> and (e) NeuN<sup>+</sup> stains at 32 d indicates G/F composite attenuates apoptosis and increases the number of mature neurons in the peri-infarct region compared to vehicle control. No significant difference was observed for NeuN<sup>+</sup> cells at 32 d between stroke + G/F composite and uninjured tissue, suggesting tissue repair to pre-injury levels (All results normalized to Stroke animals, mean + standard deviation, n = 5, \*p<0.05; \*\*p<0.01; \*\*\*p<0.001).

In addition to the tissue regeneration observed, the composite is capable of delivering growth factors without causing the tissue damage associated with cannula insertion through the brain parenchyma into the contralateral ventricles. TUNEL+ apoptotic cells in the contralateral SVZ and cortex significantly exceed that in the uninjured, stroke alone, or Stroke + composite groups (**Supplementary Fig. S5.8a, b**), demonstrating the significant tissue damage associated with cannula insertion. At both 18 and 32 d after stroke, the injury response as measured by GFAP and CD68 upregulation are also magnified by cannula insertion (**Supplementary Fig. S5.8c – f**) relative to epicortical composite delivery or stroke alone.

#### **5.4.4 Cellular response in the SVZ at 32 days after stroke**

The regeneration in the peri-infarct region at 32 days after stroke is likely correlated to the increased NSPC proliferation observed in the SVZ at 18 days after stroke. We further examined the SVZ at 32 days after stroke to assess if epicortical delivered EGF-PEG and EPO is likely to elicit tissue benefits in the peri-infarct area beyond the treatment period.

Stroke-injured animals treated with the epicortical G/F composite show significantly greater numbers of Ki67+ cells in the SVZ relative to all other groups studied, including animals that received G/F treatment through ICV infusion (**Supplementary Fig. S5.9a**). The number of Mash-1<sup>+</sup> neural precursors is significantly greater in G/F delivery animals relative to their appropriate controls yet not different from each other and not from stroke alone (**Supplementary Fig. S5.9b**). The extent of apoptosis in the SVZ is lowest in stroke-injured animals that receive EGF-PEG and EPO from the composite (**Supplementary Fig. S5.9c**). Use of catheter/minipumps leads to increased apoptosis in the SVZ, although growth factor delivery attenuates the number of TUNEL+ cells relative to aCSF delivery alone. The reduction in apoptotic cells observed in the composite vs. pump delivery strategies may reflect the greater concentration and duration of the neuroprotective EPO in those animals having composite vs.

pump delivery. Alternatively, the reduced apoptosis in the stroke + G/F composite and stroke + vehicle composite vs. the relevant pump infusion animals may reflect the greater invasiveness of the pump strategy relative to the epicortical HAMC strategy.

#### **5.4.5 Preliminary functional assessments**

In addition to the cellular level studies, we carried out preliminary investigation on the functional outcome of animals that receive sequential treatment of EGF-PEG followed by EPO from the composite system. Due to the preliminary nature of these studies, the results are presented in Appendix D. Our findings suggest that in agreement with the tissue-level findings, animals that receive EGF-PEG followed by EPO from the composite also obtain functional recovery compared to injured animals that received no treatment. Additionally, composite-treated animals reach pre-stroke levels of forelimb motor functions following treatment.

### **5.5 DISCUSSION**

Sequential delivery of EGF and EPO was originally shown to promote tissue repair after stroke injury in the rat PVD model<sup>22</sup>. From those studies, it was evident that repair resulted from tissue regeneration rather than neuroprotection, as EGF and EPO were not delivered until 4 and 11 days after stroke, respectively. It was also clear that the sequential delivery paradigm of EGF for 7 days followed by EPO for 7 days was key to the regeneration because simultaneous delivery did not show the same success. We mimic this ICV catheter/minipump delivery strategy in the endothelin-1 mouse model of stroke, and compare it to our new epicortical injectable hydrogel composite system. Neural tissue repair is observed in both delivery strategies; however, overall tissue repair is enhanced by cortical delivery and the tissue damage observed with cannula insertion is obviated by using the epicortical strategy.

Compared to either single protein delivery or simultaneous delivery of multiple proteins, the benefits of sequential delivery of multiple proteins have been observed in other systems<sup>347</sup>. For example, sequential delivery of basic fibroblast growth factor (bFGF) and neurotrophin-3 (NT-3) improved neuronal survival after CNS injury compared to either factor alone<sup>348</sup>. When EPO alone is delivered epicortically<sup>252</sup>, the number of mature neurons in the injured cortex is less than half of that achieved here by the sequential delivery of EGF-PEG and EPO from the composite.

In this study, we engineer the sequential release of EGF-PEG followed by EPO by encapsulating EGF-PEG in PLGA particles and EPO in PLGA-PSA biphasic microparticles, both of which are dispersed in HAMC. While the hydrogel alone is insufficient to achieve prolonged sustained release<sup>349</sup>, the inclusion of polymeric particles, which encapsulate growth factors and are dispersed in the hydrogel, results in sustained release that is localized to the site of injection by the hydrogel<sup>350</sup>. The temporal profile of drug released from the composite mimics that achieved using conventional osmotic minipump systems. To the best of our knowledge, this is the first time that a polymer composite has been used to achieve sequential delivery of growth factors to the brain without multiple surgeries. Other strategies have been used to deliver two proteins at varying rates, but the release profiles are not truly sequential. Typically, one protein is released significantly slower than the other, but with no initial delay period<sup>343</sup>.

Furthermore, the epicortical delivery strategy overcomes some of the challenges associated with drug delivery to the brain. By delivering growth factors directly to the brain tissue, this strategy circumvents the blood-brain barrier while localizing release. Unlike the ICV catheter/minipump, which causes significant tissue damage<sup>351</sup>, the epicortical composite provides a minimal invasiveness and no tissue damage. Thus the epicortical composite

comprised of polymeric particles dispersed in HAMC provides a versatile strategy for local, sustained release to the brain while obviating the need for invasive or systemic delivery strategies.

The epicortical composite outperforms the ICV catheter/minipump in terms of tissue benefit. Relative to ICV catheter/minipump infusion, epicortical composite-treated animals show similar tissue repair, but resulted in reduced apoptosis and increased proliferation in the ipsilateral SVZ. Given that growth factors were delivered to the SVZ in both systems, this result is unexpected but may be explained by greater tissue concentrations of EGF-PEG and EPO when delivered from the cortical surface vs. into the ventricle. When delivered through ICV infusion, the majority of the proteins are dispersed by the cerebrospinal fluid throughout the central nervous system<sup>352,353</sup>, resulting in low tissue accumulation. It has been shown that a population of quiescent cortical neural precursor cells is activated by brain injury<sup>354</sup>. The composite allows higher quantities of EGF-PEG to accumulate in the cortex compared to the osmotic minipumps, and since EGF stimulates NSPC proliferation, it is possible that these cortical precursors, in addition to the NSPCs from the SVZ, may be involved in tissue repair. EPO is neuroprotective, and higher concentrations of neuroprotective factors in the brain following delivery from the composite may decrease cortical apoptosis and enhance the effect of regeneration.

We observe additional evidence of tissue repair in terms of an attenuated inflammatory response, with epicortical delivered HAMC at both 18 and 32 days after stroke, thereby minimizing detrimental effects of inflammation to adult brain neurogenesis<sup>326</sup>. Hyaluronan promotes wound healing, and is anti-inflammatory in the CNS<sup>355</sup>, suggesting that the HA of HAMC is responsible for the reduced inflammatory response. Given that in the presence of HAMC alone, there is reduced inflammatory response, increased number of mature neurons, but no reduction in apoptosis in the peri-infarct area, it is possible that it is the microglia and not

the neurons in the penumbra is undergoing apoptosis<sup>356</sup>. The difference in inflammatory response between epicortical composite and intraventricular catheter/pump is heightened by the significant damage and inflammation in the tissue surrounding the ventricle resulting from cannula insertion. This is a common problem associated with metallic implants in the brain parenchyma<sup>357,358</sup>, and can be avoided by using an alternate delivery strategy, such as the epicortical composite.

One challenge in epicortical delivery is the short penetration distance of proteins in the brain, which limits the volume of tissue that can be targeted. Typical protein penetration distance in the uninjured brain tissue is 1 mm<sup>141</sup>. Since the SVZ is approximately 3 mm ventral to the cortical surface in a mouse brain<sup>359</sup>, the protein must be engineered to achieve adequate penetration. PEG-modification increases the penetration of EGF in the ischemic brain<sup>340</sup> while EPO requires no modification to penetrate to the SVZ<sup>252</sup>. This difference in EGF and EPO tissue penetration can be largely ascribed to differences in their relevant receptors in the stroke injured brain where EGFr is upregulated<sup>250</sup> and EPOr is not<sup>252</sup>. Here we demonstrate that by using the composite system, sequential accumulation of EGF-PEG and EPO at the approximate depth of the SVZ can be achieved over a 2-3 week period. Translation from the mouse to larger animal models and ultimately to humans will require additional innovations in order to achieve the penetration distances required. For example, the mouse SVZ resides 2 – 3 mm ventral to the cortical surface<sup>359</sup> whereas the human SVZ is situated at a depth between 5 – 10 cm ventral to the cortical surface<sup>360</sup>. The differences in brain size, cell composition, and cell density will impact protein transport in the brain, which is governed by both diffusivity and the rate of protein removal<sup>141</sup>. These parameters can be used to our advantage: modifying proteins with a polymer such as PEG can significantly increase tissue penetration<sup>265,361</sup>. For example, conjugating a single PEG molecule to EGF can increase penetration in a stroke-injured brain by up to 27 fold<sup>250</sup>. In addition, a constant growth factor source, such as that provided by the composite system,

results in a further 2-3 fold increase in penetration distance<sup>250</sup>. This distance can be further enhanced by varying the molecular weight and structure of PEG, by using different conjugation polymers<sup>362</sup>, or reducing protein elimination through protein caging<sup>363</sup> and point mutations<sup>364</sup>.

## **5.6 CONCLUSION**

The epicortical delivery system, comprised of HAMC hydrogel and polymeric particles, provides temporally-controlled release of therapeutically relevant factors to achieve neural tissue repair without the concomitant tissue damage of catheter/minipump system. While clinical translation of this system will be non-trivial, the polymer composite is less invasive than other local delivery strategies to the brain. The application of this composite DDS is not limited to the stimulation of endogenous NSPCs for the treatment of stroke. A number of CNS disorders, including Alzheimer's disease<sup>365</sup> and spinal cord lesions<sup>366</sup> result from loss of healthy neurons and glia. The epicortical local, minimally-invasive delivery strategy may have therapeutic use in these disorders as well.

## **6. Thesis Discussion**

Controlled local delivery of therapeutically relevant proteins to the CNS remains a major challenge today, primarily due to the inability of most proteins to penetrate the BBB. The goal of this thesis was to develop a delivery system that allows two growth factors, EGF and EPO, to be delivered to the stroke-injured brain in a controlled and sequential manner. The delivery system should allow these two proteins to achieve the same levels of therapeutic efficacy as when they are infused into the lateral ventricles using conventional devices such as the catheter/osmotic minipump system, and the delivery method should be minimally invasive. These studies were designed to demonstrate that the efficacy of protein-based treatments for CNS disorders can be enhanced through the use of polymer-based epicortical delivery systems.

### **6.1. Growth factor-mediated tissue regeneration following stroke**

Stroke is a neurodegenerative condition where loss of blood supply to the brain leads to tissue damage and related functional deficit<sup>35</sup>. Currently there is no effective clinical treatment for this condition, although treatments based on tissue regeneration have yielded promising results in treating stroke in animal models. One class of these neuroregenerative approaches rely on the proliferation of endogenous NSPCs in the brain, and the subsequent migration of these progenitor cells to the stroke site to replace the neurons, astrocytes, and oligodendrocytes in the injured tissue<sup>367</sup>. However, even though the adult mammalian brain contains a population of NSPCs that are capable of regeneration after stroke<sup>66</sup>, the rate at which endogenous repair occurs is insufficient to restore motor and functional abilities in the majority of patients<sup>32</sup>. Therefore external stimuli are required to fully realize the promise of this neuroregenerative approach. It has been shown that a number of growth factors, including EGF and EPO, are

capable of stimulating endogenous regeneration <sup>107</sup>. Additionally, given that functional cortical tissue consist of multiple neural cell types, delivering multiple growth factors to target the various lineages may have more therapeutic efficacy than using a single factor. For instance, in the mouse brain, while factors including EPO, retinoic acid, GDNF, and BDNF are most effective in enhancing maturation of NSPCs into neurons rather than other cell types <sup>335</sup>, factors such as ERK <sup>368</sup> and neuregulin <sup>369</sup> promote the maturation and migration of oligodendrocytes, and bFGF <sup>370</sup> enhance astrocyte proliferation. It is conceivable that using a combination of these factors may lead to better recovery after neurological injury.

While single-factor delivery has shown promise in neuroregeneration, delivery of multiple factors either simultaneously or sequentially has shown greater efficacy <sup>371,372</sup>. The time course of administration has direct influence on the pharmacokinetics of protein therapy, and therefore contributes significantly to the overall outcome of treatment <sup>373</sup>. Sequential delivery of growth factors has been shown to elicit superior results compared to simultaneous delivery of multiple factors. For instance, delivery of bFGF and platelet-derived growth factor (PDGF) led to greater angiogenesis compared to PDGF alone <sup>374</sup>. Similarly, co-delivery of bone morphogenic protein-2 (BMP-2) and BMP-7 led to enhanced chondrocyte stimulation compared to BMP-7 alone <sup>375</sup>. The primary reason for this is thought to be that sequential delivery paradigms allow the benefits of various proteins to be staggered and optimized <sup>375,376</sup>. Use of multiple factors has also often shown more efficacy than delivering single factors. The importance of combined sequential delivery of EGF and EPO was first demonstrated by Kolb et. al. <sup>22</sup>: recovery in stroke-injured animals were achieved only when both EGF and EPO were sequentially infused into the lateral ventricles. When either factor was infused alone, recovery was not observed. We confirmed here that when either PEG-EGF or EPO was delivered alone to the stroke-injured brain, they led to increased NSPC proliferation and neuroregeneration in the cortex. However, when both were delivered sequentially using the composite, the benefit was significantly higher. Although single

factor delivery was achieved using hydrogels and sequential delivery was achieved using the composite, which leads to differences in delivery profiles, this nevertheless demonstrates the importance of multiple factor treatment.

The rationale behind sequentially delivering EGF and then EPO to stimulate neuroregeneration after stroke is that EGF is a potent mitogen that stimulates the proliferation of NSPCs, while EPO is a neuroprotective factor that encourages the survival and maturation of newly generated progenitor cells. Kolb et. al. had demonstrated in a rat PVD stroke model that sequential infusion of EGF followed by EPO into the lateral ventricles led to the formation of a tissue plug at the stroke site, which was correlated with recovery <sup>22</sup>. However, the PVD model is a better representation of traumatic brain injury rather than stroke <sup>377</sup>. As such, there may be a lack of compatibility between the treatment developed for PVD strokes and that required to treat clinical stroke. <sup>378</sup>

In our work, we showed that PEG-EGF and EPO can be delivered in a sequential and minimally invasive manner to the brain in an endothelin-1 (ET-1) mouse model of stroke to elicit tissue benefits. Following ET-1 stroke, animals treated with PEG-EGF and EPO delivered from our composite DDS showed reduced stroke cavity volume and increased number of mature neurons in the penumbra. The results are similar to those shown previously by Kolb et. al., where the same two growth factors were infused using a catheter/osmotic minipump system into PVD-injured rats <sup>22</sup>. Significantly, when the HAMC-particle composite was used to deliver growth factors, the extent of tissue damage caused by the delivery system is significantly less than that caused by the osmotic minipump/catheter system. This is due to a number of reasons, the non-penetrating nature of composite injection, as well as the ability of HAMC to help wound healing and reduce inflammation in the CNS. These findings help to demonstrate that protein drugs that

do not readily cross the BBB can be administered epicortically in a manner that does not cause significant tissue damage while achieving therapeutic efficacy.

## 6.2. Engineering protein transport in the injured brain

Transport of proteins in the brain has been a heavily investigated topic in the field of controlled delivery in the last few decades. The mechanisms that contribute to this transport process are now well understood, which allows investigators to optimize drug delivery to the brain. The distribution of proteins in the brain is primarily governed by three mechanisms: convective transport<sup>379</sup>, diffusive transport, and elimination from the brain<sup>380</sup>.

Convection dominates drug transport in the brain during the first seconds to minutes after administration<sup>381</sup>. The convective transport of all drugs in the brain depends on the flow of the cerebral spinal fluid (CSF), which randomly distributes drugs to all areas of the brain. Convective transport is limited to transport from the CSF to the surfaces of the brain, and so its main role is that of distributing the drug rather than delivering the drug in question to specific target regions. In the context of local delivery in the CNS, convective transport is sometimes detrimental because CSF flow disperses the drugs and proteins of interest away from the site of delivery, which is often the target site in local delivery systems. Compared to other available local delivery systems such as the catheter/osmotic minipump system, hydrogel scaffolds such as the one used here have the advantage of localizing the drugs of interest to the site of interest by limiting convective transport.

After the initial convective stage, drug transport in the brain is dominated by both diffusion and elimination<sup>141</sup>. The distance of penetration into the brain tissue is directly correlated with a substance's diffusivity and inversely correlated with its rate of elimination. The diffusivity of a

drug in a tissue reflects its intrinsic diffusivity (i.e. diffusivity in a free medium such as water) and the tortuosity of the tissue. Intrinsic diffusivity is dictated by a molecule's hydrodynamic radius and hydrophobicity: small hydrophilic molecules tend to diffuse faster than large hydrophilic molecules. For example, EGF conjugated to one PEG molecule demonstrated significantly faster apparent diffusion than EGF conjugated to two or three PEG molecules (Chapter 2)<sup>250</sup>. The tortuosity is an intrinsic property of the tissue in question, and cannot be easily modified<sup>141</sup>. However, after injuries such as stroke, changes in the ECM may affect tortuosity. Studies have shown that initially after stroke, cellular edema causes slight shrinkage in ECM space, thereby increasing tortuosity. Over the intermediate and long term, however, free volume in brain tissue increases and tortuosity decreases<sup>382</sup>. These findings suggest that there is an optimal window during which proteins can be delivered epicortically to achieve maximum penetration distance.

Elimination of proteins in the brain is a complex concept that is typically comprised of the following four mechanisms: elimination due to clearance, cellular uptake (both receptor mediated endocytosis and phagocytosis), immobilization onto the ECM, and elimination through proteolytic degradation (predominantly by trypsin and serine proteases<sup>383</sup>). Each of these mechanisms contribute to the overall removal rate, and the faster the rate of elimination of a drug, the smaller its penetration distance in the brain. It is important to note that the mechanism which dominates the removal of a specific protein or drug differs for every protein and drug. We have demonstrated that both upregulation of receptors and increased protease concentration in the brain tissue contribute to faster rates of EGF elimination in the stroke-injured tissue compared to uninjured tissue. In contrast, the removal of EPO was similar in the both uninjured and stroke-injured tissues due to similar levels of receptor expression in the regions of interest. This demonstrates that the dominant mechanism of elimination differs for the two proteins investigated, and the implication is that the dominating mechanism of elimination must be determined for each individual protein. Understanding of the protein elimination process will

allow the transport to be more accurately modeled, such that the protein or DDS can be engineered to minimize removal and maximize penetration.

In non-infusion-based controlled delivery systems, it is difficult to modify either the drugs or the delivery system to significantly alter convective transport. Therefore the majority of research efforts focus on modifying properties of the protein to alter transport parameters associated with diffusion and elimination<sup>384</sup>. This is typically done through changing the size and receptor recognition of the molecule in question. One of the most common ways of modifying proteins to improve its retention time and hence its penetration distance is to conjugate PEG molecules to the protein<sup>385</sup>. PEG increases the hydrodynamic radius of the protein that it is conjugated to and masks the protein against its receptors, both of which reduce removal of the protein from its diffusion path. Additionally, PEG is mostly inert in the body and elicits a minimal foreign body response<sup>386</sup>.

PEG with different molecular weights and structures have been conjugated to a large number of proteins to enhance their tissue retention<sup>385</sup>. It has also been shown that PEG with larger molecular weights and higher degrees of branching are more effective than small linear PEG molecules at improving protein retention<sup>387</sup>. This approach has shown promise for improving protein penetration in a number of tissues<sup>388</sup> including the brain<sup>168</sup>. In this work we showed that conjugating a PEG of similar molecular weight to EGF significantly reduces elimination and enhances penetration in both the uninjured and the stroke-injured brains of mice (Chapters 2 and 3)<sup>250,251</sup>. Previous works have shown that 5 kDa PEG molecules can be conjugated to EGF to yield monoPEGylated EGF (PEG-EGF), but the conversion efficiency is typically low<sup>389</sup>. We showed in this work that by optimizing the reaction pH and the reducing agent, and by using a molar excess of PEG to EGF, we can increase the yield of PEG-EGF to approximately 50%, approximately 2 fold higher than that obtained previously. Importantly, the in vitro bioactivity of

PEG-EGF is maintained, which was not found previously<sup>389</sup>. Increasing the degree of PEGylation decreased the in vitro bioactivity, but even when three PEG molecules were conjugated to EGF, 60% in vitro bioactivity was retained.

In this work, integrative optical imaging was used to derive the parameters required in building a mathematical model to predict protein diffusion distances in the brain. This technique had previously been used to derive apparent diffusivity of proteins such as EGF, BDNF, and NGF in the brain. However, the rate of elimination has rarely been calculated in other works<sup>142,154,257,390-392</sup>. Without accurate estimations of this parameter, it is difficult to predict penetration distance with certainty. Here we modeled the elimination of EGF and PEG-modified EGF in both the uninjured and the stroke-injured brain. This allowed us to both better understand protein transport in the brain, and realize that PEG-modification is necessary for EGF to achieve maximum penetration distance and efficacy. This procedure can be applied to other proteins, such as EPO, to model and predict maximum penetration in the brain.

Using a modeling approach, we demonstrated that PEG-modification can enhance EGF penetration in the uninjured brain by three-fold. We confirmed this in vivo, and further demonstrated that in both uninjured and stroke-injured mouse brains, the amount of bioactive PEG-EGF found at the SVZ exceeded that of unmodified EGF. The penetration distance may be further enhanced by using larger PEG molecules with branched structure, as well as conjugating more than one PEG molecule onto each protein molecule. These findings imply that PEG modification of proteins may be used to facilitate epicortical delivery in larger animal models, where the distance between the cortical surface and the SVZ is larger than that in a mouse.

### 6.3. Optimizing protein delivery from polymeric drug delivery systems

Encapsulating proteins in polymeric particles allows for sustained delivery to be achieved over tunable periods of time, and the goal is typically to maximize efficacy through optimizing pharmacokinetics. Here, both PEG-EGF and EPO are encapsulated in PLGA nanoparticles, either alone or embedded in a second polymer shell. PLGA is one of the most commonly used polymer vehicles in protein delivery because it allows a large variety of proteins to be encapsulated, the formulation can be varied to yield a large range of release characteristics, and PLGA is FDA approved for clinical use<sup>393,394</sup>. One of the major limitations in using PLGA as a drug delivery agent is that the kinetics of drug release from PLGA matrices are difficult to model and predict. Consequently, a small change in process parameters may lead to drastic variations in encapsulation and release profiles<sup>395</sup>. We demonstrated that PLGA nanoparticles of similar size can be synthesized to encapsulate both PEG-EGF and EPO at therapeutically relevant encapsulation efficiencies, and the synthesis process can be modified to empirically achieve different encapsulation efficiency and release rates.

Controlling the encapsulation efficiency and the rate of protein release from PLGA nanoparticles, however, is a pragmatic rather than theoretical process: it is difficult to model the release of a specific protein from PLGA matrices<sup>396</sup>. While much effort has been devoted to deriving mathematical models that can be used for a generic protein, most of the models available today are highly specific and only applicable to proteins with a small range of molecular weights, surface charge, and hydrophobicity<sup>397-400</sup>. This is primarily due to the large number of variables involved in the particle synthesis process, such as molecular weight of PLGA, size of the particle, and the size and hydrophobicity of the protein<sup>395</sup>. Furthermore, depending on the nature of the protein, various additives must be added to or coencapsulated in the particles to preserve protein bioactivity and ensure complete release from the particles<sup>401</sup>. For instance, we

found that we can encapsulate PEG-EGF in PLGA nanoparticles to achieve high encapsulation and linear release using a specific set of process parameters. Using the same set of parameters, however, we cannot encapsulate EPO to maintain any detectable bioactivity. Rather, additives such as bovine serum albumin (BSA) were required to ensure the encapsulation and release of bioactive EPO in PLGA nanoparticles. Process parameters such as the concentration of salt in the aqueous phases and the emulsion times also played significant roles in the encapsulation of both PEG-EGF and EPO, but the effect of varying each parameter is again difficult to model and predict<sup>402</sup>. Therefore the process of optimizing protein encapsulation in PLGA particles remains very much a trial-and-error process. This is a severe limitation since enormous efforts must be put into designing the encapsulation process for each individual protein of interest.

One of the contributions of this work is the use of biphasic microparticles to encapsulate EPO to achieve a delayed release profile. Previously, double-walled microspheres have been made using a single-step process<sup>233,234</sup>. In these works, two different organic phases containing either the same polymer in two organic solvents, or two different polymers are mixed. In these processes, the formation of a distinct core-shell structure relies on the difference in the interfacial energies of the two organic solutions, and the release characteristics are highly dependent on the volume and concentration ratios of the two phases. While this process is theoretically sound and simple, it is difficult practically and has a number of limitations. For instance, a spray drying solvent evaporation process must be employed. Also, only two types of double-walled particles have been reported to date. They consist of either a poly(anhydride) core and PLGA coating, or a PLGA core and PLA/PGA coating<sup>233,234</sup>. This is likely due to the limited number of systems that have large enough interfacial energy differentials between the two organic phases to properly form a core-shell structure. Therefore the range of applications is limited. Alternatively, pan-coating can be used to add a shell layer to polymeric particles. While simple, this technique lacks reproducibility, typically is only applicable for large particle

size (600 – 5000  $\mu\text{m}$  diameter particles are typically prepared in this manner), and yields large size polydispersity<sup>403</sup>. Using the two-step process reported here, we were able to reproducibly synthesize biphasic microparticles to encapsulate EPO to yield release profiles with an initial delay followed by linear release. The particles are also injectable through thin gauge needles, therefore meeting the criteria that the injection of our composite must be minimally invasive. The two-step technique does not rely on interfacial energy differentials, and therefore it is conceivable that there is no limit on the types of polymers that can be used to form either the core or the shell of the particle. Each of the two phases can also be engineered to yield a broad range of release profiles. It is therefore likely to be more versatile than other existing techniques.

Using the hydrogel-particle composite system, rather than a single component system of hydrogel or microparticles only, we also had more degrees of freedom in optimizing protein release. Previous work from our group has demonstrated that the release of a variety of drugs from HAMC-PLGA particle composites differ significantly from release from PLGA particles alone<sup>316</sup>. This was attributed to protein sieving effect at the interface of gel and particles<sup>404</sup>. We also found this to be true for EGF encapsulated in PLGA microparticles<sup>316</sup>. In general, the presence of HAMC attenuated the burst release of various proteins from PLGA particles, and helped to yield pseudo-zero order release profiles<sup>316</sup>.

Additionally, one of the concerns of using the epicortical composite DDS is the structural stability of the composite. We require a delivery window of at least two weeks, and so the composite must retain most of its mass in vivo over this time frame. The physical crosslinks in HAMC form by dynamic hydrophobic interactions and may be disturbed by the flow of CSF. Therefore it is expected that in vivo degradation of the gel occur faster than that in vitro. Previous work from our lab has found that the addition of hydrophobic nanoparticles, such as poly(styrene), helped to stabilize HAMC<sup>405</sup>. This is attributed to the formation of hydrophobic

junctions between particles and methylcellulose, in addition to the natural hydrophobic crosslinks between the methylcellulose chains. Here we reported that degradation of the composite in vitro is significantly slower than that of HAMC, possibly due to the presence of PLGA and PSA particles, both of which are hydrophobic.

Encapsulating proteins in polymeric particles allows researchers to develop a variety of drug delivery systems that do not require prolonged infusion, which is an advantage as infusion systems can be invasive and may cause infection at the site of insertion. However it is difficult to engineer the DDS such that the delivery profile obtained matches what can be obtained with an infusion system. The work presented in this thesis demonstrated the preparation of one such system, where the desirable features of multiple protein delivery and programmable delayed release are combined.

A key learning from this work is that a versatile system is crucial in engineering controlled delivery systems. One of the advantages that our composite system has over other strategies is that the rate of protein release can be individually engineered using polymeric particles, and particles can then be incorporated into HAMC to allow for differential rates of delivery. Conceptually, separating the functionalities (i.e., that of the particles from that of the hydrogel) will allow for fine-tuning the release rates of an unlimited number of drugs.

#### **6.4. Comparison between composite delivery system and existing delivery strategies**

The last few decades saw a myriad of protein drugs developed for use in treating CNS disorders. However, despite relatively high success rates in preclinical studies, few protein drugs have passed clinical trials and been approved for human use. Specifically, EPO has been tested in a

clinical trial for stroke treatment<sup>406</sup> where EPO was infused intravenously upon patient admission, and 24 and 48 h later. The outcome of the trial was negative as none of the patients showed significant improvement compared to placebo controls. One reason for this may be attributed to the lack of appropriate delivery strategies. Most proteins lack the ability to cross the BBB if administered systemically, and the available local delivery strategies are invasive. The main advantage of both systemic and local infusion systems, which are the most commonly used systems in administering drugs to the CNS in preclinical studies, is that they can sustain a steady level of drug at the insertion site, and the rate of release is easily tunable. The main limitations include invasiveness and that the drugs are not localized to the target site. The appropriate DDS for the CNS should deliver therapeutically relevant levels of proteins to the target site without causing systemic toxicity or local tissue damage.

In this work we wanted to develop a polymer based controlled delivery system that allows the proteins delivered to achieve the same level of efficacy as the catheter/osmotic minipump infusion system. To this end we developed a composite DDS that shows promise in meeting the criteria mentioned above: spatially and temporally controlled release, minimal invasiveness, and in vivo efficacy. The HAMC-particle composite developed here can be injected epicortically to sustain the release of two different proteins over a desired time period. The hydrogel, HAMC, localizes the proteins of interest to the site of injection, such that there is low probability of systemic side effects. Since the epicortical delivery strategy does not require insertion of the composite into the brain tissue, it avoids the damage caused by cannula insertion associated with the catheter/osmotic minipump system. The anti-inflammatory and wound healing properties of HAMC also add to the benefits of this composite delivery system. Importantly, the benefit achieved by delivering PEG-EGF and EPO using the composite is equivalent to that achieved using the osmotic minipump/catheter system at the tissue level. Preliminary functional studies also suggest that treatment administered using the composite system leads to functional

improvement in stroke-injured animals. One other benefit that epicortical delivery has over ICV infusion is that the location of delivery can be adjusted as needed. This allows our epicortical composite delivery system to be easily adapted for treating other neurological disorders, where regions other than the SVZ are targeted.

Although this is not the first instance where polymer scaffolds or particles have been used to deliver drugs to the brain, the system developed here presents a number of improvements over existing systems. PLGA particles and wafers, as well as various hydrogel patches and implants have been used to deliver therapeutic agents to the brain in animal studies of CNS disorders<sup>24,407</sup>. These devices are also versatile in their use, and can be formulated to deliver drugs at controlled rates. The main difference between these systems and our epicortical composite is that they require direct insertion into the brain tissue. As such, they are invasive and have thus far been predominantly used to treat brain tumours, where it is typical for portions of the brain to be excised during surgery<sup>408,409</sup>. The wafers or implants are then placed into the void where the tissue has been removed. This is not applicable for most neurodegenerative disorders and brain injuries, such as Parkinson's disease, Alzheimer's disease, traumatic brain injury, and stroke<sup>410</sup>. In these conditions, the target site can be deep within the brain, but tissue cannot be surgically removed without causing detrimental effects. The epicortical delivery strategy overcomes this problem, since the delivery system is injected onto the cortical surface. At the same time, the proteins delivered can be engineered to penetrate through the brain to reach the target site.

Despite its numerous advantages over some existing local delivery systems, the epicortical composite delivery system developed here still faces a number of limitations. One of the most medically relevant drawbacks is that a surgery is required for the injection of this system. As such, the invasiveness associated with the composite is higher than that of systemic delivery.

Another limitation is the need to engineer proteins to penetrate to stem cell niches deep in the brain, which is often non-trivial.

The significance in this work lies in engineering a device where the benefits of the overall system exceeds that of the sum of the components. Each component of this thesis, including PEG-modification of EGF, investigating the effect of PEGylation on protein penetration in the brain, and the preparation of the composite DDS all contribute to the final outcome, but it is the combination of all the different parts of the system that ultimately elicited tissue repair in stroke-injured mice.

## **6.5 Potential issues in translation**

One question remains regarding the mechanism of tissue repair after NSPC stimulation. Once NSPCs from the SVZ migrate to the injury site, tissue regeneration may occur if the precursor cells differentiate into mature cells and integrate with host tissue, or the cells may release cytokines and mediate repair indirectly. While this investigation is beyond the scope of this thesis, one can identify the mechanism by conducting an experiment where the newly generated tissue is removed after stroke-injured animals begin to show functional recovery. This can be done either physically using targeted local ablation, or chemically by delivering a toxin to which only the new tissue is sensitive. One way to do this is to use transgenic mice where only NSPCs express receptors to certain toxins. Conceptually, we can insert toxin receptor genes (e.g. diphtheria toxin receptor<sup>411</sup>) into NSPCs but not other cells in the body. This can be done by inserting toxin receptors downstream of NSPC-specific transcription factors. One such factor is PQBP1<sup>412</sup>: studies have shown that PQBP1 mRNA is dominantly expressed by SOX2+ stem cells in the subventricular zone region. We can then induce stroke in mice that have diphtheria toxin receptor gene inserted downstream of the PQBP1, and locally administer diphtheria toxin to these animals post recovery, This experiment will allow us to effectively ablate the newly-

regenerated tissue without damaging other tissue. If incorporation of the newly generated cells into the host tissue is required for recovery after stroke, removal of the tissue will reverse recovery. On the other hand, if the cells lead to repair by secreting cytokines, removal of the new tissue should have minimal impact on recovery. Additionally, if the newly formed neurons are required for recovery, they should have neurite extensions and communicate with surrounding neurons<sup>413</sup>. Neuroelectric activities in functional neurons are positively correlated with cognitive processes and functional improvement, and lack of signaling between neurons often indicates dead or dying tissue, or tissue that has not made connections with neighbouring cells<sup>413</sup>. The mechanism of repair can therefore be determined using a combination of electrophysiology, immunohistochemistry, and large functional assays to compare animals with the new tissue plug intact vs. removed.

Another potential issue with translating a treatment that is effective in a mouse model into humans is that the cytoarchitecture of the SVZ is different between the two species. In the human SVZ, there is a hypocellular gap between the ependymal wall of the lateral ventricle and the inner layer of astrocytes that is filled with astrocytic cell processes<sup>294</sup>. Transport of proteins through this type of tissue will likely differ significantly from transport in the mouse brain tissue, both in terms of tortuosity and elimination rate. The exact transport will need to be investigated in more detail to predict diffusion distance for a given protein drug. Additionally some mature astrocytes in the human SVZ niche express proliferative markers, but not in mice<sup>414</sup>. Studies showed that these mature astrocytes interact with NSPCs to promote proliferation. These findings suggest that compared to the amount of protein that we need to deliver to the mouse brain to stimulate neuroregeneration, the amount of proteins that we have to deliver in humans may not need to scale linearly with size. Another point of difference is the growth conditions that murine vs. human NSPCs are responsive toward. Human NSPCs have been shown to have greater sensitivity to their environments (e.g., oxygen and insulin levels<sup>415</sup>) compared to

murine NSPCs, and the sensitivity to various proteins and growth factors are also different between species<sup>416</sup>). Therefore the amount and types of factors required for stimulating endogenous neurogenesis may be different for mice vs. humans.

In a few recent studies, the ongoing potential of neurogenesis in the human olfactory bulbs and the presence of an active rostral migratory stream are questioned<sup>417</sup>. These findings raise the question of whether the adult human brain has enough neurogenesis potential to facilitate endogenous stimulation strategies. Interestingly, the same study showed that the extent of neurogenesis in the adult human olfactory bulb follows a temporal profile that is different from that in the mouse. Others found that the maximal neuronal proliferation and maturation are reached in the first month post-injection in mice and rat whereas in primates and other mammals the first new mature neurons are only observed at 3 months<sup>417</sup>. These suggest that in higher order mammals, neuronal proliferation, differentiation, and maturation occur at a longer time scale compared to rodents, and that to optimize endogenous regeneration, we need to not only identify the appropriate factors to deliver and the appropriate site for delivery, but also the optimal time point after injury to initiate treatment.

The other obvious challenge lies in the size difference between the mouse brain and the brain human. In the mouse brain, the SVZ is approximately 2 mm ventral to the cortical surface, whereas the SVZ in the average adult human is more than 10 cm from the cortical surface<sup>378</sup>. Given this significantly greater distance, proteins that are engineered to reach the mouse SVZ after epicortical delivery may not be able to reach the SVZ in humans. In order to increase penetration distance, modifications such as conjugating the proteins to branched or longer PEG chains, conjugating proteins to liposomes and nanoparticles, or designing fusion proteins that have altered binding kinetics to cell surface receptors may be necessary.

Despite the promise that endogenous stimulation strategies have shown in animal models of stroke, there has been a lack of clinical success to date. Indeed, using endogenous stimulation to treat neurological injuries such as stroke is a challenging prospect. Given these potential translational issues, it may be worthwhile to study endogenous stimulation along with other treatment strategies in a combination approach. For instance, transplanting exogenous stem cells into the injured brain has shown efficacy in animal models both through cytokines released by transplanted cells and through integration of these cells into the host tissue. Using a two-pronged approach of endogenous stimulation and exogenous transplantation may increase the likelihood of clinical success.

## 7. Thesis Conclusions

### 7.1. Achievement of objectives

The original hypothesis of this work was:

*A drug delivery system consisting of a hyaluronan-methylcellulose (HAMC) hydrogel and polymeric particles will enable epicortical delivery of EGF followed by EPO to the brain to elicit tissue regeneration in a mouse model of stroke.*

Four objectives were defined to answer this question.

1. Investigate the effect of PEG modification on protein diffusion in the stroke-injured brain.

To address this question, the diffusion and elimination of EGF and PEG-EGF with various degrees of PEG-modification were investigated in both uninjured and stroke-injured brain tissue of a mouse. Integrative optical imaging in combination with mathematical modeling was used as a method for studying protein transport. We found that stroke injury significantly increases the rate of protein elimination from the tissue, which consequently leads to decreased penetration distance. By conjugating one PEG molecule to EGF, where the PEG has similar molecular weight as EGF, we show that we can improve tissue penetration, and modeling results show that the distance of penetration would allow epi-cortically delivered proteins to reach SVZ in a mouse model of stroke. These data were presented in Chapter 2 and published in the Journal of Controlled Release<sup>250</sup>.

## 2. Assess the feasibility of epicortical HAMC-mediated EGF delivery for stroke treatment

To examine the ability of PEG-EGF to penetrate through the stroke-injured cortex following epicortical delivery, we incorporated this growth factor into the HAMC hydrogel and monitored its transport *in vivo*. Compared to unmodified EGF, we found that PEG-EGF showed greater stability and slower elimination *in vivo*, which led to greater penetration depth. PEG-EGF delivered from HAMC reached the depth of tissue that corresponds to the SVZ in a mouse, stimulated proliferation of cells in the SVZ. Greater NSPC stimulation was observed following the delivery of PEG-EGF compared to unmodified EGF. These data were presented in chapter 3 and published in *Biomaterials*<sup>340</sup>.

## 3. Assess the feasibility of epicortical HAMC-mediated EPO delivery for stroke treatment

The transport of EPO in the stroke-injured mouse brain following epicortical delivery was examined. The transport of this protein was similar in the stroke-injured tissue compared to uninjured tissue due to a lack of receptor upregulation following injury. We demonstrated that EPO penetrated to the SVZ and enhanced neurogenesis. Additionally, EPO demonstrated both neuroprotective and neuroregenerative functions in the stroke-injured mouse and increased tissue regeneration in the injured cortex. These results were presented in chapter 4 and published in *Biomaterials*<sup>252</sup>.

## 4. Design and optimize a composite DDS for epicortical delivery of PEG-EGF followed by EPO

A composite DDS was developed with the following components: HAMC hydrogel for spatially localizing the system; PLGA nanoparticles for encapsulating PEG-EGF, and biphasic microparticles with a PLGA core and PSA coating for encapsulating EPO. The system was

engineered such that PEG-EGF can be delivered first, followed by delivery of EPO. This allowed the temporal profile of delivery to match that achieved using osmotic minipumps. We demonstrated that growth factors delivered using this composite stimulated NSPCs in the SVZ and enhanced tissue regeneration in the ET-1 mouse model of stroke. This new method of delivery also achieved similar efficacy and was less invasive than conventional osmotic minipump/catheter infusion system. These data were presented in Chapter 5 and accepted for publication in the Journal of Controlled Delivery.

## **7.2. Major contributions**

In this work it was demonstrated that two growth factors can be delivered sequentially to enhance brain repair after stroke using a minimally invasive delivery approach. To this end, a composite DDS of HAMC hydrogel and polymeric particles was prepared, and the formulation of the particles was engineered such that two different growth factors, PEG-EGF and EPO, can be encapsulated to yield sequential linear release profiles. To delay the release of EPO by approximately one week, we developed a two-step encapsulation strategy that is versatile and may be used for various polymeric systems.

It was also found that a single PEG molecule of similar molecular weight as EGF can be conjugated to this protein to significantly increase the penetration distance in both uninjured and stroke-injured brain. This was investigated using both a mathematical modeling approach and confirmed using an in vivo model. We attributed the change in protein penetration to increased number of EGFR in the injured brain, as well as the global upregulation of proteases<sup>250</sup>. The transport of proteins and the impact of PEG modification on protein penetration in the stroke

injured brain helped us to understand the morphological and proteomic changes in the brain after injury.

This work also showed that the time of protein delivery has a significant impact on the outcome of growth factor treatment. When we delivered EPO at two different time points after stroke, we found that EPO showed neuroprotective effects 4 days after stroke, whereas it showed neuroregenerative effect when injected one week later. These results help to demonstrate that for growth factors, the timing of administering contributes significantly to the therapeutic outcome of the treatment, and that the therapeutic windows must be tightly controlled to achieve optimal results.

Finally, the method for preparing biphasic microparticles for encapsulating EPO is novel and will likely allow a variety of proteins to be encapsulated. Unlike conventional one-step process for synthesizing double-walled particles, this two-step process does not rely on the interfacial energy differences between the two polymer phases to form the double-walled structure<sup>234</sup>. Therefore a larger number of polymers can be used to synthesize these particles, and a broader range of release profiles may be achieved.

## **8. Recommendations for future work**

### **8.1 Encapsulating more clinically relevant proteins in composite DDS**

In the present composite DDS, two proteins were encapsulated to stimulate endogenous brain repair after stroke. PEG-EGF stimulates proliferation of endogenous NSPCs while EPO is thought to encourage their maturation into neurons<sup>22</sup>. The sequential delivery of these two growth factors led to tissue repair in a mouse model of stroke. The limitation in the current work, however, is with respect to clinical translation of our system. EGF is a potent mitogen and is associated with tumor formation<sup>418,419</sup>. For safety reasons, it is necessary to investigate other factors that can stimulate NSPC proliferation without causing tumor formation.

The drug or growth factor that can replace EGF in our delivery system must have the following properties: 1) able to enhance the proliferation of NSPCs; 2) penetrate through the cortex to reach the SVZ; and 3) safe for use in humans. A number of growth factors that have been studied by other groups may satisfy these criteria. For instance, Cyclosporin A (CsA) is an immunosuppressant commonly used in organ transplant operations<sup>420</sup>. It interferes with the activity of T cells and reduces the ability of the immune system to recognize foreign substances. In the central nervous system, recent findings have shown that CsA has both neuroprotective effects and the ability to stimulate neural precursor proliferation<sup>421</sup>. Since CsA is safe for prolonged use in humans, it is a promising candidate for replacing EGF. Another potential candidate is human chorionic gonadotrophin (hCG)<sup>422</sup>. This hormone is associated with reproduction in humans, but has shown considerable promise in human stroke treatment. Combining hCG with EPO is of particular interest because in a recent Phase II clinical study<sup>422</sup>. The possibility of delivering multiple factors using our system can therefore be used to improve the clinical translation of this system.

## **8.2 Additional functional assessment of composite delivery system**

In this study we focused on examining the tissue level benefits of protein drugs delivered through the composite system. As a next step, once the more clinically relevant molecules to be delivered has been decided upon and successfully encapsulated, it would be interesting to assess both the tissue level and the functional level benefit of the strategy. The ET-1 mouse model of stroke is appropriate for this purpose, as demonstrated by Sachewsky *et. al.*<sup>423</sup>. In this thesis, we examined the preliminary effect of our composite system on the functional outcome of ET-1 stroke-injured mice, but as the studies were unblinded, further assessment with larger cohorts of animals would be required for definitive conclusions.

## **8.3 Translating composite DDS into larger animal models**

The current version of the HAMC-particle composite DDS is able to deliver two growth factors sequentially to the stroke-injured mouse brain such that tissue repair can be observed. One potential limitation in this system is the penetration distance that proteins are able to achieve in the brain of larger animals, where the SVZ is significantly deeper in the brain compared to that in the mice<sup>296</sup>. It may be necessary, therefore, to develop strategies to further enhance protein penetration in the stroke-injured brain.

The following approaches may be effective for increasing protein penetration distance. First, the length of PEG chain conjugated to the protein can be increased. It has been shown that increase in PEG molecular weight has significant impact in decreasing the rate of protein degradation and elimination, and therefore may serve to increase penetration<sup>387</sup>. Second, the degree of branching of the PEG molecule also has significant impact on the rate of elimination<sup>387</sup>. PEG molecules with higher degree of branching lead to slower elimination rates compared

to linear PEG chains with the same molecular weight <sup>385</sup>. Third, the number of PEG chains conjugated to each protein molecule also has significant impact on the rate of protein removal <sup>269</sup>. All these PEG-based methods for reducing protein elimination, however, should be considered in combination with any reduction in bioactivity due to PEG-conjugation. Typically, the higher degree of shielding due to PEG will lower recognition of the protein by its receptors, and therefore may decrease bioactivity <sup>424</sup>.

Another method for increasing protein penetration is to modify the protein, either by mutagenesis or post-translational modification, by replacing certain amino acid residues in the receptor recognition site of the protein <sup>425</sup>. This will reduce receptor recognition and therefore decrease protein elimination. The concern for this method is again the possible reduction in protein bioactivity.

An alternative approach to increase protein penetration may be to scale up the composite system. The penetration distance will be directly correlated with the concentration of drugs in the reservoir device: the higher the concentration, the greater the driving force for diffusion in the extracellular space of the brain <sup>382</sup>. Therefore if we are able to increase the length of time during which there is a constant driving force, we may increase protein penetration accordingly. Mathematical modeling may be used to first predict the length of time required for proteins to reach specific distances in the brain, and the concentration required can be calculated through reverse engineering. We can then take advantage of this knowledge and design a delivery system that is capable of delivering this quantity of proteins.

#### 8.4 Develop more clinically translatable drug delivery casing

The drug delivery composite is currently fixed in place on the mouse skull using a set of two custom-made polycarbonate disks. The disks are molded to the shape of the skull to ensure a tight seal. A burr hole is opened on the skull so that the composite can be injected onto the cortical surface, and these disks help to prevent the composite from flowing away during treatment. The limitation with the current version of this system is that the polycarbonate disks are bio-inert and nondegradable. As such, it must be removed at the completion of the treatment, and does not have any therapeutic advantages.

One way to improve the current system is to manufacture the disks with materials that are biodegradable, and helps to expedite skull and dura healing. For instance, the disks may be synthesized from PLGA matrices containing therapeutic molecules such as bone morphogenic protein (BMPs)<sup>426</sup> and fibroblast growth factors (FGFs)<sup>427,428</sup>. BMPs may be incorporated into the scaffold so that when released, they will help with the process of skull healing. The rate of dura healing may be increased by incorporating growth factors such as FGF-2 into the drug delivery composite, as FGF-2 has been incorporated into poly(lactide) scaffolds to enhance skull healing<sup>428</sup>.

Another method for improving the biocompatibility and usefulness of the drug delivery casing is to construct it from osteoinductive and osteoconductive materials, such as hydroxyapatite<sup>429</sup>. Hydroxyapatite has been shown to expedite bone healing in various animal models, and is also biodegradable in vivo. Incorporating hydroxyapatite particles into polymer matrices<sup>430</sup> have been used as bone grafts in various applications to help heal fractured bones<sup>431</sup>.

## 9. References

- 1 Audebert, H. J. Stroke treatment in 2011. Update on new therapeutic options. *Gefasschirurgie* **16**, 603-612 (2011).
- 2 Lloyd-Jones, D. Heart Disease and Stroke Statistics-2010 Update: A Report From the American Heart Association (vol 121, pg e46, 2010). *Circulation* **121**, E260-E260 (2010).
- 3 Hartmann, A. *et al.* Outcome in critically ill stroke patients - comparing ischemia and hemorrhage. *Eur J Neurol* **12**, 297-297 (2005).
- 4 Hatcher, M. A. & Starr, J. A. Role of Tissue Plasminogen Activator in Acute Ischemic Stroke. *Ann Pharmacother* **45**, 364-371 (2011).
- 5 Machumpurath, B., Davis, S. M. & Yan, B. Rapid Neurological Recovery after Intravenous Tissue Plasminogen Activator in Stroke: Prognostic Factors and Outcome. *Cerebrovasc Dis* **31**, 278-283 (2011).
- 6 Fonarow, G. C. *et al.* Relationship between Door-to-Needle Times for Tissue Plasminogen Activator and In-Hospital Clinical Outcomes in Acute Ischemic Stroke. *Stroke* **42**, E86-E87 (2011).
- 7 Adeoye, O., Hornung, R., Khatri, P. & Kleindorfer, D. Recombinant Tissue-Type Plasminogen Activator Use for Ischemic Stroke in the United States A Doubling of Treatment Rates Over the Course of 5 Years. *Stroke* **42**, 1952-1955 (2011).
- 8 Curry, S. H. Why have so many drugs with stellar results in laboratory stroke models failed in clinical trials? A theory based on allometric relationships. *Ann Ny Acad Sci* **993**, 69-74 (2003).
- 9 De Keyser, J., Sulter, G. & Luiten, P. G. Clinical trials with neuroprotective drugs in acute ischaemic stroke: are we doing the right thing? *Trends Neurosci* **22**, 535-540 (1999).
- 10 Martinez-Vila, E. & Sieira, P. I. Current status and perspectives of neuroprotection in ischemic stroke treatment. *Cerebrovasc Dis* **11**, 60-70 (2001).
- 11 Lyden, P. *et al.* Clomethiazole Acute Stroke Study in ischemic stroke (CLASS-I) - Final results. *Stroke* **33**, 122-128 (2002).

- 12 Qureshi, I. A. & Mehler, M. F. The Emerging Role of Epigenetics in Stroke III. Neural Stem Cell Biology and Regenerative Medicine. *Arch Neurol-Chicago* **68**, 294-302 (2011).
- 13 Onteniente, B. & Polentes, J. Regenerative Medicine for Stroke - Are We There Yet? *Cerebrovasc Dis* **31**, 544-551 (2011).
- 14 Kalra, L. & Ratan, R. R. Advances in stroke regenerative medicine 2007. *Stroke* **39**, 273-275 (2008).
- 15 Wang, T. W., Zhang, H. L., Gyetko, M. R. & Parent, J. M. Hepatocyte growth factor acts as a mitogen and chemoattractant for postnatal subventricular zone-olfactory bulb neurogenesis. *Mol Cell Neurosci* **48**, 38-50 (2011).
- 16 Mani, N., Khaibullina, A., Krum, J. M. & Rosenstein, J. M. Vascular Endothelial Growth Factor Enhances Migration of Astroglial Cells in Subventricular Zone Neurosphere Cultures. *J Neurosci Res* **88**, 248-257 (2010).
- 17 Nicoleau, C. *et al.* Endogenous Hepatocyte Growth Factor Is a Niche Signal for Subventricular Zone Neural Stem Cell Amplification and Self-Renewal. *Stem Cells* **27**, 408-419 (2009).
- 18 Yu, J. & Zeng, J. Exogeneous epidermal growth factor promotes the migration and differentiation of neural stem cells in the subventricular zone to cortical infarct cavity in adult hypertensive rats. *Stroke* **35**, E253-E253 (2004).
- 19 Zheng, W., Nowakowski, R. S. & Vaccarino, F. M. Fibroblast growth factor 2 is required for maintaining the neural stem cell pool in the mouse brain subventricular zone. *Dev Neurosci-Basel* **26**, 181-196 (2004).
- 20 Decker, L., Picard-Riera, N., Lachapelle, F. & Baron-Van Evercooren, A. Growth factor treatment promotes mobilization of young but not aged adult subventricular zone precursors in response to demyelination. *J Neurosci Res* **69**, 763-771 (2002).
- 21 Duong, A. V. *et al.* Temporal sequence of subventricular zone cell proliferation in response to transforming growth factor alpha administration in the adult rat forebrain in vivo. *Faseb J* **15**, A1074-A1074 (2001).
- 22 Kolb, B. *et al.* Growth factor-stimulated generation of new cortical tissue and functional recovery after stroke damage to the motor cortex of rats. *J Cerebr Blood F Met* **27**, 983-997 (2007).

- 23 Lindvall, O. & Kokaia, Z. Stem cells in human neurodegenerative disorders - time for clinical translation? *J Clin Invest* **120**, 29-40 (2010).
- 24 Misra, A., Ganesh, S., Shahiwala, A. & Shah, S. P. Drug delivery to the central nervous system: a review. *J Pharm Pharm Sci* **6**, 252-273 (2003).
- 25 Rosenow, U. F. & Wojcicka, J. B. Clinical Implementation of Stereotaxic Brain Implant Optimization. *Med Phys* **18**, 266-272 (1991).
- 26 During, M. J. *et al.* Controlled Release of Dopamine from a Polymeric Brain Implant - In vivo Characterization. *Ann Neurol* **25**, 351-356 (1989).
- 27 Roger. Heart Disease and Stroke Statistics-2011 Update: A Report From the American Heart Association (vol 123, pg e18, 2011). *Circulation* **123**, E240-E240 (2011).
- 28 Szczesniewska, D., Kurjata, P., Broda, G., Polakowska, M. & Kupsc, W. Comparison of Official Mortality Statistics with Data Obtained from Myocardial-Infarction and Stroke Registers. *Rev Epidemiol Sante* **38**, 435-439 (1990).
- 29 Bleic, S. A., Jeanette, S. M., De Windt, A., Bier, J. C. & Pandolfo, M. Stroke in the young: Fixing the upper age limit of youth leads to individualize a new subpopulation. *Neurology* **58**, A118-A118 (2002).
- 30 Cumming, T. B. & Brodtmann, A. Can stroke cause neurodegenerative dementia? *Int J Stroke* **6**, 416-424 (2011).
- 31 Morris, J. C. *et al.* Post-Stroke Dementia Is a Function of Presymptomatic Alzheimer Disease. *Neurology* **76**, A168-A168 (2011).
- 32 Di Carlo, A. Human and economic burden of stroke. *Age Ageing* **38**, 4-5 (2009).
- 33 Zhang, Y. R. *et al.* Lifestyle Factors on the Risks of Ischemic and Hemorrhagic Stroke. *Arch Intern Med* **171**, 1811-1818 (2011).
- 34 Smith, S. D. & Eskey, C. J. Hemorrhagic Stroke. *Radiol Clin N Am* **49**, 27-+ (2011).
- 35 Guiraud, V., Ben Amor, M., Mas, J. L. & Touze, E. Triggers of Ischemic Stroke A Systematic Review. *Stroke* **41**, 2669-2677 (2010).

- 36 Godoy, D. A., Pinero, G. & Di Napoli, M. Predicting mortality in spontaneous intracerebral Hemorrhage - Can modification to original score improve the prediction? *Stroke* **37**, 1038-1044 (2006).
- 37 Fandino-Rivera, J. Traumatic brain injury and ischemic stroke: A delayed sequela? *Rev Neurologia* **38**, 912-915 (2004).
- 38 Kidwell, C. S. *et al.* Late secondary ischemic injury in patients receiving intraarterial thrombolysis. *Ann Neurol* **52**, 698-703 (2002).
- 39 Wang, Y. & Qin, Z. H. Molecular and cellular mechanisms of excitotoxic neuronal death. *Apoptosis* **15**, 1382-1402 (2010).
- 40 Gilgun-Sherki, Y., Rosenbaum, Z., Melamed, E. & Offen, D. Antioxidant therapy in acute central nervous system injury: Current state. *Pharmacol Rev* **54**, 271-284 (2002).
- 41 Aarts, M. M. & Tymianski, M. Molecular mechanisms underlying specificity of excitotoxic signaling in neurons. *Curr Mol Med* **4**, 137-147 (2004).
- 42 Bano, D. & Nicotera, P. Ca<sup>2+</sup> signals and neuronal death in brain ischemia. *Stroke* **38**, 674-676 (2007).
- 43 Castillo, J., Davalos, A. & Noya, M. Progression of ischaemic stroke and excitotoxic aminoacids. *Lancet* **349**, 79-83 (1997).
- 44 Hasbani, M. J., Underhill, S. M., de Erausquin, G. & Goldberg, M. P. Synapse loss and regeneration: A mechanism for functional decline and recovery after cerebral ischemia? *Neuroscientist* **6**, 110-119 (2000).
- 45 Dominguez, C. *et al.* Oxidative Stress After Thrombolysis-Induced Reperfusion in Human Stroke. *Stroke* **41**, 653-660 (2010).
- 46 Aoki, J. & Uchino, K. Treatment of Risk Factors to Prevent Stroke. *Neurotherapeutics* **8**, 463-474 (2011).
- 47 Towfighi, A. & Ovbiagele, B. Metabolic Syndrome and Stroke. *Curr Diabetes Rep* **8**, 37-41 (2008).
- 48 Hillbom, M., Juvela, S. & Numminen, H. Alcohol intake and the risk of stroke. *J Cardiovasc Risk* **6**, 223-228 (1999).

- 49 Lee, I. M., Hennekens, C. H., Berger, K., Buring, J. E. & Manson, J. E. Exercise and risk of stroke in male physicians. *Stroke* **30**, 1-6 (1999).
- 50 Marx, P. Prevention of stroke. *Nervenheilkunde* **16**, 472-481 (1997).
- 51 Mohr, J. P. Neuroprotective agents in acute ischemic stroke. *Abstr Pap Am Chem S* **211**, 103-MEDI (1996).
- 52 Pyne-Geithman, G. Brain, heal thyself! Neuroregeneration in the subventricular zone after ischemic stroke. *Neurology* **74**, 352-353 (2010).
- 53 Pulsinelli, W. A., Jacewicz, M., Levy, D. E., Petito, C. K. & Plum, F. Ischemic brain injury and the therapeutic window. *Frontiers of Neurology* **835**, 187-193 (1997).
- 54 Konstas, A. A., Wintermark, M. & Lev, M. H. CT Perfusion Imaging in Acute Stroke. *Neuroimag Clin N Am* **21**, 215-+ (2011).
- 55 Jager, H. R. Diagnosis of stroke with advanced CT and MR imaging. *Brit Med Bull* **56**, 318-333 (2000).
- 56 Bi, M. *et al.* Local mild hypothermia with thrombolysis for acute ischemic stroke within a 6-h window. *Clin Neurol Neurosur* **113**, 768-773 (2011).
- 57 Groysman, L. I., Emanuel, B. A., Kim-Tenser, M. A., Sung, G. Y. & Mack, W. J. Therapeutic hypothermia in acute ischemic stroke. *Neurosurg Focus* **30** (2011).
- 58 Sheehan, J. J. & Tsirka, S. E. Fibrin-modifying serine proteases thrombin, tPA, and plasmin in ischemic stroke: A review. *Glia* **50**, 340-350 (2005).
- 59 Saver, J. L. Improving reperfusion therapy for acute ischaemic stroke. *J Thromb Haemost* **9**, 333-343 (2011).
- 60 Molina & Saver. Extending reperfusion therapy for acute ischemic stroke: Emerging pharmacological, mechanical, and imaging strategies (vol 36, pg 2311, 2005). *Stroke* **37**, 931-931 (2006).
- 61 Donnan, G. A. *et al.* How to make better use of thrombolytic therapy in acute ischemic stroke. *Nat Rev Neurol* **7**, 400-409 (2011).

- 62 Kalra, L. & Eade, J. Role of Stroke Rehabilitation Units in Managing Severe Disability after Stroke. *Stroke* **26**, 2031-2034 (1995).
- 63 Tilling, K. *et al.* A new method for predicting recovery after stroke. *Stroke* **32**, 2867-2873 (2001).
- 64 Alexander, M. P. Stroke Rehabilitation Outcome - a Potential Use of Predictive Variables to Establish Levels of Care. *Stroke* **25**, 128-134 (1994).
- 65 Bliss, T., Guzman, R., Daadi, M. & Steinberg, G. K. Cell transplantation therapy for stroke. *Stroke* **38**, 817-826 (2007).
- 66 Borlongan, C. V. & Hess, D. C. New hope for stroke patients: mobilization of endogenous stem cells. *Can Med Assoc J* **174**, 954-955 (2006).
- 67 Titomanlio, L. *et al.* Stem cell therapy for neonatal brain injury: Perspectives and Challenges. *Ann Neurol* **70**, 698-712 (2011).
- 68 Sicard, K. M. & Fisher, M. Emerging drugs for acute ischemic stroke. *Expert Opin Emerg Dr* **14**, 33-42 (2009).
- 69 Ford, G. A. Clinical pharmacological issues in the development of acute stroke therapies. *Brit J Pharmacol* **153**, S112-S119 (2008).
- 70 Knight, A. Systematic reviews of animal experiments demonstrate poor human clinical and toxicological utility. *Atla-Altern Lab Anim* **35**, 641-659 (2007).
- 71 Casals, J. B. *et al.* The Use of Animal Models for Stroke Research: A Review. *Comparative Medicine* **61**, 305 - 313 (2011).
- 72 Culp, W. C., Erdem, E., Roberson, P. K. & Husain, M. M. Microbubble Potentiated ultrasound as a method of stroke therapy in a pig model: Preliminary findings. *J Vasc Interv Radiol* **14**, 1433-1436 (2003).
- 73 Prusty, S., Kemper, T., Moss, M. B. & Hollander, W. Occurrence of Stroke in a Nonhuman Primate Model of Cerebrovascular-Disease. *Stroke* **19**, 84-90 (1988).
- 74 Lee, S. H., Heros, R. C., Mullan, J. C. & Korosue, K. Optimum Degree of Hemodilution for Brain Protection in a Canine Model of Focal Cerebral-Ischemia. *J Neurosurg* **80**, 469-475 (1994).

- 75 Durukan, A. & Tatlisumak, T. Acute ischemic stroke: Overview of major experimental rodent models, pathophysiology, and therapy of focal cerebral ischemia. *Pharmacol Biochem Be* **87**, 179-197 (2007).
- 76 Zarruk, J. G. *et al.* Neurological tests for functional outcome assessment in rodent models of ischaemic stroke. *Rev Neurologia* **53**, 607-618 (2011).
- 77 van der Worp, H. B. *et al.* Can Animal Models of Disease Reliably Inform Human Studies? *Plos Med* **7** (2010).
- 78 Liu, F. D. & McCullough, L. D. Middle Cerebral Artery Occlusion Model in Rodents: Methods and Potential Pitfalls. *J Biomed Biotechnol* (2011).
- 79 Orset, C. *et al.* Mouse model of in situ thromboembolic stroke and reperfusion. *Stroke* **38**, 2771-2778 (2007).
- 80 Jiang, W., Gu, W. G., Hossmann, K. A., Mies, G. & Wester, P. Establishing a photothrombotic 'ring' stroke model in adult mice with late spontaneous reperfusion: quantitative measurements of cerebral blood flow and cerebral protein synthesis. *J Cerebr Blood F Met* **26**, 927-936 (2006).
- 81 Nakahara, T., Oki, S., Muttaqin, Z., Kuwabara, S. & Uozumi, T. A New Model of Brain-Stem Ischemia by Embolization Technique in Cats. *Neurosurg Rev* **14**, 221-229 (1991).
- 82 Wang, K. & Walz, W. Unusual topographical pattern of proximal astrogliosis around a cortical devascularizing lesion. *J Neurosci Res* **73**, 497-506 (2003).
- 83 Virley, D. *et al.* A new primate model of focal stroke: Endothelin-1-induced middle cerebral artery occlusion and reperfusion in the common marmoset. *J Cerebr Blood F Met* **24**, 24-41 (2004).
- 84 Horie, N. *et al.* Mouse model of focal cerebral ischemia using endothelin-1. *J Neurosci Meth* **173**, 286-290 (2008).
- 85 Fisher, M. Neuroprotection for acute ischemic stroke. *Zh Nevropatol Psikh*, 43-45 (2003).
- 86 Culmsee, C. & Krieglstein, J. Ischaemic brain damage after stroke: new insights into efficient therapeutic strategies - International Symposium on Neurodegeneration and Neuroprotection. *Embo Rep* **8**, 129-133 (2007).

- 87 Antonelli, M. C. *et al.* New Strategies in Neuroprotection and Neurorepair. *Neurotox Res* **21**, 49-56 (2012).
- 88 Kriegelstein, J. Excitotoxicity and neuroprotection. *Eur J Pharm Sci* **5**, 181-187 (1997).
- 89 Hasselblatt, M., Ehrenreich, H. & Siren, A. L. The brain erythropoietin system and its potential for therapeutic exploitation in brain disease. *J Neurosurg Anesth* **18**, 132-138 (2006).
- 90 Wiltout, C., Lang, B., Yan, Y. P., Dempsey, R. J. & Vemuganti, R. Repairing brain after stroke: A review on post-ischemic neurogenesis. *Neurochem Int* **50**, 1028-1041 (2007).
- 91 Luque, J. M. & Ribotta, M. G. Y. Neural stem cells and the quest for restorative neurology. *Histol Histopathol* **19**, 271-280 (2004).
- 92 Wang, L., Zhang, Z. G., Wang, Y., Zhang, R. L. & Chopp, M. Treatment of stroke with erythropoietin enhances neurogenesis and angiogenesis and improves neurological function in rats. *Stroke* **35**, 1732-1737 (2004).
- 93 Mabuchi, T., Lucero, J., Feng, A., Koziol, J. A. & del Zoppo, G. J. Focal cerebral ischemia preferentially affects neurons distant from their neighboring microvessels. *J Cerebr Blood F Met* **25**, 257-266 (2005).
- 94 Dewar, D., Underhill, S. M. & Goldberg, T. P. Oligodendrocytes and ischemic brain injury. *J Cerebr Blood F Met* **23**, 263-274 (2003).
- 95 Cramer, S. C. Repairing the human brain after stroke: I. Mechanisms of spontaneous recovery. *Ann Neurol* **63**, 272-287 (2008).
- 96 Savitz, S. I., Rosenbaum, D. M., Dinsmore, J. H., Wechsler, L. R. & Caplan, L. R. Cell transplantation for stroke. *Ann Neurol* **52**, 266-275 (2002).
- 97 Kawai, H. *et al.* Tridermal tumorigenesis of induced pluripotent stem cells transplanted in ischemic brain. *J Cerebr Blood F Met* **30**, 1487-1493 (2010).
- 98 Boncoraglio, G. B., Bersano, A., Candelise, L., Reynolds, B. A. & Parati, E. A. Stem Cell Transplantation for Ischemic Stroke. *Stroke* **42**, E33-E33 (2011).
- 99 Locatelli, F. *et al.* Stem cell therapy in stroke. *Cell Mol Life Sci* **66**, 757-772 (2009).

- 100 Deverman, B. E. & Patterson, P. H. Cytokines and CNS Development. *Neuron* **64**, 61-78 (2009).
- 101 Doetsch, F., Caille, I., Lim, D. A., Garcia-Verdugo, J. M. & Alvarez-Buylla, A. Subventricular zone astrocytes are neural stem cells in the adult mammalian brain. *Cell* **97**, 703-716 (1999).
- 102 Doetsch, F., Petreanu, L., Caille, I., Garcia-Verdugo, J. M. & Alvarez-Buylla, A. EGF converts transit-amplifying neurogenic precursors in the adult brain into multipotent stem cells. *Neuron* **36**, 1021-1034 (2002).
- 103 Blanchard, J. *et al.* Beneficial Effect of a CNTF Tetrapeptide on Adult Hippocampal Neurogenesis, Neuronal Plasticity, and Spatial Memory in Mice. *J Alzheimers Dis* **21**, 1185-1195 (2010).
- 104 Kallos, M. S., Sen, A. & Behie., L. A. Large-scale expansion of mammalian neural stem cells: a review *Medical and Biological Engineering and Computing* **21**, 271 - 282 (2003).
- 105 Ford, G. A., Bryant, C. A., Mangoni, A. A. & Jackson, S. H. D. Stroke, dementia, and drug delivery. *Brit J Clin Pharmacol* **57**, 15-26 (2004).
- 106 Jin, K. L. *et al.* Post-ischemic administration of heparin-binding epidermal growth factor-like growth factor (HB-EGF) reduces infarct size and modifies neurogenesis after focal cerebral ischemia in the rat. *J Cerebr Blood F Met* **24**, 399-408 (2004).
- 107 Lanfranconi, S. *et al.* Growth factors in ischemic stroke. *J Cell Mol Med* **15**, 1645-1687 (2011).
- 108 Ay, H., Ay, I., Koroshetz, W. J. & Finklestein, S. P. Potential usefulness of basic fibroblast growth factor as a treatment for stroke. *Cerebrovasc Dis* **9**, 131-135 (1999).
- 109 Lin, D. A. & Finklestein, S. P. Basic fibroblast growth factor: A treatment for stroke? *Neuroscientist* **3**, 247-250 (1997).
- 110 Watanabe, T. *et al.* Postischemic intraventricular administration of FGF-2 expressing adenoviral vectors improves neurologic outcome and reduces infarct volume after transient focal cerebral ischemia in rats. *J Cerebr Blood Flow Metab* **24**, 1205-1213, doi:00004647-200411000-00002 [pii]  
10.1097/01.WCB.0000136525.75839.41 (2004).

- 111 Diederich, K. *et al.* Successful Regeneration After Experimental Stroke by Granulocyte-Colony Stimulating Factor Is Not Further Enhanced by Constraint-Induced Movement Therapy Either in Concurrent or in Sequential Combination Therapy. *Stroke* **43**, 185 - 192 (2011).
- 112 Dong, F. & Lerner, A. C. Activation of Akt kinase by granulocyte colony-stimulating factor (G-CSF): evidence for the role of a tyrosine kinase activity distinct from the janus kinases. *Blood* **95**, 1656-1662 (2000).
- 113 Pennington, A., Sava, V., Song, S., Patel, N. & Sanchez-Ramos, J. Direct Actions of Granulocyte-Colony Stimulating Factor on Human Neuronal and Monocytic Cell Lines. *Journal of Alzheimer's Disease and Parkinsonism* **3** (2013).
- 114 Gonzalez-Perez, O., Romero-Rodriguez, R., Soriano-Navarro, M., Garcia-Verdugo, J. M. & Alvarez-Buylla, A. Epidermal Growth Factor Induces the Progeny of Subventricular Zone Type B Cells to Migrate and Differentiate into Oligodendrocytes (vol 27, pg 2032, 2009). *Stem Cells* **27**, 3122-3122 (2009).
- 115 Wang, K. *et al.* Infusion of epidermal growth factor and basic fibroblast growth factor into the striatum of parkinsonian rats leads to in vitro proliferation and differentiation of adult neural progenitor cells. *Neuroscience Letters* **364**, 154-158 (2004).
- 116 Brines, M. & Cerami, A. Erythropoietin-mediated tissue protection: reducing collateral damage from the primary injury response. *J Intern Med* **264**, 405-432 (2008).
- 117 Sargin, D., Friedrichs, H., El-Kordi, A. & Ehrenreich, H. Erythropoietin as neuroprotective and neuroregenerative treatment strategy: comprehensive overview of 12 years of preclinical and clinical research. *Best Practice and Research Clinical Anaesthesiology* **24**, 573 - 594 (2010).
- 118 Ehrenreich, H. *et al.* Erythropoietin therapy for acute stroke is both safe and beneficial. *Mol Med* **8**, 495-505 (2002).
- 119 Genc, S., Zadeoglulari, Z., Oner, M. G., Genc, K. & Digicaylioglu, M. Intranasal erythropoietin therapy in nervous system disorders. *Expert Opin Drug Del* **8**, 19-32 (2011).
- 120 Pardridge, W. M., Boado, R. J., Black, K. L. & Cancilla, P. A. Blood-Brain-Barrier and New Approaches to Brain Drug Delivery. *Western J Med* **156**, 281-286 (1992).
- 121 Ferber, D. Bridging the blood-brain barrier: New methods improve the odds of getting drugs to the brain cells that need them. *Plos Biol* **5**, 1191-1194 (2007).

- 122 Sandoval, K. E. & Witt, K. A. Blood-brain barrier tight junction permeability and ischemic stroke. *Neurobiol Dis* **32**, 200-219 (2008).
- 123 Biondi, M., Ungaro, F., Quaglia, F. & Netti, P. A. Controlled drug delivery in tissue engineering. *Adv Drug Deliver Rev* **60**, 229-242 (2008).
- 124 Namba, H., Zheng, Y., Abe, Y. & Nawa, H. Epidermal Growth Factor Administered in the Periphery Influences Excitatory Synaptic Inputs onto Midbrain Dopaminergic Neurons in Postnatal Mice. *Neuroscience* **158**, 1731-1741 (2009).
- 125 Pean, J. M. *et al.* NGF release from poly(D,L-lactide-co-glycolide) microspheres. Effect of some formulation parameters on encapsulated NGF stability. *J Control Release* **56**, 175-187 (1998).
- 126 Rao, R. Oxidative stress-induced disruption of epithelial and endothelial tight junctions. *Frontiers in Bioscience* **13**, 7210-7226 (2008).
- 127 Siepmann, J., Siepmann, F. & Florence, A. T. Local controlled drug delivery to the brain: Mathematical modeling of the underlying mass transport mechanisms. *Int J Pharm* **314**, 101-119 (2006).
- 128 Greenhalgh, A. D., Ogungbenro, K., Rothwell, N. J. & Galea, J. P. Translational pharmacokinetics: challenges of an emerging approach to drug development in stroke. *Expert Opin Drug Met* **7**, 681-695 (2011).
- 129 Lestage, P., Lockhart, B. & Roger, A. In vivo exploration of stroke: animal models and pharmacology. *Therapie* **57**, 554-563 (2002).
- 130 Shemesh, E., Rudich, A., Harman-Boehm, I. & Cukierman-Yaffe, T. Effect of Intranasal Insulin on Cognitive Function: A Systematic Review. *Journal of Clinical Endocrinology and Metabolism* **97**, 366 (2012).
- 131 de Boer, A. G. & Gaillard, P. J. Strategies to improve drug delivery across the blood-brain barrier. *Clin Pharmacokinet* **46**, 553-576 (2007).
- 132 Zhou, Q. H., Lu, J. Z., Hui, E. K. W., Boado, R. J. & Pardridge, W. M. Delivery of a Peptide Radiopharmaceutical to Brain with an IgG-Avidin Fusion Protein. *Bioconjugate Chem* **22**, 1611-1618 (2011).

- 133 Zhou, Q. H., Hui, E. K. W., Lu, J. Z., Boado, R. J. & Pardridge, W. M. Brain penetrating IgG-erythropoietin fusion protein is neuroprotective following intravenous treatment in Parkinson's disease in the mouse. *Brain Res* **1382**, 315-320 (2011).
- 134 Fu, A. L., Hui, E. K. W., Lu, J. Z., Boado, R. J. & Pardridge, W. M. Neuroprotection in stroke in the mouse with intravenous erythropoietin-Trojan horse fusion protein. *Brain Res* **1369**, 203-207 (2011).
- 135 Zheng, W., Aschner, M. & Ghersi-Egea, J. F. Brain barrier systems: a new frontier in metal neurotoxicological research. *Toxicology and Applied Pharmacology* **192**, 1-11 (2003).
- 136 Jonhagen, M. E. *et al.* Intracerebroventricular infusion of nerve growth factor in three patients with Alzheimer's disease. *Dement Geriatr Cogn* **9**, 246-257 (1998).
- 137 Kobayashi, T. *et al.* Intracerebral infusion of glial cell line-derived neurotrophic factor promotes striatal neurogenesis after stroke in adult rats. *Stroke* **37**, 2361-2367 (2006).
- 138 Jain, K. K. Nanobiotechnology - Based drug delivery to the central nervous system. *Neurodegener Dis* **4**, 287-291 (2007).
- 139 Kerenyi, S. Z. & Hartgraves, S. L. Premature Excess Release from the Alzet Osmotic Pump. *Pharmacol Biochem Be* **27**, 199-201 (1987).
- 140 Jasmin, L. & Ohara, P. T. Long-term intrathecal catheterization in the rat. *J Neurosci Meth* **110**, 81-89 (2001).
- 141 Saltzman, W. M. & Radomsky, M. L. Drugs released from polymers - diffusion and elimination in brain-tissue. *Chem Eng Sci* **46**, 2429-2444 (1991).
- 142 Thorne, R. G., Hrabetova, S. & Nicholson, C. Diffusion of epidermal growth factor in rat brain extracellular space measured by integrative optical imaging. *J Neurophysiol* **92**, 3471-3481 (2004).
- 143 Haller, M. F. & Saltzman, W. M. Localized delivery of proteins in the brain: Can transport be customized? *Pharmaceut Res* **15**, 377-385 (1998).
- 144 Shortle, D. Mutational Studies of Protein Structures and Their Stabilities. *Q Rev Biophys* **25**, 205-250 (1992).

- 145 Shortle, D., Dimaio, D. & Nathans, D. Directed Mutagenesis. *Annu Rev Genet* **15**, 265-294 (1981).
- 146 de Graaf, A. J., Kooijman, M., Hennink, W. E. & Mastrobattista, E. Nonnatural Amino Acids for Site-Specific Protein Conjugation. *Bioconjugate Chem* **20**, 1281-1295 (2009).
- 147 Matzuk, M. M. & Boime, I. Site-Specific Mutagenesis Defines the Intracellular Role of the Asparagine-Linked Oligosaccharides of Chorionic Gonadotropin-Beta Subunit. *J Biol Chem* **263**, 17106-17111 (1988).
- 148 Zhan, H. J. *et al.* Engineering a soluble extracellular erythropoietin receptor (EPObp) in *Pichia pastoris* to eliminate microheterogeneity, and its complex with erythropoietin. *Protein Eng* **12**, 505-513 (1999).
- 149 Cunningham, B. C. & Wells, J. A. Comparison of a Structural and a Functional Epitope. *J Mol Biol* **234**, 554-563 (1993).
- 150 Cohen, S. & Carpenter, G. Human Epidermal Growth-Factor - Isolation and Chemical and Biological Properties. *P Natl Acad Sci USA* **72**, 1317-1321 (1975).
- 151 Seo, J. & Lee, K. J. Post-translational modifications and their biological functions: Proteomic analysis and systematic approaches. *J Biochem Mol Biol* **37**, 35-44 (2004).
- 152 Katre, N. V. The Conjugation of Proteins with Polyethylene-Glycol and Other Polymers - Altering Properties of Proteins to Enhance Their Therapeutic Potential. *Adv Drug Deliver Rev* **10**, 91-114 (1993).
- 153 Lee, H. & Park, T. G. Conjugation of trypsin by temperature-sensitive polymers containing a carbohydrate moiety: Thermal modulation of enzyme activity. *Biotechnol Progr* **14**, 508-516 (1998).
- 154 Stroh, M., Zipfel, W. R., Williams, R. M., Webb, W. W. & Saltzman, W. M. Diffusion of nerve growth factor in rat striatum as determined by multiphoton microscopy. *Biophys J* **85**, 581-588 (2003).
- 155 Vicent, M. J., Dieudonne, L., Carbajo, R. J. & Pineda-Lucena, A. Polymer conjugates as therapeutics: future trends, challenges and opportunities. *Expert Opin Drug Del* **5**, 593-614 (2008).
- 156 Hoffman, A. S. & Stayton, P. S. Conjugates of stimuli-responsive polymers and proteins. *Progress in Polymer Science* **32**, 922-932 (2007).

- 157 Tong, R. & Cheng, J. J. Anticancer polymeric nanomedicines. *Polymer Reviews* **47**, 345-381 (2007).
- 158 Vicent, M. J. Polymer-drug conjugates as modulators of cellular apoptosis. *Aaps Journal* **9**, E200-E207 (2007).
- 159 Lele, B. S., Murata, H., Matyjaszewski, K. & Russell, A. J. Synthesis of uniform protein-polymer conjugates. *Biomacromolecules* **6**, 3380-3387 (2005).
- 160 Veronese, F. M. *et al.* Improvement of pharmacokinetic, immunological and stability properties of asparaginase by conjugation to linear and branched monomethoxy poly(ethylene glycol). *J Control Release* **40**, 199-209 (1996).
- 161 Delgado, C., Francis, G. E. & Fisher, D. The Uses and Properties of Peg-Linked Proteins. *Critical Reviews in Therapeutic Drug Carrier Systems* **9**, 249-304 (1992).
- 162 Woghiren, C., Sharma, B. & Stein, S. Protected Thiol Polyethylene-Glycol - a New Activated Polymer for Reversible Protein Modification. *Bioconjugate Chem* **4**, 314-318 (1993).
- 163 Roberts, M. J., Bentley, M. D. & Harris, J. M. Chemistry for peptide and protein PEGylation. *Adv Drug Deliver Rev* **54**, 459-476 (2002).
- 164 Otsuka, H., Nagasaki, Y. & Kataoka, K. Characterization of aldehyde-PEG tethered surfaces: Influence of PEG chain length on the specific biorecognition. *Langmuir* **20**, 11285-11287 (2004).
- 165 Ananda, K., Nacharaju, P., Smith, P. K., Acharya, S. A. & Manjula, B. N. Analysis of functionalization of methoxy-PEG as maleimide-PEG. *Anal Biochem* **374**, 231-242 (2008).
- 166 Veronese, F. M. Peptide and protein PEGylation: a review of problems and solutions. *Biomaterials* **22**, 405-417 (2001).
- 167 Xu, Z. L. & Qusay, F. A. Effect of polyethylene glycol molecular weights and concentrations on polyethersulfone hollow fiber ultrafiltration membranes. *J Appl Polym Sci* **91**, 3398-3407 (2004).
- 168 Mehvar, R. Modulation of the pharmacokinetics and pharmacodynamics of proteins by polyethylene glycol conjugation. *J Pharm Pharm Sci* **3**, 125-136 (2000).

- 169 Dixon, H. B. F. N-Terminal Modification of Proteins - a Review. *J Protein Chem* **3**, 99-108 (1984).
- 170 Kinstler, O. B. *et al.* Characterization and stability of N-terminally PEGylated rhG-CSF. *Pharmaceut Res* **13**, 996-1002 (1996).
- 171 Lee, H. & Park, T. G. Preparation and characterization of mono-PEGylated epidermal growth factor: Evaluation of in vitro biologic activity. *Pharmaceut Res* **19**, 845-851 (2002).
- 172 Yoshioka, Y. *et al.* Site-specific PEGylation of a lysine-deficient TNF superfamily with full bioactivity. *Cytokine* **39**, 47-47 (2007).
- 173 Yoshioka, Y., Tsunoda, S. & Tsutsumi, Y. Development of a novel DDS for site-specific PEGylated proteins. *Chem Cent J* **5** (2011).
- 174 Gilmore, J. M., Scheck, R. A., Esser-Kahn, A. P., Joshi, N. S. & Francis, M. B. N-terminal protein modification through a biomimetic transamination reaction. *Angew Chem Int Edit* **45**, 5307-5311 (2006).
- 175 Scheck, R. A., Dedeo, M. T., Lavarone, A. T. & Francis, M. B. Optimization of a biomimetic transamination reaction. *J Am Chem Soc* **130**, 11762-11770 (2008).
- 176 Guo, X. Q., Wang, Q. L., Swarts, B. M. & Guo, Z. W. Sortase-Catalyzed Peptide-Glycosylphosphatidylinositol Analogue Ligation. *J Am Chem Soc* **131**, 9878-+ (2009).
- 177 Ton-That, H., Mazmanian, S. K., Faull, K. F. & Schneewind, O. Anchoring of surface proteins to the cell wall of *Staphylococcus aureus* - Sortase catalyzed in vitro transpeptidation reaction using LPXTG peptide and NH<sub>2</sub>-Gly(3) substrates. *J Biol Chem* **275**, 9876-9881 (2000).
- 178 Metzler, D. E., Olivard, J. & Snell, E. E. Transamination of Pyridoxamine and Amino Acids with Glyoxylic Acid. *J Am Chem Soc* **76**, 644-648 (1954).
- 179 Sonomura, K., Kuyama, H., Matsuo, E., Tsunasawa, S. & Nishimura, O. The specific isolation of C-terminal peptides of proteins through a transamination reaction and its advantage for introducing functional groups into the peptide. *Rapid Commun Mass Sp* **23**, 611-618 (2009).
- 180 Parthasarathy, R., Subramanian, S. & Boder, E. T. Sortase A as a novel molecular "stapler" for sequence-specific protein conjugation. *Bioconjugate Chem* **18**, 469-476 (2007).

- 181 Pritz, S. *et al.* Synthesis of biologically active peptide nucleic acid-peptide conjugates by sortase-mediated ligation. *Journal of Organic Chemistry* **72**, 3909-3912 (2007).
- 182 Kumar, M. N. V. R. Nano and microparticles as controlled drug delivery devices. *J Pharm Pharm Sci* **3**, 234-258 (2000).
- 183 Nicholas, A. P. *et al.* The fate of biodegradable microspheres injected into rat brain. *Neuroscience Letters* **323**, 85-88 (2002).
- 184 Kabanov, A. V. & Gendelman, H. E. Nanomedicine in the diagnosis and therapy of neurodegenerative disorders. *Progress in Polymer Science* **32**, 1054-1082 (2007).
- 185 Gibas, I. & Janik, H. Review: synthetic polymer hydrogels for biomedical applications. *Chemistry & Chemical Technology* **4**, 297 - 304 (2010).
- 186 Meyvis, T. K. L. *et al.* A comparison between the use of dynamic mechanical analysis and oscillatory shear rheometry for the characterisation of hydrogels. *Int J Pharm* **244**, 163-168 (2002).
- 187 Lazzeri, L. *et al.* Physicochemical and Mechanical Characterization of Hydrogels of Poly(Vinyl Alcohol) and Hyaluronic-Acid. *J Mater Sci-Mater M* **5**, 862-867 (1994).
- 188 Shalaby, W. S. W. & Park, K. Biochemical and Mechanical Characterization of Enzyme-Digestible Hydrogels. *Pharmaceut Res* **7**, 816-823 (1990).
- 189 Westman, L. & Lindstrom, T. Swelling and Mechanical-Properties of Cellulose Hydrogels .1. Preparation, Characterization, and Swelling Behavior. *J Appl Polym Sci* **26**, 2519-2532 (1981).
- 190 Hennink, W. E. & van Nostrum, C. F. Novel crosslinking methods to design hydrogels. *Adv Drug Deliver Rev* **54**, 13-36 (2002).
- 191 Hubbell, J. A. Synthetic biodegradable polymers for tissue engineering and drug delivery. *Curr Opin Solid St M* **3**, 246-251 (1998).
- 192 Warren, P. B. Flory-huggins theory for the solubility of heterogeneously modified polymers. *Macromolecules* **40**, 6709-6712 (2007).
- 193 Slaughter, B. V., Khurshid, S. S., Fisher, O. Z., Khademhosseini, A. & Peppas, N. A. Hydrogels in Regenerative Medicine. *Adv Mater* **21**, 3307-3329 (2009).

- 194 Peppas, N. A., Bures, P., Leobandung, W. & Ichikawa, H. Hydrogels in pharmaceutical formulations. *Eur J Pharm Biopharm* **50**, 27-46 (2000).
- 195 Sun, J. X., Wang, Y. L., Dou, S. H., Ruan, C. S. & Hu, C. B. PEG derived hydrogel: A novel synthesis route under mild condition. *Mater Lett* **67**, 215-218 (2012).
- 196 PEG-based 3D hydrogel slide shows promise. *Future Med Chem* **1**, 1208-1208 (2009).
- 197 Dziubla, T. D. & Lowman, A. M. Vascularization of PEG-grafted macroporous hydrogel sponges: A three-dimensional in vitro angiogenesis model using human microvascular endothelial cells. *J Biomed Mater Res A* **68A**, 603-614 (2004).
- 198 Gayet, J. C. & Fortier, G. High water content BSA-PEG hydrogel for controlled release device: Evaluation of the drug release properties. *J Control Release* **38**, 177-184 (1996).
- 199 Qiu, Y. & Park, K. Environment-sensitive hydrogels for drug delivery. *Adv Drug Deliver Rev* **53**, 321-339 (2001).
- 200 Lin, C. C. & Anseth, K. S. PEG Hydrogels for the Controlled Release of Biomolecules in Regenerative Medicine. *Pharmaceut Res* **26**, 631-643 (2009).
- 201 Stasko, J., Kalnins, M., Dzene, A. & Tupureina, V. Poly(vinyl alcohol) hydrogels. *P Est Acad Sci* **58**, 63-66 (2009).
- 202 Muratoglu, O. K. *et al.* Optical analysis of surface changes on early retrievals of highly cross-linked and conventional polyethylene tibial inserts. *J Arthroplasty* **18**, 42-47 (2003).
- 203 Dini, L. *et al.* In vitro study of the interaction of polyalkylimide and polyvinyl alcohol hydrogels with cells. *Tissue Cell* **37**, 479-487 (2005).
- 204 Fan, C. X. *et al.* Cellular biological evaluation of medical polyacrylamide hydrogel. *Key Eng Mat* **288-289**, 413-416 (2005).
- 205 Ramires, P. A., Miccoli, M. A., Panzarini, E., Dini, L. & Protopapa, C. In vitro and in vivo biocompatibility evaluation of a polyalkylimide hydrogel for soft tissue augmentation. *J Biomed Mater Res B* **72B**, 230-238 (2005).
- 206 Rahimi, S., Sarraf, E. H., Wong, G. K. & Takahata, K. Implantable drug delivery device using frequency-controlled wireless hydrogel microvalves. *Biomed Microdevices* **13**, 267-277 (2011).

- 207 Lee, K. K. *et al.* Polyimide-based intracortical neural implant with improved structural stiffness. *J Micromech Microeng* **14**, 32-37 (2004).
- 208 Abraham, G. A., de Queiroz, A. A. A. & San Roman, J. S. Hydrophilic hybrid IPNs of segmented polyurethanes and copolymers of vinylpyrrolidone for applications in medicine. *Biomaterials* **22**, 1971-1985 (2001).
- 209 Akita, S. *et al.* A polyurethane dressing is beneficial for split-thickness skin-graft donor wound healing. *Burns* **32**, 447-451 (2006).
- 210 Cho, H. K. & Noh, S. T. Swelling behavior of polyurethane hydrogels based on poly(ethylene oxide) glycol (PEG) or poly(ethylene oxide-co-propylene oxide) glycol (PEPG). *J Ind Eng Chem* **6**, 19-24 (2000).
- 211 Kazmierska, K. A., Kuc, K. & Ciach, T. Polyvinylpyrrolidone-Polyurethane Interpolymer Hydrogel Coating as a Local Drug Delivery System. *Acta Pol Pharm* **65**, 763-766 (2008).
- 212 Sano, K., Tokoro, T. & Imai, Y. A new drug delivery system utilizing piggyback contact lenses. *Acta Ophthalmologica Scandinavica* **74**, 243-248 (1996).
- 213 Ruszczak, Z. & Friess, W. Collagen as a carrier for on-site delivery of antibacterial drugs. *Adv Drug Deliver Rev* **55**, 1679-1698 (2003).
- 214 Ahmad, Z. & Khuller, G. K. Alginate-based sustained release drug delivery systems for tuberculosis. *Expert Opin Drug Del* **5**, 1323-1334 (2008).
- 215 Andrews, G. P., Laverty, T. P. & Jones, D. S. Mucoadhesive polymeric platforms for controlled drug delivery. *Eur J Pharm Biopharm* **71**, 505-518 (2009).
- 216 Ganji, F. & Vasheghani-Farahani, E. Hydrogels in Controlled Drug Delivery Systems. *Iranian Polymer Journal* **18**, 63-88 (2009).
- 217 Lapcik, L., Lapcik, L., De Smedt, S., Demeester, J. & Chabreck, P. Hyaluronan: Preparation, structure, properties, and applications. *Chem Rev* **98**, 2663-2684 (1998).
- 218 Burdick, J. A. & Prestwich, G. D. Hyaluronic Acid Hydrogels for Biomedical Applications. *Adv Mater* **23**, H41-H56 (2011).
- 219 Segura, T. *et al.* Crosslinked hyaluronic acid hydrogels: a strategy to functionalize and pattern. *Biomaterials* **26**, 359-371 (2005).

- 220 Gupta, D., Tator, C. H. & Shoichet, M. S. Fast-gelling injectable blend of hyaluronan and methylcellulose for intrathecal, localized delivery to the injured spinal cord. *Biomaterials* **27**, 2370-2379 (2006).
- 221 Li, L., Wang, Q. Q. & Xu, Y. R. Thermoreversible association and gelation of methylcellulose in aqueous solutions. *Nihon Reoroji Gakk* **31**, 287-296 (2003).
- 222 Xu, Y., Wang, C., Tam, K. C. & Li, L. Salt-assisted and salt-suppressed sol-gel transitions of methylcellulose in water. *Langmuir* **20**, 646-652 (2004).
- 223 Lin, Y. K., Matsumoto, Y., Kuroyanagi, Y. & Kagawa, S. A Bilayer Hyaluronic Acid Wound Dressing to Promote Wound Healing in Diabetic Ulcer. *J Bioact Compat Pol* **24**, 424-443 (2009).
- 224 Wang, Y., Lapitsky, Y., Kang, C. E. & Shoichet, M. S. Accelerated Release of a Sparingly Soluble Drug from a Hyaluronan-Methylcellulose Hydrogel. *J Control Release* **140**, 218-223 (2009).
- 225 Vulic, K. & Shoichet, M. S. Tunable growth factor delivery from injectable hydrogels for tissue engineering. *Journal of American Chemical Society*, doi:doi: 10.1021/ja210638x (2011).
- 226 Taluja, A., Youn, Y. S. & Bae, Y. H. Novel approaches in microparticulate PLGA delivery systems encapsulating proteins. *J Mater Chem* **17**, 4002-4014 (2007).
- 227 Soppimath, K. S., Aminabhavi, T. M., Kulkarni, A. R. & Rudzinski, W. E. Biodegradable polymeric nanoparticles as drug delivery devices. *J Control Release* **70**, 1-20 (2001).
- 228 Bai, X. L., Yang, Y. Y., Chung, T. S., Ng, S. & Heller, J. Effect of polymer composites on the fabrication of poly(ortho-ester) microspheres for controlled release of protein (vol 80, pg 1630, 2001). *J Appl Polym Sci* **81**, 3083-3083 (2001).
- 229 Gopferich, A. & Tessmar, J. Polyanhydride degradation and erosion. *Adv Drug Deliver Rev* **54**, 911-931 (2002).
- 230 Cohen-Sela, E. *et al.* Single and Double Emulsion Manufacturing Techniques of an Amphiphilic Drug in PLGA Nanoparticles: Formulations of Mithramycin and Bioactivity. *J Pharm Sci-U.S.* **98**, 1452-1462 (2009).
- 231 Heller, J., Barr, J., Ng, S. Y., Abdellauoi, K. S. & Gurny, R. Poly(ortho esters): synthesis, characterization, properties and uses. *Adv Drug Deliver Rev* **54**, 1015-1039 (2002).

- 232 Grimsley, G. R. *et al.* Increasing protein stability by altering long-range coulombic interactions. *Protein Sci* **8**, 1843-1849 (1999).
- 233 Pekarek, K. J., Jacob, J. S. & Mathiowitz, E. Double-Walled Polymer Microspheres for Controlled Drug-Release. *Nature* **367**, 258-260 (1994).
- 234 Pekarek, K. J., Jacob, J. S. & Mathiowitz, E. One-Step Preparation of Double-Walled Microspheres. *Adv Mater* **6**, 684-687 (1994).
- 235 Mumper, R. J. & Jay, M. Biodegradable Radiotherapeutic Polyester Microspheres - Optimization and Invitro Invivo Evaluation. *J Control Release* **18**, 193-204 (1992).
- 236 Kim, H. K. & Park, T. G. Microencapsulation of human growth hormone within biodegradable polyester microspheres: Protein aggregation stability and incomplete release mechanism. *Biotechnol Bioeng* **65**, 659-667 (1999).
- 237 Li, Z. H. & Huang, L. Sustained delivery and expression of plasmid DNA based on biodegradable polyester, poly(D,L-lactide-co-4-hydroxy-L-proline). *J Control Release* **98**, 437-446 (2004).
- 238 Chun, K. W., Yoo, H. S., Yoon, J. J. & Park, T. G. Biodegradable PLGA microcarriers for injectable delivery of chondrocytes: Effect of surface modification on cell attachment and function. *Biotechnol Progr* **20**, 1797-1801 (2004).
- 239 Langer, R. New Methods of Drug Delivery. *Science* **249**, 1527-1533 (1990).
- 240 Mundargi, R. C., Babu, V. R., Rangaswamy, V., Patel, P. & Aminabhavi, T. M. Nano/micro technologies for delivering macromolecular therapeutics using poly(D,L-lactide-co-glycolide) and its derivatives. *J Control Release* **125**, 193-209 (2008).
- 241 Pollauf, E. J., Kim, K. K. & Pack, D. W. Small-molecule release from poly(D,L-lactide)/poly(D,L-lactide-co-glycolide) composite microparticles. *J Pharm Sci-US* **94**, 2013-2022 (2005).
- 242 Morlock, M., Koll, H., Winter, G. & Kissel, T. Microencapsulation of rh-erythropoietin, using biodegradable poly(D,L-lactide-co-glycolide): Protein stability and the effects of stabilizing excipients. *Eur J Pharm Biopharm* **43**, 29-36 (1997).
- 243 Song, X. R. *et al.* Dual agents loaded PLGA nanoparticles: Systematic study of particle size and drug entrapment efficiency. *Eur J Pharm Biopharm* **69**, 445-453 (2008).

- 244 Kim, T. H., Lee, H. & Park, T. G. Pegylated recombinant human epidermal growth factor (rhEGF) for sustained release from biodegradable PLGA microspheres. *Biomaterials* **23**, 2311-2317 (2002).
- 245 Wischke, C. & Schwendeman, S. P. Principles of encapsulating hydrophobic drugs in PLA/PLGA microparticles. *Int J Pharm* **364**, 298-327 (2008).
- 246 Kang F., S. J. Effect of additives on the release of a model protein from PLGA microspheres. *AAPS PharmSciTech* **2**, 30 (2001).
- 247 Cohen-Sela, E., Chorny, M., Koroukhov, N., Danenberg, H. D. & Golomb, G. A new double emulsion solvent diffusion technique for encapsulating hydrophilic molecules in PLGA nanoparticles. *J Control Release* **133**, 90-95 (2009).
- 248 Morita, T., Sakamura, Y., Horikiri, Y., Suzuki, T. & Yoshino, H. Protein encapsulation into biodegradable microspheres by a novel S/O/W emulsion method using poly(ethylene glycol) as a protein micronization adjuvant. *J Control Release* **69**, 435-444 (2000).
- 249 Perez, C. & Griebenow, K. Effect of salts on lysozyme stability at the water-oil interface and upon encapsulation in poly(lactic-co-glycolic) acid microspheres. *Biotechnol Bioeng* **82**, 825-832 (2003).
- 250 Wang, Y. F. *et al.* Transport of epidermal growth factor in the stroke-injured brain. *J Control Release* **149**, 225-235 (2011).
- 251 Cooke, M. J., Wang, Y. F., Morshead, C. M. & Shoichet, M. S. Controlled epi-cortical delivery of epidermal growth factor for the stimulation of endogenous neural stem cell proliferation in stroke-injured brain. *Biomaterials* **32**, 5688-5697 (2011).
- 252 Wang, Y., Cooke, M. J., Morshead, C. M. & Shoichet, M. S. Hydrogel delivery of erythropoietin to the brain for endogenous stem cell stimulation after stroke injury. *Biomaterials* **33**, 2681-2692 (2011).
- 253 McMurry, J. *Fundamentals of Organic Chemistry*. 5 edn, (Thomson Brooks/Cole, 2003).
- 254 Panchuk-Voloshina, N. *et al.* Alexa dyes, a series of new fluorescent dyes that yield exceptionally bright, photostable conjugates. *Journal of Histochemistry & Cytochemistry* **47**, 1179-1188 (1999).
- 255 Invitrogen, M. P. Amine-reactive Probes. (2009).

- 256 Tennant, K. A. & Jones, T. A. Sensorimotor behavioral effects of endothelin-1 induced small cortical infarcts in C57BL/6 mice. *J Neurosci Meth* **181**, 18-26 (2009).
- 257 Stroh, M. *et al.* Multiphoton microscopy guides neurotrophin modification with poly(ethylene glycol) to enhance interstitial diffusion. *Nat Mater* **3**, 489-494 (2004).
- 258 Franklin KBJ, P. G. *The mouse brain in stereotaxic coordinates*. 1 edn, (Academic Press, 1996).
- 259 Liu, B., Chen, H. Y., Johns, T. G. & Neufeld, A. H. Epidermal growth factor receptor activation: An upstream signal for transition of quiescent astrocytes into reactive astrocytes after neural injury. *J Neurosci* **26**, 7532-7540 (2006).
- 260 Nicholson, C. Diffusion and related transport mechanisms in brain tissue. *Rep Prog Phys* **64**, 815-884 (2001).
- 261 Levitt, B. P. An Introduction to Error Analysis - the Study of Uncertainties in Physical Measurements - Taylor, Jr. *Journal of the Chemical Society-Faraday Transactions I* **79**, 2269-2269 (1983).
- 262 Hammoud, L., Burger, D. E., Lu, X. R. & Feng, Q. P. Tissue inhibitor of metalloproteinase-3 inhibits neonatal mouse cardiomyocyte proliferation via EGFR/JNK/SP-1 signaling. *American Journal of Physiology-Cell Physiology* **296**, C735-C745 (2009).
- 263 Zar, H. H. *Biostatistical Analysis*. 3 edn, (Prentice-Hall, 1996).
- 264 Fee, C. J. & Van Alstine, J. A. PEG-proteins: Reaction engineering and separation issues. *Chem Eng Sci* **61**, 924-939 (2006).
- 265 Caliceti, P. & Veronese, F. M. Pharmacokinetic and biodistribution properties of poly(ethylene glycol)-protein conjugates. *Adv Drug Deliver Rev* **55**, 1261-1277 (2003).
- 266 Carpenter, G., Lembach, K. J., Morrison, M. M. & Cohen, S. Characterization of Binding of I-125-Labeled Epidermal Growth-Factor to Human Fibroblasts. *J Biol Chem* **250**, 4297-4304 (1975).
- 267 Murphy, T. H. & Corbett, D. Plasticity during stroke recovery: from synapse to behaviour. *Nature Reviews Neuroscience* **10**, 861-872 (2009).

- 268 Windle, V. *et al.* An analysis of four different methods of producing focal cerebral ischemia with endothelin-1 in the rat. *Experimental Neurology* **201**, 324-334 (2006).
- 269 Pasut, G. & Veronese, F. M. PEGylation of proteins as tailored chemistry for optimized bioconjugates. *Adv Polym Sci* **192**, 95-134 (2006).
- 270 Tropepe, V. *et al.* Distinct neural stem cells proliferate in response to EGF and FGF in the developing mouse telencephalon. *Dev Biol* **208**, 166-188 (1999).
- 271 Buga, A. M. *et al.* The genomic response of the ipsilateral and contralateral cortex to stroke in aged rats. *J Cell Mol Med* **12**, 2731-2753 (2008).
- 272 Comi, A. M., Johnston, M. V. & Wilson, M. A. Strain variability, injury distribution, and seizure onset in a mouse model of stroke in the immature brain. *Dev Neurosci-Basel* **27**, 127-133 (2005).
- 273 Futrell, N. Pathophysiology of acute ischemic stroke: New concepts in cerebral embolism. *Cerebrovasc Dis* **8**, 2-5 (1998).
- 274 Fee, C. J. Size comparison between proteins PEGylated with branched and linear Poly(Ethylene glycol) molecules. *Biotechnol Bioeng* **98**, 725-731 (2007).
- 275 Kubetzko, S., Sarkar, C. A. & Pluckthun, A. Protein PEGylation decreases observed target association rates via a dual blocking mechanism. *Mol Pharmacol* **68**, 1439-1454 (2005).
- 276 Hellen, E. & Axelrod, D. Dissociation Rate-Constant of Epidermal Growth-Factor Specifically Bound to Its Receptor Measured with Prismless Tir/Fpr. *Biophys J* **57**, A293-a293 (1990).
- 277 Waters, C. M., Oberg, K. C., Carpenter, G. & Overholser, K. A. Rate Constants for Binding, Dissociation, and Internalization of Egf - Effect of Receptor Occupancy and Ligand Concentration. *Biochemistry* **29**, 3563-3569 (1990).
- 278 Wiley, H. S. Anomalous Binding of Epidermal Growth-Factor to a431 Cells Is Due to the Effect of High Receptor Densities and a Saturable Endocytic System. *Journal of Cell Biology* **107**, 801-810 (1988).
- 279 Knauer, D. J., Wiley, H. S. & Cunningham, D. D. Relationship between Epidermal Growth-Factor Receptor Occupancy and Mitogenic Response - Quantitative-Analysis Using a Steady-State Model System. *J Biol Chem* **259**, 5623-5631 (1984).

- 280 Myers, A. C., Kovach, J. S. & Vukpavlovic, S. Binding, Internalization, and Intracellular Processing of Protein Ligands - Derivation of Rate Constants by Computer Modeling. *J Biol Chem* **262**, 6494-6499 (1987).
- 281 Lloyd, C. E. & Ascoli, M. On the Mechanisms Involved in the Regulation of the Cell-Surface Receptors for Human Chorio-Gonadotropin and Mouse Epidermal Growth-Factor in Cultured Leydig Tumor-Cells. *Journal of Cell Biology* **96**, 521-526 (1983).
- 282 Planas, A. M., Justicia, C., Soriano, M. A. & Ferrer, I. Epidermal growth factor receptor in proliferating reactive glia following transient focal ischemia in the rat brain. *Glia* **23**, 120-129 (1998).
- 283 Soderquist, R. G. *et al.* PEGylation of brain-derived neurotrophic factor for preserved biological activity and enhanced spinal cord distribution. *J Biomed Mater Res A* **91A**, 719-729 (2009).
- 284 Belcheva, N., Woodrow-Mumford, K., Mahoney, M. J. & Saltzman, W. M. Synthesis and biological activity of polyethylene glycol-mouse nerve growth factor conjugate. *Bioconjugate Chem* **10**, 932-937 (1999).
- 285 Kang, C. E., Clarkson, R., Yeung, I., Tator, C. H. & Shoichet, M. S. Localized Delivery of Fibroblast Growth Factor 2 to the Injured Spinal Cord. *Journal of Neurotrauma* **26**, A61-a61 (2009).
- 286 Krewson, C. E. & Saltzman, W. M. Transport and elimination of recombinant human NGF during long-term delivery to the brain. *Brain Res* **727**, 169-181 (1996).
- 287 Correia, M. L. G., Morgan, D. A., Sivitz, W. I., Mark, A. L. & Haynes, W. G. Leptin acts in the central nervous system to produce dose-dependent changes in arterial pressure. *Hypertension* **37**, 936-942 (2001).
- 288 Jablonska B., G. M., Kublik A., Skangiel-Kramska J., Kossut M. Effects of implantation of Alzet 1007D osmotic minipumps upon 2-deoxyglucose uptake in the cerebral cortex of mice. *Acta neurobiologiae experimentalis* **53**, 577-580 (1993).
- 289 Bear, M. F., Kleinschmidt, A., Gu, Q. & Singer, W. Disruption of Experience-Dependent Synaptic Modifications in Striate Cortex by Infusion of an Nmda Receptor Antagonist. *J Neurosci* **10**, 909-925 (1990).
- 290 Paradiso, M. A., Bear, M. F. & Daniels, J. D. Effects of Intracortical Infusion of 6-Hydroxydopamine on the Response of Kitten Visual-Cortex to Monocular Deprivation. *Exp Brain Res* **51**, 413-422 (1983).

- 291 Nave, K. A., Probstmeier, R. & Schachner, M. Epidermal Growth-Factor Does Not Cross the Blood-Brain-Barrier. *Cell Tissue Res* **241**, 453-457 (1985).
- 292 Erlandsson A., L. A., Yu F., Morshead CM. . Immunosuppression promotes endogenous neural stem and progenitor cell migration and tissue regeneration after ischemic injury *Experimental Neurology*.
- 293 Ghosh, P., Salman, H. & Kernie, S. G. The subventricular zone is a source of neural stem cells that remodel the brain following traumatic brain injury. *Crit Care Med* **30**, A13-A13 (2002).
- 294 Riquelme, P. A., Drapeau, E. & Doetsch, F. Brain micro-ecologies: neural stem cell niches in the adult mammalian brain. *Philos T R Soc B* **363**, 123-137, doi:DOI 10.1098/rstb.2006.2016 (2008).
- 295 Jin, K. L. *et al.* Evidence for stroke-induced neurogenesis in the human brain. *P Natl Acad Sci USA* **103**, 13198-13202, doi:DOI 10.1073/pnas.0603512103 (2006).
- 296 Marti-Fabregas, J. *et al.* Proliferation in the human ipsilateral subventricular zone after ischemic stroke. *Neurology* **74**, 357-365 (2010).
- 297 Teramoto, T., Qu, J. H., Plumier, J. C. & Moskowitz, M. A. EGF amplifies the replacement of parvalbumin-expressing striatal interneurons after ischemia. *J Clin Invest* **111**, 1125-1132 (2003).
- 298 Kalluri, H. S. G. & Dempsey, R. J. Growth factors, stem cells, and stroke. *Neurosurg Focus* **24**, -, doi:Artn E13  
Doi 10.3171/Foc/2008/24/3-4/E13 (2008).
- 299 Sprigg, N. & Bath, P. M. W. Colony stimulating factors (blood growth factors) are promising but unproven for treating stroke. *Stroke* **38**, 1997-1998 (2007).
- 300 Kang, C. E., Tator, C. H. & Shoichet, M. S. Poly(ethylene glycol) modification enhances penetration of fibroblast growth factor 2 to injured spinal cord tissue from an intrathecal delivery system. *J Control Release* **144**, 25-31 (2010).
- 301 Franklin K.B.J., P. G. *The Jouse Brain in Stereotaic Coordinates*. 3 edn, (Academic Press, 2008).

- 302 Wang, Y., Cooke, MJ., Lapitsky, Y., Wylie, RG., Sachewsky, N., Corbett, D., Morshead, CM., Shoichet, MS. Transport of epidermal growth factor in the stroke injured brain. *J Control Release* (2010).
- 303 Wang, Y., Cooke, MJ., Lapitsky, Y., Wylie, RG., Sachewsky, N., Corbett, D., Morshead, CM., Shoichet, MS. Transport of Epidermal Growth Factor in the Stroke-injured Brain. *J Control Release* **In press** (2010).
- 304 Shashoua, V. E., Hesse, G. W. & Moore, B. W. Proteins of the Brain Extracellular Fluid - Evidence for Release of S-100 Protein. *J Neurochem* **42**, 1536-1541 (1984).
- 305 Lin, M. *et al.* Novel biodegradable blend matrices for controlled drug release. *J Pharm Sci-U.S.* **97**, 4240-4248, doi:Doi 10.1002/Jps.21297 (2008).
- 306 Bailon, P. & Berthold, W. Polyethylene glycol-conjugated pharmaceutical proteins. *Pharm Sci Technol To* **1**, 352-356 (1998).
- 307 Lo, E. H., Wang, X. Y. & Cuzner, M. L. Extracellular proteolysis in brain injury and inflammation: Role for plasminogen activators and matrix metalloproteinases. *J Neurosci Res* **69**, 1-9 (2002).
- 308 Iwata, A., Browne, K. D., Chen, X. H., Yuguchi, T. & Smith, D. H. Traumatic brain injury induces biphasic upregulation of ApoE and ApoJ protein in rats. *J Neurosci Res* **82**, 103-114, doi:Doi 10.1002/Jnr.20607 (2005).
- 309 Van den Heuvel, C. *et al.* Upregulation of amyloid precursor protein messenger RNA in response to traumatic brain injury: an ovine head impact model. *Experimental Neurology* **159**, 441-450 (1999).
- 310 Enwere E \*, S. T., Gregg C, Fujikawa H, Ohta H, Weiss S. Aging Results in Reduced Epidermal Growth Factor Receptor Signaling, Diminished Olfactory Neurogenesis, and Deficits in Fine Olfactory Discrimination. *J Neurosci* **24**, 8354-8365, doi:doi:10.1523/JNEUROSCI.2751-04.2004 (2004).
- 311 Bouab M., P. G., Aumont A., Forest-Bérard K., Fernandes KJ. Aging of the subventricular zone neural stem cell niche: evidence for quiescence-associated changes between early and mid-adulthood. *J Neurosci*, doi:10.1016/j.neuroscience.2010.11.032 (2010).
- 312 Hawryluk, G. W. J., Rowland, J., Kwon, B. K. & Fehlings, M. G. Protection and repair of the injured spinal cord: a review of completed, ongoing, and planned clinical trials for acute spinal cord injury. *Neurosurg Focus* **25**, -, doi:Artn E14

Doi 10.3171/Foc.2008.25.11.E14 (2008).

- 313 Saltzman, W. M. Biomaterials for drug delivery to the brain. *Protein Eng* **10**, 78-78 (1997).
- 314 Saltzman, W. M., Mak, M. W., Mahoney, M. J., Duenas, E. T. & Cleland, J. L. Intracranial delivery of recombinant nerve growth factor: Release kinetics and protein distribution for three delivery systems. *Pharmaceut Res* **16**, 232-240 (1999).
- 315 Mahoney, M. J. & Saltzman, W. M. Millimeter-scale positioning of a nerve-growth-factor source and biological activity in the brain. *P Natl Acad Sci USA* **96**, 4536-4539 (1999).
- 316 Baumann, M. D. *et al.* An injectable drug delivery platform for sustained combination therapy. *J Control Release* **138**, 205-213, doi:DOI 10.1016/j.jconrel.2009.05.009 (2009).
- 317 Fricker-Gates, R. A. *et al.* EGF infusion stimulates the proliferation and migration of embryonic progenitor cells transplanted in the adult rat striatum. *Experimental Neurology* **165**, 237-247, doi:DOI 10.1006/exnr.2000.7482 (2000).
- 318 Novaes, L. C. D., Mazzola, P. G., Pessoa, A. & Penna, T. C. V. Effect of Polyethylene Glycol on the Thermal Stability of Green Fluorescent Protein. *Biotechnol Progr* **26**, 252-256, doi:Doi 10.1002/Btpr.296 (2010).
- 319 Felling, R. J. & Levison, S. W. Enhanced neurogenesis following stroke. *J Neurosci Res* **73**, 277-283 (2003).
- 320 Matsumoto, M. Neurogenesis and stem cell supply as therapeutic approach to overcome ischemic stroke. *Neurosci Res* **55**, S37-S37 (2006).
- 321 Warren, R. A., Green, F. A. & Enns, C. A. Saturation of the endocytic pathway for the transferrin receptor does not affect the endocytosis of the epidermal growth factor receptor. *J Biol Chem* **272**, 2116-2121 (1997).
- 322 Bakhshi, S. & North, R. B. Implantable pumps for drug delivery to the brain. *J Neuro-Oncol* **26**, 133-139 (1995).
- 323 Heiss, J. D., Walbridge, S., Asthagiri, A. R. & Lonser, R. R. Image-guided convection-enhanced delivery of muscimol to the primate brain Laboratory investigation. *J Neurosurg* **112**, 790-795 (2010).

- 324 Ooneda, G. Pathology of stroke. *Japanese circulation journal* **50**, 1224-1234 (1986).
- 325 Ceulemans, A. G. *et al.* The dual role of the neuroinflammatory response after ischemic stroke: modulatory effects of hypothermia. *J Neuroinflamm* **7** (2010).
- 326 Ekdahl, C. T., Claassen, J. H., Bonde, S., Kokaia, Z. & Lindvall, O. Inflammation is detrimental for neurogenesis in adult brain. *P Natl Acad Sci USA* **100**, 13632-13637 (2003).
- 327 Rogalewski, A., Schneider, A., Ringelstein, E. B. & Schabitz, W. R. Toward a multimodal neuroprotective treatment of stroke. *Stroke* **37**, 1129-1136, doi:10.1161/01.STR.0000209330.73175.34 (2006).
- 328 Lichtenwalner, R. J. & Parent, J. M. Adult neurogenesis and the ischemic forebrain. *J Cereb Blood Flow Metab* **26**, 1-20, doi:10.1038/sj.jcbfm.9600170 (2006).
- 329 Jin, K. *et al.* Evidence for stroke-induced neurogenesis in the human brain. *Proc Natl Acad Sci U S A* **103**, 13198-13202, doi:10.1073/pnas.0603512103 (2006).
- 330 Arvidsson, A., Collin, T., Kirik, D., Kokaia, Z. & Lindvall, O. Neuronal replacement from endogenous precursors in the adult brain after stroke. *Nat Med* **8**, 963-970 (2002).
- 331 Abrous, D. N., Koehl, M. & Le Moal, M. Adult neurogenesis: from precursors to network and physiology. *Physiological reviews* **85**, 523-569, doi:10.1152/physrev.00055.2003 (2005).
- 332 Shingo, T., Sorokan, S. T., Shimazaki, T. & Weiss, S. Erythropoietin regulates the in vitro and in vivo production of neuronal progenitors by mammalian forebrain neural stem cells. *J Neurosci* **21**, 9733-9743 (2001).
- 333 Jin, K. *et al.* Vascular endothelial growth factor (VEGF) stimulates neurogenesis in vitro and in vivo. *Proc Natl Acad Sci U S A* **99**, 11946-11950, doi:10.1073/pnas.182296499 (2002).
- 334 Yoshimura, S. *et al.* FGF-2 regulation of neurogenesis in adult hippocampus after brain injury. *P Natl Acad Sci USA* **98**, 5874-5879 (2001).
- 335 Robertson, M. J., Gip, P. & Schaffer, D. V. Neural stem cell engineering: directed differentiation of adult and embryonic stem cells into neurons. *Frontiers in bioscience: a journal and virtual library* **13**, 21-50 (2008).

- 336 Lo, E. H., Singhal, A. B., Torchilin, V. P. & Abbott, N. J. Drug delivery to damaged brain. *Brain research. Brain research reviews* **38**, 140-148 (2001).
- 337 Pardridge, W. M. The blood-brain barrier: bottleneck in brain drug development. *NeuroRx : the journal of the American Society for Experimental NeuroTherapeutics* **2**, 3-14, doi:10.1602/neurorx.2.1.3 (2005).
- 338 Stamatovic, S. M., Keep, R. F. & Andjelkovic, A. V. Brain endothelial cell-cell junctions: How to "Open" the blood brain barrier. *Curr Neuropharmacol* **6**, 179-192 (2008).
- 339 Pathan, S. A. *et al.* CNS drug delivery systems: novel approaches. *Recent patents on drug delivery & formulation* **3**, 71-89 (2009).
- 340 Cooke, M. J., Wang, Y., Morshead, C. M. & Shoichet, M. S. Controlled epi-cortical delivery of epidermal growth factor for the stimulation of endogenous neural stem cell proliferation in stroke-injured brain. *Biomaterials* **32**, 5688-5697 (2011).
- 341 Wang, Y., Cooke, M. J., Morshead, C. M. & Shoichet, M. S. Hydrogel delivery of erythropoietin to the brain for endogenous stem cell stimulation after stroke injury. *Biomaterials* **33**, 2681-2692, doi:10.1016/j.biomaterials.2011.12.031 (2012).
- 342 Wang, Y., Lapitsky, Y., Kang, C. E. & Shoichet, M. S. Accelerated release of a sparingly soluble drug from an injectable hyaluronan-methylcellulose hydrogel. *J Control Release* **140**, 218-223 (2009).
- 343 Hans, M. L. & Lowman, A. M. Biodegradable nanoparticles for drug delivery and targeting. *Curr Opin Solid St M* **6**, 319-327 (2002).
- 344 Craig, C. G. *et al.* In vivo growth factor expansion of endogenous subependymal neural precursor cell populations in the adult mouse brain. *J Neurosci* **16**, 2649-2658 (1996).
- 345 Wang, Q., Tang, X. N. & Yenari, M. A. The inflammatory response in stroke. *J Neuroimmunol* **184**, 53-68 (2007).
- 346 Cheng, Y. D., Al-Khoury, L. & Zivin, J. A. Neuroprotection for ischemic stroke: two decades of success and failure. *NeuroRx : the journal of the American Society for Experimental NeuroTherapeutics* **1**, 36-45, doi:10.1602/neurorx.1.1.36 (2004).
- 347 Lee, K., Silva, E. A. & Mooney, D. J. Growth factor delivery-based tissue engineering: general approaches and a review of recent developments. *Journal of the Royal Society, Interface / the Royal Society* **8**, 153-170, doi:10.1098/rsif.2010.0223 (2011).

- 348 Logan, A., Ahmed, Z., Baird, A., Gonzalez, A. M. & Berry, M. Neurotrophic factor synergy is required for neuronal survival and disinhibited axon regeneration after CNS injury. *Brain* **129**, 490-502 (2006).
- 349 Lin, C. C. & Metters, A. T. Hydrogels in controlled release formulations: Network design and mathematical modeling. *Adv Drug Deliver Rev* **58**, 1379-1408 (2006).
- 350 Pillai, O. & Panchagnula, R. Polymers in drug delivery. *Curr Opin Chem Biol* **5**, 447-451 (2001).
- 351 Ung, K. & Arenkiel, B. R. Fiber-optic implantation for chronic optogenetic stimulation of brain tissue. *Journal of visualized experiments : JoVE*, e50004, doi:10.3791/50004 (2012).
- 352 Johanson, C. E. *et al.* Multiplicity of cerebrospinal fluid functions: New challenges in health and disease. *Cerebrospinal fluid research* **5**, 10, doi:10.1186/1743-8454-5-10 (2008).
- 353 Perrin, C., Knauf, C. & Burcelin, R. Intracerebroventricular infusion of glucose, insulin, and the adenosine monophosphate-activated kinase activator, 5-aminoimidazole-4-carboxamide-1-beta-D-ribofuranoside, controls muscle glycogen synthesis. *Endocrinology* **145**, 4025-4033, doi:10.1210/en.2004-0270 (2004).
- 354 Nakagomi, T. *et al.* Isolation and characterization of neural stem/progenitor cells from post-stroke cerebral cortex in mice. *The European journal of neuroscience* **29**, 1842-1852, doi:10.1111/j.1460-9568.2009.06732.x (2009).
- 355 Austin, J. W. *et al.* The effects of intrathecal injection of a hyaluronan-based hydrogel on inflammation, scarring and neurobehavioural outcomes in a rat model of severe spinal cord injury associated with arachnoiditis. *Biomaterials* (2012).
- 356 Patel, A. R., Ritzel, R., McCullough, L. D. & Liu, F. Microglia and ischemic stroke: a double-edged sword. *International Journal of Physiology and Pathophysiological Pharmacology* **5**, 73 - 90 (2013).
- 357 Biran, R., Martin, D. C. & Tresco, P. A. Neuronal cell loss accompanies the brain tissue response to chronically implanted silicon microelectrode arrays. *Exp Neurol* **195**, 115-126, doi:10.1016/j.expneurol.2005.04.020 (2005).
- 358 Jaquins-Gerstl, A. & Michael, A. C. Comparison of the brain penetration injury associated with microdialysis and voltammetry. *J Neurosci Methods* **183**, 127-135, doi:10.1016/j.jneumeth.2009.06.023 (2009).

- 359 MacKenzie-Graham, A. *et al.* The informatics of a C57BL/6J mouse brain atlas. *Neuroinformatics* **1**, 397-410, doi:10.1385/NI:1:4:397 (2003).
- 360 Toh, M. Y., Falk, R. B. & Main, J. S. Interactive brain atlas with the Visible Human Project data: development methods and techniques. *Radiographics: a review publication of the Radiological Society of North America, Inc* **16**, 1201-1206 (1996).
- 361 Fishburn, C. S. The pharmacology of PEGylation: balancing PD with PK to generate novel therapeutics. *J Pharm Sci* **97**, 4167-4183, doi:10.1002/jps.21278 (2008).
- 362 Veronese, F. M., Caliceti, P. & Schiavon, O. Branched and linear poly(ethylene glycol): Influence of the polymer structure on enzymological, pharmacokinetic, and immunological properties of protein conjugates. *J Bioact Compat Pol* **12**, 196-207 (1997).
- 363 Takagi, F., Koga, N. & Takada, S. How protein thermodynamics and folding mechanisms are altered by the chaperonin cage: Molecular simulations. *P Natl Acad Sci USA* **100**, 11367-11372 (2003).
- 364 Foit, L. *et al.* Optimizing Protein Stability In Vivo. *Mol Cell* **36**, 861-871 (2009).
- 365 Sugaya, K., Alvarez, A., Marutle, A., Kwak, Y. D. & Choumkina, E. Stem cell strategies for Alzheimer's disease therapy. *Panminerva Med* **48**, 87-96 (2006).
- 366 Okano, H., Okada, S., Nakamura, M. & Toyama, Y. Neural stem cells and regeneration of injured spinal cord. *Kidney Int* **68**, 1927-1931 (2005).
- 367 Hol, E. Neurogenic Astrocytes in the Human Subventricular Zone in Health and Disease. *Glia* **59**, S26-S27 (2011).
- 368 Vora, P. *et al.* Differential effects of growth factors on oligodendrocyte progenitor migration. *European Journal of Cell Biology* **90**, 649-656 (2011).
- 369 Viehover, A., Miller, R. H., Park, S., Fischbach, G. & Vartanian, T. Neuregulin: An Oligodendrocyte Growth Factor Absent in Active Multiple Sclerosis Lesions. *Developmental Neuroscience* **23**, 377-386 (2001).
- 370 Riboni, L., Viani, P., Bassi, R., Giussani, P. & Tettamanti, G. Basic Fibroblast Growth Factor-induced Proliferation of Primary Astrocytes. *J Biol Chem* **276**, 12797-12804 (2001).

- 371 Wang, Z. & Ho, P. C. A nanocapsular combinatorial sequential drug delivery system for antiangiogenesis and anticancer activities. *Biomaterials* **31**, 7115-7123 (2010).
- 372 Bangham, J. Drug delivery - A tiny timely vehicle. *Nat Rev Cancer* **5**, 670-671 (2005).
- 373 Alavijeh, M. S. & Palmer, A. M. The pivotal role of drug metabolism and pharmacokinetics in the discovery and development of new medicines. *Idrugs* **7**, 755-763 (2004).
- 374 Tengood, J. E., Ridenour, R., Brodsky, R., Russell, A. J. & Little, S. R. Sequential Delivery of Basic Fibroblast Growth Factor and Platelet-Derived Growth Factor for Angiogenesis. *Tissue Eng Pt A* **17**, 1181-1189 (2011).
- 375 Basmanav, F. B., Kose, G. T. & Hasirci, V. Sequential growth factor delivery from complexed microspheres for bone tissue engineering. *Biomaterials* **29**, 4195-4204, doi:10.1016/j.biomaterials.2008.07.017 (2008).
- 376 Hao, X. J. *et al.* Angiogenic effects of sequential release of VEGF-A(165) and PDGF-BB with alginate hydrogels after myocardial infarction. *Cardiovasc Res* **75**, 178-185 (2007).
- 377 Bartnik, B. L., Kendall, E. J. & Obenaus, A. Cortical devascularization: quantitative diffusion weighted magnetic resonance imaging and histological findings. *Brain Res* **915**, 133-142 (2001).
- 378 University of California, S. D. *The Brain Observatory*, <<http://thebrainobservatory.ucsd.edu/cortex-1>> (2005 - 2013).
- 379 Arifin, D. Y., Lee, K. Y. T., Wang, C. H. & Smith, K. A. Role of Convective Flow in Carmustine Delivery to a Brain Tumor. *Pharmaceut Res* **26**, 2289-2302 (2009).
- 380 Jahnchen, E. Stereoselectivity in Protein-Binding and Drug Distribution. *Pharm Int* **4**, 185-185 (1983).
- 381 Bobo, R. H. *et al.* Convection-Enhanced Delivery of Macromolecules in the Brain. *P Natl Acad Sci USA* **91**, 2076-2080 (1994).
- 382 Sykova, E. & Nicholson, C. Diffusion in brain extracellular space. *Physiological reviews* **88**, 1277-1340 (2008).

- 383 Wang, Y., Luo, W. & Reiser, G. Trypsin and trypsin-like proteases in the brain: proteolysis and cellular functions. *Cell Molecular Life Science* **65**, 237-252 (2008).
- 384 Meulemans, A. A Model of Cefoperazone Tissue Penetration - Diffusion-Coefficient and Protein-Binding. *Antimicrob Agents Ch* **36**, 295-298 (1992).
- 385 Roberts, M. J. & Harris, J. M. Attachment of degradable poly(ethylene glycol) to proteins has the potential to increase therapeutic efficacy. *J Pharm Sci-U.S.* **87**, 1440-1445 (1998).
- 386 Alcantar, N. A., Aydil, E. S. & Israelachvili, J. N. Polyethylene glycol-coated biocompatible surfaces. *J Biomed Mater Res* **51**, 343-351 (2000).
- 387 Treethammathurot, B., Ovarlarnporn, C., Wungsintaweekul, J., Duncan, R. & Wiwattanapatapee, R. Effect of PEG molecular weight and linking chemistry on the biological activity and thermal stability of PEGylated trypsin. *Int J Pharm* **357**, 252-259 (2008).
- 388 Knauf, M. J. *et al.* Relationship of Effective Molecular-Size to Systemic Clearance in Rats of Recombinant Interleukin-2 Chemically Modified with Water-Soluble Polymers. *J Biol Chem* **263**, 15064-15070 (1988).
- 389 Lee, H., Jang, I. H., Ryu, S. H. & Park, T. G. N-terminal site-specific mono-PEGylation of epidermal growth factor. *Pharmaceut Res* **20**, 818-825 (2003).
- 390 Thorne, R. G., Lakkaraju, A., Rodriguez-Boulan, E. & Nicholson, C. In vivo diffusion of lactoferrin in brain extracellular space is regulated by interactions with heparan sulfate. *P Natl Acad Sci USA* **105**, 8416-8421 (2008).
- 391 Thorne, R. G. & Nicholson, C. In vivo diffusion analysis with quantum dots and dextrans predicts the width of brain extracellular space. *P Natl Acad Sci USA* **103**, 5567-5572 (2006).
- 392 Thorne, R. G., Hrabetova, S. & Nicholson, C. Diffusion measurements for drug design. *Nat Mater* **4**, 713-713 (2005).
- 393 Blanco, D. & Alonso, M. J. Protein encapsulation and release from poly(lactide-co-glycolide) microspheres: effect of the protein and polymer properties and of the co-encapsulation of surfactants. *Eur J Pharm Biopharm* **45**, 285-294 (1998).
- 394 Gaspar, M. M., Blanco, D., Cruz, M. E. M. & Alonso, M. J. Formulation of L-asparaginase-loaded poly(lactide-co-glycolide) nanoparticles: influence of polymer

- properties on enzyme loading, activity and in vitro release. *J Control Release* **52**, 53-62 (1998).
- 395 Fredenberg, S., Wahlgren, M., Reslow, M. & Axelsson, A. The mechanisms of drug release in poly(lactic-co-glycolic acid)-based drug delivery systems-A review. *Int J Pharm* **415**, 34-52 (2011).
- 396 Barat, A., Ruskin, H. J. & Crane, M. 3D multi-agent models for protein release from PLGA spherical particles with complex inner morphologies. *Theor Biosci* **127**, 95-105 (2008).
- 397 Jelvehgari, M., Valizadehl, H., Rezapour, M. & Nokhodchi, A. Control of encapsulation efficiency in polymeric microparticle system of tolmetin. *Pharm Dev Technol* **15**, 71-79 (2010).
- 398 Zhao, Y. L., Tian, F., Liu, C. J., Li, F. & Xing, N. Preparation and Evaluation of Poly(3-hydroxybutyrate) Microspheres Containing Bovine Serum Albumin for Controlled Release. *J Appl Polym Sci* **110**, 3826-3835 (2008).
- 399 Peng, D. M., Huang, K. L., Liu, Y. F. & Liu, S. Q. Preparation of novel polymeric microspheres for controlled release of finasteride. *Int J Pharm* **342**, 82-86 (2007).
- 400 Yeo, Y. & Park, K. N. Control of encapsulation efficiency and initial burst in polymeric microparticle systems. *Arch Pharm Res* **27**, 1-12 (2004).
- 401 Srinivasan, C., Katare, Y. K., Muthukumaran, T. & Panda, A. K. Effect of additives on encapsulation efficiency, stability and bioactivity of entrapped lysozyme from biodegradable polymer particles. *J Microencapsul* **22**, 127-138 (2005).
- 402 Mao, S. R. *et al.* Effect of WOW process parameters on morphology and burst release of FITC-dextran loaded PLGA microspheres. *Int J Pharm* **334**, 137-148 (2007).
- 403 Gopferich, A., Alonso, M. J. & Langer, R. Development and Characterization of Microencapsulated Microspheres. *Pharmaceut Res* **11**, 1568-1574 (1994).
- 404 Mochizuki, S. & Zydney, A. L. Effect of Protein Adsorption on the Transport Characteristics of Asymmetric Ultrafiltration Membranes. *Biotechnol Progr* **8**, 553-561 (1992).

- 405 Baumann, M. D., Kang, C. E., Tator, C. H. & Shoichet, M. S. Intrathecal delivery of a polymeric nanocomposite hydrogel after spinal cord injury. *Biomaterials* **31**, 7631-7639 (2010).
- 406 Ehrenreich, H. *et al.* Recombinant Human Erythropoietin in the Treatment of Acute Ischemic Stroke. *Stroke* **40**, E647-E656 (2009).
- 407 Langer, R. Polymer Implants for Drug Delivery in the Brain. *J Control Release* **16**, 53-59 (1991).
- 408 Brem, H. *et al.* Interstitial Chemotherapy with Drug Polymer Implants for the Treatment of Recurrent Gliomas. *J Neurosurg* **74**, 441-446 (1991).
- 409 Brem, H. *et al.* Placebo-Controlled Trial of Safety and Efficacy of Intraoperative Controlled Delivery by Biodegradable Polymers of Chemotherapy for Recurrent Gliomas. *Lancet* **345**, 1008-1012 (1995).
- 410 Popovic, N. & Brundin, P. Therapeutic potential of controlled drug delivery systems in neurodegenerative diseases. *Int J Pharm* **314**, 120-126 (2006).
- 411 Abematsu, M. *et al.* Neurons derived from transplanted neural stem cells restore disrupted neuronal circuitry in a mouse model of spinal cord injury. *J Clin Invest* **120**, 3255-3266 (2010).
- 412 Li, C. *et al.* Sox2 transcriptionally regulates PQBP1, an intellectual disability-microcephaly causative gene, in neural stem progenitor cells. *PLoS One* **8**, doi:doi: 10.1371/journal.pone.0068627 (2013).
- 413 Weber, R. *et al.* Early Prediction of Functional Recovery after Experimental Stroke: Functional Magnetic Resonance Imaging, Electrophysiology, and Behavioral Testing in Rats *J Neuroscience* **28**, 1022-1029 (2008).
- 414 Sanai, N. *et al.* Unique astrocyte ribbon in adult human brain contains neural stem cells but lacks chain migration. *Nature* **427**, 740-744 (2004).
- 415 Rhee, H. *et al.* Insulin concentration is critical in culturing human neural stem cells and neurons. *Cell Death and Disease* **2013**, e766 (2013).
- 416 Jakel, R., Schneider, B. & Svendsen, C. Using human neural stem cells to model neurological disease. *Nature Reviews* **5**, 136-144 (2004).

- 417 Brus, M., Keller, M. & Levy, F. Temporal features of adult neurogenesis: differences and similarities across mammalian species. *Frontiers in Neuroscience*, doi:doi: 10.3389/fnins.2013.00135 (2013).
- 418 Wong, A. J. *et al.* Increased Expression of the Epidermal Growth-Factor Receptor Gene in Malignant Gliomas Is Invariably Associated with Gene Amplification. *P Natl Acad Sci USA* **84**, 6899-6903 (1987).
- 419 Masui, H. *et al.* Growth-Inhibition of Human-Tumor Cells in Athymic Mice by Anti-Epidermal Growth-Factor Receptor Monoclonal-Antibodies. *Cancer Res* **44**, 1002-1007 (1984).
- 420 Laupacis, A., Keown, P. A., Ulan, R. A., Mckenzie, N. & Stiller, C. R. Cyclosporin-a - a Powerful Immunosuppressant. *Can Med Assoc J* **126**, 1041-1046 (1982).
- 421 Hunt, J., Cheng, A., Hoyles, A., Jervis, E. & Morshead, C. M. Cyclosporin A Has Direct Effects on Adult Neural Precursor Cells. *J Neurosci* **30**, 2888-2896 (2010).
- 422 Cramer, S. C. *et al.* The Beta-hCG plus Erythropoietin in Acute Stroke (BETAS) Study A 3-Center, Single-Dose, Open-Label, Noncontrolled, Phase IIa Safety Trial. *Stroke* **41**, 927-931 (2010).
- 423 Horie, N. *et al.* Mouse model of focal cerebral ischemia using endothelin-1. *J Neurosci Methods* **173**, 286 - 290 (2008).
- 424 Keefe, A. J. & Jiang, S. Y. Poly(zwitterionic)protein conjugates offer increased stability without sacrificing binding affinity or bioactivity. *Nat Chem* **4**, 60-64 (2012).
- 425 He, J. T. *et al.* Simultaneous elimination of T- and B-cell epitope by structure-based mutagenesis of single Glu80 residue within recombinant staphylokinase. *Acta Bioch Bioph Sin* **42**, 209-215 (2010).
- 426 Gao, T. J., Lindholm, T. S. & Kommonen, B. Composite delivery devices of bone morphogenetic proteins with osteoinduction and osteoconduction in the healing of large bone defect in sheep model. *Bone* **24**, 413-413 (1999).
- 427 Behr, B., Panetta, N. J., Longaker, M. T. & Quarto, N. Application of FGF-2 mimics bone healing potential of frontal bones in parietal calvarial defects by recruitment of dura mater cells. *J Am Coll Surgeons* **209**, S75-S75 (2009).

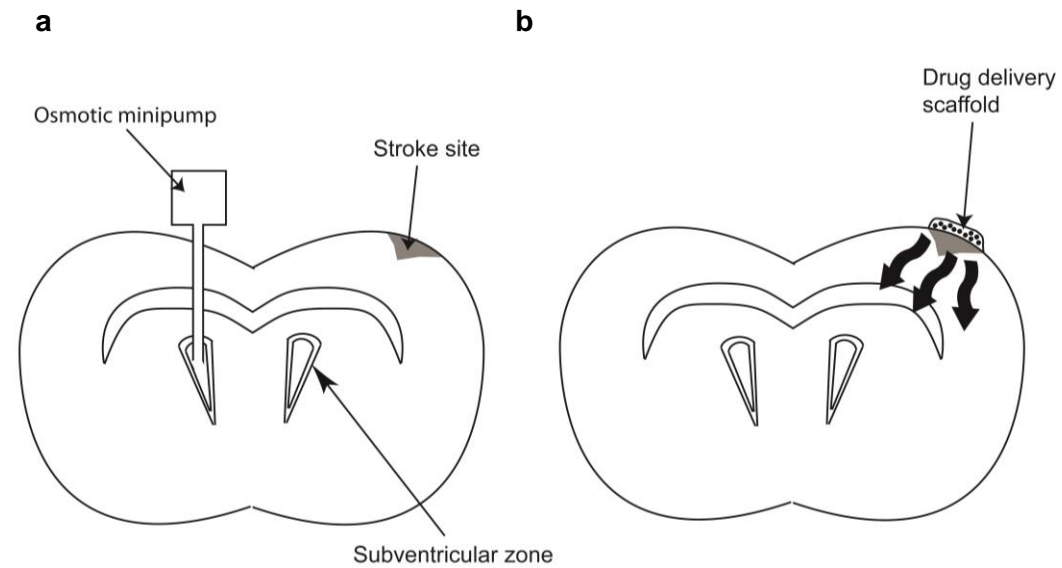
- 428 Gomez, G. *et al.* Effect of FGF and polylactide scaffolds on calvarial bone healing with growth factor on biodegradable polymer scaffolds. *J Craniofac Surg* **17**, 935-942 (2006).
- 429 Albrektsson, T. & Johansson, C. Osteoinduction, osteoconduction and osseointegration. *Eur Spine J* **10**, S96-S101 (2001).
- 430 Rainer, A. *et al.* Electrospun Hydroxyapatite-Functionalized PLLA Scaffold: Potential Applications in Sternal Bone Healing. *Ann Biomed Eng* **39**, 1882-1890 (2011).
- 431 Peterson, L. J., Larsen, P. E., Mcglumphy, E. A. & Walsh, E. C. Initial Bone Healing Response to Hydroxyapatite-Coated Implants. *J Dent Res* **74**, 169-169 (1995).
- 432 Zhang, L. *et al.* A test for detecting long-term sensorimotor dysfunction in the mouse after focal cerebral ischemia. *J Neurosci Meth* **117**, 207-214 (2002).
- 433 Li, X. L. *et al.* Chronic behavioral testing after focal ischemia in the mouse: functional recovery and the effects of gender. *Experimental Neurology* **187**, 94-104 (2004).

## Appendix A: Abbreviations

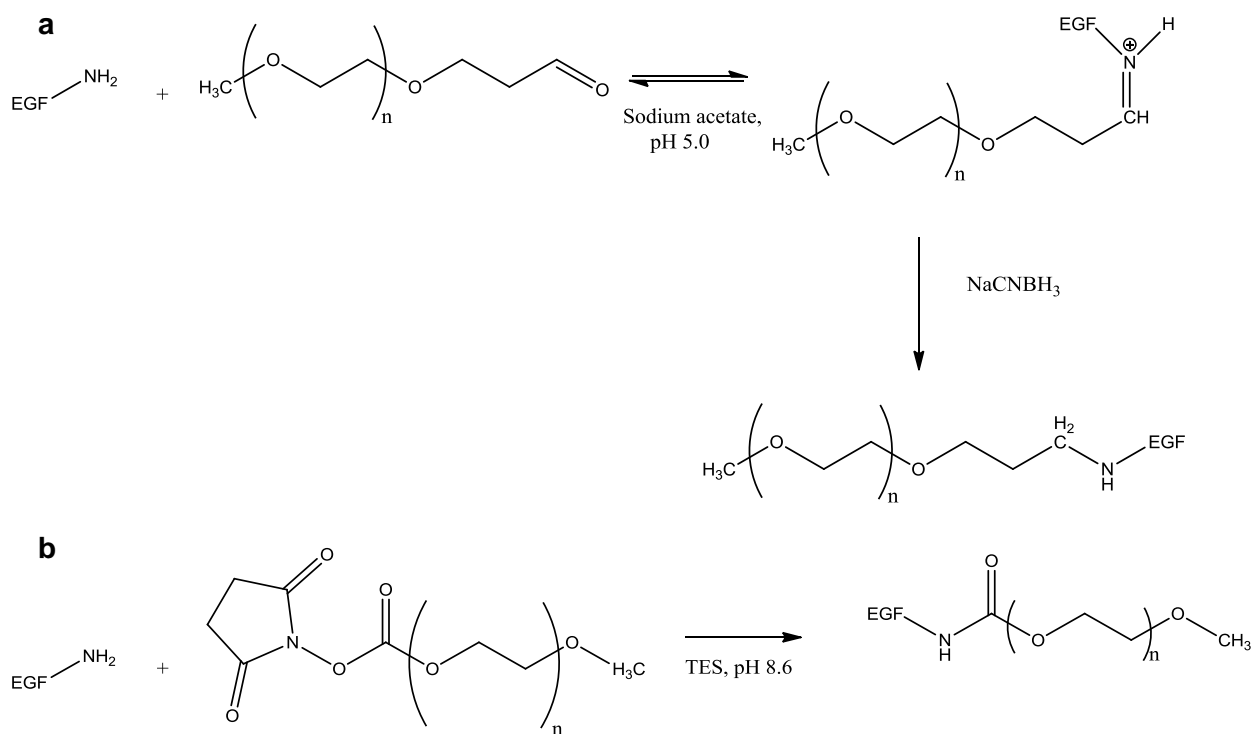
$\alpha$ :	Free space ratio in extracellular space
$\lambda$ :	Tissue tortuosity
aCSF:	Artificial cerebrospinal fluid
AMPA:	$\alpha$ -amino-3-hydroxyl-5-methyl-4-isoxazole-propionate
BBB:	Blood-brain-barrier
BSA:	Bovine serum albumin
CT:	Computed tomography
D:	Intrinsic diffusivity ( $\text{cm}^2/\text{s}$ )
$D^*$ :	Apparent diffusivity ( $\text{cm}^2/\text{s}$ )
DCX:	Double cortin
DDS:	Drug delivery system
DG:	Dentate gyrus
DMTMM	4-(4,6-Dimethoxy-1,3,5-triazin-2-yl)-4- methylmorpholinium
ECM:	Extracellular matrix
ECS	Extracellular space
EGF:	Epidermal growth factor
EGFR:	EGF receptor
ELISA:	Enzyme linked immunosorbant assay
EPO:	Erythropoietin
EPOR:	EPO receptor
ET-1:	Endothelin-1
GAG:	glycosaminoglycans
GFAP:	Glial fibrillary acidic protein

HAMC:	Hyaluronan methylcellulose
IC:	Intraberebral
ICV:	Intracerebroventricular
IOI:	Integrated optical imaging
$k_e$ :	Elimination coefficient ( $s^{-1}$ )
MCAo:	Middle cerebral artery occlusion
MRI:	Magnetic resonance imaging
MSC:	Mesenchymal stem cell
LDH:	Lactate dehydrogenase
NHS:	n-hydroxysuccinimide
NMDA:	N-methyl-D-aspartic acid
NSPC:	Neural stem/progenitor cell
PEG:	Poly(ethylene glycol)
PLGA:	Poly(lactic-co-glycolic acid)
POE:	Poly(ortho ester)
PPA:	Propionic acid
PSA:	Poly(sebacic acid)
PVA:	Poly(vinyl alcohol)
PVD:	Pial vessel disruption
ROS:	Reactive oxygen species
SGZ:	Subgranular zone
SVZ:	Subventricular zone
tPA:	Tissue plasminogen activator
TUNEL:	Terminal deoxynucleotidyl transferase dUTP nick end labeling

## Appendix B: Supplementary Figures

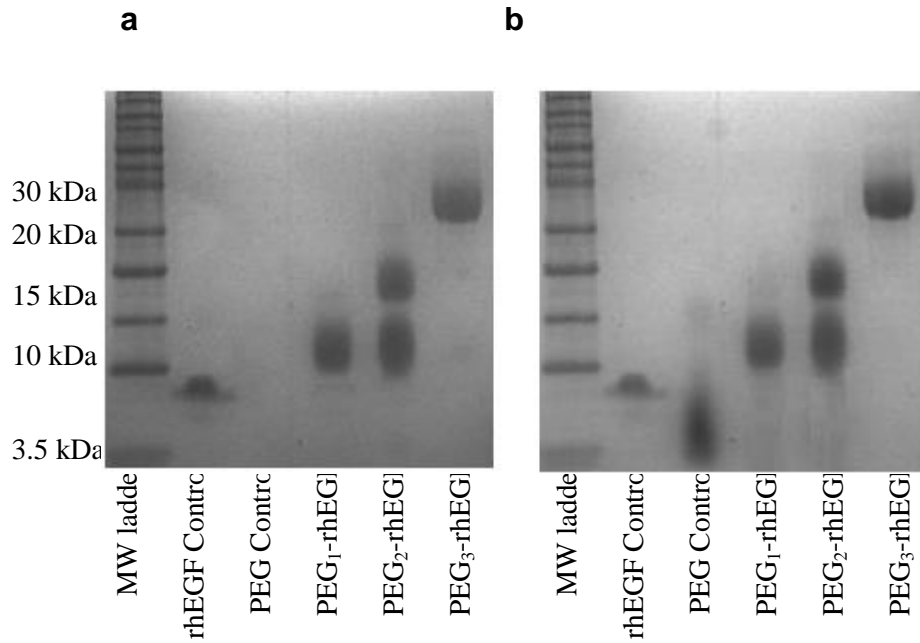


**Supplementary Figure S2.1 | Schematic comparing traditional invasive and novel drug delivery strategies.** (a) Osmotic minipump/catheter system for infusing drug solutions into the lateral ventricles of the brain. A catheter is directly inserted through the brain tissue into the ventricles, leading to a highly invasive strategy with the potential for infection. (b) A drug delivery scaffold positioned on top of the brain cortex is minimally-invasive and eliminates the need for highly invasive surgeries.

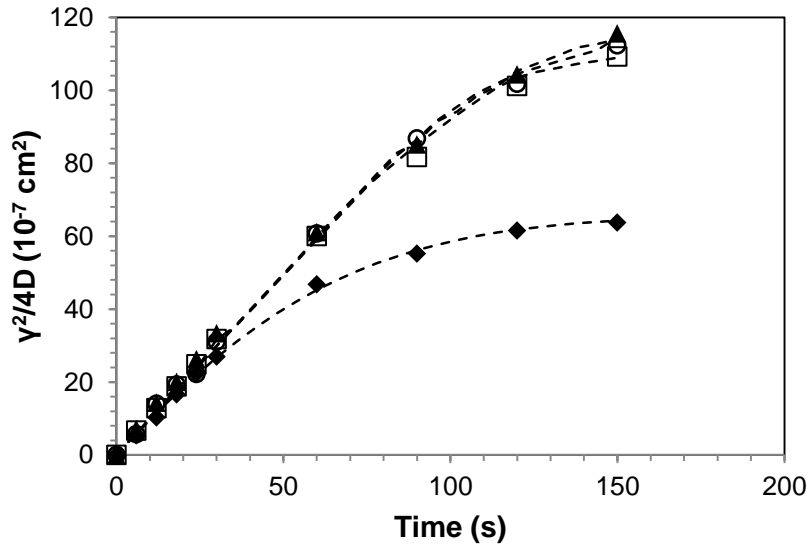


**Supplementary Figure S2.2 | Reaction schemes for conjugating rhEGF with methoxy-poly(ethylene glycol).** (a) Reaction scheme for synthesizing PEG<sub>1</sub>- and PEG<sub>2</sub>-rhEGF.

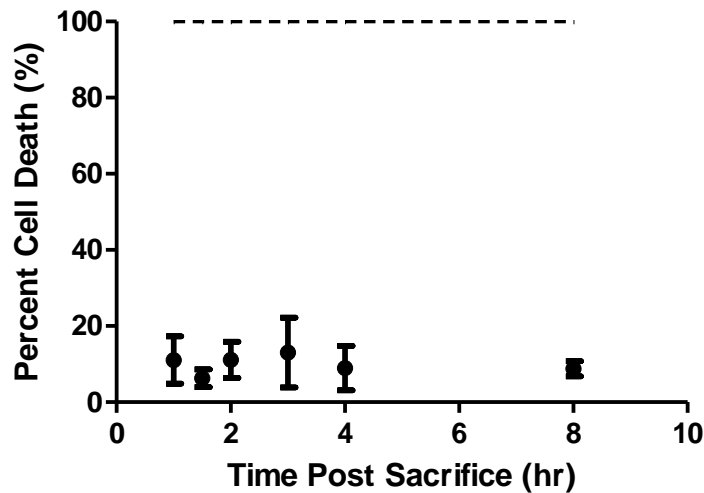
Reactions carried out at pH 5.0 in MES buffer, with 3 or 6 molar excess mPEG-PPA to produce PEG<sub>1</sub>- and PEG<sub>2</sub>-rhEGF, respectively. The reducing agent NaCNBH<sub>3</sub> was added at 140 molar excess to rhEGF. (b) Reaction scheme for synthesizing PEG<sub>3</sub>-rhEGF. Reaction was carried out at pH 8.6 in TES buffer, with 100 molar excess mPEG-NHS added batch-wise over four additions.



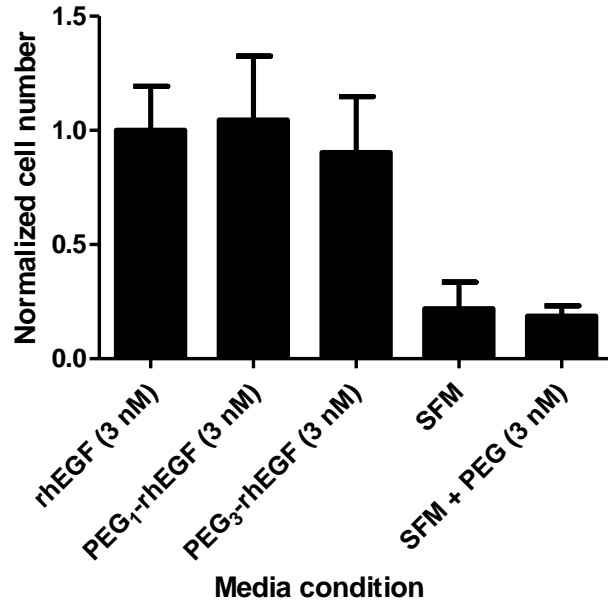
**Supplementary Figure S2.3 | Gel electrophoresis images of rhEGF and PEG<sub>x</sub>-rhEGF showing degrees of PEG modification.** Gels are sequentially stained with (a) Invitrogen Simply-Blue Safe Protein Stain and (b) a solution of BaCl<sub>2</sub>/KI/I<sub>(s)</sub> PEG stain. Both images (A) and (B) show a molecular weight ladder (lane 1), rhEGF (lane 2), 5 kDa PEG-propionaldehyde (lane 3), PEG<sub>1</sub>-rhEGF (lane 4), PEG<sub>2</sub>-rhEGF (lane 5), and PEG<sub>3</sub>-rhEGF (lane 6).



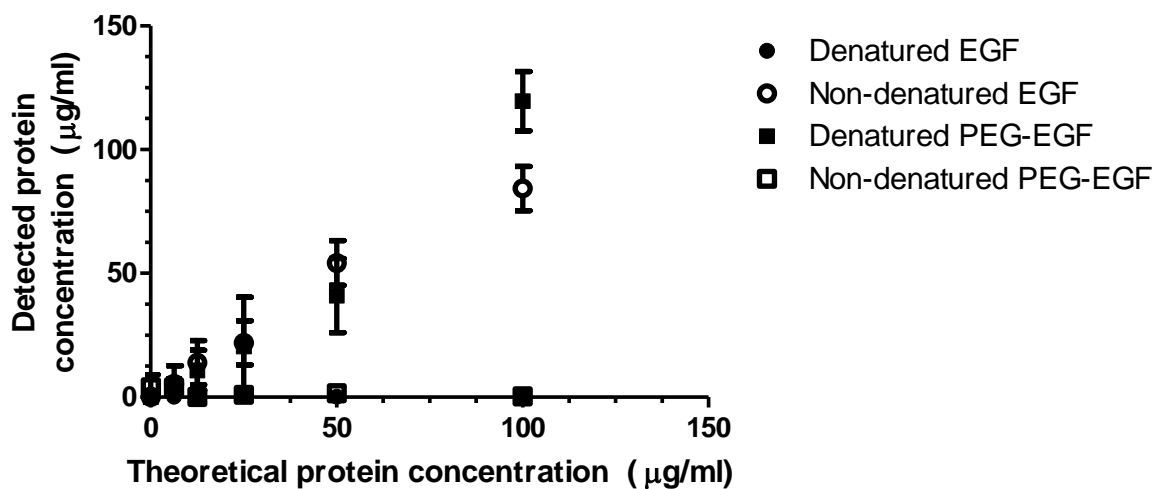
**Supplementary Figure S2.4 | Representative plot demonstrating accuracy in estimated values of  $k_e$ .** Data points represent the  $\gamma^2/4D$  vs. time plot obtained experimentally for ( $\blacklozenge$ ) rhEGF, ( $\circ$ ) PEG<sub>1</sub>-rhEGF, ( $\blacktriangle$ ) PEG<sub>2</sub>-rhEGF and ( $\square$ ) PEG<sub>3</sub>-rhEGF. Dashed lines represent model fittings generated from experimentally obtained values of  $D$  and  $\lambda$ , as well as values of  $k_e$  numerically obtained using MatLab. The model fittings correspond well to experimental data, indicating the goodness of fit and model accuracy.



**Supplementary Figure S2.5 | Cortical brain slices are viable 8 hours after animals are sacrificed.** The percent cell death over time ( $\bullet$ ) is determined using the LDH cytotoxicity assay and normalized to the maximum cell death possible obtained from homogenized tissue (dashed). Measurements at each time point are reported as mean  $\pm$  s.d. ( $n = 4$  brain slices).

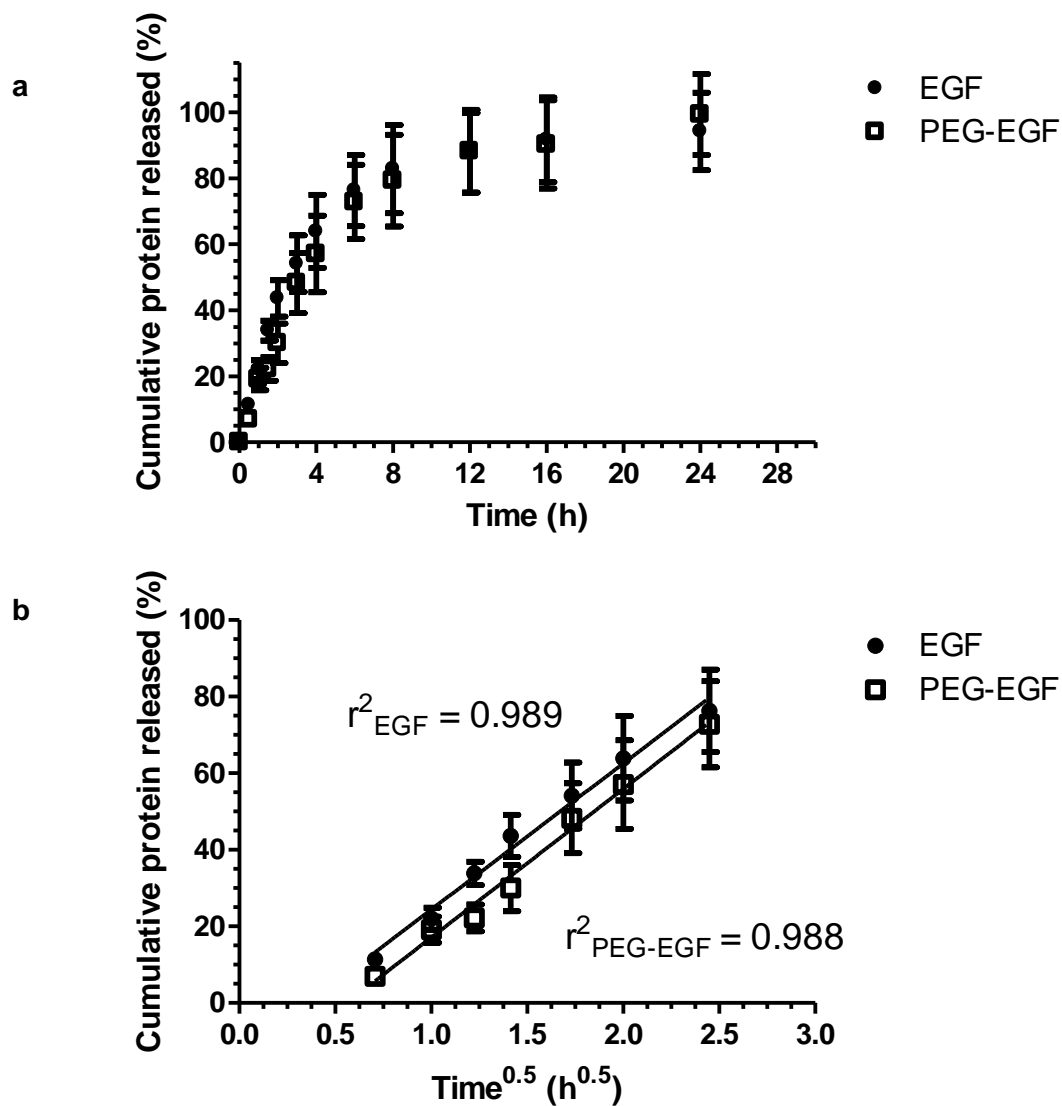


**Supplementary Figure S2.6 | PEG modification does not affect the in vitro bioactivity of rhEGF.** Neural stem cells (NSCs) are cultured for 1 week in serum free media (SFM), SFM with PEG, or SFM with rhEGF or PEG<sub>x</sub>-rhEGF. The number of NSCs in culture after 1 week is not significantly different between rhEGF, PEG<sub>1</sub>-rhEGF, and PEG<sub>3</sub>-rhEGF, while SFM lead to significantly smaller number of NSCs.



**Supplementary Figure S3.1 | Denatured EGF and PEG-EGF are not detectable by ELISA.**

Various concentrations of EGF and PEG-EGF are denatured by boiling in the presence of 2 mM  $\beta$ -mercaptoethanol. Denatured (●) EGF and (■) PEG-EGF were undetectable by ELISA whereas non-denatured (○) EGF and (□) PEG-EGF were accurately detected.

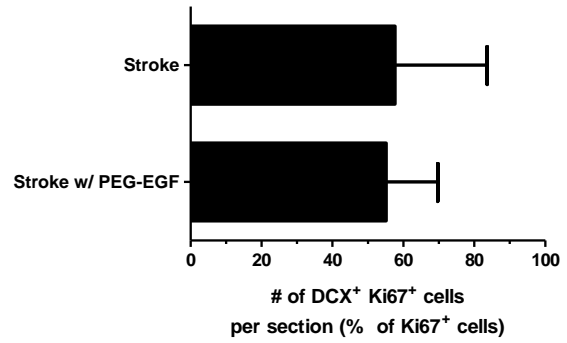


**Supplementary Figure S3.2 | Diffusion-controlled release of EGF and PEG-EGF from HAMC in vitro.** (a) HAMC serves as a vehicle to sustain the release of EGF and PEG-EGF over 24 hours in vitro. (b) The first 80% of release follows a linear relationship with respect to the square root of time for both EGF and PEG-EGF, indicating that release is diffusion-controlled. Between 0 and 30 min, the release is dependent both on diffusion and gel swelling.

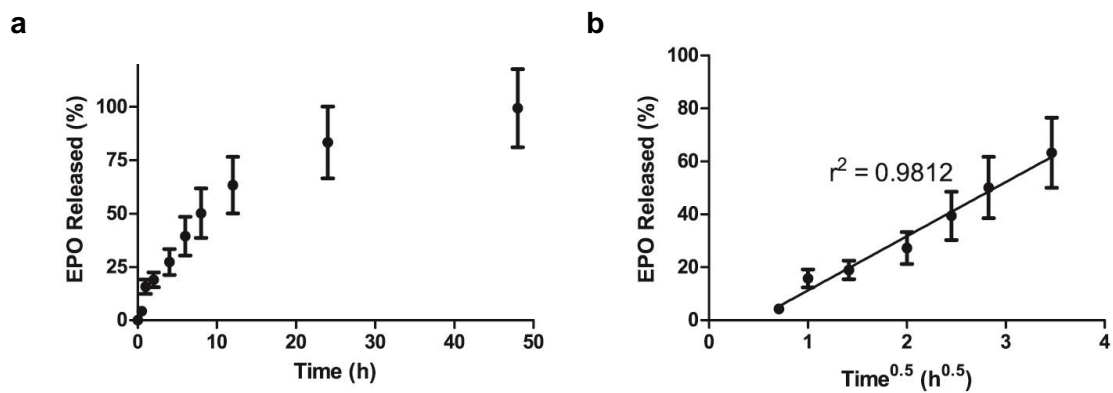
a



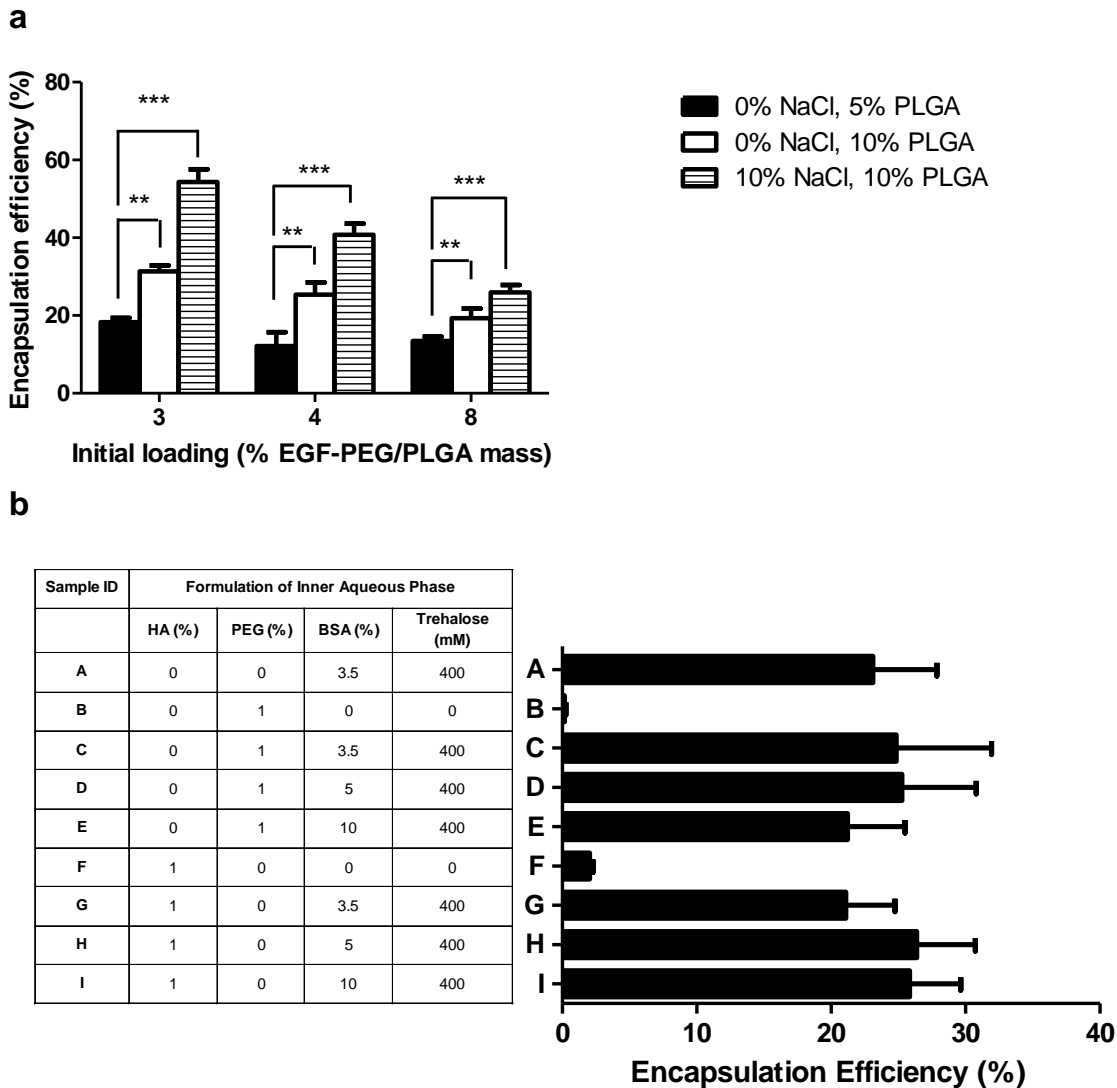
b



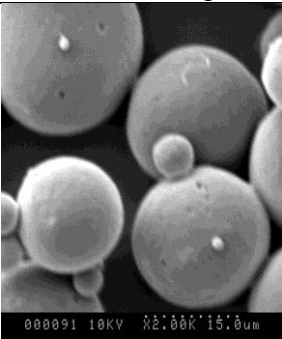
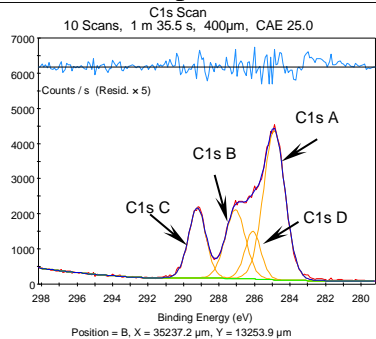
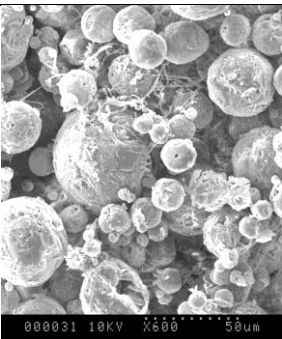
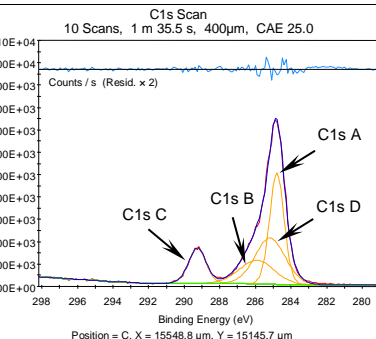
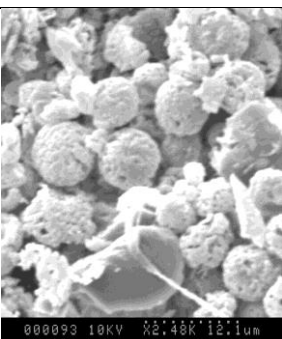
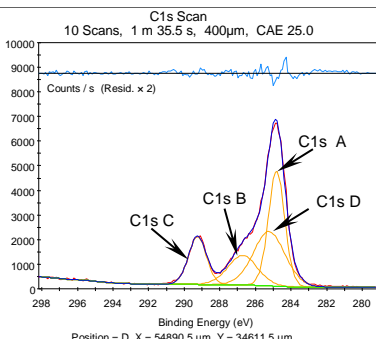
**Supplementary Figure 3.3S | Ki67 is a representative marker for neural precursor cells in the SVZ.** Brain tissue sections were stained with both Ki67 and either (a) nestin for neuroprecursors or (b) DCX for neuroblasts. Between stroke-injured and stroke/PEG-EGF treated groups, the number of cells positive for both markers as a percent of Ki67<sup>+</sup> only cells remain constant.



**Supplementary Figure S4.1 | In vitro release profile of EPO from HAMC.** (a) EPO is completely released from HAMC within 48 h. (b) Release of EPO from HAMC is diffusion controlled for the first 12 h, as the fractional protein released follows a linear relationship with  $t^{0.5}$ . Plotted are mean  $\pm$  standard deviation,  $n = 3$ .



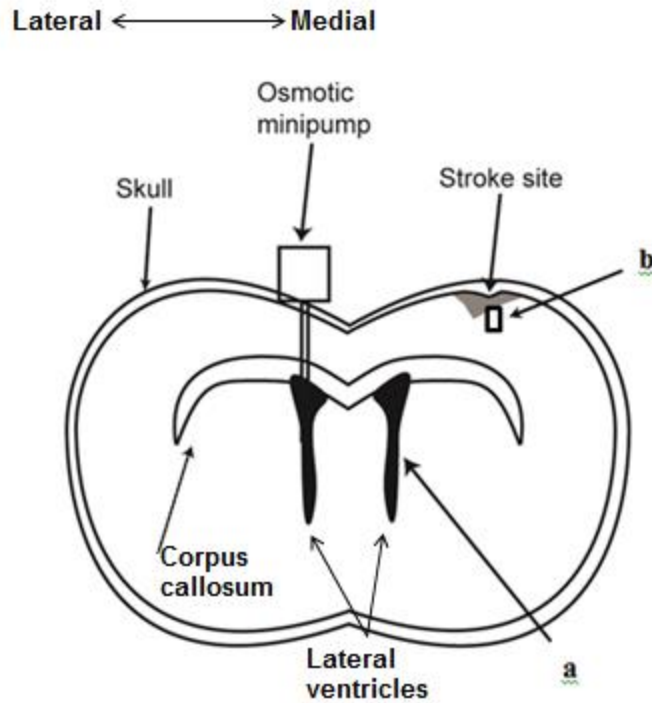
**Supplementary Figure S5.1 | Encapsulation efficiency of proteins in composite can be controlled by varying double emulsion process parameters.** (a) Encapsulation efficiency of EGF-PEG in PLGA nanoparticles were tuned using the concentration of PLGA in the organic phase and salt in the outer aqueous phase. Increasing the salt concentration and PLGA concentration increase the encapsulation efficiency. (\* $p < 0.05$ , \*\* $p < 0.01$ , \*\*\* $p < 0.001$ ) (b) Encapsulation efficiency of EPO in biphasic particles can be tuned by varying the formulation of the inner aqueous phase. BSA is a protein carrier required to achieve high encapsulation efficiency. Other factors have minimal impact on encapsulation efficiency. (Mean  $\pm$  standard deviation,  $n = 3$ ).

	Particle Image	XPS Spectrum	XPS Peak Analysis										
PLGA particle			<table border="1"> <thead> <tr> <th>Name</th> <th>Peak Area normalized to C1s D</th> </tr> </thead> <tbody> <tr> <td>C1s A</td> <td>8.31 ± 0.51</td> </tr> <tr> <td>C1s B</td> <td>3.165 ± 0.14</td> </tr> <tr> <td>C1s C</td> <td>2.70 ± 0.09</td> </tr> <tr> <td>C1s D</td> <td>1</td> </tr> </tbody> </table>	Name	Peak Area normalized to C1s D	C1s A	8.31 ± 0.51	C1s B	3.165 ± 0.14	C1s C	2.70 ± 0.09	C1s D	1
Name	Peak Area normalized to C1s D												
C1s A	8.31 ± 0.51												
C1s B	3.165 ± 0.14												
C1s C	2.70 ± 0.09												
C1s D	1												
PSA particle			<table border="1"> <thead> <tr> <th>Name</th> <th>Peak Area normalized to C1s D</th> </tr> </thead> <tbody> <tr> <td>C1s A</td> <td>1.14 ± 0.24</td> </tr> <tr> <td>C1s B</td> <td>0.59 ± 0.11</td> </tr> <tr> <td>C1s C</td> <td>0.44 ± 0.09</td> </tr> <tr> <td>C1s D</td> <td>1</td> </tr> </tbody> </table>	Name	Peak Area normalized to C1s D	C1s A	1.14 ± 0.24	C1s B	0.59 ± 0.11	C1s C	0.44 ± 0.09	C1s D	1
Name	Peak Area normalized to C1s D												
C1s A	1.14 ± 0.24												
C1s B	0.59 ± 0.11												
C1s C	0.44 ± 0.09												
C1s D	1												
Biphasic particles			<table border="1"> <thead> <tr> <th>Name</th> <th>Peak Area normalized to C1s D</th> </tr> </thead> <tbody> <tr> <td>C1s A</td> <td>1.08 ± 0.13</td> </tr> <tr> <td>C1s B</td> <td>0.51 ± 0.07</td> </tr> <tr> <td>C1s C</td> <td>0.50 ± 0.04</td> </tr> <tr> <td>C1s D</td> <td>1</td> </tr> </tbody> </table>	Name	Peak Area normalized to C1s D	C1s A	1.08 ± 0.13	C1s B	0.51 ± 0.07	C1s C	0.50 ± 0.04	C1s D	1
Name	Peak Area normalized to C1s D												
C1s A	1.08 ± 0.13												
C1s B	0.51 ± 0.07												
C1s C	0.50 ± 0.04												
C1s D	1												

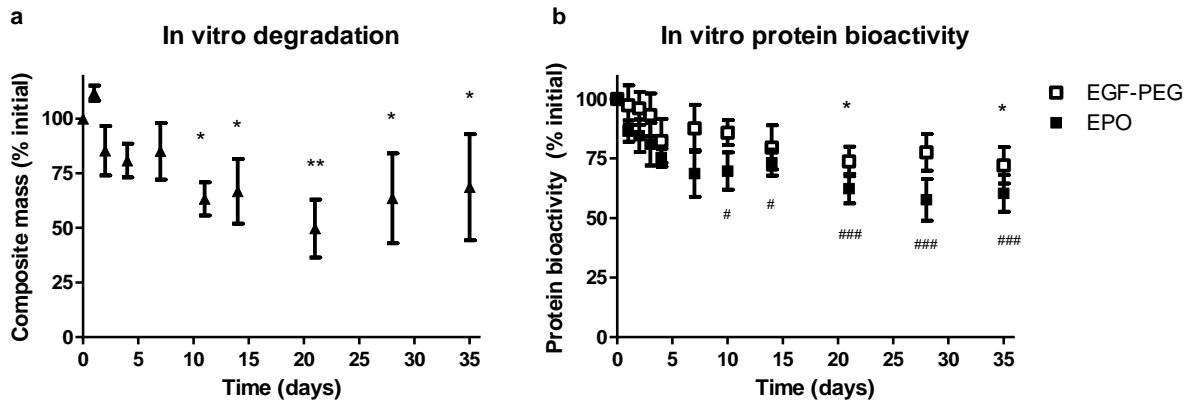
**Supplementary Figure S5.2 | Poly(sebacic acid) (PSA) is used to coat PLGA particles, resulting in biphasic particles.** PLGA particles show smooth surface morphology while PSA particles and PSA-coated PLGA particles show rough surface morphology. XPS surface analysis indicates that the surface chemical composition of biphasic particles reflect that of the PSA particle and not that of the PLGA particle. Areas under the peak for all peaks are normalized to Peak C1sD, which is associated with the C-OH bond typically used as the reference peak in analyzing polymers in XPS.



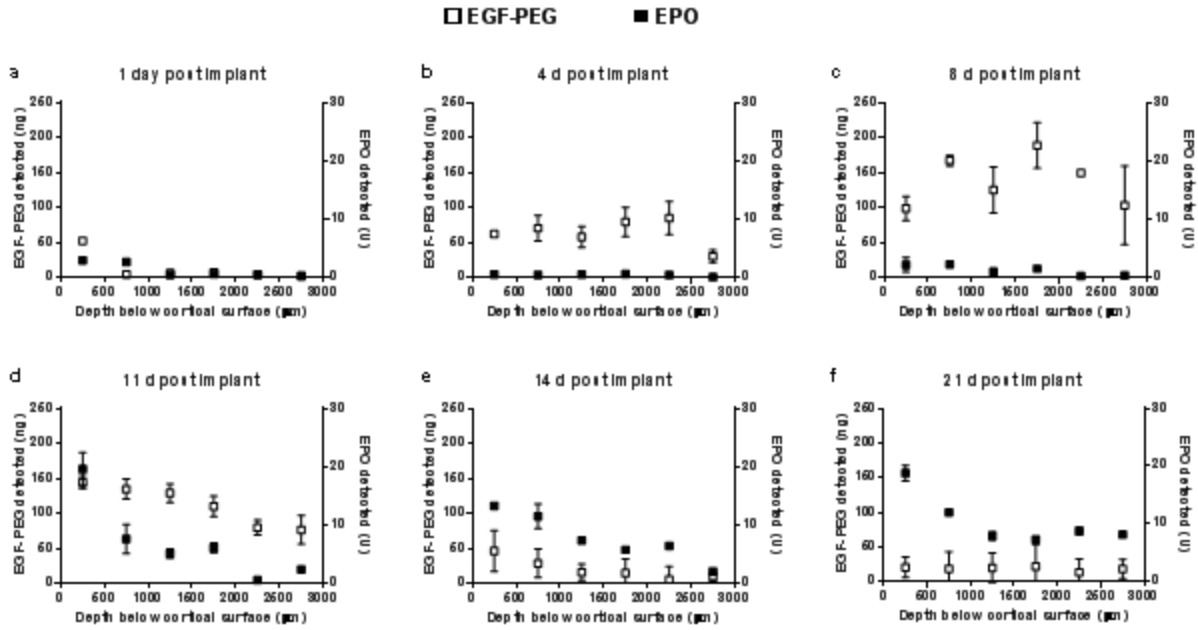
**Supplementary Figure S5.3 | Stroke surgery and the implantation of the drug delivery composite.** (a) Mice were anaesthetized with isoflurane, shaved and placed into a Kopf stereotaxic instrument. A midline incision in the scalp was made and a small burr hole was made in the skull at the coordinates 2.25 lateral to the midline and 0.6 anterior to the Bregma. 1  $\mu$ l of endothelin-1 was injected 1.0 mm ventral to the brain surface at 0.1  $\mu$ l/min. The needle was left in place for 10 min prior to removal and the incision was sutured. Uninjured mice were similarly treated, but no injection was carried out. The drug delivery system was injected 4 days post stroke to ensure that the majority of neuronal death has occurred, and any neurons found in the peri-infarct site at the completion of treatment are due to neurogenesis. The burr hole was exposed and any tissue debris was removed. (b) The disk with 2 mm central opening was fixed over the burr hole with bone glue. 3  $\mu$ l of the composite was injected into the hole such that it is in direct contact with the brain's cortical surface. (c) A second disk with no opening was fixed over the first disk and (d) the skin was sutured over the system.



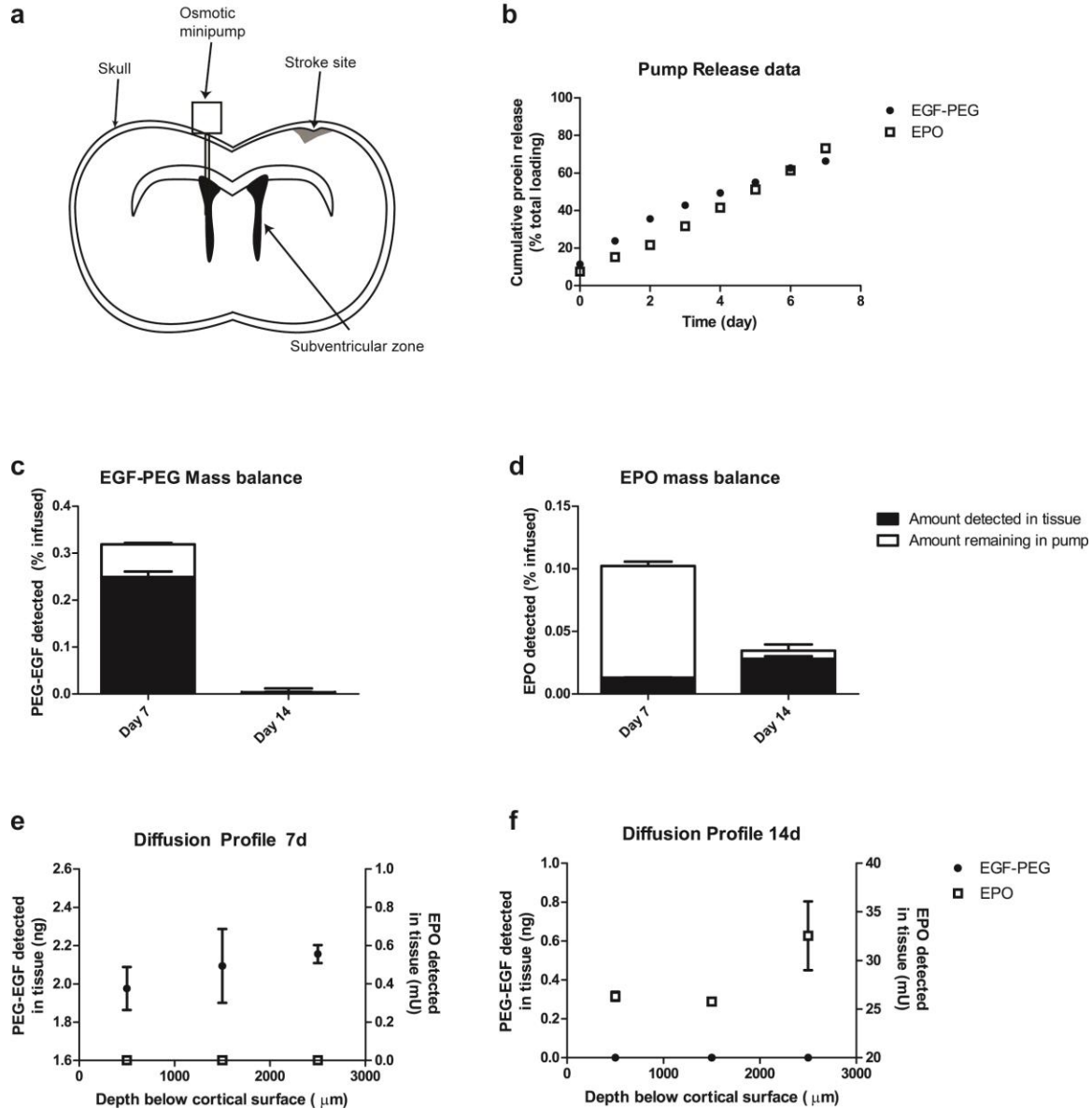
**Supplementary Figure S5.4 | The ipsilateral SVZ is analyzed for NSPC proliferation, while the peri-infarct region is analyzed for tissue repair.** Immunohistochemistry was used to analyze two regions in the brain. The number of Ki67+ and Mash-1+ cells were analyzed in the subependymal layers of the ipsilateral SVZ (a) to assess the level of NSPC proliferation. The number of NeuN+ mature neurons, GFAP+ reactive astrocytes, and CD68+ macrophages and microglia were analyzed in the peri-infarct region (b) to assess tissue repair and inflammatory response.



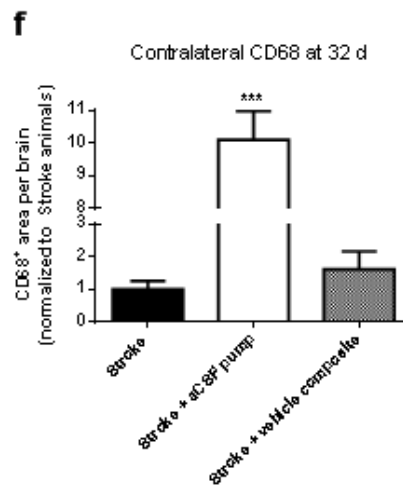
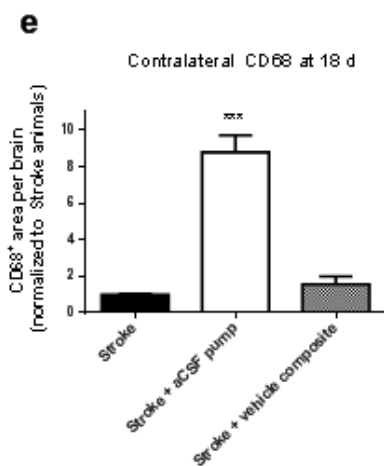
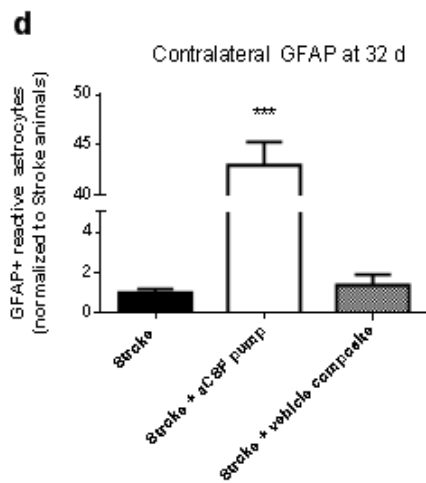
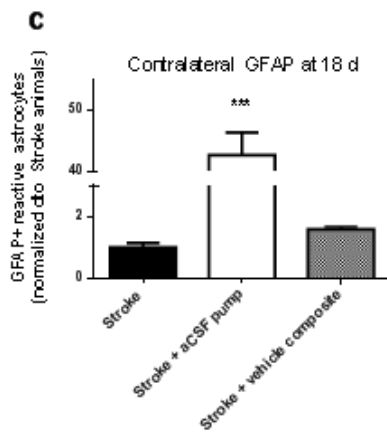
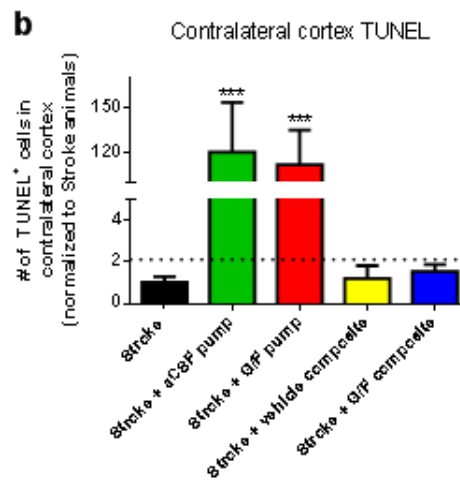
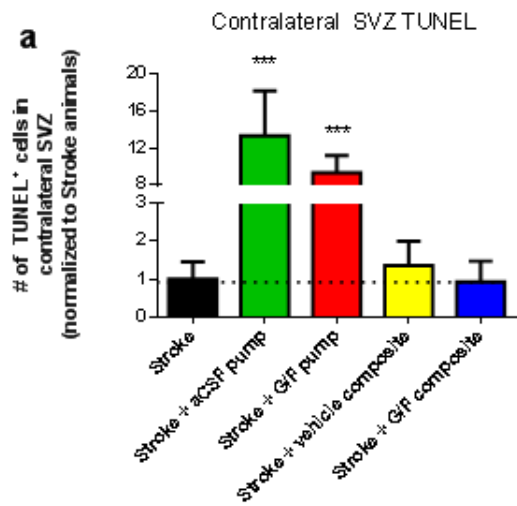
**Supplementary Figure S5.5 | Composite DDS is biodegradable and released protein remains bioactive in vitro.** (a) The HAMC/particle composite degrades/dissolves to 50% of initial wet mass is over 5 weeks, providing sufficient stability to allow controlled protein release over the 1-3 weeks observed herein (\* $p < 0.05$ , \*\* $p < 0.01$ , each time point compared to  $t = 0$  d). (b) Both (□) EGF-PEG and (■) EPO remain at least 60% bioactive during release in vitro over 5 weeks. Bioactivity of proteins was determined by cellular assays using the MTT metabolic assay as a measure of cell viability over time: EGF-PEG was tested using mouse NSPCs and EPO was tested using TF-1 cells, where each factor is required for cell viability. (Mean  $\pm$  standard deviation,  $n = 3$ , \* $p < 0.05$ , \*\* $p < 0.01$ , \*\*\* $p < 0.001$  for EGF-PEG; # $p < 0.05$ , ## $p < 0.01$ , ### $p < 0.001$  for EPO; each time point compared to  $t = 0$  d).



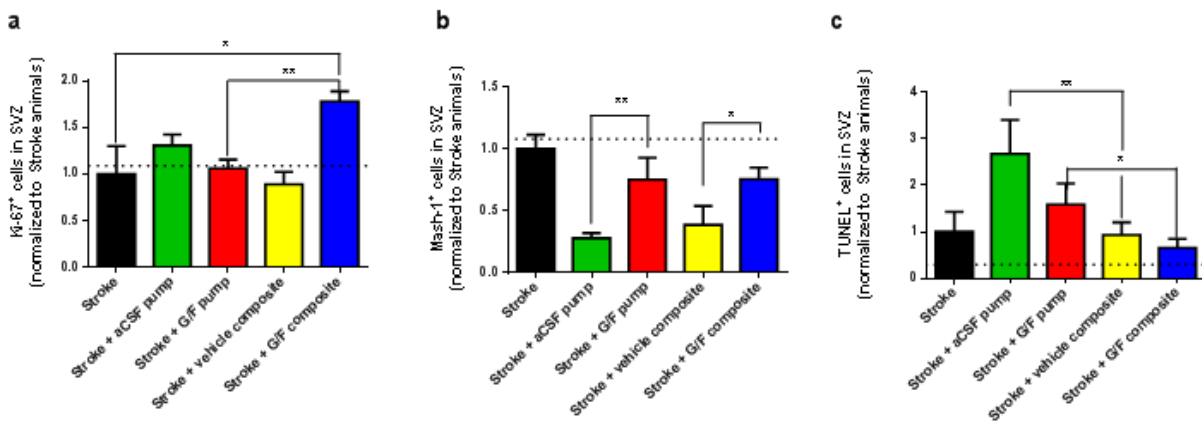
**Supplementary Figure S5.6 | Time course of EGF-PEG and EPO penetration in the stroke-injured brain tissue after epi-cortical delivery from composite.** The concentration profiles of (□)EGF-PEG and (■) EPO are shown at (a) 1, (b) 4, (c) 8, (d) 11, (e) 14, and (f) 21 d post implant using ELISA analysis of tissue samples at defined depths. EGF-PEG is found in the tissue between 1 d and 14 d post implant, with peak concentration of  $833 \pm 75$  ng observed at 8 d. EPO is not found in the tissue in the first 8 d, but detectable levels are found at 11, 14, and 21 days post implant. A peak EPO concentration of  $46.7 \pm 2.2$  U was detected at 14 d. (Mean  $\pm$  standard deviation,  $n = 3$ ).



**Supplementary Figure S5.7 | Delivery and tissue penetration of EGF-PEG and EPO from osmotic minipumps.** (a) Representation of osmotic minipump delivery system. (b) In vitro release of EGF-PEG and EPO follow linear release profiles for 7 days, with approximately 30% protein loss. Even though the same amounts of EGF-PEG and EPO were delivered here using the osmotic minipump system as was released from the epicortical composite system, significantly less growth factors were observed in the brain tissue. (c) Specifically,  $0.25 \pm 0.01\%$  (6.2 ng) of infused EGF-PEG is detected in tissue at day 7 and (d)  $0.028 \pm 0.002\%$  ( $0.0846 \pm 0.0063$  U) of infused EPO was detected at day 14. (e) Only EGF-PEG was detected in brain tissue at 7 d whereas (f) only EPO was detected in brain tissue at 14 d, reflecting the time that each factor was delivered from the pump. (Mean  $\pm$  standard deviation,  $n = 3$ ).



**Supplementary Figure S5.8 | Osmotic minipump causes significantly more damage compared to composite DDS.** Osmotic minipump cannulas are inserted through the cortex into the ventricles contralateral to the stroke site. This procedure causes significant cell death both in the (a) contralateral SVZ and the (b) contralateral cortex, compared to the composite DDS. Dashed line indicates the level of TUNEL signal in the uninjured brain. Additionally, both 18 and 32 days after stroke, the cannula significantly increases the number of (c, d) GFAP<sup>+</sup> reactive astrocytes and (e, f) CD68<sup>+</sup> active microglia in the contralateral cortex compared to both stroke alone and vehicle composite treatments. (Results are normalized to Stroke animals. Mean + standard deviation, n = 5, \*\*\*p<0.001.)



**Supplementary Figure S5.9 | EGF-PEG and EPO delivered sequentially from composite DDS increase proliferation of NSPCs and decrease cell death in the SVZ 32 d post stroke.** Quantification of (a) Ki67<sup>+</sup> proliferating cells, (b) Mash-1<sup>+</sup> neuroprecursors, and (c) TUNEL<sup>+</sup> apoptotic cells in the ipsilateral SVZ 32 d after stroke. Composite-mediated growth factor delivery significantly increases the number of proliferating cells in the SVZ compared to stroke alone, blank composite controls, and growth factors delivered with osmotic minipumps. Mash-1<sup>+</sup> neuroprecursors are increased following growth factor treatment compared to vehicle controls, regardless of the method of delivery. Composite also significantly decreases the number of cell death events in the SVZ compared to osmotic minipumps. The dashed line indicates the level of response in the uninjured brain. Results are normalized to stroke animals. Mean + standard deviation, n = 5, \*p<0.05; \*\*p<0.01; \*\*\*p<0.001.

### Appendix C: Supplementary Tables

**Supplementary Table S2.1** Number of fluorescent molecules conjugated to rhEGF and PEG<sub>x</sub>-rhEGF samples. Degree of Alexa Fluor 488 conjugation to each sample is expressed as number of fluorescent dye molecules per molecule of EGF or PEG<sub>x</sub>-EGF.

Sample	Number of Alexa Fluor 488 Molecules Conjugated
rhEGF	0.88
PEG <sub>1</sub> -rhEGF	1.04
PEG <sub>2</sub> -rhEGF	0.80
PEG <sub>3</sub> -rhEGF	0.87

**Supplementary Table S2.2** Diffusion parameters for rhEGF and PEG<sub>x</sub>-rhEGF in dilute agarose and uninjured brain tissue. Values are reported as mean ± s.e.m. (n = 25).

Sample	Diffusivity (10 <sup>-7</sup> cm <sup>2</sup> /s)		
	<i>D</i> in Agarose	<i>D</i> <sup>*</sup> in Tissue with Saturation	<i>D</i> <sup>*</sup> in Tissue with Elimination
rhEGF	16.8 ± 0.47	5.01 ± 0.88	2.22 ± 0.32
PEG <sub>1</sub> -rhEGF	13.2 ± 0.28	3.34 ± 0.52	2.64 ± 0.35
PEG <sub>2</sub> -rhEGF	8.88 ± 0.35	2.09 ± 0.31	1.78 ± 0.28
PEG <sub>3</sub> -rhEGF	7.68 ± 0.40	1.66 ± 0.40	1.17 ± 0.25

**Supplementary Table S2.3** Model parameters for fitting  $k_e$ . The values of parameters used for each diffusing species in every medium are shown. Constants obtained from literature include  $\alpha$ <sup>141</sup> and  $\varepsilon$ <sup>259</sup>; constants obtained experimentally include tortuosity ( $\lambda$ ), intrinsic diffusivity ( $D$ ), concentration of injected protein solution ( $C_p$ ), initial fluorescent peak intensity ( $I_o$ ) and volume of injected solution ( $U$ );  $k_e$  is the fitted parameter, which was varied between  $0 \text{ s}^{-1}$  to  $10^{-1} \text{ s}^{-1}$  with increments of  $10^{-7} \text{ s}^{-1}$ .

Sample	Constants from literature		Experimentally derived parameters					Fitted Parameter
	$\alpha$	$\varepsilon$	$\lambda$	$D$ ( $10^{-7} \text{ cm}^2/\text{s}$ )	$I_o$ ( $\text{nl}/\text{nmol} \cdot \text{AU}\dagger$ )	$C_p$ ( $10^{-3} \text{ nmol}/\text{nl}$ )	$U$ (nl)	$k_e$ ( $\text{s}^{-1}$ )
rhEGF	0.2	1	2.75	16.7	0.5	0.18	4.6	$0 - 10^{-1}$
PEG <sub>1</sub> -rhEGF	0.2	1	2.24	13.2	0.1	0.18	4.6	$0 - 10^{-1}$
PEG <sub>2</sub> -rhEGF	0.2	1	2.23	8.88	0.1	0.18	4.6	$0 - 10^{-1}$
PEG <sub>3</sub> -rhEGF	0.2	1	2.56	7.68	0.1	0.18	4.6	$0 - 10^{-1}$

†AU – arbitrary fluorescence units

**Supplementary Table S2.4** Diffusion parameters for rhEGF and PEG<sub>1</sub>-rhEGF in stroke-injured brain tissue. Apparent diffusivities in tissue without elimination (i.e. saturation) and tissue with elimination are reported as mean  $\pm$  s.e.m. ( $n = 25$ ).

Sample	Diffusivity ( $10^{-7} \text{ cm}^2/\text{s}$ )			
	Ipsilateral Hemisphere		Contralateral Hemisphere	
	With Saturation ( $D^*$ )	With Elimination ( $D^*$ )	With Saturation ( $D^*$ )	With Elimination ( $D^*$ )
rhEGF	$7.29 \pm 0.82$	$4.54 \pm 0.90$	$5.40 \pm 0.97$	$3.67 \pm 0.67$
PEG <sub>1</sub> -rhEGF	$3.89 \pm 0.96$	$3.78 \pm 0.59$	$3.14 \pm 0.46$	$3.24 \pm 0.68$

## Appendix D: Supplementary Results

In addition to the studies carried out in Chapter 5 of this thesis to examine the benefits of our composite delivery system, we conducted preliminary investigations on the functional outcome of animals that received EGF-PEG and and EPO sequential treatment. Our preliminary findings show that animals receiving treatment from the composite delivery system achieve functional recovery in the endothelin-1 model of stroke. However, one caveat in the study is that functional assays were not blinded, so further confirmations are necessary before definitive conclusions can be made.

### Materials and Methods

Behavioral assessments were carried out weekly from 3 days pre-stroke to 32 days post stroke. Two sets of behavioral tests were carried out: foot fault and cylinder tasks.

**Foot fault task**<sup>432</sup>: Mice were placed on a metal square grid (1.2 cm x 1.2 cm mesh size, 24 cm x 36 cm grid size) elevated above ground and allowed to explore freely. A mirror was placed underneath the grid and used for filming the animals' movements. Each slip of the impaired, contralateral forepaw was recorded as a foot fault. Eight paired weight-bearing steps were required before a set was recorded. The total number of steps was recorded for 5 min per animal.

**Cylinder task**<sup>433</sup>: Mice were placed in a pyrex cylinder (11 cm i.d. x 15 cm h) for 5 min. Animals reared and used the forepaws to explore the environment. A movement where only the ipsilateral or contralateral paw was used was recorded as either an "ipsilateral" (I) or a

“contralateral”(C) movement. If both paws were used simultaneously, the action was recorded as a “both” (B). If a single paw movement was followed by lateral or vertical exploration using both paws, the movement was recorded as an “I” and a “B” or a “C” and a “B”. The extent of contralateral injury was calculated as  $C / (I + C + B)$ .

## Results

### ***Functional Repair in mouse model of stroke: release via epicortical composite vs. intraventricular catheter/minipump***

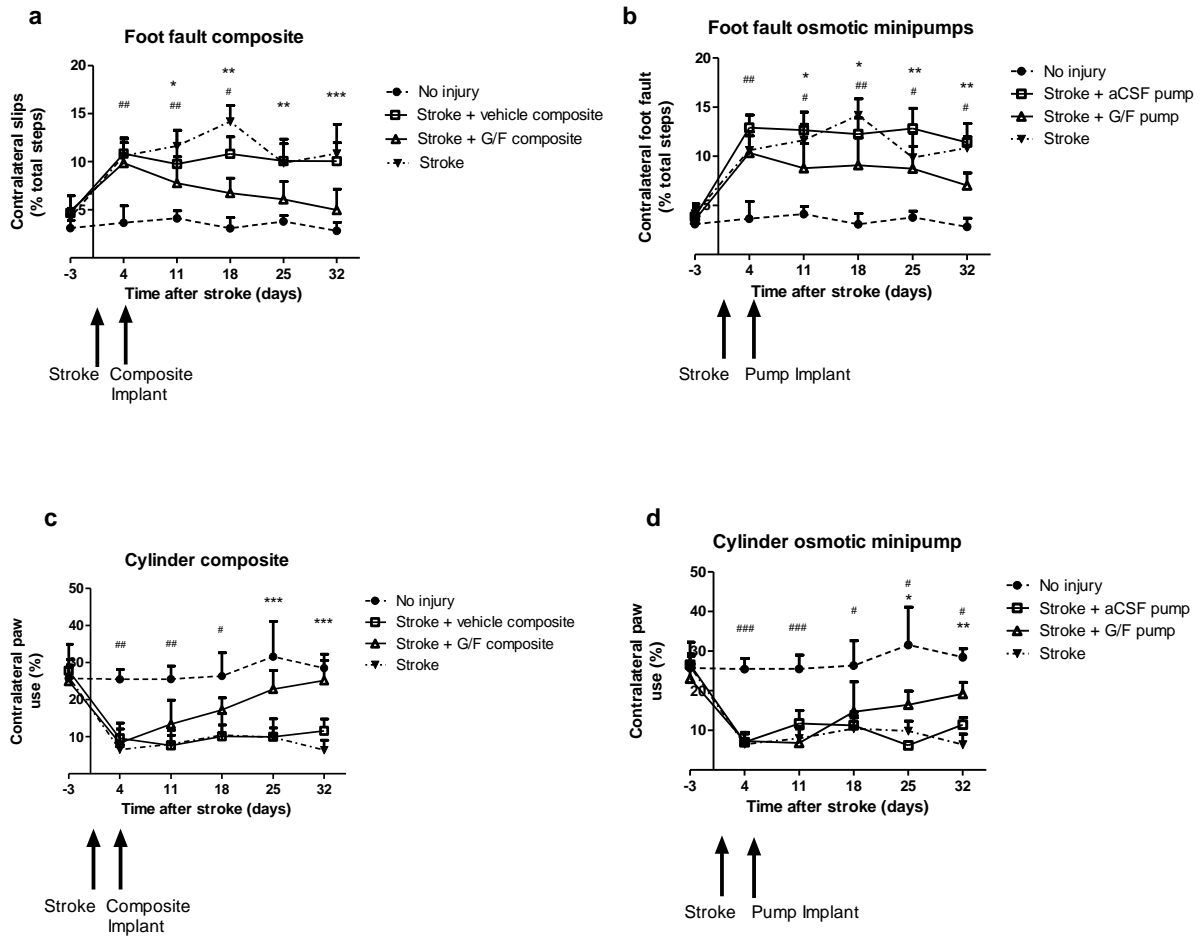
Functional repair after endothelin-1 stroke was monitored using two well-established behavioral tasks for mice that received EGF-PEG and EPO by epicortical composite vs. intraventricular catheter/minipump infusion: the foot fault and the cylinder assays. Injured animals that receive growth factors (G/F) from the composite (Stroke + G/F composite) or the catheter/minipumps (Stroke + G/F pump) are compared against controls of: no injury, vehicle composite (Stroke + vehicle composite), and vehicle pump (Stroke + aCSF pump). We ensured normal mouse behavior 3 days prior to stroke (-3 d) and deficits in the contralateral paw 4 days after stroke, prior to initiation of the controlled release strategy of EGF-PEG and EPO at 4 days.

In the foot fault assay, animals were allowed to ambulate freely on a grid and slippage of the injured forepaw was recorded relative to the number of total steps taken in a 5 minute period. The control animals behaved as expected: no injury controls show no deficits whereas stroke-injured animals that received vehicle treatments maintain the deficit from 4 – 32 days after stroke. Remarkably, stroke-injured mice that had epicortical delivery of EGF-PEG and EPO show significant improvements from 11 to 32 days after stroke compared to those that receive the vehicle composite (**Supplementary Fig. D.1a**). More importantly, these stroke + G/F composite animals show no significant difference from the no-injury controls at 25 and 32 days

after stroke, demonstrating functional recovery to pre-injury levels. EGF-PEG followed by EPO infusion from catheter/minipumps also results in improvement from 11 to 32 days after stroke compared to aCSF infusion (**Supplementary Fig. D.1b**). There remained, however, a significant difference between the stroke + G/F pump animals and the no injury animals even at the terminal time points, demonstrating that the catheter/minipump system is not as efficacious as the epicortical composite delivery of G/Fs.

In the cylinder assay, animals were placed in a glass cylinder and allowed to explore their surroundings, and the extent of injured contralateral paw use was compared to total paw use in a 5 minute period. Notably, the behavior observed between all of the groups in the cylinder task was similar to that observed in the foot fault study (**Supplementary Fig. D.1c, d**). Controls of injury alone or aCSF vehicle delivery showed no improvement over time whereas stroke + G/F animals performed significantly better. Importantly, only the stroke + G/F composite animals showed comparable performance to the no injury controls at the last two time points.

These results correspond to tissue-level findings, and show that the composite drug delivery system is a promising tool for administering proteins to the brain by a minimally invasive method.



**Supplementary Figure D.1 | Epi-cortical delivery of EGF- PEG followed by EPO using composite drug delivery system (DDS) improves functional outcome in ET-1 mouse model of stroke.** Foot fault test indicates that: (a) growth factors delivered from composite DDS (G/F composite) (n = 11) and (b) osmotic minipumps (G/F pumps) (n = 6) lead to significant functional recovery compared to vehicle control (blank composite, n = 11, and aCSF pump, n = 6) and stroke-only control (n = 6). Composite-treated animals showed no functional deficit compared to no-injury control (n = 6) at 25 and 32 d after stroke. Cylinder test confirms that (c) G/F composite and (d) G/F pump treated animals showed significant functional improvement at 25 and 32 d after stroke, but only G/F composite led to full recovery, indicating that G/F composite resulted in faster rate of recovery compared to G/F pump. Arrows indicate the dates of stroke and implant surgeries (Mean + standard deviation). \*Statistically significant difference between treatment group and vehicle control: \*p<0.05; \*\*p<0.01; \*\*\*p<0.001. #Statistically significant difference between treatment group and no-injury group: #p<0.05; ##p<0.01; ###p<0.001.

## **Copyright Acknowledgements**

Chapters 2, 3, 4, and 5 were adapted from published original research articles. Proper copyright permissions were granted by the respective publishers. These works were primarily written by Yuanfei Wang.

## Yuanfei Wang

155 Marlee Avenue, Apt#1410, Toronto, ON, M6B 4B5, Canada

Phone: (416) 882-1823

Email: yuanfei.wang@utoronto.ca

### EDUCATION

- September 2008 – Present:* University of Toronto, Doctorate in Chemical Engineering. Controlled Delivery of Growth Factors for Stimulating Brain Repair after Stroke. Professor Molly Shoichet
- September 2005 – June 2008:* University of Toronto, B.A.Sc in Chemical Engineering (Honours).

### PUBLICATIONS

#### Peer-Reviewed

1. **Wang** et al (2013). "*Bioengineered sequential growth factor delivery stimulates brain tissue regeneration after stroke*". Journal of Controlled Release 2013. Accepted.
2. **Wang** et al (2012). "*Hydrogel delivery of erythropoietin to the brain for endogenous stem cell stimulation after stroke injury*". Biomaterials, 2012(33):2681-2692.
3. McLean, D.; Cooke, M.J.; **Wang, Y.**; Fraser, P.; St. George-Hyslop, P.; Shoichet, M.S. (2012) "*Targeting the amyloid- $\beta$  antibody in the brain tissue of a mouse model of Alzheimer's disease*", in press xx1-xx8; doi: 10.1016/j.jconrel.2011.12.036
4. **Wang** et al (2011). "*Controlled Epi-cortical Delivery of Epidermal Growth Factor Stimulates Endogenous Neural Stem Cell Proliferation in Stroke-Injured Brain*". Biomaterials, 2011, 32(24):5688-97.
5. **Wang** et al (2010). "*Transport of epidermal growth factor in the stroke-injured brain*". Journal of Controlled Release. Doi: 10.1016/j.jconrel.2010.10.022.
6. **Wang** et al (2009). "*Accelerated release of a sparingly soluble drug from an injectable hyaluronan-methylcellulose hydrogel*". Journal of Controlled Release, 2009, 140(3):218-23.
7. Baumann, Kang, **Wang** et al (2009). "*An injectable drug delivery platform for sustained combination therapy*". Journal of Controlled Release, 138 (2009) 205–213.

## Patents

8. Shoichet, M.S., **Wang, Y.**, Cooke, M.C., Baumann, M.D., McLean, D., Morshead, C.M. Provisional patent application 2011, "Methods and devices for local delivery of an agent to the brain" (2011). US Provisional Application No. 61/475,466.
9. Shoichet, M.S.; Lapitsky, Y.; **Wang, Y.** Provisional patent application 2010, "Tunable sustained release of a sparingly soluble hydrophobic therapeutic agent from a hydrogel matrix" (201). U.S. Patent Application No. 12/785,083.

## Conference Presentations

10. **Wang, Y.**, Cooke, M.J., Morshead, C.M., Shoichet, M.S. (2010) "*Transport of epidermal growth factor after epi-cortical delivery from a hydrogel in a mouse stroke model*". Society for biomaterials meeting 2011.
11. **Wang, Y.**, Cooke, M.J., Shoichet, M.S. (2010) "*Controlled delivery of epidermal growth factor for neural stem cell stimulation after stroke*". Society for biomaterials meeting 2010.
12. **Wang, Y.**, Shoichet, M.S. (2009). "*Controlled drug release from hyaluronan-methylcellulose hydrogels*". 8th World Congress of Chemical Engineering.
13. Cooke, **Wang**, Morshead, Shoichet "Regenerative Stem Cell Strategies for Repair of the Injured Brain Using Endogenous and Exogenous Neural Stem/Progenitor Cells" OSCI, Toronto, ON, June 2011
14. Cooke, **Wang**, Morshead, Shoichet "Repair of the Injured Brain Using Neural Stem/Progenitor Cell Transplantation" ISSCR, Toronto, ON, June 2011
15. Cooke, **Wang**, Morshead, Shoichet "Repair of the Injured Brain Using Neural Stem/Progenitor Cell Transplantation" Gordon Research Conference, Holderness School, NH, July 2011
16. Cooke, **Wang**, Morshead, Shoichet "Regenerative Stem Cell Strategies for Repair of the Injured Brain Using Endogenous and Exogenous Neural Stem/Progenitor Cells" New York Stem Cell Foundation Translational Stem Cell Research Conference, New York, NY, October 2011

17. Cooke, **Wang**, Morshead, Shoichet "Regenerative Stem Cell Strategies for Repair of the Injured Brain Using Endogenous and Exogenous Neural Stem/Progenitor Cells" BMES Hartford, CT, October 2011

## **AWARDS**

NSERC CGS D (UofT)	2008 – 2012
Chemical Institute of Canada Silver Medal	September 2007
Shell Canada Engineering Scholarship (UofT)	2006 – 2007
Shell Canada Engineering Scholarship (UofT)	2005 – 2006
NSERC USRA (UofT)	May 2007 – August 2007
NSERC USRA (UofT)	May 2006 – August 2006